



**DCU**

Dublin City University  
Ollscoil Chathair Bhaile Átha Cliath

**THE APPLICATION OF NANOMATERIALS  
IN ELECTROCHEMICAL SENSORS AND  
BIOSENSORS**

by

**Adriano Ambrosi**

**Thesis submitted for the Degree of Doctor of Philosophy**


**Supervisors:  
Prof. Malcolm R. Smyth  
&  
Dr. Anthony J. Killard**

**School of Chemical Sciences**

**September 2007**

## Declaration

I hereby certify that this material, which I now submit for assessment on the programme of study leading to the award of PhD, is entirely my own work and has not been taken from the work of others save and to the extent that such work has been cited and acknowledged within the text of my work.

Signed: 

ID No.: 54141001

Date: 19 / 09 / 07

## Acknowledgements

The first person I want to acknowledge is prof. Malcolm Smyth who made this achievement possible and who always looked after me, making sure that my research career was going to the right direction in every moment. Thank you very much Malcolm for giving me this opportunity.

The second acknowledgement is for Dr. Tony Killard who represented a guide and the indispensable source of inspiration during all these years. Thank you so much Tony for teaching me this job, for all the advices and the invaluable help you have given me.

I would like to thank now all the members of sensors and separations group I have met during my time in DCU: First of all Aoife, Blànaid and Gill who from the very first day have always been so special to me and will always have a place in my heart. Xiliang who I had the fortune to work with for nearly two years, a great research partner but over all a good friend. Michele, Kyriaki, Ewa, Eimer, Ciàran and Karl. I had a really good time with them and I am glad to have met such nice people. Finally Kathleen, Joseph, Padraic, Car, Heidi, Eric, Claire, Ciara, Maire, Geoff, Amy, Aaron and Combs who shared with me the lab life only for a short time but leaving pleasant memories.

A big thanks also to the DCU italian beauties Stefania and Elena for the essential support and the nice friendship.

I also would like to acknowledge all the people I met in Barcelona during my visit, especially Arben for the precious supervision.

A special thanks to my family, Màm, Pàm and Annalisa for bearing the big weight of my distance and at the same time encouraging me.

Two final thoughts: One for her, Ale, for making me begin this adventure, for sharing every single bad and good moment, for supporting me, for existing and all the rest. The last one for myself, who I am very proud of.

## **Dedication**

*To Mā & Pā*

# TABLE OF CONTENTS

	<b>PAGE NUMBER</b>
TITLE PAGE	I
DECLARATION	II
ACKNOWLEDGEMENTS	III
DEDICATION	IV
TABLE OF CONTENTS	V
ABBREVIATIONS	XI
ABSTRACT	XIV
THESIS OUTLINE	XVI
<b>CHAPTER ONE</b>	<b>1</b>
<i>Electrochemical sensing applications based on nanoparticles:     A Literature Review</i>	
<b>1.1 INTRODUCTION</b>	<b>2</b>
<b>1.2 CHEMICAL SENSORS</b>	<b>4</b>
1.2.1 Catalysis of electrochemical reactions	5
1.2.2 Acting as a reactant	6
<b>1.3 ENZYME-BASED BIOSENSORS</b>	<b>7</b>
1.3.1 Immobilisation of enzymes on electrode surfaces	7
1.3.2 Enhancement of electron transfer	11
1.3.3 Nanoparticles acting as a reactant in combination with enzymes	12
<b>1.4 IMMUNOSENSORS</b>	<b>13</b>
1.4.1 Principles of immunoassays	14
1.4.2 Nanoparticle-modified electrode surfaces for the immobilisation of antibodies	17
1.4.3 Nanoparticles as labels for immunosensing	18
<b>1.5 CONCLUSIONS</b>	<b>23</b>
<b>1.6 REFERENCES</b>	<b>25</b>

*The application of conducting polymer nanoparticle electrodes  
for the sensing of ascorbic acid and hydrogen peroxide*

<b>2.1</b>	<b>INTRODUCTION</b>	<b>34</b>
2.1.1	Electrocatalytic properties of conducting polymers	34
2.1.1.1	Electrocatalytic oxidation of ascorbic acid	35
2.1.1.2	Electrocatalysis of hydrogen peroxide	40
2.1.2	Processability of polyaniline	41
<b>2.2</b>	<b>MATERIALS AND METHODS</b>	<b>44</b>
2.2.1	Materials	44
2.2.2	Buffers and solutions	44
2.2.3	Instrumentation	44
2.2.4	Synthesis of polyaniline nanoparticles	45
2.2.5	Electrode modification with PANI nanoparticles	45
2.2.6	Electropolymerisation of bulk aniline on the electrode surface	46
2.2.7	Electrochemical characterisations	46
2.2.8	Inkjet printing of PANI nanoparticles	47
<b>2.3</b>	<b>RESULTS AND DISCUSSION</b>	<b>49</b>
2.3.1	Voltammetric study of nanoPANI modified electrode	49
2.3.2	Oxidation of ascorbic acid at nanoPANI modified electrode	50
2.3.3	Investigation of the working potential for the analysis of ascorbic acid	55
2.3.4	Optimisation of the working pH for the analysis of ascorbic acid	57
2.3.5	Calibration of the nanoPANI-based sensor for the analysis of ascorbic acid	59
2.3.6	Application of the nanoPANI-modified electrode for the analysis of hydrogen peroxide	62
2.3.7	Investigation of the working potential for the analysis of hydrogen peroxide	66
2.3.8	Optimisation of the working pH and calibration of the nanoPANI based sensor for the analysis of hydrogen peroxide	67
2.3.9	Development of an inkjet printed nanoPANI film electrode for ascorbic acid and hydrogen peroxide detection	72
<b>2.4</b>	<b>CONCLUSION</b>	<b>75</b>

<b>2.5</b>	<b>REFERENCES</b>	<b>77</b>
<b>CHAPTER THREE</b>		<b>85</b>
	<i>Development of an electrochemical immunosensor platform based on enhancement of enzyme-channeling using nanoparticles</i>	
<b>3.1</b>	<b>INTRODUCTION</b>	<b>86</b>
3.1.1	Bienzyme biosensors	88
3.1.2	Bienzyme immunosensors	89
<b>3.2</b>	<b>MATERIALS AND METHODS</b>	<b>92</b>
3.2.1	Materials	92
3.2.2	Buffers and solutions	93
3.2.3	Instrumentation	93
3.2.4	Screen-printed electrode modification with PANI/PVS	93
3.2.5	Immobilisation of HRP on PANI/PVS-modified screen printed electrode	95
3.2.6	Flow-injection analysis of H <sub>2</sub> O <sub>2</sub>	95
3.2.7	Immobilisation of HRP and GOX in a single step	95
3.2.8	Investigation of the bienzyme-based biosensor using a mathematical approach	96
3.2.9	Flow-injection analysis of glucose	97
3.2.10	Immobilisation of avidin and HRP in a single step	97
3.2.11	Assessment of different avidin/HRP platforms on binding GOX or biotin-GOX	97
3.2.12	Calibration curve for GOX and biotin-GOX on avidin/HRP platform	98
3.2.13	Competition assay system for real time biotin determination	98
3.2.14	Preparation of gold nanoparticle solutions	98
3.2.15	Formation and characterisation of gold-HRP and gold-GOX conjugates	99
3.2.16	Application of Au-biotin-GOX conjugates to the immunosensing system	99
<b>3.3</b>	<b>RESULTS AND DISCUSSION</b>	<b>100</b>

3.3.1	HRP binding capacity of PANI/PVS modified electrode	100
3.3.2	Assessment of immobilisation time of HRP	102
3.3.3	Assessment of the optimal pH for the immobilisation of HRP	103
3.3.4	Calibration of the HRP-based biosensor for H <sub>2</sub> O <sub>2</sub> analysis and stability study	104
3.3.5	Optimisation of HRP/GOX ratio for the bienzyme-based biosensor for glucose analysis	107
3.3.6	Assessment of different avidin/HRP platforms on binding GOX or biotin-GOX	115
3.3.7	Calibration curve for GOX and biotin-GOX on avidin/HRP platform	119
3.3.8	Competition assay system for real-time biotin determination	120
3.3.9	Conjugation of AuNPs with GOX and HRP	122
3.3.10	Spectrophotometric activity study of HRP on gold nanoparticles	126
3.3.11	Amperometric activity study of HRP on gold nanoparticles	129
3.3.12	Amperometric activity study of GOX on gold nanoparticles	135
3.3.13	Comparison between free biotin-GOX and Au-biotin-GOX conjugate applied to the immunosystem	139
<b>3.4</b>	<b>CONCLUSION</b>	<b>141</b>
<b>3.5</b>	<b>REFERENCES</b>	<b>143</b>

## **CHAPTER FOUR** **148**

### *Enhanced electrochemical immunoassay based on paramagnetic platforms and gold nanoparticle labels*

<b>4.1</b>	<b>INTRODUCTION</b>	<b>149</b>
<b>4.2</b>	<b>MATERIALS AND METHODS</b>	<b>151</b>
4.2.1	Materials	151
4.2.2	Buffers and solutions	151
4.2.3	Instrumentation	151
4.2.4	Synthesis and characterisation of gold nanoparticles	152
4.2.5	Preparation of gold nanoparticle-based immuno label	152
4.2.6	Preparation of magnetic bead sandwich-type immunocomplexes	154
4.2.7	Spectrophotometric analysis	156



4.2.8	Construction of the graphite-epoxy composite-magnet electrodes	158
4.2.9	Electrochemical analysis	159
<b>4.3</b>	<b>RESULTS AND DISCUSSION</b>	<b>160</b>
4.3.1	Gold nanoparticles characterisation	160
4.3.2	Preparation of gold-labelled anti-human-HRP	163
4.3.3	Characterisation of magnetic bead-immunocomplexes by TEM and SEM	168
4.3.4	Spectrophotometric analysis	169
4.3.5	Electrochemical measurements	173
<b>4.4</b>	<b>CONCLUSION</b>	<b>178</b>
<b>4.5</b>	<b>REFERENCES</b>	<b>179</b>
 <b>CHAPTER FIVE</b>		 <b>182</b>
<i>The use of nanoparticle enhancement to characterise immunological interactions at a modified electrode by Scanning Electron Microscopy</i>		
<b>5.1</b>	<b>INTRODUCTION</b>	<b>183</b>
5.1.1	Scanning electron microscopy	185
5.1.2	Energy dispersive X-ray spectroscopy	188
<b>5.2</b>	<b>MATERIALS AND METHODS</b>	<b>189</b>
5.2.1	Materials	189
5.2.2	Buffers and solutions	189
5.2.3	Instrumentation	189
5.2.4	Electrode preparation	190
5.2.5	SEM /EDX Analysis	190
5.2.5.1	Optimisation of assay conditions	190
5.2.5.2	Preparation of anti-atrazine immunosensor	191
5.2.5.3	Preparation of anti-biotin immunosensor	192
<b>5.3</b>	<b>RESULTS AND DISCUSSION</b>	<b>192</b>
5.3.1	Silver enhancement optimisation	192
5.3.2	Protein immobilisation time optimisation	194
5.3.3	Anti-atrazine immunosensor surface	195

5.3.4	Anti-biotin immunosensor surface	199
5.4	CONCLUSION	201
5.5	REFERENCES	202
	<b>CHAPTER SIX</b>	<b>204</b>
	<i>Future developments</i>	
6.1	NOVEL DEVELOPMENTS FOR ELECTROCATALYSIS OF HYDROGEN PEROXIDE (CHAPTER 2)	205
6.2	ALTERNATIVE IMMOBILISATION STRATEGIES IN DEVELOPING ELECTROCHEMICAL ENZYME-BASED IMMUNOSENSORS (CHAPTER 3)	207
6.3	TOWARDS MINIATURISATION OF ELECTROCHEMICAL IMMUNOASSAYS (CHAPTER 4)	209
6.4	CHARACTERISATION OF IMMUNOSENSING SURFACES BY SEM (CHAPTER 5)	210
6.5	REFERENCES	211
	<b>LIST OF PUBLICATIONS AND PRESENTATIONS</b>	<b>213</b>

## Abbreviations

A	Area of electrode
a.c.	Alternating current
A.U.	Absorbance unit
Ab	Antibody
Abs	Absorbance
ABTS	2,2'-Azino-bis(3-ethylbenzthiazoline-6-sulphonic acid)
AFM	Atomic force microscopy
Ag	Antigen or Silver
Ag/AgCl	Silver/silver chloride reference electrode
AgNPs	Silver nanoparticles
AuNPs	Gold nanoparticles
BSA	Bovine serum albumin
B&W	Binding and washing buffer
C	Concentration of redox active species in bulk solution
CME	Chemically modified electrode
CNT	Carbon nanotubes
CPE	Carbon paste electrode
CV	Cyclic voltammetry
$D_0$	Diffusion coefficient
DBSA	Dodecylbenzene sulphonic acid
DNA	Deoxyribonucleic acid
E	Applied Potential
$E_{1/2}$	Half-wave potential
EDX	Electron dispersive x-ray
$E_{eq}$	Equilibrium potential
EFM	Electrochemical force microscopy
ELISA	Enzyme-linked immunosorbent assay
EM	Emeraldine
$EM^{++}$	Emeraldine radical cation
$E^0$	Standard electrode potential

$E_{p,a}$	Anodic peak potential
$E_{p,c}$	Cathodic peak potential
F	Faraday's constant
FET	Field effect transistor
FFT	Fast Fourier Transform
FIA	Flow injection analysis
GECE-M	Magnetic graphite-epoxy composite electrode
GOX	Glucose oxidase
HCG	Human chorionic gonadotropin
HF	Hydrofluoric acid
HRP	Horseradish peroxidase
$i$	Current
$I_{max}$	Maximum current
$i_{p,a}$	Anodic peak current
$i_{p,c}$	Cathodic peak current
ISFET	Ion-selective field effect transistor
ITO	Indium tin oxide
$j_{p,a}$	Anodic peak current density
$j_{p,c}$	Cathodic peak current density
$k^0$	Electron rate transfer constant
$k^{0'}$	Apparent electron rate transfer constant
LB	Langmuir-Blodgett
LDH	L-lactate dehydrogenase
LM	Leucoemeraldine
$LM^{*+}$	Leucoemeraldine radical cation
$m$	Slope
MB	Magnetic beads
$M_w$	Molecular weight
MWNT	Multi-walled nanotubes
$n$	Number of electrons transferred
NADH	Nicotinamide-adenine dinucleotide
NHS	N-hydroxysuccinimide
NMR	Nuclear magnetic resonance
NTA	Nitrilotriacetic acid

OPD	<i>o</i> -phenylenediamine dihydrochloride
PANI	Polyaniline
PBS	Phosphate buffered saline
PET	Polyethylene terephthalate
ppb	Parts per billion
ppm	Parts per million
ppt	Parts per trillion
PPy	Polypyrrole
PVC	Polyvinylchloride
PVS	Polyvinylsulphonate
Q	Charge
$Q_{\text{Bare}}$	Charge at a bare gold electrode
R	Universal gas constant
RE	Reference electrode
RVC	Reticulated vitreous carbon
s	Seconds
SAM	Self-assembled monolayer
SAMMS	Self-assembled monolayer on mesoporous silica
SCE	Saturated calomel electrode
SDS	Sodium dodecyl sulphate
SECM	Scanning electrochemical microscopy
SEM	Scanning electron microscopy
SPE	Screen-printed electrode
SPR	Surface plasmon resonance
SWNT	Single-walled nanotubes
T	Temperature
t	Time
TEM	Transmission electron microscopy
THF	Tetrahydrofuran
UV	Ultra violet
WE	Working electrode
$\Delta E_p$	Peak potential separation

## **Abstract**

### **The application of nanomaterials in electrochemical sensors and biosensors**

Nanotechnology has recently become one of the most exciting forefront fields in analytical chemistry. A wide variety of nanoscale materials of different sizes, shapes and compositions at the 1-100 nm scale, are now available. Metal and polymeric nanoparticles were applied in this work for designing novel sensing systems, enhancing the performance of bioanalytical assays and improving the visualisation of biointeractions occurring on sensing surfaces.

A novel nanoparticulate formulation of the conducting polymer polyaniline (PANI) was applied for the development of a chemical sensor device capable of detecting both ascorbic acid and hydrogen peroxide. The “nanoPANI”-modified electrode showed enhanced electrocatalysis over traditional bulk PANI films for hydrogen peroxide. Inkjet printing deposition of this highly processable nanomaterial onto screen-printed electrodes was also demonstrated for simple and rapid sensor device production.

An enzyme-channelling system for the detection of glucose was optimised with HRP and GOX enzymes and applied to an immunosensor platform to report the immunological interaction between biotin and avidin. After the evaluation of the efficiency of this system, a signal enhancement approach was then attempted by means of AuNPs as multi-enzyme carriers. Characterisation of the enzyme-NP conjugates was also performed by spectrophotometric and electrochemical analyses.

AuNPs were also used to develop a multi-detection immunoassay system. A sandwich-type platform was prepared using streptavidin-modified paramagnetic beads as supporting material, biotinylated anti-human IgG as primary antibody specific to human IgG and Au-labelled anti-human-HRP as secondary antibody. Using AuNPs as labels offered the possibility of the spectrophotometric analysis based on either AuNP absorption or HRP enzymatic activity and also electrochemical analysis based on the direct detection of AuNPs. Both the optical and the electrochemical analysis of a human IgG model protein resulted in enhanced sensitivity when compared to the classical ELISA tests where HRP-labelled antibodies are used.

Silver-enhanced AuNPs were finally used to visualize an immunointeraction occurring at an electrode surface by means of SEM. A AuNP-labelled anti-goat antibody was used as the target protein to interact with two immunosensor platforms prepared immobilising anti-atrazine (single chain) and anti-biotin antibodies onto PANI-modified electrodes. Comparing the images of the immunosensor surfaces with those of different control surfaces, it was possible to gain an appreciation of the extent and distribution of the immunological interaction and the level of non-specific binding occurring at the electrode.

In general, the application of these nanoparticles resulted in many advantages for the sensing systems investigated in this work. These include the observation of enhanced electrocatalytic phenomena with benefits in chemical and biosensing, in improved analytical performance of classical sensing platforms where metal NPs were used as electrical tracers, as well as the application of metal NPs to assist in the detailed physical characterisation of immunosensing systems.

## THESIS OUTLINE

The main aim of the work presented in this thesis is the application of nanomaterials, especially nanoparticles, in the development of chemical and biological electrochemical sensing devices. An overall evaluation of the benefits brought by the use of these NPs will be made for each application. The chemical and catalytic properties of novel conducting polymer NPs are investigated and applied in the fabrication of chemical sensors for ascorbic acid and hydrogen peroxide analysis. AuNPs are used both to enhance analytical performances of different immunosensing platforms, and also as tracer for the visualization of an immunointeraction occurring at an electrode surface by means of scanning electron microscopy techniques.

In Chapter 1 an overview on recent applications of nanomaterials, with particular emphasis on NPs, to electrochemical sensing and biosensing devices is presented.

Chapter 2 describes the application of a novel nanoparticulate formulation of the conducting polymer polyaniline (PANI) for the development of a chemical sensor device capable of detecting both ascorbic acid (AA) and hydrogen peroxide ( $H_2O_2$ ). The sensor device comprised a thin film of PANI NPs deposited on a disposable carbon-paste SPE. Electrochemical studies were performed to demonstrate that the electrochemical response to AA and  $H_2O_2$  showed enhanced electrocatalysis over traditional bulk films. The platform was then optimised in terms of its analytical performance for sensor development for these two analytes. In addition to the unique electrocatalytic nature of this nanomaterial, in particular towards  $H_2O_2$ , the work highlights the potential for using a combination of the inkjet printing deposition technique with a highly processable form of conducting polymer for large scale sensor device production.

In chapter 3 the development and the optimisation of a bienzyme-based biosensor using HRP and GOX enzymes is described, with the aim of evaluating the efficiency of the “enzyme-channelling” assay approach. This enzyme-channelling system was then applied to an immunosensor platform to report the immunological interaction between biotin and avidin. A signal enhancement approach was then attempted by means of AuNPs as multi-enzyme carriers. Characterisation of the enzyme-NP conjugates were also performed by spectrophotometric and electrochemical analysis.



Chapter 4 illustrates the development of an electrochemical immunoassay based on the use of AuNPs as labels. Streptavidin-modified paramagnetic beads were used as supporting material. A sandwich-type immunosensor, with biotinylated goat anti-human IgG primary antibody specific to human IgG and Au-labelled anti-human-HRP secondary antibody, was prepared in order to exploit the possibility of double-detection. Spectrophotometric analysis based on either AuNP absorption or HRP enzymatic activity and the electrochemical analysis based on the direct detection of AuNPs are presented and compared. Optical sensitivity enhancement attributable to the use of AuNPs as a multi-IgG-HRP carrier which therefore amplify the enzymatic signal, as well as the high sensitivity in the direct electrochemical detection, represent the most important achievements in the use of this doubly-labelled protein. A comparison with the classical spectrophotometric methods (ELISA) using HRP-labelled antibodies was also performed.

In chapter 5 a method to visualize an immunointeraction occurring at an electrode surface by the use of scanning electron microscopy (SEM) is demonstrated. A AuNP-labelled anti-goat antibody was used for the visualization of two immunosensor platforms where anti-atrazine (single chain) and anti-biotin antibodies were immobilized on the electrode surface. Firstly, a silver enhancement treatment was used and optimized in order to improve the visualization of the Au label. Subsequently, protein distribution on the surface was evaluated in relation to the immobilization time. Finally, this method was adopted to evaluate specific immunological interactions. Comparing the images of the immunosensor surfaces with those of different control surfaces, it was established that the immunological interactions were effectively occurring at the electrode and it was also possible to gain an appreciation of the extent and distribution of the immunological interaction at the electrode surface and the level of non-specific binding occurring. Energy Dispersive X-ray (EDX) analysis was also performed for a qualitative evaluation of the electrode surface composition.

Overall conclusions and suggestions for future work arising from this thesis are given in Chapter 6.

# **Chapter 1**

**Electrochemical sensing applications based on  
nanoparticles:  
A Literature Review**

## 1.1 INTRODUCTION

Nanotechnology is any technology which exploits phenomena and structures that exist at the nanometer scale, which is the scale of single atoms and small molecules. One of the definitions is as follows: “Nanotechnology is the understanding and control of matter at dimensions of roughly 1 to 100 nanometers, where unique phenomena enable novel applications”<sup>1</sup>. Nanomaterials or matrices, with at least one of their dimensions ranging in scale from 1 to 100 nm, display unique physical and chemical features that lead to new properties depending on the size. One of the most intuitive effects is due to the change in the surface area/volume ratio. When the size of the structure is decreased, this ratio increases considerably and the surface phenomena predominate over the chemistry and physics in the bulk. Therefore, although the reduction in the size of the sensing part and/or the transducer in a sensor are important in order to better miniaturise the devices, nanoscience deals with new phenomena, and new sensor devices are being built that take advantage of these phenomena. New effects appear and play an important role that is often related to quantum mechanics and quantum mechanisms<sup>2</sup>. Consequently, important characteristics and quality parameters of the nanosensors can be improved over the case of classically modelled systems merely reduced in size. For example, sensitivity can be increased due to higher conductivity; lower limits of detection can be reached, lower volume samples can be analysed, cost reductions can be gained etc. In addition, direct detection is being realised and assays are being simplified<sup>3</sup>. To better visualise what nanoscience and nanobiotechnology are concerned with, different sized materials are compared on a logarithmic dimensional scale in *Figure 1.1*.

Within nanomaterials, metal and semiconductor nanoparticles (NPs) are certainly the most studied and applied in electrochemical analysis<sup>4</sup>. Owing to their small size (normally in the range of 1 – 100 nm), NPs exhibit unique chemical, physical and electronic properties that are different from those of bulk materials, and can be used to construct novel and improved sensing devices; in particular, electrochemical sensors and biosensors. Such properties strongly depend on the number and kind of atoms that make up the particle. The properties of the particles generally depend on their size, shape, distribution and stabilizing agents, which are controlled by the preparation conditions<sup>5</sup>. Metal NPs can be prepared by physical and chemical methods. The

physical methods consist of using a low-pressure evaporation of the metal, followed by a controlled condensation in a stream of inert gas. Chemical procedures consist of the chemical reduction of metal ions to metal atoms in the presence of a stabilizer (capping agent such as citrate or thiol) which binds to their surface to impart high stability and rich linking chemistry and provide the desired charge and solubility properties. The latter preparative method is more suitable to obtain small and uniform NPs than the former; moreover, the size and uniformity of the NPs depend on the kind and amount of the reducing agent employed<sup>6</sup>.

Many types of NPs of different sizes and compositions are now available, which facilitate their application in electroanalysis, bringing important advantages: A) their immobilization on electrode surfaces generates a roughened conductive high-surface area interface that enables the sensitive electrochemical detection of molecular and biomolecular analytes; B) NPs act as effective labels for the amplified electrochemical analysis of the respective analytes; C) the conductivity properties of metal NPs enable the design of biomaterial architectures with pre-designed and controlled electrochemical functions.

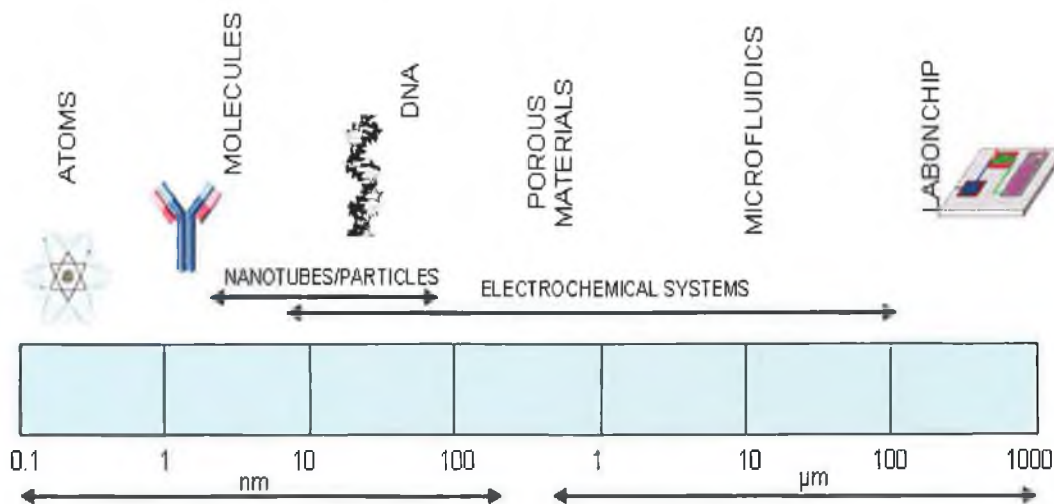


**Figure 1.1. Dimensional scale for biomaterials.**

Electrochemical sensors offer elegant routes for interfacing, at the molecular level, chemical or biological recognition events and electronic signal-transduction processes. In addition, electrochemical devices are uniquely qualified for meeting the size, cost, low-volume, and power requirements of decentralized testing and indicate great promise for a wide range of biomedical<sup>7</sup> or environmental applications<sup>8</sup>.

Nanomaterials in general and NPs in particular can be used in a variety of electrochemical sensing schemes. This review will focus on the application of NPs to three different types of electrochemical sensing devices: a) chemical sensors; b) enzyme-based biosensors and c) immunosensors.

Different kinds of NPs, and sometimes the same kind of NPs of different sizes and compositions can play different roles in these three electrochemical sensing systems in order to achieve enhanced analytical performances.

## 1.2 CHEMICAL SENSORS

A chemical sensor can be defined as a device that provides continuous information about its environment. Ideally, a chemical sensor provides a certain type of response directly related to the quantity of a specific chemical species. All chemical sensors consist of a transducer, which transforms the response into a detectable signal on modern instrumentation, and a chemically selective layer, which isolates the response of the analyte from its immediate environment. Compared to optical, mass and thermal sensors, electrochemical sensors are especially attractive because of their remarkable sensitivity, experimental simplicity and low cost. They have a leading position among the presently available sensors that have reached the commercial stage and which have found a vast range of important applications in the fields of clinical, industrial, environmental and agricultural analyses.

Nanomaterials have been introduced in the development of new kinds of electrochemical sensors with improved performances. NPs in particular have been used and exploited for two main types of actions: 1) catalysis of electrochemical reactions and 2) acting as direct reactant.

### 1.2.1 Catalysis of electrochemical reactions

Many NPs, especially metal NPs have excellent catalytic properties combining, as they do, the intrinsic catalytic properties of the metal with the nanoparticulate properties of high surface area/volume ratio. The introduction of NPs with catalytic properties into electrochemical sensors and biosensors can decrease overpotentials of many analytically important electrochemical reactions, and even realize the reversibility of some redox reactions, which are irreversible at common unmodified electrodes. For instance, a sensitive NO microsensor was developed through the modification of a platinum microelectrode with gold NPs (AuNPs) in which AuNPs catalyze the electrochemical oxidation of NO with an overpotential decrease of about 250 mV<sup>9</sup>. The catalytic oxidation of NO can also be observed at dense AuNPs film modified electrodes<sup>10</sup>. Based on the selective catalysis of NPs, selective electrochemical analysis could be achieved. Ohsaka and co-workers (2003) developed an electrochemical sensor for the selective detection of dopamine in the presence of ascorbic acid, which was based on the catalytic effect of AuNPs on the ascorbic acid oxidation. This resulted in the decrease of the oxidation overpotential of ascorbic acid and the effective separation of the oxidation potentials of ascorbic acid and dopamine, thus allowing the selective electrochemical detection<sup>11</sup>.

Platinum NPs (PtNPs) are another type of NP that exhibit good catalytic properties and have been used in electrochemical analysis. Niwa *et al.* prepared a highly sensitive H<sub>2</sub>O<sub>2</sub> sensor based on the modification of a carbon film electrode with PtNPs. Due to the catalytic oxidation of H<sub>2</sub>O<sub>2</sub> by PtNPs, the modified electrode exhibited a sensitive response to H<sub>2</sub>O<sub>2</sub>, with the oxidation peak potential at this electrode at about 170 mV lower than than at a platinum bulk electrode<sup>12</sup>. Replacing PtNPs with nickel NPs (NiNPs), the same group further developed an electrochemical sensor for sugar determination. It was reported that a graphite-like carbon film electrode containing 0.8% highly dispersed NiNPs had excellent electrocatalytic ability with regard to the electrooxidation of sugars, such as glucose, fructose, sucrose and lactose. Compared with the Ni-bulk electrode, the proposed electrode exhibited a high oxidation current for the detection of sugars at comparatively low applied potentials, and the detection limits obtained were at least one order of magnitude lower<sup>13</sup>. Electrochemical sensors based on the catalytic properties of other metal NPs

have also been reported, such as the application of copper NPs (CuNPs) for amino acid detection<sup>14</sup>.

Some of the non-metal NPs that have special catalytic properties can also be applied in electrochemical analysis systems. For example, a carbon paste electrode doped with copper oxide NPs was developed for the detection of amikacin based on the catalytic properties of the copper oxide NPs, and the oxidation current of amikacin at the prepared electrode was about 40 times higher than that at a bulk copper oxide modified carbon paste electrode<sup>15</sup>. Recently, Torresi *et al.* reported the application of Prussian Blue nanoparticles in electrochemical sensing devices. Prussian Blue nanoparticles with the size of about 5 nm were immobilized onto ITO electrodes through the layer-by-layer technique, and the resulting electrodes exhibited sensitive responses to H<sub>2</sub>O<sub>2</sub> (103.5 mA/mM·cm<sup>2</sup> for the electrode containing 15 bilayers) due to the catalytic reduction of H<sub>2</sub>O<sub>2</sub> by the Prussian Blue NPs<sup>16</sup>.

### 1.2.2 Acting as a reactant

The chemical properties of some NPs are different from those of the bulk materials, and normally the NPs are chemically more active than the related bulk materials due to their high surface energy. For example, bulk MnO<sub>2</sub> is known to catalyze the decomposition of H<sub>2</sub>O<sub>2</sub>, while MnO<sub>2</sub> NPs can react with H<sub>2</sub>O<sub>2</sub> directly<sup>17</sup>. Taking advantage of the active properties of NPs and using these NPs as special reactants, some novel electrochemical analysis systems could be constructed. MnO<sub>2</sub> NPs can also react with ascorbic acid, and a sensitive ion-sensitive field effect transistor (ISFET)-based ascorbic acid sensor was constructed based on this reaction. MnO<sub>2</sub> NPs were simply deposited on the gate of an ISFET, and its reaction with ascorbic acid resulted in the production of hydroxyl ions, which was related to the concentration of ascorbic acid that could be monitored by the ISFET. This ascorbic acid sensor was more stable and sensitive than the enzyme-based ISFET sensor, and it could be easily prepared and renewed<sup>18</sup>. Moreover, the reaction of MnO<sub>2</sub> NPs with ascorbic acid has also been used to eliminate interference in a glucose biosensor. A chitosan film containing MnO<sub>2</sub> NPs was introduced on the surface of an amperometric

glucose biosensor, and the MnO<sub>2</sub> NPs could effectively oxidize ascorbic acid to an electrochemically inactive product before it reached the electrode surface<sup>19</sup>.

The application of the special reactivity of NPs in electrochemical sensors and biosensors has not been extensively studied, and more attention should be paid to this field. Other NPs besides MnO<sub>2</sub> with unique reactive properties can be applied to the development of novel sensor systems. For instance, PbO<sub>2</sub> and TiO<sub>2</sub> NPs have been used recently by Jin *et al.* (2006) to develop a sensor for the catalytic oxidation of organic substances in water for the determination of Chemical Oxygen Demand (COD). This sensor exhibited a wider linear range and a lower limit of detection than conventional methods<sup>20</sup>. Rao *et al.* (2007) prepared and compared three sensors for ammonia detection, based on ZnO, In<sub>2</sub>O<sub>3</sub> and SnO<sub>2</sub> NPs respectively. The highest sensitivity was revealed by the sensor built with ZnO NPs<sup>21</sup>. Special reactive properties have also been found in CeO<sub>2</sub> NPs which can be used to construct novel electrochemical sensors<sup>22</sup>.

### **1.3 ENZYME-BASED BIOSENSORS**

Electrochemical enzyme-based biosensors exploit the extraordinary selectivity and sensitivity of enzymes as a biological recognition element and detect the catalytic biological reaction with the specific substrate/analyte by electrochemical transduction<sup>23</sup>. Metal, oxide, semiconductor and even composite NPs, have been widely used in electrochemical enzyme-based biosensors. Although these NPs play different roles in different electrochemical sensing systems, the basic functions of NPs can be mainly classified as: 1) immobilisation of biomolecules; 2) enhancement of electron transfer; 3) acting as reactants.

#### **1.3.1 Immobilisation of enzymes on electrode surfaces**

Due to their large specific surface area and high surface free energy, NPs can adsorb biomolecules strongly and play an important role in the immobilization of biomolecules in biosensor construction. Generally, the adsorption of biomolecules



directly onto naked surfaces of bulk materials may frequently result in their denaturation and loss of bioactivity. However, the adsorption of such biomolecules onto the surfaces of NPs can retain their bioactivity. Having comparable dimensions, biomolecules conjugated to NPs maintain the natural conformation/structure and hence the functionality.

The functionalisation of NPs with biomolecules in general and with enzyme in this particular context can be obtained through three main mechanisms:

1. Electrostatic adsorption
2. Chemisorption of thiol derivatives
3. Specific affinity interactions

#### *Electrostatic adsorption*

The simple adsorption of biomolecules on NPs has frequently been performed and studied for biomolecules, which range from low-molecular-weight organic substances (e.g. vitamin C) to large protein/enzyme molecules<sup>24,25</sup>. In the case of NPs that are stabilized by anionic ligands such as carboxylic acid derivatives (citrate, tartrate, lipoic acid), the adsorption of positively charged proteins originates from electrostatic interactions<sup>26,27</sup> as illustrated in *Figure 1.2*.



**Figure 1.2. Electrostatic interaction of biomolecules with AuNPs.**

AuNPs and silver NPs (AgNPs) produced by citrate reduction have been functionalized with immunoglobulin G (IgG) molecules at pH values that lie slightly above the isoelectric point of the citrate ligand<sup>28</sup>. This allowed effective binding between the positively charged amino acid side chains of the protein and the negatively charged citrate groups of the colloids. Other examples of protein coating through electrostatic interactions include the direct adsorption of heme-containing redox enzymes at citrate-stabilized AgNPs<sup>29</sup>.

The electrostatic deposition of biomolecules, particularly proteins or enzymes, can also be extended to multilayer-level assemblies<sup>30</sup>. Proteins that are electrostatically attracted to the charged NPs can provide an interface for the further deposition of an oppositely charged polyelectrolyte polymer, which again allows the deposition of a secondary protein layer. Multilayer films of glucosidase<sup>31</sup>, glucose oxidase (GOX)<sup>32</sup>, urease<sup>33</sup> and horseradish peroxidase (HRP)<sup>34</sup> have been assembled on polystyrene NPs by the alternate deposition of the proteins and an oppositely charged synthetic polyelectrolyte as a linker, e.g. poly(diallyldimethylammonium) chloride (positively charged) or poly(sodium 4-styrenesulfonate) (negatively charged). The protein/polymer multilayer shell could be varied from several to hundreds of nanometers in thickness. This strategy permits the preparation of functional films on NPs with a high density of enzyme molecules.

#### *Chemisorption of thiol derivatives*

Chemisorption of proteins on AuNPs can originate from the binding of thiol groups from cysteine residues that exist in the proteins to the Au surface (*Figure 1.3*). If no thiolated residues are available in the native proteins, thiol groups can be incorporated by chemical means; for example, with 2-iminothiolane<sup>35</sup> or through genetic engineering<sup>36</sup>. For example, the immobilisation of endoglucanase enzyme onto AuNPs through the covalent bonds formed between the Au atoms and the cysteine residues of the protein, has been reported<sup>37</sup>.



**Figure 1.3.** Covalent interaction of biomolecules with AuNPs through thiol groups.

Among the NPs used for the immobilization of proteins, AuNPs are probably the most frequently used<sup>38</sup>. In the early 1990s, Crumbliss *et al.* immobilized several kinds of enzyme with AuNPs and further fabricated different enzyme electrodes, and the prepared enzyme electrodes retained enzymatic activity<sup>39</sup>. Chen *et al.* firstly attached AuNPs to gold electrodes modified with cysteamine monolayer, and then successfully

immobilized horseradish peroxidase on these NPs. They also studied the influence of NP size on the performance of the prepared biosensors and NPs with smaller size were found to be more suitable for enzyme immobilization<sup>40</sup>. Many similar studies have been reported for the construction of biosensors based on the immobilization of different proteins with AuNPs, such as horseradish peroxidase<sup>41,42</sup>, microperoxidase-11<sup>43</sup> and tyrosinase<sup>44</sup>. SiO<sub>2</sub> NPs are also excellent matrices for enzyme immobilization due to their good biocompatibility and ease of preparation. Hu *et al.* (2004) immobilized several heme proteins with SiO<sub>2</sub> NPs through the layer-by-layer assembly<sup>45</sup>, and investigated the driving forces for the assembly procedure<sup>46</sup>. Other NPs, such as Pt, Ag, TiO<sub>2</sub>, ZrO<sub>2</sub> NPs and so on can also be used for the immobilization of enzymes.

#### *Specific affinity interactions*

NPs functionalized with groups that provide sites for the binding of biomolecules have been used for the specific attachment of proteins and oligonucleotides. For example, streptavidin (SAv)-functionalized AuNPs have been used for the affinity binding of biotinylated proteins (e.g. immunoglobulins and serum albumins) (*Figure 1.4*) or biotinylated oligonucleotides<sup>47</sup>. Likewise, biotinylated CdSe<sub>core</sub>/CdS<sub>shell</sub> NPs can be bound to SAv<sup>48</sup>.

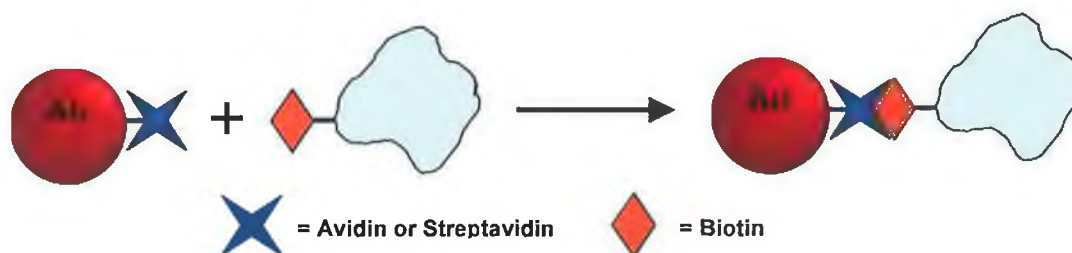


**Figure 1.4. Bioconjugation of AuNPs by the use of bioaffinity interactions upon (strept)avidin –biotin binding.**

However, this kind of interaction, is mainly exploited to attach metal NPs to antibodies and oligonucleotides and used in bioaffinity sensing systems, with the aim of having a sensitive and easily detectable label, rather than for immobilisation of enzymes.

### 1.3.2 Enhancement of electron transfer

The electrical contacting of redox enzymes with electrodes is a key process in the design of enzyme electrodes for bioelectronic applications such as biosensors<sup>49</sup>, or biofuel cell elements<sup>50</sup>. Enzymes usually lack direct electrical communication with electrodes due to the fact that their active centres are surrounded by considerably thick insulating protein shells which therefore block the direct electron transfer. The conductive properties of NPs - mostly metal NPs at nanoscale dimensions - make them suitable for enhancing the electron transfer between the enzyme active centres and electrodes, thus acting as “mediators” or “electrical wires”.

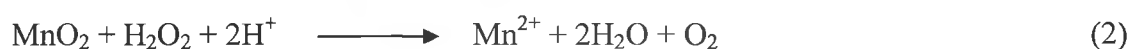
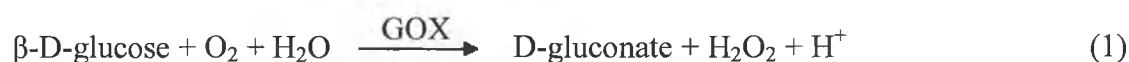
Biocatalytic electrodes for biosensor applications have been prepared by the co-deposition of redox enzymes/proteins and AuNPs on electrode supports<sup>51,52</sup>. In one example, direct electron transfer between hemoglobin and a glassy carbon electrode was facilitated by lipid-protected AuNPs. The biocatalytic electrodes were reported to operate without electron transfer mediators. However, the random and non-optimized positioning of the redox proteins on the conductive NPs did not allow efficient electron transfer between the active sites of the enzyme and the electrode support. Highly efficient electrical contacting of the redox enzyme glucose oxidase (GOX) through a single AuNP was demonstrated by Willner *et al.* in 2003. They reconstituted the apo-flavoenzyme, apo-glucose oxidase (apo-GOX), on a 1.4 nm AuNP that was functionalized with *N*<sup>6</sup>-(2-aminoethyl)flavin adenine dinucleotide (FAD cofactor, amine derivative). The resulting conjugate was assembled on a thiolated monolayer by using different dithiols as linkers. Alternatively, the FAD-functionalized AuNP could be assembled on a thiolated monolayer associated with an electrode, and apo-GOX was subsequently reconstituted on the functional NPs. The enzyme electrodes prepared by these two routes revealed similar surface coverages of about  $1 \times 10^{-12}$  mol/cm<sup>2</sup> of the protein. The NP-reconstituted glucose oxidase layer was found to be electrically contacted with the electrode without any additional mediators, and the enzyme assembly stimulated the bioelectrocatalyzed oxidation of glucose. The resulting NP-reconstituted enzyme electrodes revealed unprecedented electrical communication efficiency with the electrode showing an electron-transfer turnover rate of about 5000 s<sup>-1</sup>; nearly seven times faster than that between GOX and its natural substrate, oxygen<sup>53</sup>.

The electron transfer between other redox proteins and electrodes has also been revealed with the help of AuNPs. For example, Wang *et al.* self assembled AuNPs onto a three-dimensional silica gel network-modified gold electrode, and obtained the direct electrochemistry of cytochrome c. These AuNPs acted as a bridge to transfer electrons between protein and electrode<sup>54</sup>. AgNPs, as well as AuNPs, have good conductivity, and they can also be used to enhance the electron transfer between enzymes and electrodes. Li *et al.* assembled AgNPs onto pyrolytic graphite electrodes, and then immobilized cytochrome c on these NPs. It was reported that AgNPs act as the electrical bridge that “wires” the electron transfer between cytochrome c and the electrode, and the electron transfer rate constant was about  $15.8 \text{ s}^{-1}$ <sup>55</sup>. Some non-metal NPs, such as oxide NPs and semiconductor NPs, can also enhance the electron transfer between enzymes and electrodes in certain systems. For instance, horseradish peroxidase (HRP) was mixed with  $\text{TiO}_2$  NPs and immobilized onto pyrolytic graphite electrodes, which resulted in direct electron transfer<sup>56</sup>. Hemoglobin immobilized with  $\text{ZrO}_2$  NPs also exhibited direct electrochemistry at pyrolytic graphite electrodes and could be used for constructing mediator-free biosensors<sup>57</sup>. Other oxide NPs such as  $\text{Fe}_3\text{O}_4$ <sup>58</sup> and  $\text{MnO}_2$ <sup>59</sup> NPs have also been used to immobilize enzymes and enhance their direct electrochemistry. Recently, the application of semiconductor NPs for the enhancement of electron transfer between redox proteins and electrode surfaces has been reported. Hemoglobin and CdS NPs were mixed and immobilized onto pyrolytic graphite electrodes, and the immobilized hemoglobin exhibited direct electrochemistry. In fact, the effective enhancement of electron transfer was dependent not only on the conductivity of NPs, but also the arrangement between NPs and biomolecules<sup>60</sup>. It is believed that creating defined and ordered arrangements of NPs using nanotechnology is a promising approach to the construction of biosensors with greatly enhanced electron transfer properties.

### **1.3.3 Nanoparticles acting as a reactant in combination with enzymes**

It has already been discussed in section 1.2.2 that some metal NPs exhibit special chemical properties that are not present in the bulk material. The ability to directly react with  $\text{H}_2\text{O}_2$  for  $\text{MnO}_2$  NPs could be exploited, for example, in conjunction with an enzyme for a biosensing device development. Chen *et al.* developed two types of

biosensors for glucose and lactate detection. Glucose oxidase and MnO<sub>2</sub> NPs were co-immobilized on the gate of an ion-selective field effect transistor (ISFET), and the resulting glucose biosensor showed a significant pH increase at the selective membrane with increasing glucose concentration, which was essentially different from the pH changes of conventional ISFET-based glucose biosensors<sup>61</sup>. Generally, the response of an ISFET-based glucose biosensor is based on local pH changes in biomembranes resulting from the formation of gluconic acid, as in reaction (1), while the driving force for pH change in the proposed biosensor was due to the special reaction of MnO<sub>2</sub> NPs with H<sub>2</sub>O<sub>2</sub> as in reaction (2).



Thus the total reaction in the proposed glucose biosensor is given in reaction (3):



Obviously, one hydrogen ion is consumed and no oxygen is needed in (3), which results in the novel response mechanism and extended dynamic range of the MnO<sub>2</sub> NP-based glucose biosensor. Making use of a similar response mechanism, a sensitive biosensor for lactate was further developed based on layer-by-layer assembly of MnO<sub>2</sub> NPs and lactate oxidase on an ISFET, and its response to lactate was about 50 times higher than that of the biosensor without MnO<sub>2</sub> NPs<sup>62</sup>.

#### 1.4 IMMUNOSENSORS

Electrochemical immunosensors exploit the extraordinary selectivity and sensitivity of antibodies as a biological recognition element and detect the immunological interaction with specific antigens by electrochemical transduction. Today, new biological, chemical and genetic methods show the potential of producing antibodies against any chemical substance; so theoretically an immunosensing device can be built to specifically determine any analyte. Electrochemical techniques, which are highly sensitive and applicable by means of very simple instruments, have also proved

to be very suitable for developing disposable, low cost biosensors. The high selectivity of the antibodies combined with the simplicity of the electrochemical transduction, determines the increasing use of electrochemical immunosensors in clinical, food and environmental analysis<sup>63</sup>.

#### **1.4.1 Principles of immunoassays**

An immunoassay is a technique that uses the binding of antibodies to antigens to identify and measure certain substances. Direct measurements of the antibody-antigen interaction during the binding event are very difficult to perform, due to the fact that this interaction results only in a very small and localised conformational and electronic change in the structure of the antibody. Indirect measurements, therefore, represent the most widely used methodology for immunoassays and consist of labelling either the antigen or the antibody with a tracer which can be more easily detected. A tracer could be, among others, a fluorescent molecule (fluoroimmunoassay), a radioisotope (radio-immunoassay) or an enzyme (enzyme-linked immunosorbent assay) (ELISA). Using this labelled species a very sensitive and accurate evaluation of the immunointeraction can be performed. Enzymes are the most widely used species for labelling, especially horseradish peroxidase (HRP)<sup>64</sup>, glucose oxidase (GOX)<sup>65</sup> and alkaline phosphatase (AP)<sup>66</sup> due to their low cost, high turnover rates and ease of conjugation. Adding a substrate, the enzyme-labelled component, participating in the immunointeraction, forms a detectable product.

There are two different categories of immunoassays: heterogeneous and homogeneous. Heterogeneous assays require the separation of the antibody-antigen-label complex from the unbound immunoreactants before the measurement. That can be performed immobilizing either the antibody or the antigen on a solid support (plastic plate, particle etc.) and then, after the interaction, washing away the reagents in excess or not bound.

A further two subdivisions exist for the heterogeneous assays depending on the technique adopted for the detection: competitive and non-competitive (or sandwich).

In competitive formats, unlabelled analyte (usually antigen) in the test sample is measured by its ability to compete with a labelled antigen in the immunoassay. The unlabelled antigen prevents the binding of the labelled one because the antibody's

specific site is already occupied. In this situation, the higher the concentration of the unlabelled antigen in solution (test sample), the lower is the response due to a lower amount of labelled antigen bound (*Figure 1.5a*)<sup>67</sup>.

Non-competitive assay formats generally provide the highest level of assay sensitivity and specificity and are applied to the measurement of critical analytes. This format is referred to as a “sandwich” assay because analyte is bound (sandwiched) between two highly specific antibody reagents. A primary antibody is immobilised on a solid support. Then the antigen binds specifically to available sites. Finally, a secondary labelled antibody binds the same antigen on a different epitope. In this case the signal is due to the secondary labelled antibody and it is proportional to the amount of antigen already bound (*Figure 1.5b*)<sup>68</sup>.

Heterogeneous immunoassays (competitive or non-competitive) involve the use of several processes of washing in order to remove unbound materials or those interacting non-specifically with the antibody. The presence of these additional steps increases the complexity of the assay, lengthens the analysis time and often requires skilled operators. This represents the main drawback of the heterogeneous assays which are, however, the most commonly used.

Homogeneous assays are theoretically simpler because they do not require the separation of unbound reagents from the bound immunocomplexes. They consist of a competition format where an antigen and a labelled antigen compete for binding to the antibody free in solution. The antibody-antigen interaction causes a change to the tracer properties which results in an alteration of the response. For example, an enzyme label reduces the activity after the binding event, due to a change in conformation or to a steric hindrance and hence resulting in a lower response. Also the chemiluminescence of a molecular label could change with the antibody-antigen interaction, resulting in a lower or higher energy emission and therefore a different response. In this scenario, the higher the concentration of free antigen, the bigger is the signal alteration (*Figure 1.5c*)<sup>69,70</sup>. It requires only one step with no washing processes, but high background signals and the possibility of interferences from other matrix constituents represent the drawbacks which limit the applicability of this technique.



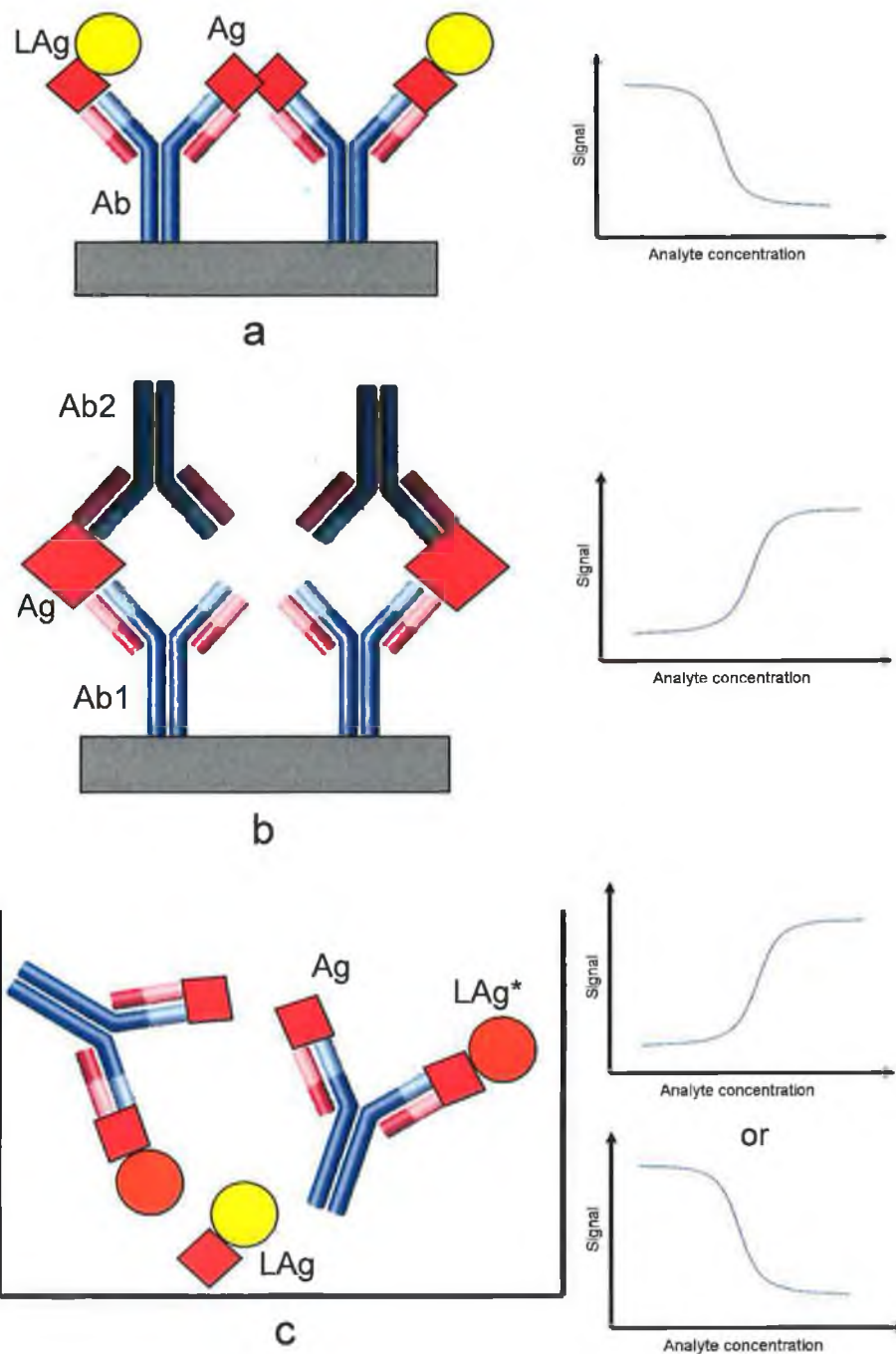


**Figure 1.5.** Immunoassay techniques. (a) The heterogeneous competition assay. An antibody (Ab) is bound to the solid phase and the antigen (Ag) introduced with a labelled antigen (LAg) which compete for the binding sites. More free antigen results in less labelled antigen being bound and so a lower signal is produced. (b) The heterogeneous sandwich assay. Here, an antibody (Ab1) is immobilized to a solid substrate, the antigen (Ag) is introduced and a secondary labelled antibody (Ab2) is introduced. The presence of the labelled antibody is detected and is proportional to the antigen concentration. (c) The homogeneous competition assay. Here, antigen (Ag) and a labelled antigen (LAg) compete for binding to the antibody free in solution (Ab). When the labelled antigen binds, the activity of the label changes (LAg\*), resulting in an alteration of the response. High levels of free antigen result in high levels of signal alteration.

NPs of different sizes and compositions can be adopted and integrated into the development of novel electrochemical immunosensors and immunoassays in order to achieve higher sensitivity, better stability and enhanced analytical performances. Two main uses can be made with NPs in developing immunosensing systems: 1) improve the immobilisation of antibodies on electrode surfaces and 2) utilisation of NPs as sensitive labels.

#### **1.4.2 Nanoparticle-modified electrode surfaces for the immobilisation of antibodies**

AuNPs are certainly the most exploited to enhance the immobilization of antibodies or antigens in proximity to the electrode surface with, in most of the cases, improvements of the stability. One approach consists of assembling on the electrode surface, a monolayer of AuNPs where antibodies can be electrostatically attached without loss of activity.

An amperometric immunosensor for *Schistosoma japonicum* antigen (SjAg) assay based on nano-size particulate gold (nano-Au) monolayer as a sensing platform was proposed by Lei *et al.* in 2003. The nano-Au monolayer was obtained through a chitosan-entrapped carbon paste electrode (CCPE). The high affinity of chitosan for nano-Au associated with its amino groups facilitated the formation of a nano-Au monolayer on the surface of the CCPE. A sequential competitive immunoassay format was performed on the CCPE supported nano-Au monolayer using *S. japonicum* antibody (SjAb) and SjAg as a model system. The assay comprised first loading of SjAb on the nano-Au monolayer, then blocking with a bovine serum solution (BSA), followed by a competitive incubation in the buffer containing the SjAg (analyte) and SjAg labelled with HRP and finally the amperometric detection with hydroquinone as an enzymatic substrate. The dynamic concentration range for SjAg assay was 0.11–22.4 µg/ml with a detection limit of 0.06 µg/ml. The feasibility of regenerating the nano-Au monolayer for consecutive assays was demonstrated by a simple chemical treatment after each determination. The simple construction of the nano-Au monolayer and the improved sensitivity were main features of the proposed immunosensing method<sup>71</sup>.

A similar approach was followed by Li *et al.* (2005), who have recently developed a reusable capacitive immunosensor based on 1,6-hexanedithiol (HDT) and colloidal gold layers. The organic monolayer film was first formed by the spontaneous assembly of HDT from solution onto a gold electrode. When these thiol-rich surfaces were exposed to gold colloid, the sulphides formed strong bonds with AuNPs, anchoring the clusters to the electrode substrate. After the assembly of the AuNPs layer, the antibody could be immobilized through electrostatic adsorption between nano-Au and the antibody proteins. After use, the formed immunocomplex layer could be rinsed out, via a saline solution with extreme pH<sup>72</sup>. The use of AuNPs in these types of immunosensor developments has certainly brought advantages with respect to classical immunoassays employing covalent immobilization of the antibodies. However, the need of regenerating the sensing surface after each measurement still represents the main drawback for a practical analytical application of this type of immunosensor. The assay procedure consists of complex operations which require specialised operators.

Another approach was based on using membranes<sup>73,74</sup> or sol-gel composites<sup>75,76</sup> to entrap AuNPs and biomaterials. In all these systems, the presence of AuNPs improved the conductivity of the composite and enhanced the stability and sensitivity of the sensor due to a higher attachment surface availability for the biomolecules. Silica NPs do not possess conductive properties. However, due to the porosity of the material, they exhibit a very high surface area and therefore they are usually used to immobilize biomolecules. A higher number of biological molecules can be attached with a very stable interaction resulting in enhanced sensor performance<sup>77</sup>.

### **1.4.3 Nanoparticles as labels for immunosensing**

The unique optical, photophysical, electronic, and catalytic properties of metal and semiconductor NPs offer great promise as labels for biorecognition and biosensing processes. Biomolecules labelled with NPs can retain their bioactivity and interact with their counterparts, and based on the electrochemical detection of those NPs the amount or concentration of analytes can be determined. Several electrochemical protocols offer great promise for ultrasensitive NP-based transduction of biological

interactions. Stripping voltammetry has been particularly useful for detecting metal-NP tags, owing to its 'built-in' preconcentration (electrodeposition) step that leads to a remarkable sensitivity<sup>78</sup>.

One of the first electroanalytical procedures adopted in NP-based immunosensors, consisted of the dissolution of the NP labels – mostly metal and semiconductor NPs – and the measurement of the dissolved ions with stripping voltammetry, which already represents a very powerful electrochemical technique for trace metal analysis<sup>79</sup>. Metal NP labels can be used in both immunosensors and DNA sensors (genosensors), and AuNPs are the most frequently used among all the metal NP labels available.

For example, Limoges *et al.* (2000) reported a sensitive electrochemical immunoassay for goat immunoglobulin G (IgG) based on a AuNP label. The primary donkey anti-goat IgG was immobilized on a microwell surface and interacted with the goat IgG to be determined, and then AuNP-labelled donkey anti-goat IgG was added to the conjugate. The immunocomplex was treated with acidic bromine-bromide solution resulting in the oxidative dissolution of the AuNPs. The solubilised gold ions were then electrochemically reduced and accumulated on the electrode and subsequently detected by anodic stripping voltammetry using carbon-based SPEs. The combination of the sensitive detection of Au ions with anodic stripping voltammetry and the release of a large number of Au ions upon the dissolution of AuNPs associated with a single recognition event provides an amplification path that allowed the detection of the goat IgG at a concentration of 3 pM<sup>80</sup>.

Alternatively to AuNPs, inorganic nanocrystals have been used with the advantage of having an electrodiverse population of electrical tags as needed for designing electronic coding. A multi-target electronic detection of proteins was demonstrated by Liu *et al.* (2004) using different inorganic-nanocrystal tracers. Three encoding NPs (zinc sulphide, cadmium sulphide and lead sulphide) were used to differentiate the signals of three protein targets in connection with a sandwich immunoassay and stripping voltammetry of the corresponding metals (*Figure 1.6*). Each binding thus yielded a distinct voltammetric peak, whose position and size reflected the identity and level of the corresponding antigen, respectively<sup>81</sup>.

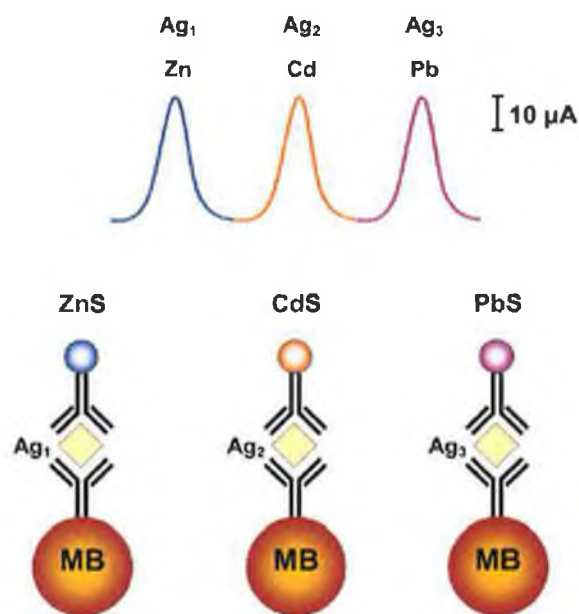


**Figure 1.6.** Multi-antigen immunoassay based on different inorganic nanocrystal tracers. Each binding yields a distinct voltammetric peak, whose position and amplitude reflects the identity and concentration of the corresponding antigen, respectively.

Libraries of electrical codes have been created by encapsulating different predetermined levels of multiple inorganic nanocrystals into polymeric carrier beads or depositing various metal tracers onto the pores of a host membrane. The resulting voltammetric signatures reflect the predetermined proportions of the corresponding metals in such “identification” nanomaterials<sup>82</sup>.

Since the sensitivity of such electrical (stripping-based) bioassays depends on the size of the metallic tag, a dramatic amplification of the signals is expected using larger tracers. For example, a substantial sensitivity enhancement can be achieved by using the metal-nanosphere tags as catalytic labels for subsequent enlargement and further amplification. A catalytic enlargement of a AuNP tracer was achieved by the precipitation of metal gold promoted by the NP itself<sup>83</sup> or by the precipitation of metal silver induced by hydroquinone<sup>84</sup>. Combining such enlargement of the metal-particle tracers with stripping voltammetry, paved the way to sub-picomolar detection limits. A triple-amplification bioassay, using polymeric spheres (loaded with numerous AuNP tags) has also been demonstrated<sup>85</sup>. Such an enlargement of numerous gold-nanoparticle tags (on a supporting sphere carrier) represents the fourth generation of amplification (*Figure 1.7*), starting with the early use of single AuNP tags.

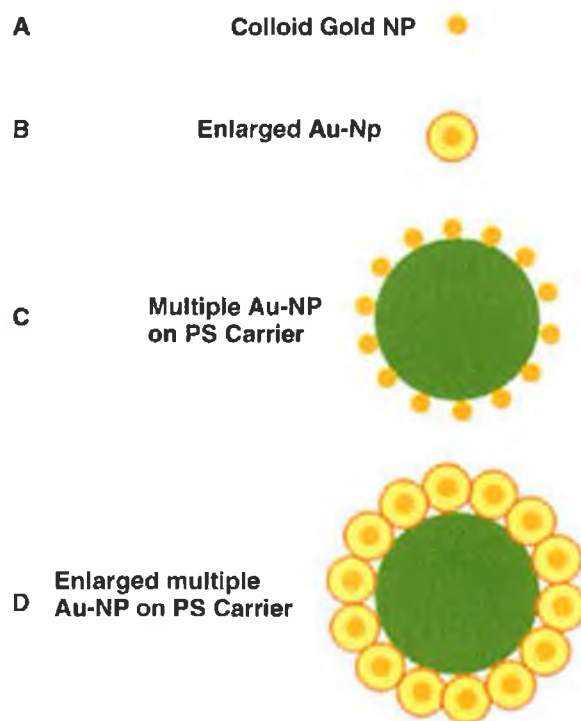


**Figure 1.7. Generations of amplification platforms for bioelectronic detection based on AuNP tracers: A) A single NP tag; B) catalytic enlargement of the NP tag; C) polymer carrier bead loaded with numerous AuNP tags; D) catalytic enlargement of multiple tags on the carrier bead.**

The use of metal NP labels coupled with electroanalytical stripping analysis has brought several advantages for both DNA analysis and immunoassays. However, the need to dissolve the metallic labels by means of acidic bromine-bromide solution or concentrated acidic solution, represents a distinct disadvantage. These solutions are toxic, dangerous and difficult to handle and hence limit the use of these systems.

An improvement in this regard was achieved with the introduction of solid-state measurements which were demonstrated by Wang *et al.* (2002) for the detection of DNA hybridisation. Such bioassays involved the hybridization of a target oligonucleotide to probe-coated magnetic spheres, followed by the binding of the streptavidin-coated AuNPs to the captured target. After the catalytic silver precipitation on the Au-particle tags, a magnetic “collection” of the DNA-linked particle assembly was achieved by means of an external magnet positioned under the screen-printed electrode. Using a constant-current chronopotentiometric stripping analysis of the metallic silver adsorbed on the surface, a limit of detection of 150

pg/ml was estimated<sup>86</sup>. The use of an external magnet to “collect” the particles onto the electrode surface could affect the reproducibility of the method considering that the electrochemical response depends entirely on the amount of Ag touching the electrode.

The catalytic features of metal NPs that enable the electroless deposition of metals on the NP clusters allows the enlargement of the particles to conductive interparticle-connected entities. The formation of conductive domains as a result of biorecognition events provides an alternative path for the electrical transduction of biorecognition events. This was exemplified by the design of a miniaturized immunosensor based on AuNPs and their catalytic properties (*Figure 1.8*). Latex particles which were stabilized by an anionic protective layer were attracted to a gap between micron-sized Au electrodes upon the application of a non-uniform alternating electric field between the electrodes (dielectrophoresis). Removal of the protective layer from the latex particles by an oppositely charged polyelectrolyte resulted in the aggregation of the latex particles and their fixation in the gap domain. Adsorption of protein A on the latex surface yielded a sensing interface for the specific association of the human immunoglobulin (IgG) antigen. The association of human IgG on the surface was probed by the binding of the secondary AuNP-labelled anti-human IgG antibodies to the surface, followed by the catalytic deposition of a layer of Ag on the AuNPs. The Ag layer bridged the gap between the two microelectrodes to result in a conductive “wire”. Typical resistances between the microelectrodes were 50-70  $\Omega$ , whereas control experiments conducted without the specific catalytic enlargement of the domain by the Au NP-antibody conjugate yielded resistances  $>10^3 \Omega$ . The method enabled the analysis of human IgG with a detection limit of about 0.2 pM<sup>87</sup>.

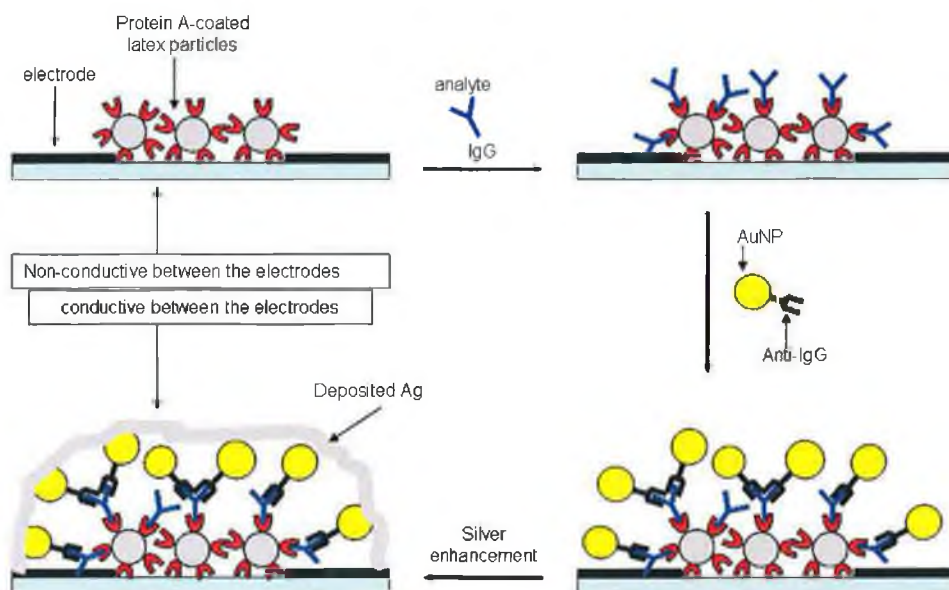


**Figure 1.8.** Immunosensing at microsized Au electrodes by the change of conductivity between the Au strips upon the binding of AuNPs and the deposition of silver.

Normally, electrochemical immunosensors or immunoassays exploiting NP labels are based on the final detection of the NP itself. Therefore, the preparation and application of “special” NP labels is of great importance. Composite NPs with special components, for example, a core-shell NP with a shell suitable for labelling and a core containing special materials that can be sensitively detected with electrochemical methods, may play an important role in developing novel ultra-sensitive methods.

## 1.5 CONCLUSIONS

This review has summarized the different roles that NPs can play in the development of novel electrochemical sensors and biosensors. Due to the unique and attractive properties of NPs, these novel sensing systems exhibit attractive and promising analytical performances. The special physical or chemical properties of NPs can be exploited, for example, to improve the stability of biosensors, being excellent substrates for biomolecule immobilisation, ensuring the retention of their biofunctionality. NP catalytic properties can be used to develop electrochemical sensors and biosensors with enhanced sensitivity and selectivity. Enzyme-based electrochemical biosensors could achieve impressive signal amplifications making use



of metal NPs to enhance the electron-transfer between the enzyme and the electrode. Acting as a sensitive detection label represents the most widely used role played by the NPs in immunosensing systems. Coupling metal NP labels with very sensitive electrochemical techniques, extremely low limits of detection can be reached. In this scenario, metal NPs can also represent the starting point for a catalytic metal deposition enlargement which causes a signal amplification reaching, sub-picomolar detection limits. Different metal NPs have also been applied in the same immunosensing platform to perform multi-target analysis.

In addition to the NPs seen and discussed in this review, a new kind of nanoparticulate material is finding increasing application in electrochemical sensor and biosensor platforms. It is represented by nanodimensional conducting polymers which are known to exhibit unique properties such as greater conductivity and more rapid electrochemical switching speeds<sup>88</sup>. Moulton *et al.* have synthesized a type of conducting polymer nanoparticle by a micellar emulsion chemical polymerization of polyaniline (PANI), using dodecylbenzenesulfonic acid (DBSA) as the micelle and dopant<sup>89</sup>. Modification of electrodes were achieved from this nanodispersion by both electrochemical<sup>90</sup> and casting methods<sup>91</sup> resulting in a nanostructured film which permitted the uniform adsorption of proteins. These novel conducting polymer NPs present also a great Processability. In fact, they can be coupled to inkjet printing technology to easily pattern this material on electrode surfaces for a practical fabrication of sensing devices. A more detailed discussion on this novel nanoparticulate conducting polymer features, will be presented in Chapter 2 of this thesis.

The unique range of properties imparted by nanoparticles and the nanoscale dimensions of the active sensing elements holds great promise for the development of a new generation of sensing devices, with improvements in analytical performance, device production, cost and applicability in a range of applications.

## 1.6 REFERENCES

- 1 J. Riu, A. Maroto, F.X. Rius. Nanosensors in environmental analysis. *Talanta*, **69**, (2006), 288-301.
- 2 C. Jianrong, M. Yuqing, H. Nongyue, W. Xiaohua, L. Sijiao. Nanotechnology and biosensors. *Biotechnology Advances*, **22**, (2004), 505-518.
- 3 A. Vaseashta, D. Dimova-Malinovska. Nanostructured and nanoscale devices, sensors and detectors. *Science and Technology of Advanced Materials*, **6**, (2005), 312-318.
- 4 S.G. Penn, L. He, M.J. Natan. Nanoparticles for bioanalysis. *Current opinion in chemical biology*, **7**, (2003), 609-615.
- 5 H. Bonnemann, F.J.M. Richards. Nanoscopic metal particles - synthetic methods and potential applications. *European Journal of Inorganic Chemistry*, **0**, 2455-2480.
- 6 C.M. Niemeyer. Nanoparticles, proteins, and nucleic acids: biotechnology meets materials science. *Angewandte Chemie International Edition*, **40**, (2001), 4128-4158.
- 7 J. Wang. Portable electrochemical systems. *Trends in Analytical Chemistry*, **21**, (2002), 226-232.
- 8 J. Wang. Real-time electrochemical monitoring: toward green analytical chemistry. *Accounts of Chemical Research*, **35**, (2002), 811-817.
- 9 M. Zhu, M. Liu, G. Shi, F. Xu, X. Ye, J. Chen, L. Jin, J. Jin. Novel nitric oxide microsensor and its application to the study of smooth muscle cells. *Analytica Chimica Acta*, **455**, (2002), 199-206.
- 10 A.M. Yu, Z.J. Liang, J.H. Cho, F. Caruso. Nanostructured electrochemical sensor based on dense gold nanoparticle films. *Nano Letters*, **3**, (2003), 1203-1207.
- 11 C.R. Raj, T. Okajima, T. Ohsaka. Gold nanoparticle arrays for the voltammetric sensing of dopamine. *Journal of Electroanalytical Chemistry*, **543**, (2003), 127-133.
- 12 T. You, O. Niwa, M. Tomita, S. Hirono. Characterization of platinum nanoparticle-embedded carbon film electrode and its detection of hydrogen peroxide. *Analytical Chemistry*, **75**, (2003), 2080-2085.
- 13 T.Y. You, O. Niwa, Z.L. Chen, K. Hayashi, M. Tomita, S. Hirono. An amperometric detector formed of highly dispersed Ni nanoparticles embedded in a graphite-like carbon film electrode for sugar determination. *Analytical Chemistry*, **75**, (2003), 5191-5196.

- 
- 14 J.M. Zen, C.T. Hsu, A.S. Kumar, H.J. Lyuu, K.Y. Lin. Amino acid analysis using disposable copper nanoparticle plated electrodes. *Analyst*, **129**, (2004), 841-845.
  - 15 J.Z. Xu, J.J. Zhu, H. Wang, H.Y. Chen. Nano-sized copper oxide modified carbon paste electrodes as an amperometric sensor for amikacin. *Analytical Letters*, **36**, (2003), 2723-2733.
  - 16 P.A. Fiorito, V.R. Goncales, E.A. Ponzio, S.I.C. de Torresi. Synthesis, characterization and immobilization of Prussian blue nanoparticles. A potential tool for biosensing devices. *Chemical Communications*, **3**, (2005), 366-368.
  - 17 X.L. Luo, J.J. Xu, W. Zhao, H.Y. Chen. A novel glucose ENFET based on the special reactivity of MnO<sub>2</sub> nanoparticles. *Biosensors and Bioelectronics*, **19**, (2004), 1295-1300.
  - 18 X.L. Luo, J.J. Xu, W. Zhao, H.Y. Chen. Ascorbic acid sensor based on ion-sensitive field-effect transistor modified with MnO<sub>2</sub> nanoparticles. *Analytica Chimica Acta*, **512**, (2004), 57-61.
  - 19 J.J. Xu, X.L. Luo, Y. Du, H.Y. Chen. Application of MnO<sub>2</sub> nanoparticles as an eliminator of ascorbate interference to amperometric glucose biosensors. *Electrochemistry Communications*, **6**, (2004), 1169-1173.
  - 20 L. Jiaqing, Z. Lei, L. Luoping, S. Guoyue, X. Yuezhong, J. Litong. Photoelectro-synergistic catalysis at Ti/TiO<sub>2</sub>/PbO<sub>2</sub> electrode and its application on determination of chemical oxygen demand. *Electroanalysis*, **18**, (2006), 2251-2256.
  - 21 C.S. Rout, M. Hegde, A. Govindaraj, C.N.R. Raol. Ammonia sensors based on metal oxide nanostructures. *Nanotechnology*, **18**, (2007), 205504-205513.
  - 22 Y. Qing, G. Qi, Z. Xin-Rong, X. Bo-Qing. Cataluminescence and catalytic reactions of ethanol oxidation over nanosized Ce<sub>1-x</sub>Zr<sub>x</sub>O<sub>2</sub> (0 ≤ x ≤ 1) catalysts *Catalysis Communications*, **7**, (2006), 589-592.
  - 23 D.R. Thévenot, K. Toth, R.A. Durst, G.S. Wilson. Electrochemical biosensors: recommended definitions and classification. *Biosensors and Bioelectronics*, **16**, (2001), 121-131.
  - 24 J.B. Broderick, M.J. Natan, T.V. O'Halloran, R.P. Van Duyne. Evidence for retention of biological activity of a non-heme iron enzyme adsorbed on a silver colloid: a surface-enhanced Resonance Raman Scattering study. *Biochemistry*, **32**, (1993), 13771-13776.
  - 25 C. Yongli, Z. Xiufang, G. Yandao, Z. Nanming, Z. Tingying, S. Xinqi. Conformational changes of fibrinogen adsorption onto hydroxyapatite and titanium oxide nanoparticles. *Journal of Colloid and Interface Science*, **214**, (1999), 38-45.

- 
- 26 B.N. Rospendowski, K. Kelly, C.R. Wolf, W.E. Smith. Surface-enhanced Resonance Raman Scattering from cytochromes P-450 adsorbed on citrate-reduced silver sols. *Journal of the American Chemical Society*, **113**, (1991), 1217-1225.
- 27 H. Mattoussi, J.M. Mauro, E.R. Goldman, G.P. Anderson, V.C. Sundar, F.V. Mikulec, M.G. Bawendi. Self-assembly of CdSe-ZnS Quantum dot bioconjugates using an engineered recombinant protein. *Journal of the American Chemical Society*, **122**, (2000), 12142-12150.
- 28 W. Shenton, S.A. Davis, S. Mann. Directed self-assembly of Nanoparticles into macroscopic materials using antibody-antigen recognition. *Advanced Materials*, **11**, (1999), 449-452.
- 29 I.D.G. MacDonald, W.E. Smith. Orientation of cytochrome *c* adsorbed on a citrate-reduced silver colloid surface. *Langmuir*, **12**, (1996), 706-713.
- 30 F. Caruso. Nanoengineering of particle surfaces advanced materials. *Advanced Materials*, **13**, (2001), 11-22.
- 31 F. Caruso, H. Fiedler, K. Haage. Assembly of  $\beta$ -glucosidase multilayers on spherical colloidal particles and their use as active catalysts. *Colloids and Surfaces A: Physicochemical and Engineering Aspects*, **169**, (2000), 287-293.
- 32 C. Schtler, F. Caruso. Preparation of enzyme multilayers on colloids for biocatalysis. *Macromolecular Rapid Communications*, **21**, (2000), 750-753.
- 33 Y. Lvov, F. Caruso. Biocolloids with ordered urease multilayer shells as enzymatic reactors. *Analytical Chemistry*, **73**, (2001), 4212-4217.
- 34 F. Caruso, C. Schtler. Enzyme multilayers on colloid particles: assembly, stability, and enzymatic activity. *Langmuir*, **16**, (2000), 9595-9603.
- 35 E. Droz, M. Tadorelli, P. Descouts, T.N.C. Wells, R.C. Werlen. Covalent immobilization of immunoglobulins G and Fab fragments on gold substrates for scanning force microscopy imaging in liquids. *Journal of Vacuum Science & Technology B*, **14**, (1996), 1422-1426.
- 36 S. Kanno, Y. Yanagida, T. Haruyama, E. Kobatake, M. Aizawa. Assembling of engineered IgG-binding protein on gold surface for highly oriented antibody immobilization. *Journal of Biotechnology*, **76**, (2000), 207-214.
- 37 A. Gole, S. Vyas, S. Phadtare, A. Lachke, M. Sastry. Studies on the formation of bioconjugate of endoglucanase with colloidal gold. *Colloids and Surfaces B: Biointerfaces*, **25**, (2002), 129-138.
- 38 S.Q. Liu, D. Leech, H.X. Ju. Application of colloidal gold in protein immobilization, electron transfer, and biosensing. *Analytical Letters*, **36**, (2003), 1-19.

- 
- 39 A.L. Crumbliss, S.C. Perine, J. Stonehuerner, K.R. Tubergen, J. Zhao, R.W. Henkens. Colloidal gold as a biocompatible immobilization matrix suitable for the fabrication of enzyme electrodes by electrodeposition. *Biotechnology and Bioengineering*, **40**, (1992), 483-490.
- 40 Y. Xiao, H.X. Ju, H.Y. Chen. Hydrogen peroxide sensor based on horseradish peroxidase-labeled Au colloids immobilized on gold electrode surface by cysteamine monolayer. *Analytica Chimica Acta*, **391**, (1999), 73-82.
- 41 J.B. Jia, B.Q. Wang, A.G. Wu, G.J. Cheng, Z. Li, S.J. Dong. A method to construct a third-generation horseradish peroxidase biosensor: self-assembling gold nanoparticles to three-dimensional sol-gel network. *Analytical Chemistry*, **74**, (2002), 2217-2223.
- 42 X.L. Luo, J.J. Xu, Q. Zhang, G.J. Yang, H.Y. Chen. Electrochemically deposited chitosan hydrogel for horseradish peroxidase immobilization through gold nanoparticles self-assembly. *Biosensors and Bioelectronics*, **21**, (2005), 190-196.
- 43 F. Patolsky, T. Gabriel, I. Willner. Controlled electrocatalysis by microperoxidase-11 and Au-nanoparticle superstructures on conductive supports. *Journal of Electroanalytical Chemistry*, **479**, (1999), 69-73.
- 44 Z.M. Liu, H. Wang, Y. Yang, H.F. Yang, S.Q. Hu, G.L. Shen, R.Q. Yu. Amperometric tyrosinase biosensor using enzyme-labeled Au colloids immobilized on cystamine/chitosan modified gold surface. *Analytical Letters*, **37**, (2004), 1079-1091.
- 45 P.L. He, N.F. Hu. Electrocatalytic properties of heme proteins in layer-by-layer films assembled with SiO<sub>2</sub> nanoparticles. *Electroanalysis*, **16**, (2004), 1122-1131.
- 46 P.L. He, N.F. Hu, J.F. Rusling. Driving forces for layer-by-layer self-assembly of films of SiO<sub>2</sub> nanoparticles and heme proteins. *Langmuir*, **20**, (2004), 722-729.
- 47 J.E. Gestwicki, L.E. Strong, L.L. Kisseling. Visualization of single multivalent receptor-ligand complexes by Transmission Electron Microscopy. *Angewandte Chemie*, **112**, (2000), 4741-4744.
- 48 M. Bruchez Jr., M. Moronne, P. Gin, S. Weiss, A.P. Alivisatos. Semiconductor nanocrystals as fluorescent biological labels. *Science*, **281**, (1998), 2013-2015.
- 49 F.A. Armstrong, G.S. Wilson. Recent developments in faradaic bioelectrochemistry. *Electrochimica Acta*, **45**, (2000), 2623-2645.
- 50 I. Willner, G. Arad, E. Katz. A biofuel cell based on pyrroloquinoline quinone and microperoxidase-11 monolayer-functionalized electrodes. *Bioelectrochemistry and Bioenergetics*, **44**, (1998), 209-214.

- 
- 51 X. Han, W. Cheng, Z. Zhang, S. Dong, E. Wang. Direct electron transfer between hemoglobin and a glassy carbon electrode facilitated by lipid-protected gold nanoparticles. *Biochimica et Biophysica Acta-Bioenergetics*, **1556**, (2002), 273-277.
- 52 S. Liu, Z. Dai, H. Chen, H. Ju. Immobilization of hemoglobin on zirconium dioxide nanoparticles for preparation of a novel hydrogen peroxide biosensor. *Biosensors and Bioelectronics*, **19**, (2004), 963-969.
- 53 Y. Xiao, F. Patolsky, E. Katz, J.F. Hainfeld, I. Willner. "Plugging into enzymes": nanowiring of redox enzymes by a gold nanoparticle. *Science*, **299**, (2003), 1877-1881.
- 54 L. Wang, E.K. Wang. Direct electron transfer between cytochrome c and a gold nanoparticles modified electrode. *Electrochemistry Communications*, **6**, (2004), 49-54.
- 55 T. Liu, J. Zhong, X. Gan, C. Fan, G. Li, N. Matsuda, Wiring electrons of cytochrome c with silver nanoparticles in layered films. *Chemphyschem*, **4**, (2003), 1364-1366.
- 56 Y. Zhang, P.L. He, N.F. Hu. Horseradish peroxidase immobilized in TiO<sub>2</sub> nanoparticle films on pyrolytic graphite electrodes: direct electrochemistry and bioelectrocatalysis. *Electrochimica Acta*, **49**, (2004), 1981-1988.
- 57 S.Q. Liu, Z.H. Dai, H.Y. Chen, H.X. Ju. Immobilization of hemoglobin on zirconium dioxide nanoparticles for preparation of a novel hydrogen peroxide biosensor. *Biosensors and Bioelectronics*, **19**, (2004), 963-969.
- 58 D.F. Dao, P.L. He, N.F. Hu. Electrochemical biosensors utilising electron transfer in heme proteins immobilised on Fe<sub>3</sub>O<sub>4</sub> nanoparticles. *Analyst*, **128**, (2003), 1268-1274.
- 59 Y. Lvov, B. Munge, O. Giraldo, I. Ichinose, S.L. Suib, J.F. Rusling. Films of manganese oxide nanoparticles with polycations or myoglobin from alternate-layer adsorption. *Langmuir*, **16**, (2000), 8850-8857.
- 60 H. Zhou, X. Gan, T. Liu, Q.L. Yang, G.X. Li. Effect of nano-cadmium sulphide on the electron transfer reactivity and peroxidase activity of haemoglobin. *Journal of Biochemical and Biophysical Methods*, **64**, (2005), 38-45.
- 61 X.L. Luo, J.J. Xu, W. Zhao, H.Y. Chen. A novel glucose ENFET based on the special reactivity of MnO<sub>2</sub> nanoparticles. *Biosensors and Bioelectronics*, **19**, (2004), 1295-1300.
- 62 J.J. Xu, W. Zhao, X.L. Luo, H.Y. Chen. A sensitive biosensor for lactate based on layer-by-layer assembling MnO<sub>2</sub> nanoparticles and lactate oxidase on ion-sensitive field-effect transistors. *Chemical Communications*, (2005), 792-794.

- 
- 63 A.J. Killard and M.R. Smyth. C. Grines (Ed). Electrochemical immunosensors. *Encyclopedia of Sensors*, **10**, (2006), 1-29. American Scientific Publication, New York.
- 64 E. Katz, L. Alfonta, I. Willner. Chronopotentiometry and faradaic impedance spectroscopy as methods for signal transduction in immunosensors. *Sensors and Actuators B*, **76**, (2001), 134-141.
- 65 R.M. Carter, M.A. Poli, M. Pesavento, D.E.T. Sibley, G.J. Lubrano, G.G. Guilbault. Immunochemical biosensors for detection of saxitoxin and brevetoxin. *Immunomethods*, **3**, (1993), 128-133.
- 66 C. Ruan, L. Yang, Y. Li. Immunobiosensor chips for detection of *Escherichia coli* O157:H7 using electrochemical impedance spectroscopy. *Analytical Chemistry*, **74**, (2002), 4814-4820.
- 67 R.W. Keay, C.J. McNeil. Separation-free electrochemical immunosensor for rapid determination of atrazine. *Biosensors and Bioelectronics*, **13**, (1998), 963-970.
- 68 A.L. Ghindilis, R. Krishnan, P. Atanasov, E. Wilkins. Flow-through amperometric immunosensor: fast 'sandwich' scheme immunoassay. *Biosensors and Bioelectronics*, **12**, (1997), 415-423.
- 69 M.L. Sánchez-Martínez, M.P. Aguilar-Caballos, A. Gómez-Hens. Homogeneous stopped-flow fluorimmunoassay for gliadin determination in food samples. *Analytica Chimica Acta*, **523**, (2004), 35-41.
- 70 A.K. Campbell, A. Patel. A homogeneous immunoassay for cyclic nucleotides based on chemiluminescence energy transfer. *Biochemical Journal*, **216**, (1983), 185-194.
- 71 C.X. Lei, F.C. Gong, G.L. Shen and R.Q. Yu. Amperometric immunosensor for *Schistosoma japonicum* antigen using antibodies loaded on a nano-Au monolayer modified chitosan-entrapped carbon paste electrode. *Sensors and Actuators B: Chemical*, **96**, (2003), 582-588.
- 72 J. Li, Z. Wu, H. Wang, G. Shen and R. Yu. A reusable capacitive immunosensor with a novel immobilization procedure based on 1,6-hexanedithiol and nano-Au self-assembled layers. *Sensors and Actuators B: Chemical*, **110**, (2005), 327-334.
- 73 S.Q. Hu, J.W. Xie, Q.H. Xu, K.T. Rong, G.L. Shen and R.Q. Yu. A label-free electrochemical immunosensor based on gold nanoparticles for detection of paraoxon. *Talanta*, **61**, (2003), 769-777.
- 74 D.P. Tang, R. Yuan, Y.Q. Chai, X. Zhong, Y. Liu, J.Y. Dai and L.Y. Zhang. Novel potentiometric immunosensor for hepatitis B surface antigen using a gold nanoparticle-based biomolecular immobilization method. *Analytical Biochemistry*, **333**, (2004), 345-350.

- 
- 75 T. Yin, W. Wei, L. Yang, X. Gao, Y. Gao. A novel capacitive immunosensor for transferrin detection based on ultrathin alumina sol-gel-derived films and gold nanoparticles. *Sensors and Actuators B: Chemical*, **117**, (2006), 286-294.
- 76 J. Chen, J. Tang, F. Yan, H. Ju. A gold nanoparticles/sol-gel composite architecture for encapsulation of immunoconjugate for reagentless electrochemical immunoassay. *Biomaterials*, **27**, (2006), 2313-2321.
- 77 D. Tang, R. Yuan, Y. Chai, Y. Fu. Study on electrochemical behavior of a diphtheria immunosensor based on silica/silver/gold nanoparticles and polyvinyl butyral as matrices. *Electrochemistry Communications*, **7**, (2005), 177-182.
- 78 J. Wang. *Stripping Analysis*, (1985), VCH, New York.
- 79 E. Katz, I. Willner, J. Wang. Electroanalytical and bioelectroanalytical systems based on metal and semiconductor nanoparticles. *Electroanalysis*, **16**, (2004), 19-44.
- 80 M. Dequaire, C. Degrand, B. Limoges. An electrochemical metalloimmunoassay based on a colloidal gold label. *Analytical Chemistry*, **72**, (2000), 5521-5528.
- 81 G. Liu, J. Wang, J. Kim, M.R. Jan. Electrochemical coding for multiplexed immunoassays of proteins. *Analytical Chemistry*, **76**, (2004), 7126-7130.
- 82 J. Wang, G. Liu, G. Rivas. Encoded beads for electrochemical identification. *Analytical Chemistry*, **75**, (2003), 4667-4671.
- 83 J. Wang, D. Xu, A. Kawde, R. Polsky. Metal nanoparticle-based electrochemical stripping potentiometric detection of DNA hybridization. *Analytical Chemistry*, **73**, (2001), 5576-5581.
- 84 J. Wang, R. Polsky, X. Danke. Silver-enhanced colloidal gold electrochemical stripping detection of DNA hybridization. *Langmuir*, **17**, (2001), 5739-5741.
- 85 A. Kawde, J. Wang. Amplified electrical transduction of DNA hybridization based on polymeric beads loaded with multiple gold nanoparticle tags. *Electroanalysis*, **16**, (2004), 101-107.
- 86 J. Wang, D. Xu, R. Polsky. Magnetically-induced solid-state electrochemical detection of DNA hybridization. *Journal of the American Chemical Society*, **124**, (2002), 4208-4209.
- 87 O.D. Velev, E.W. Kaler. In situ assembly of colloidal particles into miniaturized biosensors. *Langmuir*, **15**, (1999), 3693-3698.
- 88 P. Innis, G. Wallace. Inherently conducting polymer nanostructures. *Journal of Nanoscience and Nanotechnology*, **2**, (2002), 441-451.



- 
- 89 S.E. Moulton, P.C. Innis, L.A.P. Kane-Maguire, O. Ngamna, G.G. Wallace. Polymerisation and characterisation of conducting polyaniline nanoparticle dispersions. *Current Applied Physics*, 4, (2004), 402-406.
- 90 A. Morrin, O. Ngamna, S.E. Moulton, A.J. Killard, G.G. Wallace, M.R. Smyth. An amperometric enzyme biosensor fabricated from polyaniline nanoparticles. *Electroanalysis*, 17, (2004), 423-430.
- 91 A. Morrin, F. Wilbeer, O. Ngamna, S.E. Moulton, A.J. Killard, G.G. Wallace, M.R. Smyth. Novel biosensor fabrication methodology based on processable conducting polyaniline nanoparticles. *Electrochemistry Communications*, 7, (2005), 317-322.

## **Chapter 2**

**The application of conducting polymer nanoparticle  
electrodes for the sensing of ascorbic acid and  
hydrogen peroxide**

## 2.1 INTRODUCTION

### 2.1.1 Electrocatalytic properties of conducting polymers

Since the discovery of the organic conducting polymers more than 20 years ago, these materials are finding increasing use in various branches of technology, such as metallization of dielectrics, primary and secondary batteries<sup>1</sup>, anti-static coatings<sup>2</sup>, electromagnetic shielding, electrochromic systems<sup>3</sup> and electrochemical sensors<sup>4,5,6</sup>. One of the most striking properties of conducting polymers is their ability to catalyze some electrode reactions. Thin layers of a conducting polymer deposited onto the surfaces of electrodes are able to enhance the kinetics of electrode processes of some solution species. These electrocatalytic processes, proceeding at conducting polymer electrodes, present a fast growing area of investigation, which may yield many unexpected applications in various fields of applied electrochemistry.

At conducting polymer modified electrodes, at least three processes should be considered to be taking place during electrocatalytic conversion of solution species. The first process is the heterogeneous electron transfer between the electrode and the conducting polymer layer, and electron transfer within the polymer film. As usual, this process is accompanied by the movement of charge compensating anions and solvent molecules within the conducting polymer film, and possible conformational changes of polymer structure as well. The rate of this process is determined by many factors. Among these, electrical conductivity of the polymer layer, electron self-exchange rates between the chains and/or clusters of polymer, and anion movement within the polymer film are of great importance. The second process is the diffusion of solution species to the reaction zone, where the electrocatalytic conversion occurs. As compared to simple electrode reactions, this process can be more complicated in cases where the electrocatalytic conversion occurs within the polymer film due to the fact that the diffusion of species within the film, as well as the possible electrostatic interaction of this species with the polymer itself should be taken into account. The last process is represented by the actual chemical (heterogeneous) reaction taking place between the solution species and the conducting polymer<sup>7</sup>.

From both theoretical and practical points of view, the question on the location of electrocatalytic process seem to be of primary interest. If the charge transfer within the layer of conducting polymer proceeds much faster than the mass transfer of

reacting species and their electrochemical conversion, the electrocatalytic process should proceed at the outer conducting polymer/solution interface. In an opposite case, if the mass transfer and electrochemical reaction proceed faster than the electron transfer in the conducting polymer, an electrocatalytic process occurs at the inner substrate electrode/conducting polymer interface, assuming that the permeability of a porous conducting polymer layer is sufficiently high to penetrate the reacting species and solution ions. Finally, if both processes occur at comparable rates, the electrocatalytic process is located within the conducting polymer layer. The depth of the reaction zone within the conducting polymer layer will be determined, in this case, by the balance between charge and mass transfer, and the rate of electrocatalytic conversion as well. Taking into account the described processes, the electrocatalysis at conducting polymer modified electrodes can be subdivided into two main categories<sup>8</sup>:

1. Metal-like electrocatalysis, that occurs at conducting polymer/solution interface at a high conductivity of electrode material. In this case, an overall rate is determined by the flux of solution species, or by the rate of catalytic conversion.
2. Redox catalysis, that occurs within the polymer layer, or at inner substrate electrode/conducting polymer interface at a limited conductivity of the modifier layer.

Among all of the conducting polymers, polyaniline (PANI) is probably the most widely studied because it has a broad range of tuneable properties derived from its structural flexibility. Much work has been published with regard to the catalytic properties of PANI modified electrodes, which do not contain additional catalytically active substances<sup>9,10,11</sup>.

#### ***2.1.1.1 Electrocatalytic oxidation of ascorbic acid***

Ascorbic acid and its two-electron oxidation product, dehydroascorbic acid, present a quasi-reversible redox couple with a formal redox potential of  $E_0' = +0.058$  V vs. RHE in a pH-neutral solution. In an aqueous solution, ascorbic acid shows two

deprotonation steps with  $pK_a$  values of 4.30 and 11.57. Thus, in a neutral solution ascorbic acid exists as a monodeprotonated ascorbate anion.

The development of sensitive and reproducible sensing systems for the analysis of ascorbic acid can be considered of great importance for both the increasingly strict government guidelines of foodstuff which require precise quantifications of vitamins within these product<sup>12</sup>, and also for the recent association of the ascorbate concentration in biological fluids to the amount of oxidative stress in human metabolism, causing cancer, diabetes and hepatic disease<sup>13,14,15</sup>.

The analytical problem in the electrochemical analysis of ascorbic acid is represented by the high overpotential required for his oxidation. At bare glassy carbon electrodes the oxidation reaction occurs only a potential of +0.6 V vs. SCE. In this situation, the numerous species present in real analyte solutions can be easily oxidised generating an anodic current equivalent or even greater than that generated by the ascorbate electrooxidation.

Therefore, it would seem to be of some importance to create electrocatalytically active electrode surfaces able to oxidize ascorbate at lower potentials, avoiding the anodic discharge of interfering substances<sup>16</sup>.

On the other hand, for some other analytical applications, ascorbic acid represents the undesired interfering species, since it is able to discharge anodically at potentials similar to other analytically important substances. For example, the discrimination of dopamine and other neurotransmitters from ascorbate represents a typical analytical problem due to their co-presence in biological samples. Thus, as well as the electrocatalytically active surfaces able to detect ascorbate at low potentials, it is also important to develop sensing systems able to distinguish and isolate the ascorbate responses from those of other substances.

Two problems are of critical importance for an efficient electrocatalytic oxidation of ascorbate. One of them relates to the chemical redox interaction between ascorbate and a conducting polymer, i.e. the reduction of a polymer layer by ascorbate. As for polyaniline, the redox potential for the redox transition between its leucoemeraldine (i.e., fully reduced) and emeraldine (i.e., half oxidized) forms appears ca. 0.3 V more positive than for ascorbate/dehydroascorbate redox couple in an acidic solution. Thus,

the reduction of polyaniline by ascorbate appears as a possible and thermodynamically favourable process.

Since both redox forms of polyaniline differ significantly in their light absorbance characteristics, the occurrence of this reaction can be followed by photometric means. Based on this, a polyaniline optical sensor was developed and used as an optical detector for ascorbate, integrated into a capillary electrophoresis column<sup>17</sup>. Similarly, microtiter reader plates were modified with polyaniline and used for optical detection of ascorbate<sup>18</sup>.

The second problem relates to the charge propagation within the conducting polymer layer. For an efficient electrocatalysis, a high electrical conductivity of a polymer layer is desirable. The electrical conductivity of many conducting polymers depends on their redox state (i.e. on electron doping level), and on solution acidity (i.e. on proton doping level). For polyaniline, three different redox forms are known. From these, only the emeraldine (half-oxidized) form appears electrically conducting, whereas both leucoemeraldine (fully reduced) and pernigraniline (fully oxidized) forms are semiconducting or even insulating. To be conducting, the emeraldine form must be protonated. Thus, it shows its conductivity only in acidic solutions up to pH of 2.5–3.0. Above this pH, the conductivity drops by several orders of magnitude, and emeraldine becomes insulating. This situation seems to be highly unfavourable for electroanalytical applications, since most assays must be performed in pH neutral or slightly acidic solutions, where no electrical conductivity of polyaniline films is expected<sup>19</sup>.

However, much work on electrochemical oxidation of ascorbic acid has been performed at pH neutral buffered solutions, and efficient electrocatalytic properties of polyaniline towards anodic oxidation of ascorbate in these solutions has been demonstrated. Casella and Guascito (1997) showed glassy carbon electrodes, covered with an electropolymerized layer of PANI to exhibit electrocatalytic properties towards the oxidation of ascorbic acid. Based on their experiments using the rotating disk electrode (RDE), the authors dealt with the question of the location of the electrocatalytic reaction, and stated the cross-exchange reaction to be the rate-determining step of the process. The electrode prepared was used for ascorbate assay, performed by flow injection analysis at a controlled potential of 0.35 V vs. Ag/AgCl<sup>20</sup>. In 2001 O'Connell *et al.* developed an amperometric sensor for the

detection of ascorbic acid at low potential (+100 mV) and a neutral pH modifying both glassy carbon and screen-printed electrodes with PANI. Using the batch and the flow injection mode, the limit of detections were 0.4  $\mu\text{M}$  and 2.45  $\mu\text{M}$ , respectively<sup>21</sup>. The electrocatalytic oxidation of ascorbic acid on polyaniline electrodes has been studied by cyclic voltammetry, electrolysis at controlled potential, and impedance spectroscopy<sup>22,23</sup>. In a pH 5.64 solution, the anodic peak for ascorbic acid has been found to shift from 0.32 V vs. SCE on platinum electrode to 0.05 V on polyaniline modified platinum electrode<sup>18</sup>. As shown by cyclic voltammetry for a polyaniline modified nickel electrode, a gradual decrease of anodic peak corresponding to the leucoemeraldine to emeraldine redox transition at increasing ascorbic acid concentration proceeds, whereas, at higher ascorbate concentration (1 mM), another peak corresponding to oxidation of ascorbate appears in 0.1 M sulphuric acid solution. The electrooxidation of ascorbic acid, resulting in a linear dependence of the current output on concentration, was shown to proceed over a wide pH range<sup>19</sup>. Electrocatalytic current for anodic oxidation of ascorbate was found to be 5–15 times greater for PANI-, polypyrrole-, and poly(3-methylthiophene)-modified electrodes, than for a bare platinum electrode<sup>24</sup>.

The use of “self-doped” polyaniline bearing large anionic groups, basically solved the problem of extension of electrical conductivity for polyaniline towards higher solution pH values. These derivatives, although less conducting than the parent polyaniline, have extended the pH range of electrical conductivity and show their specific redox behaviour even in neutral or alkaline solutions. Sun *et al.* (1998) reported the cathodic overpotential for ascorbate to be significantly reduced by ca. 0.2 V for a microdisk gold electrode, covered with an electrochemically copolymerized layer of aniline with 3,4-dihydroxybenzoic acid<sup>25</sup>. A self-doped polyaniline derivative, prepared by electrochemical copolymerization of aniline with *o*-aminobenzoic acid, has been shown to decrease the over-potential for electro-oxidation of ascorbate by 0.2 V, and has been used as a thin coating at a gold electrode for ascorbate assay within a linear range of response of 12  $\mu\text{M}$  to 2.4 mM<sup>26</sup>. Self-doped copolymer of aniline with *m*-aminobenzoic acid has been deposited at dual band platinum microelectrode with a gap of 10  $\mu\text{m}$ , showing an on–off response to ascorbate up to 6 mM<sup>27</sup>.

In 2001 Bartlett and Wallace proposed a model for the oxidation of ascorbate at PANI-poly(vinylsulfonate) composite coated electrode. They demonstrated that the

reaction occurs at the polymer surface being independent from the film thickness at the highest ascorbate concentrations where it is not mass transport limited and that it occurs through a kinetic scheme in which a complex is formed between the polymer and the ascorbate and that this is followed by the oxidation of bound ascorbate<sup>28</sup>. Heras *et al.* (2007) developed an ascorbate sensor with improved conducting and electrochemical properties at neutral pH, compared to a polyaniline modified electrode, using a sequential electrochemical polymerisation of aniline and N-(3-propane sulfonic acid)aniline (PSA) to modify a glassy carbon electrode. The developed sensor detected ascorbate at 0 mV versus Ag/AgCl, avoiding the interference of uric acid and dopamine and reaching the detection limit of 2.2  $\mu\text{M}$ <sup>29</sup>.

However, to explain the autocatalytic reaction for the anodic oxidation of ascorbate in nearly pH-neutral buffered solutions at “non-doped” polyaniline modified electrodes, Jurevičiūtė *et al.* in 2005 proposed a mechanism. In an aqueous solution, ascorbic acid shows two steps of ionization with  $\text{p}K_{\text{a}}$  values of 4.17 and 11.57. Therefore, a mono-deprotonated anionic form of ascorbic acid (ascorbate) should be predominant in nearly neutral buffered solutions used in the present work. Thus, a two-electron electro-oxidation of ascorbate mono-anion should be accompanied by the liberation of one proton. Then, since electro-oxidation of ascorbate proceeds in a thin porous layer of polyaniline, a local acidifying of this layer should proceed. Obviously, a local decrease of pH within this layer leads to proton doping of polyaniline. As a result, polyaniline turns into its protonated, and thus electrically conductive and electrochemically active form, which enables an efficient electro-oxidation of ascorbate to proceed<sup>30</sup>. Using Raman spectroelectrochemistry, Mažeikienė *et al.* (2006) studied the electrocatalytic oxidation of ascorbate at electrodes modified with “non-doped” polyaniline and concluded that the reaction proceeds within the polyaniline film rather than at an outer polyaniline/solution boundary and therefore following a redox-catalysis mechanism<sup>31</sup>.

It appears interesting to note that the electrocatalytic oxidation of ascorbic acid at PANI-modified electrodes follows two distinct mechanisms depending on whether the polymer is doped or not. In fact, according to Bartlett and Wallace’s investigation, the electrocatalytic oxidation of ascorbate at PANI-poly(vinylsulfonate)-coated electrodes occurs at the polymer surface for a metal-like catalysis. On the contrary, for non-doped PANI-modified electrodes the reaction occurs within the polymer film



following a redox-like catalysis as Mažeikiene *et al.* demonstrated with Raman spectroelectrochemical measurements.

### ***2.1.1.2 Electrocatalysis of hydrogen peroxide***

Because of the importance of H<sub>2</sub>O<sub>2</sub> in several fields such as environmental, industrial, food, clinical and biochemical analysis, the development of reliable, rapid and economic methods of sensing H<sub>2</sub>O<sub>2</sub> is of great significance for numerous processes and has become a subject of study for decades. Many analytical methods have been reported for the determination of H<sub>2</sub>O<sub>2</sub> such as titrimetry<sup>32</sup>, fluorimetry<sup>33</sup>, chemiluminescence<sup>34</sup>, spectrophotometry<sup>35</sup> and electrochemistry<sup>36,37</sup>. Among these, electrochemical detection is one of the promising approaches to achieve accurate, specific, economic and rapid H<sub>2</sub>O<sub>2</sub> monitoring. In earlier days, amperometric detection of H<sub>2</sub>O<sub>2</sub> was usually performed at platinum surfaces<sup>38</sup>. A great drawback in this approach is represented by the high over potential needed for H<sub>2</sub>O<sub>2</sub> oxidation (ca. 0.7 V vs. Ag/AgCl) at which many electroactive species such as ascorbic acid, uric acid could also be oxidised to give interfering signals.

One of the most common ways to overcome this problem, has been the use of an enzyme, namely horseradish peroxidase (HRP), a prototypical heme protein peroxidase, which catalyses the reduction of H<sub>2</sub>O<sub>2</sub> and, due to its peculiar structure, allows the direct electron transfer between its active site and the electrode surface<sup>39,40</sup>. Using this system, the electrochemical detection of hydrogen peroxide can be performed at much lower potentials (-0.1 to 0 V vs. Ag/AgCl) where the responses from the enzyme-catalyzed reaction are based on the reduction of the enzyme active centre and not the direct reduction of hydrogen peroxide<sup>41</sup>. Though direct electrical communication between HRP and common electrodes is observed, generally, it is a slow process<sup>42</sup>. A faster electron transfer could be achieved by means of mediators<sup>43</sup> and, in reagentless biosensor systems, by means of conducting polymers which can transfer charges from the electrode to the enzyme active site more efficiently<sup>44</sup>. Despite the advantages of good sensitivity and accuracy, biosensors suffer from important shortcomings such as high cost, low stability and limited binding of the enzyme to solid surfaces<sup>45</sup>.

Conducting polymers in general, and PANI in particular, have been investigated with regard to direct electrocatalysis of various species without the need of enzymes. Ascorbic acid as seen in the previous section, is only one of the possible analytes. Some investigation has also been carried out with regard to the electrochemical behaviour of hydrogen peroxide on bare platinum and glassy carbon electrodes and on the same modified with a PANI film. In this work no response current of the reduction of hydrogen peroxide was observed at both the bare and PANI-modified glassy carbon electrodes and only a very small response was observed at both the bare and the PANI-modified platinum electrode at low potentials (+0.075 V vs. SCE)<sup>46</sup>.

Generally, the catalysis of hydrogen peroxide can be observed only for PANI composites prepared with other catalytically active substances, such as carbon nanotubes<sup>47</sup>, metal complexes<sup>48</sup>, etc. However, the catalytic effects are attributed to the composite rather than to the polyaniline itself. More recently, Aussawasathien *et al.* (2005) observed the direct catalysis of H<sub>2</sub>O<sub>2</sub> on a form of nanostructured polyaniline: electrospun nanofibers. However, the potential at which the catalysis of H<sub>2</sub>O<sub>2</sub> was carried out was not given and the analytical capabilities of the sensor were not quoted.

### 2.1.2 Processability of Polyaniline

Similar to many other conducting polymers, the exploitation of polyaniline for commercial sensing applications has proved very difficult for a number of reasons. It is insoluble in common solvents, seriously hindering its material processing. The monomer, aniline, is a carcinogen. It must be distilled prior to use and stored under nitrogen. Finally, acidic conditions are required for the formation of the most highly conductive form of PANI, which does not lend itself to entrapment of pH-sensitive materials such as proteins. As such, proteins have to be subsequently deposited, adding complexity to the sensor fabrication<sup>49</sup>. Much effort has been spent improving the processability of PANI. Dispersion of this polymer is one of the useful ways to overcome the problems with solubility and processability. In addition, little or no aniline should be present in dispersions, thereby removing its carcinogenic properties. These dispersions have been studied by many research groups<sup>50,51,52</sup>. Recently, Moulton *et al.* (2004)<sup>53</sup> used a micelle polymerisation method developed by Han *et al.*

(2002)<sup>54</sup> to synthesise PANI nanoparticles, using dodecylbenzenesulphonic acid (DBSA), where DBSA plays the role of both dopant and surfactant in aqueous dispersions. These nanoparticles were characterised as spherical particles,  $10 \pm 2$  nm in diameter with an electrical conductivity of  $15 \pm 3$  S/cm. Polyaniline nanofibres were synthesized using a method termed as the “rapid mixing method” by Huang and Kaner (2004). This rapid mixing concept was based on using oxidant (APS) as a limiting reagent with respect to monomer. Therefore, during polymerisation, the oxidant molecules were rapidly consumed by polymerizing aniline monomer and inducing formation of nanofibres in their vicinity. Complete depletion of oxidant resulted in secondary growth of the fibres being suppressed, resulting in individual fibrillar structures of the polymer<sup>55</sup>. This concept was applied by Ngamna *et al.* (2007) to the synthesis of PANI nanoparticles, where an emulsion polymerization approach was used (using DBSA as dopant) in order to induce a spherical nanoparticulate formation. The inherent morphology of PANI-DBSA nanoparticulates was spherical, rather than fibrillar, as the polymer was formed inside the DBSA micelles<sup>56</sup>. Recent breakthroughs in synthesis and fabrication of conducting polymers with nanodimensional control have managed to overcome the issue of processability. A stable nanodispersion has an indistinguishable appearance from a true solution, and more importantly can be handled and applied similarly. In addition, enhanced properties of conducting polymer materials become apparent at the nanodimension such as higher conductivity<sup>57</sup> and more rapid, discrete, electrochemical switching processes<sup>58</sup>; properties directly applicable to electrochemical devices.

To date, several techniques have been employed in the fabrication of polymer thin films, such as thermal evaporation, electropolymerisation<sup>59</sup>, spin-coating<sup>60</sup>, dipping<sup>61</sup>, electrophoretic patterning<sup>62</sup>, and printing. Among the printing techniques available, inkjet printing has arguably caught the most attention in recent years due to its unique characteristics of simplicity, high speed, compatibility with a wide range of substrates, non-contact patterning, additive properties (low waste), ability to deposit very small droplets (2 - 12 pl), and low cost. Inkjet printing is an ideal method to deposit conducting polymer solutions provided they are in a readily soluble or nanoparticulate form. Conducting polymers are attractive for electronic applications and using inkjet printing, ultra-thin films can be patterned with resolution up to  $20\text{-}30 \mu\text{m}$ <sup>63</sup>.

Many applications of this technology are emerging through both patents and publications. Chen *et al.* (2003) inkjet printed an all-polymer RC filter circuit in 2003 for the first time using soluble conducting polyaniline and poly(3,4-ethylenedioxythiophene). The paper illustrated the clear advantages in terms of fabrication technology over more traditional methods such as lithography<sup>64</sup>. Other devices fabricated by inkjet printing of conducting polymers in the electronics field include thin-film transistors<sup>65</sup>, transistor circuits<sup>66</sup> and a chemical fuse<sup>67</sup>. Electrochromic displays have also been fabricated using conducting polymer materials in conjunction with inkjet printing technology<sup>68</sup>.

Research on the coupling of conducting polymers with inkjet patterning techniques for sensor devices, and more specifically, biosensor devices is beginning to emerge<sup>69,70</sup>. Morrin *et al.* in 2007 illustrated a unique method to pattern conducting polymer in a simple economical and environmentally safe manner. Coupling the novel use of conducting polymer nanoparticles as the building material, inkjet printing enabled a practical route to a desktop fabrication system of sensing devices<sup>71</sup>.

The novel nanoparticulate formulation of polyaniline, synthesized according to Moulton *et al.*<sup>53</sup>, has been used in this work as the foundation for a chemical sensor development for the analysis of ascorbic acid and hydrogen peroxide. Electrochemical experiments have been carried out with the aim of optimizing all the analytical parameters, demonstrating also the catalytic features of this novel nanomaterial towards both ascorbic acid and hydrogen peroxide. Screen-printed carbon electrodes were modified with polyaniline nanoparticles using a simple drop-coating technique and used to perform all the characterisations and studies. Finally, the inkjet-printing deposition technique was used to pattern polyaniline nanoparticles on the electrode surface and further measurements were performed to show the behaviour of the sensors fabricated in this manner.

## 2.2 MATERIALS AND METHODS

### 2.2.1 Materials

Aniline was purchased from Aldrich (13,293-4), vacuum distilled and stored frozen under nitrogen. polyvinylsulphonate (PVS, 27,842-4) was purchased from Aldrich.. Ammonium peroxydisulfate (APS-215589) and sodium dodecylsulfate (SDS-L4509) were purchased from Aldrich and used as received. Dodecylbenzenesulphonic acid (DBSA-D0989) was purchased from Tokyo Kasei Kogyo Co., Ltd. 30% (v/v) hydrogen peroxide solution and ascorbic acid were purchased from Merck. Dialysis membrane (D9402), 12,000 Da molecular weight cut-off, was purchased from Sigma and soaked in Milli-Q water before the use. Silver/silver chloride (Ag/AgCl) electrodes were purchased from Bioanalytical Systems Ltd. (Cheshire, UK). The platinum mesh (29,809-3) was purchased from Aldrich. All solutions were prepared using Milli-Q water.

### 2.2.2 Buffers and solutions

Unless otherwise stated, all electrochemical measurements were carried out in phosphate buffered saline (PBS), (0.002 M  $\text{KH}_2\text{PO}_4$ , 0.008 M  $\text{Na}_2\text{HPO}_4$ , 0.137 M NaCl, 0.003 M KCl, pH 6.8). Unless otherwise stated, all biochemicals were prepared in PBS.

### 2.2.3 Instrumentation

Screen-printed carbon-paste electrodes were produced using an automated DEK 248 machine (Weymouth, UK) according to Grennan *et al*<sup>72</sup>. Briefly, electrodes were screen-printed onto pre-shrunk PET substrate. Initially a layer of silver was deposited as the conducting path. Two layers of Gwent carbon paste ink (C10903D14) were deposited as the working electrode. Finally, an insulation layer was deposited to eliminate cross-talk and to define the working electrode area ( $9 \text{ mm}^2$ ). The silver and carbon layers were cured using a conventional oven at  $120^\circ\text{C}$  for 5 minutes. The insulating layer was cured using the UV lamp curing system. All electrochemical measurements were performed on a BAS100W electrochemical analyser with

BAS100W software using either cyclic voltammetry or time-based amperometric modes. An Ag/AgCl pseudo-reference electrode and a platinum mesh auxiliary electrode were used for bulk electrochemical experiments. Scanning Electron Microscopy (SEM) using Secondary Electron (SE) detection and Back-Scattered Electron (BSE) detection were carried out with a Hitachi S 3000N. An acceleration voltage of 20 kV was employed.

#### **2.2.4 Synthesis of polyaniline nanoparticles**

The synthesis of polyaniline NPs is a modification of the rapid mixing method first reported by Kaner *et al.*<sup>73</sup> and optimised by Ngamna *et al.*<sup>56</sup> 1.7 g of DBSA was allowed to dissolve in 20 ml of distilled water (0.25 M) by heating the solution to 40°C. This served as both doping acid and surfactant. 10 ml of the acid was added to 0.3 g (0.294 ml) of distilled aniline (0.16 M) and the resulting solution was stirred for about 3 min. At this point it is crucial to avoid the solution being dominated by white flakes. The remaining 10 ml of DBSA were added to 0.18 g of APS (0.04 M) and the solution was stirred until the APS was dissolved. The two solutions were then mixed together to start the polymerisation process which was allowed to proceed for 2.5-3 h with vigorous stirring. The characteristic green colour of polyaniline appears after 30-50 min. After polymerisation, 20 ml of 0.05 M SDS was added to the polyaniline suspension and the mixture was stirred for several minutes. Centrifugation was then carried out at 4400 rpm for 30 min. The precipitate was discarded and the supernatant was retained and transferred to dialysis tubing (12,000 Da molecular weight cut-off point) and dialysis was allowed to proceed for 48 h at room temperature against 0.05 M SDS (2 L), with the SDS solution changed twice during this period.

#### **2.2.5 Electrode modification with PANI nanoparticles**

Screen-printed electrodes were preliminarily cleaned and activated using a single voltammetric cycle between -1200 and +1500 mV (vs. Ag/AgCl) at a scan rate of 100 mV/s in 10 ml of 0.2 M H<sub>2</sub>SO<sub>4</sub>. PANI nanoparticle solutions having a pH of about 4.3 were adjusted to pH 7.0 using a dilute solution of NaOH. An optimised volume of this

solution was then drop-coated onto pre-treated screen-printed electrode surfaces and allowed to dry at room temperature for 2 h.

### **2.2.6 Electropolymerisation of bulk aniline on the electrode surface**

For comparative studies, electrodes modified with bulk polyaniline were prepared as follows. Screen-printed electrodes were preliminarily cleaned and activated using a single voltammetric cycle between -1200 and +1500 mV (vs. Ag/AgCl) at a scan rate of 100 mV/s in 10 ml of 0.2 M H<sub>2</sub>SO<sub>4</sub>. A mixture of 7.8 ml HCl 1 M, 186 µl aniline and 2 ml polyvinylsulphonate (PVS) was degassed under nitrogen for 10 min prior the polymerisation. The electrode was then placed into this solution and aniline was polymerised onto the surface of the working electrode using cyclic voltammetry. 10 voltammetric cycles were carried out between -500 and 1100 mV versus Ag/AgCl reference electrode at 100 mV/s.

### **2.2.7 Electrochemical characterisations**

All the electrochemical characterisations as well as the calibration measurements were carried out in stirred batch system using a 10 ml volume glass cell with a three-electrode configuration. A platinum mesh and a Ag/AgCl electrode were used as auxiliary and reference electrode, respectively, while the screen-printed carbon electrode modified with nanoPANI was used as the working electrode. In all the experiments, PBS (pH 6.8) was used as the working buffer except during the optimisation of the working pH, when for lower pH values a citrate buffer was used. 1 M stock solutions of ascorbic acid and hydrogen peroxide were prepared in PBS buffer and then aliquots from these solutions were added to the batch cell containing PBS buffer, to perform both the voltammetric characterisations and the calibration studies of the sensor.

### 2.2.8 Inkjet printing of PANI nanoparticles

PANI NPs were inkjet printed on the screen-printed electrode surface according to the method optimised by Ngamna *et al.*<sup>56</sup> Briefly, Epson print cartridges (T036 and T037), compatible with the Epson C45 printer were cut open and emptied of ink and the sponge inside was removed. All colour tanks of the cartridges (black, cyan, magenta and yellow) were cleaned thoroughly with deionized water. The chip on the cartridge was then reset using a chip resetter ([www.9to6.ie](http://www.9to6.ie)) so that the printer would read the cartridge as full. Polyaniline NP dispersions were then poured into one or more of the colour tanks in the cartridge. All other tanks were left empty. The lid was replaced on top of the cartridge, and the cartridge was inserted back into the printer. Powerpoint® was used to draw coloured circles (3 mm diam.). The design was printed with the polyaniline on plain printing paper (210 mm x 210 mm). Screen-printed electrodes (3 mm diam.) were then affixed to the printed page where the Powerpoint® circles were aligned with the electrode area. Polyaniline was then printed as many times as required, on the electrodes using 'Best Photo' mode as the printer setting. The process is illustrated in *Figure 2.1*.

SEM visualisations of different nanoPANI films deposited on screen-printed electrodes by inkjet printing were also carried out. Precisely, the unmodified electrode surface and the electrode surface modified by 10, 20 and 30 prints were investigated. All the samples were gold sputtered before the analysis.



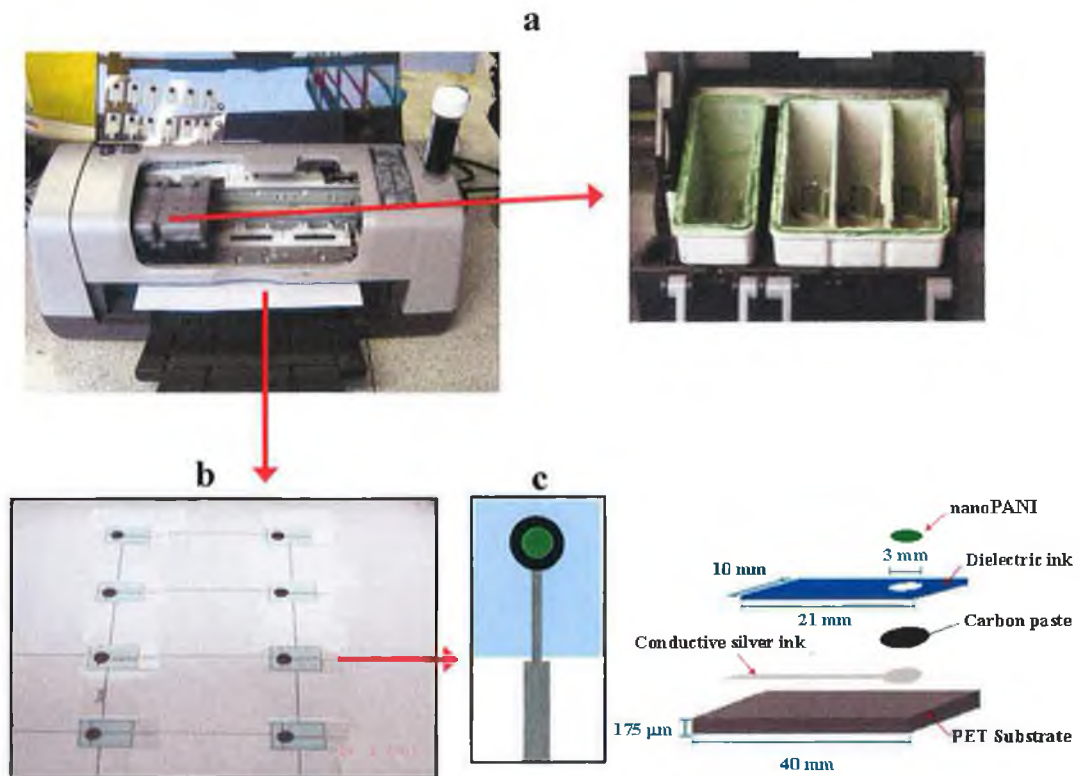


**Figure 2.1.** Inkjet printing procedure consisting of: (a) preparation of the desk printer filling the empty colour tanks with the nanoPANI suspension; (b) printing the green nanoPANI circles onto the screen-printed electrodes positioned on a template sheet; (c) after the printing and the drying process separation of the electrodes. A detailed illustration of the electrode's components is also shown.

## 2.3 RESULTS AND DISCUSSIONS

### 2.3.1 Voltammetric study of nanoPANI modified electrode

Voltammetric characterisations were performed in order to evaluate the electrochemical behaviour of the nanoPANI film deposited onto a screen-printed carbon electrode. A cyclic voltammetric study was carried out in batch system using PBS (pH 6.8) as buffer. The presence of DBSA in the polymer structure ensures the electroactivity and conductivity of the film even at neutral pH. *Figure 2.2* shows the cyclic voltammograms for nanoPANI-modified SPE recorded at pH 6.8 at different scan rates. The two oxidation peaks (at ~600 and 750 mV) correspond to the oxidation of Leucoemeraldine base (LB) to Emeraldine salt (ES) and ES to pernigraniline salt (PS), respectively. The nanoPANI film presents a quasi-reversible chemistry as confirmed by two reduction peaks (at 650 and 450 mV) corresponding to the transformation of PS to ES and ES to LB, respectively. As a matter of fact the ratio between the peak current for the oxidation and the peak current for the reduction for both reactions is very close to 1. The good stability of the film was confirmed by the overlapping of the cyclic voltammograms recorded at the same scan rate (data not shown). A scan rate study was then performed plotting the peak current values for the oxidation and the reduction process as a function of the square root of the scan rate (*Figure 2.3*).

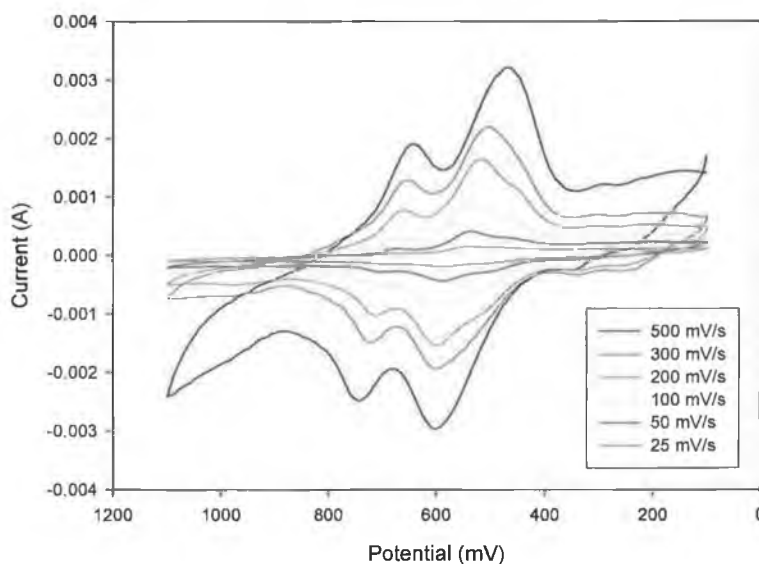


**Figure 2.2.** Cyclic voltammograms recorded between 0.1 and 1.1 V in PBS (pH 6.8) for nanoPANI-modified SPE at scan rates: 25, 50, 100, 200, 300 and 500 mV/s (vs. Ag/AgCl). (Electrode surface area: 0.07 cm<sup>2</sup>).

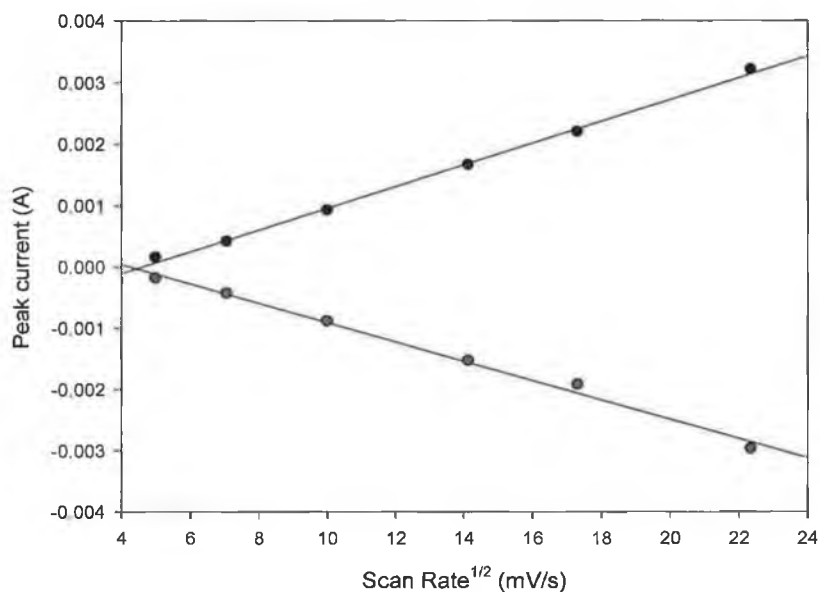


**Figure 2.3.** Plots of the peak current as a function of the square root of the scan rate at +600 mV and +500 mV for the reduction and oxidation process, respectively. (Electrode surface area: 0.07 cm<sup>2</sup>).

Increasing the rate of change of potential caused the rate of electrolysis at the surface of the electrode to increase and resulted in increased peak currents.

The fact that they present a significantly linear trend means that the nanoPANI film behaves as an electroactive specie-adsorbed thin film undergoing non-diffusional Nernstian reaction. This study also demonstrated a level of stability of the films on the screen-printed electrode surface.

### 2.3.2 Oxidation of ascorbic acid at nanoPANI modified electrode

The  $pK_a$  of ascorbic acid is 4.30, and so carrying out the experiments at pH 6.8, all of the reactant is present as ascorbate. The oxidation of L-ascorbate to dehydro-L-ascorbic acid involves the transfer of two electrons and one proton. At unmodified electrodes it is commonly proposed that ascorbate oxidation occurs *via* a radical anion intermediate in a series of first order steps<sup>74</sup> whereas at modified electrode surfaces it is possible that the reaction occurs through a hydride transfer<sup>20</sup>. Whatever the mechanism of oxidation, it is followed, at neutral pH, by rapid hydrolysis of the dehydro-L-ascorbic acid to 2,3-diketogluconic acid<sup>75</sup> (Figure 2.4).

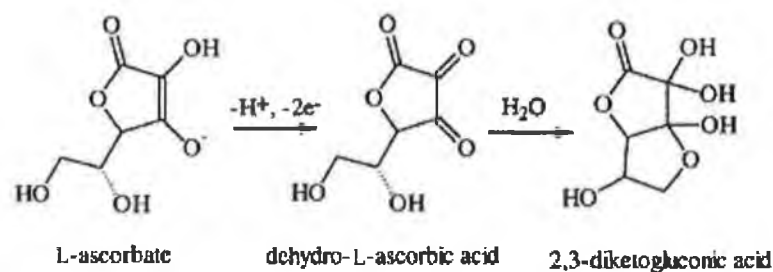


**Figure 2.4.** Oxidation of ascorbic acid to dehydro-L-ascorbic acid at neutral pH involving the transfer of two electrons and one proton and followed immediately by the hydrolysis of the dehydro-L-ascorbic acid to 2,3-diketogluconic acid.

To compare the oxidation of ascorbic acid at both unmodified and modified electrodes, cyclic voltammograms were recorded using a bare SPE and a nanoPANI-modified SPE in PBS buffer (pH 6.8) with ascorbic acid at several concentrations.

It can be seen in *Figure 2.5(a, b)* that the oxidation of ascorbic acid started from about  $-50$  mV for both electrodes and resulted in an irreversible process. As a matter of fact, the final product 2,3 diketogluconic acid is not reduced again during the cathodic scan. Both voltammograms present a very similar trend with the oxidation peak currents recorded using the nanoPANI-modified SPE of an order of magnitude higher. This confirms that the nanoPANI film is a good electrocatalyst for ascorbate oxidation as well as the bulk PANI which has been already investigated from other groups in the past<sup>28-30</sup>.

For a better visualisation of the differences between the catalytic properties in the oxidation of ascorbic acid of a bare SPE, a bulk PANI-modified SPE and a nanoPANI-modified SPE, an experiment was carried out measuring the signals at the fixed potential of  $0$  V (vs. Ag/AgCl) (see section 2.3.3 for working potential optimisation) for different ascorbate concentrations. This amperometric experiment was again performed in a batch system using PBS as buffer and adding sequentially different amounts of ascorbic acid. The results are illustrated in *Figure 2.6*. It can be clearly seen that the nanoparticulate formulation of PANI presents a very similar catalytic property in the oxidation of ascorbic acid as the bulk structured PANI, with signals recorded of about one order of magnitude higher than the bare SPE.

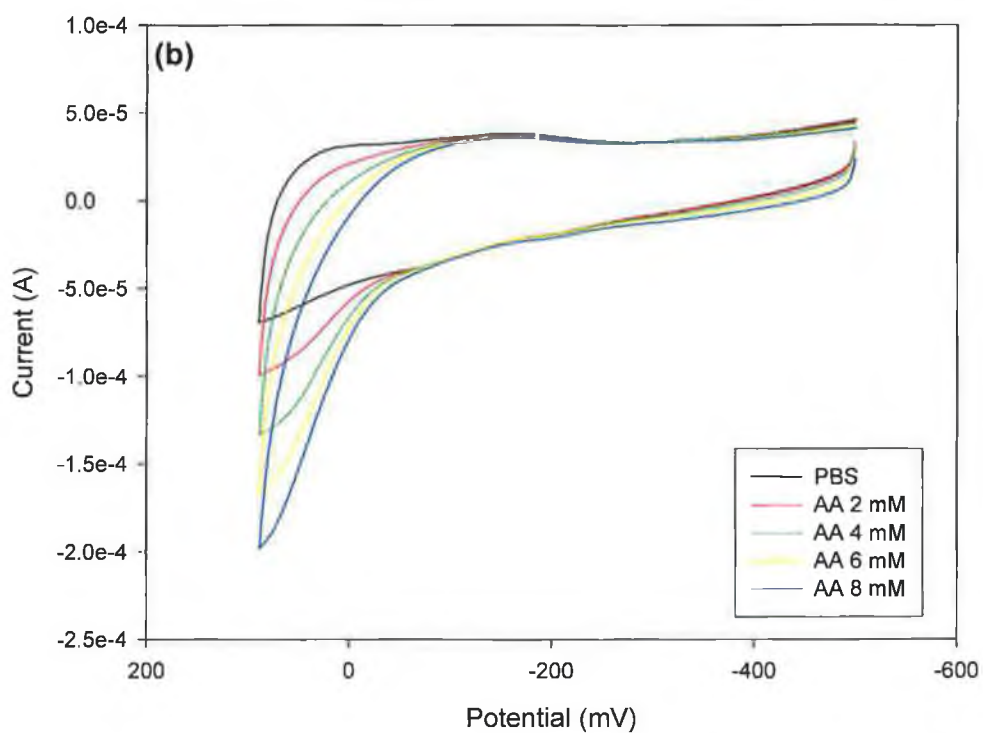
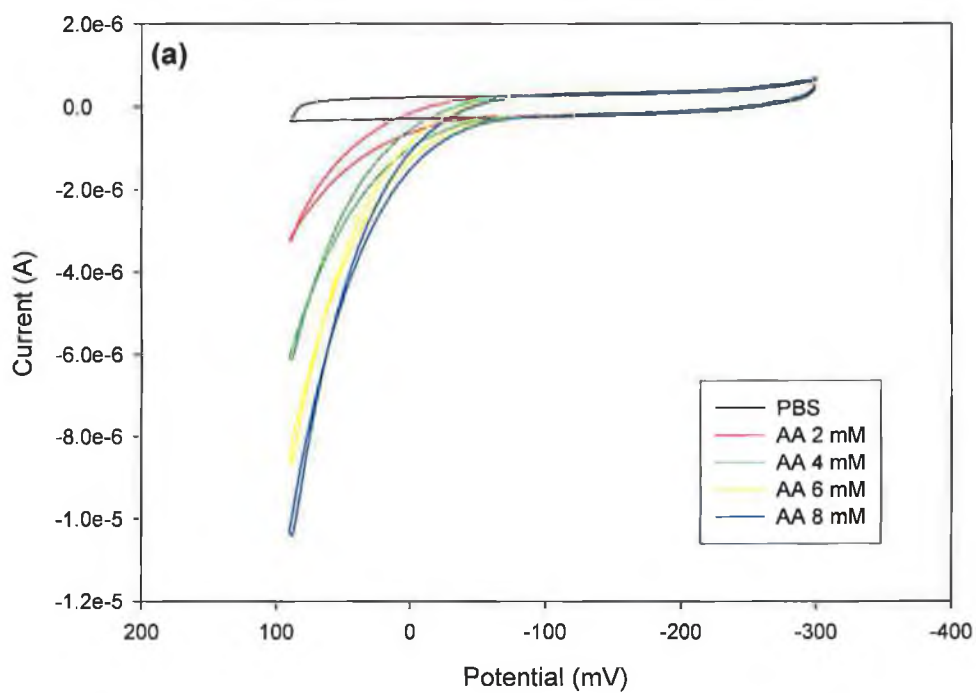


**Figure 2.5.** Cyclic voltammograms for the oxidation of ascorbic acid at (a) bare SPE and (b) nanoPANI-modified SPE in PBS and containing AA at concentrations 2, 4, 6, 8 mM (vs. Ag/AgCl). (Electrode surface area:  $0.07 \text{ cm}^2$ ).

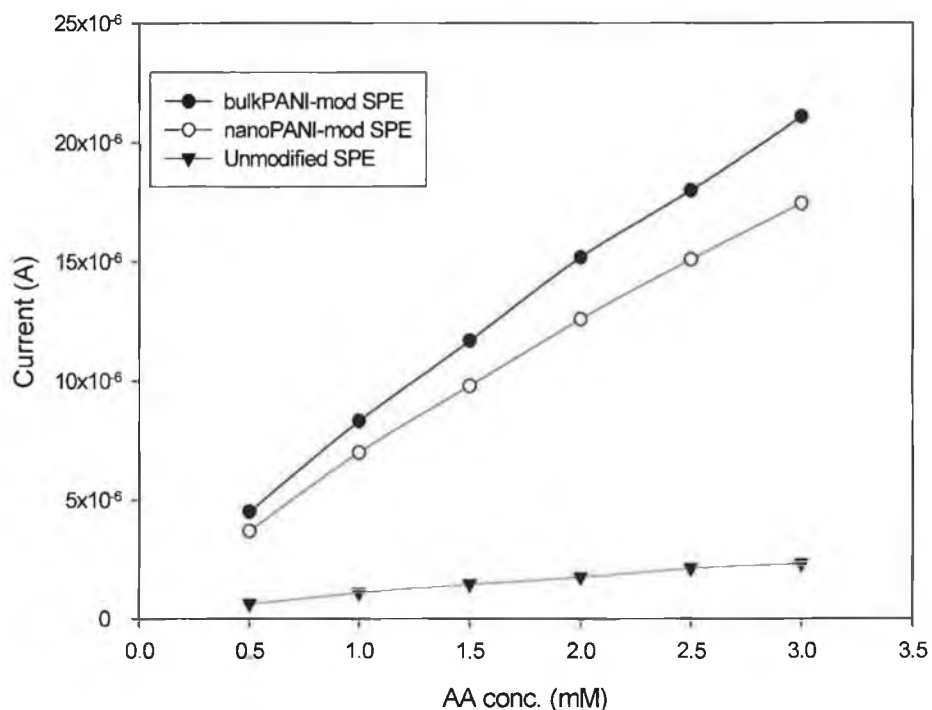


**Figure 2.6.** Signals recorded for the oxidation of ascorbic acid at potential of 0 V (vs. Ag/AgCl) for bare SPE, bulk PANI-modified SPE and nanoPANI-modified SPE at concentrations of ascorbic acid between 0.5 and 3 mM. (Electrode surface area: 0.07 cm<sup>2</sup>).

A scan rate study was also carried out to determine whether the current was entirely mass transport controlled. Plotting again the peak current values as function of the square root of the scan rate resulted in a linear trend ( $r^2 = 0.996$ ) as illustrated in *Figure 2.7*, which confirmed the above assumption. This means that the catalytic current depends on the concentration of ascorbate which reacts as soon as it reaches the nanoPANI film surface. It could be deduced also that the catalytic response was independent from the film thickness which was estimated to be about 190  $\mu\text{m}$  for the bulk PANI and 3  $\mu\text{m}$  for the nanoPANI. This metal-like behaviour of the nanoPANI film was similar to that of bulk PANI/PVS investigated by Bartlett *et al.*<sup>28</sup>

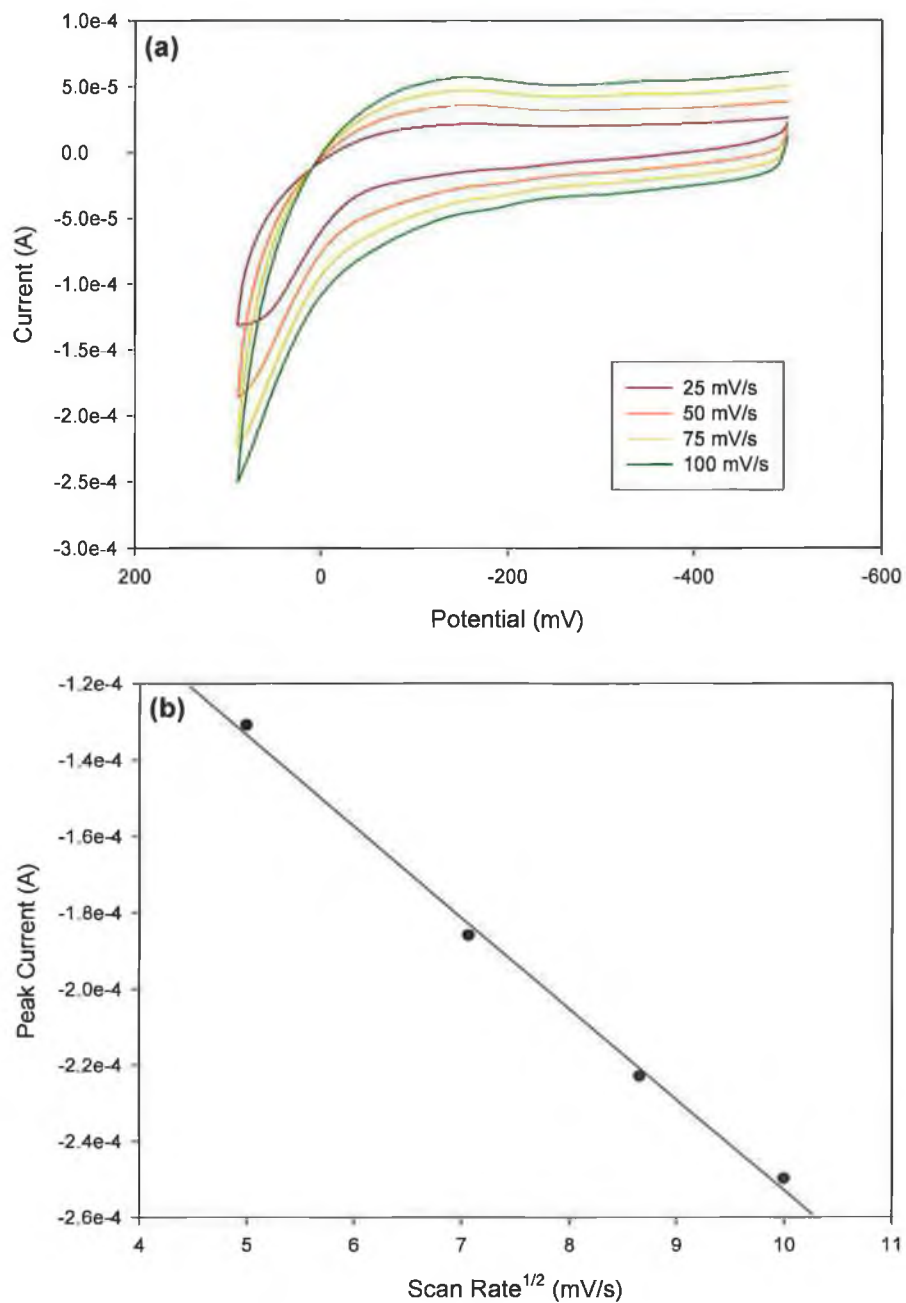


**Figure 2.7.** Scan rate study for the oxidation of ascorbic acid (AA) at nanoPANI-modified SPE. (a) Cyclic voltammograms recorded in the presence of AA 8 mM at scan rates between 25 and 100 mV/s. (b) Plot of the current values as function of the square root of scan rate at +100 mV vs. Ag/AgCl. ( $y = -2.38 \times 10^{-5}x - 1.39 \times 10^{-5}$ ,  $r^2 = 0.996$ , electrode surface area:  $0.07 \text{ cm}^2$ ).

### 2.3.3 Investigation of the working potential for the analysis of ascorbic acid

As described in section 2.2.5, the sensor was prepared by drop coating a small volume of the nanoPANI suspension onto a screen-printed electrode and then drying for 2 h at room temperature. In order to optimise the amount of nanoPANI to be deposited onto the electrode surface, an experiment was carried out in a batch system, measuring the signals generated at the potential of 0 V by the injection of 3 mM ascorbic acid. Different electrodes were prepared using different volumes of the nanoPANI suspension of 1, 3, 5, 7 and 10  $\mu\text{l}$ . The results are shown in *Figure 2.8*. An increase in the catalytic performance was recorded increasing the deposition volume from 1 to 5  $\mu\text{l}$ , while at 7 and 10  $\mu\text{l}$ , no further enhancement appeared. This seems to suggest that the entire electrode surface was covered by PANI NPs, using 5  $\mu\text{l}$  of the suspension. Using 1 and 3  $\mu\text{l}$  probably not the entire surface was covered, resulting in a lower catalytic response. However, using volumes larger than 5  $\mu\text{l}$ , it could be assumed that a thicker nanoPANI film layer resulted. Because the signal responses were found to be of the same amplitude, they might be considered independent from the film thickness, proving again that the catalytic reaction occurs at the polymer surface. From this result all of the subsequent investigations were carried out modifying screen-printed electrodes with 5  $\mu\text{l}$  of the nanoPANI suspension.

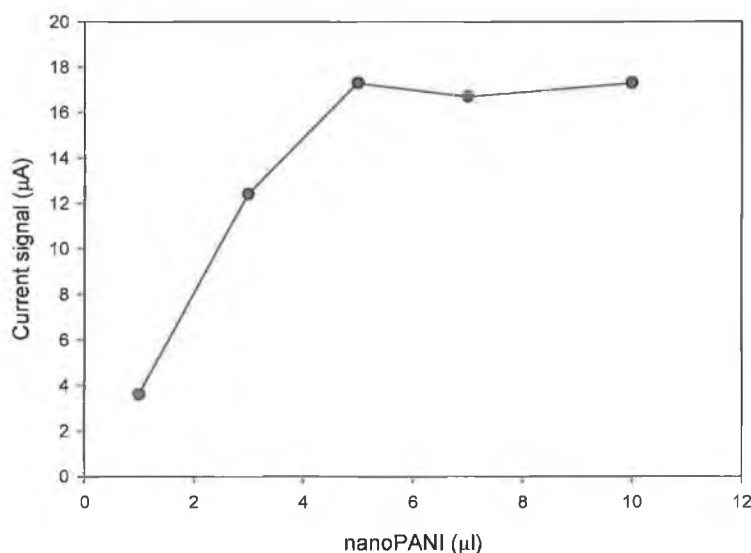


**Figure 2.8.** Optimisation of the volume of the nanoPANI suspension drop-coated onto the screen-printed electrodes. In batch system using PBS buffer (pH 6.8), at potential of 0 V (vs. Ag/AgCl), five different electrodes were prepared using 1, 3, 5, 7 and 10  $\mu\text{l}$  of the nanoPANI solution, and tested in the oxidation of a 3 mM solution of ascorbic acid. (Electrode surface area: 0.07  $\text{cm}^2$ ).



A potential study was performed in order to select the best potential to be applied for the analysis of ascorbic acid. Again in batch system, current signals were recorded for the oxidation of 1 mM solution of ascorbic acid but setting different potentials in the range  $-100$  to  $+400$  mV. As it can be seen in *Figure 2.9* there was an increased response increasing the potential up to  $+250$  mV where it reached a plateau. This behaviour was not unexpected, the higher the potential applied the easier is the oxidation process. However, the potential applied seemed to affect the sensor itself, in fact increasing the potential, together with the increase of the catalytic signal, also the background noise increased, due probably to the oxidation of impurities present in solution or inside the nanoPANI film. This further effect caused by increasing the potential was taken into account to select the optimum potential for the analysis. It was believed that the best way to quantify the noise level and to judge its effect to the analysis, was to calculate the limit of detections at each potential applied. These were estimated considering three times the height of the background noise ( $S/N=3$ ) and compared to the signals recorded injecting 1 mM ascorbic acid. The graph in *Figure 2.10* shows the limit of detections calculated for each potential applied.

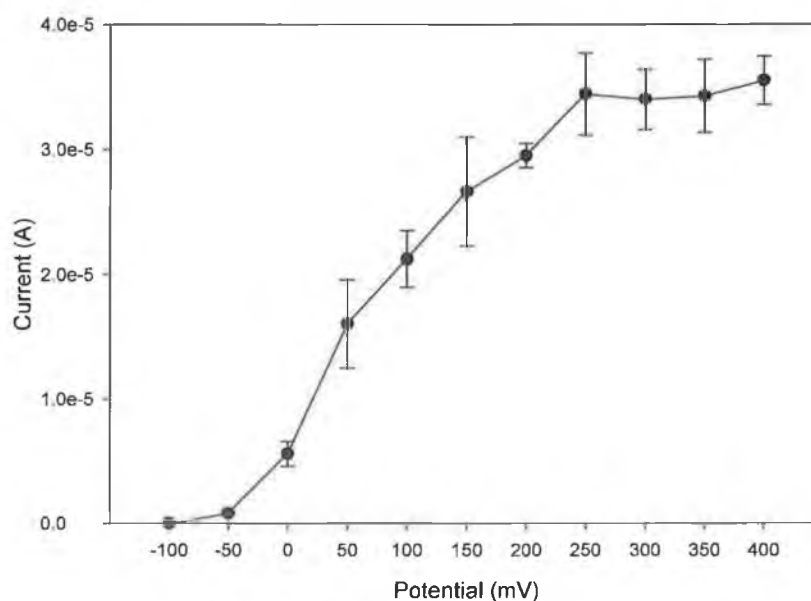


**Figure 2.9. Working potential optimisation. Amperometric signals generated by the oxidation of 1 mM solution of ascorbic acid in batch system with PBS buffer (pH 6.8) at applied potentials between  $-100$  and  $+400$  mV (vs. Ag/AgCl). (Electrode surface area:  $0.07$  cm<sup>2</sup>).**

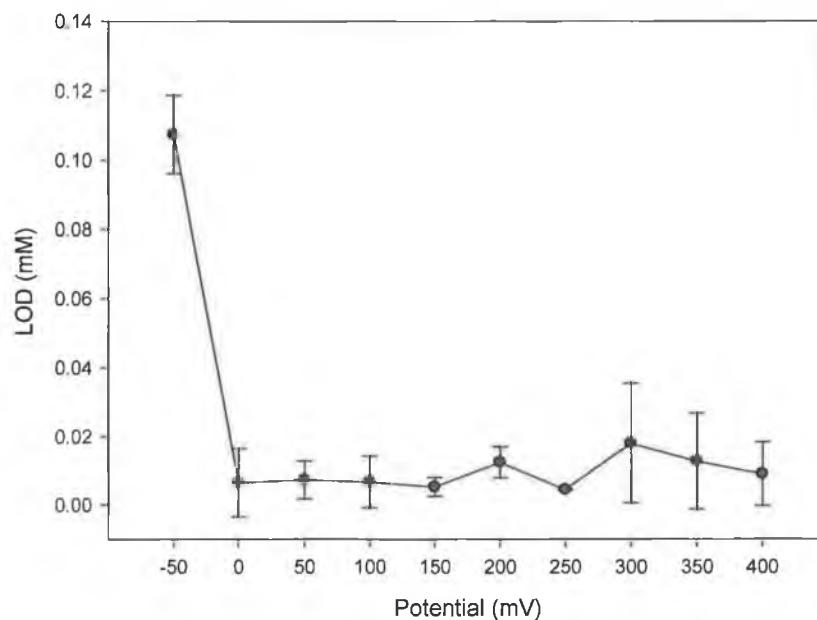


**Figure 2.10.** Investigation of the limit of detection as function of the potential applied. Experiment set up as in *Figure 2.9*.

It seemed that from potentials more anodic than 0 V the increase of the amperometric signal was equally balanced by the increase in the background noise, resulting therefore in a very similar detection limit. The potential of 0 V was then chosen as the working potential both because the limit of detection was one of the lowest and also because being the lowest applicable, reduces possible interferences by other substances that could be oxidised.

### 2.3.4 Optimisation of the working pH for the analysis of ascorbic acid

It has been already stated in section 2.3.1, that the presence of DBSA in the polyaniline structure ensures the conductivity and the electroactivity of the polymer at neutral and alkaline pH, even though at acidic pH the charge transfer within the polymer is more efficient. The investigation of the working buffer pH was carried out therefore to evaluate the optimal pH for the ascorbic acid oxidation process in relation to the polymer electroactivity. Similarly to the investigation of the working potential, an experiment was performed setting 0 V as the optimised potential and using different working buffers for the amperometric analysis. Citrate buffer was used to prepare solutions at pH between 4.0 and 5.5 and phosphate buffer for the solutions at

pH from 6.0 to 8.0. The assay was performed in triplicate for each buffer. The graph in *Figure 2.11* shows the current signal values recorded as a function of the pH used. It can be seen that increasing the pH the amperometric signal also increased. This confirmed once again, the electroactivity of polyaniline even at quite high pH, due to the dopant present in the structure which ensures the charge transfer through the polymer itself. The fact that the signal increased at higher pH could also be explained by taking into account the oxidation reaction of ascorbic acid as illustrated in section 2.3.2. The oxidation process starts with the monobasic form of the ascorbic acid, the ascorbate. Therefore the higher the pH the higher the concentration of ascorbate in solution. Moreover, the first step of the reaction involves the transfer of one proton which is certainly favoured by an alkaline pH. These processes seemed to offset any loss in conductivity of the film at elevated pH.

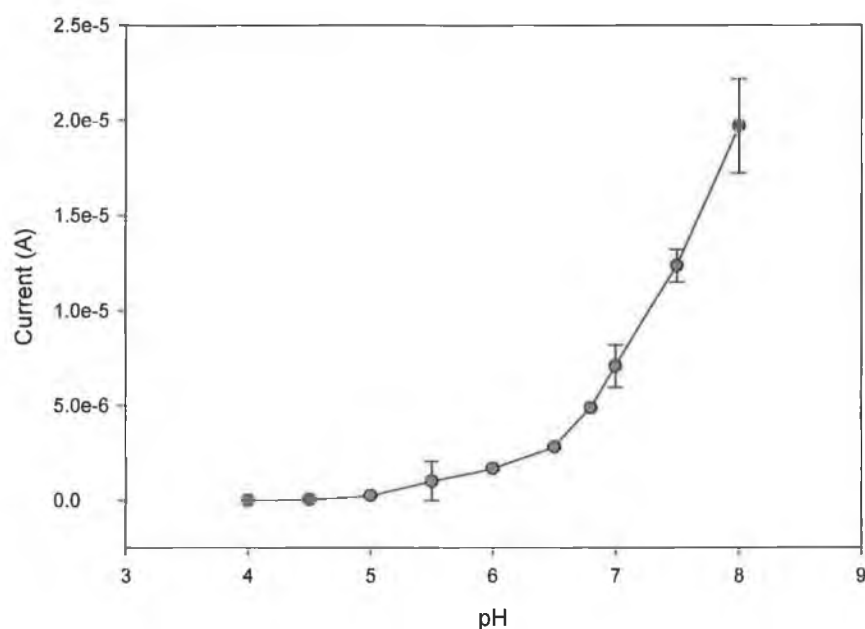


**Figure 2.11.** Working buffer optimisation. Amperometric signals generated by the oxidation of 1 mM solution of ascorbic acid in batch system at potential of 0 V (vs. Ag/AgCl) and using different working buffers at pH between 4 and 8. (Electrode surface area: 0.07 cm<sup>2</sup>).

However, similarly to the potential study, the buffer pH also seemed to affect the background noise together with the catalytic signal, with higher pH resulting in a higher background signal. Once again, therefore, the evaluation of the working pH was made in relation to the limit of detection at each working pH calculated as

explained in section 2.3.3. It can be seen in *Figure 2.12* that from pH 5 to pH 6 the catalytic response seemed to have the main effect resulting in a lower signal to noise ratio. After pH 6 the increase of the catalytic signal was well balanced by the increase of the background, resulting in similar signal to noise ratios with similar detection limits. The lowest LOD resulted using the buffer at pH 6.8, so it was chosen as the optimal working buffer for the analysis of ascorbic acid.

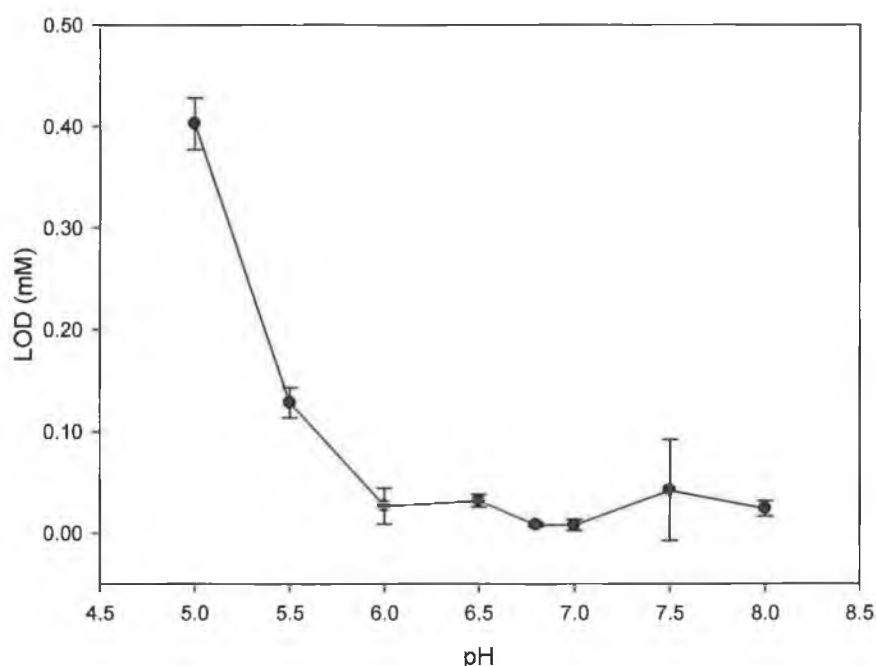


**Figure 2.12.** Investigation of the limit of detection as function of the working pH used. Experiment set up as in *Figure 2.11*.

### 2.3.5 Calibration of the nanoPANI-based sensor for the analysis of ascorbic acid

Using the optimised conditions such as the volume to be used to modify the screen-printed electrode, the potential to be applied and working buffer pH to be used for the analysis, the sensor was calibrated for the determination of ascorbic acid. The calibration curve together with the typical step-shaped amperogram is illustrated in *Figure 2.13*. The sensor showed linearity from 0.5 to 8 mM with  $r^2 = 0.996$  ( $n = 6$ ). The limit of detection was determined to be 8.3  $\mu\text{M}$  and the sensitivity 4.07  $\mu\text{A}/\text{mM}$ .

The reproducibility was also evaluated and it resulted in a relative standard deviation (RSD) for the nanoPANI-based sensor of 3.2% for nine successive measurements of 1 mM ascorbic acid. The sensor analytical performance can be evaluated in relation to other systems exploiting conducting polymer-modified electrodes, which are summarized in *Table 2.1*. It can be noted that none of them applies a potential lower than +50 mV vs. Ag/AgCl. This is an important feature for the sensor developed in this work because the applied potential of 0 V vs. Ag/AgCl significantly reduces the possibility for other species interfering. In fact, testing the selectivity of the sensor with typical interferents for ascorbic acid such as dopamine, acetamidophen, uric acid and citric acid, no response resulted at the applied potential of 0 V. The sensor therefore resulted in both a sensitive and specific response for the analysis of ascorbic acid. With regard to the limit of detection and the linearity ranges, better performances have been achieved with other systems. However, most of the work illustrated in the table utilized gold or platinum electrodes, much more expensive than the disposable screen-printed carbon electrodes used in this study. Those utilizing GC electrodes present performances similar to that of the sensor under study.

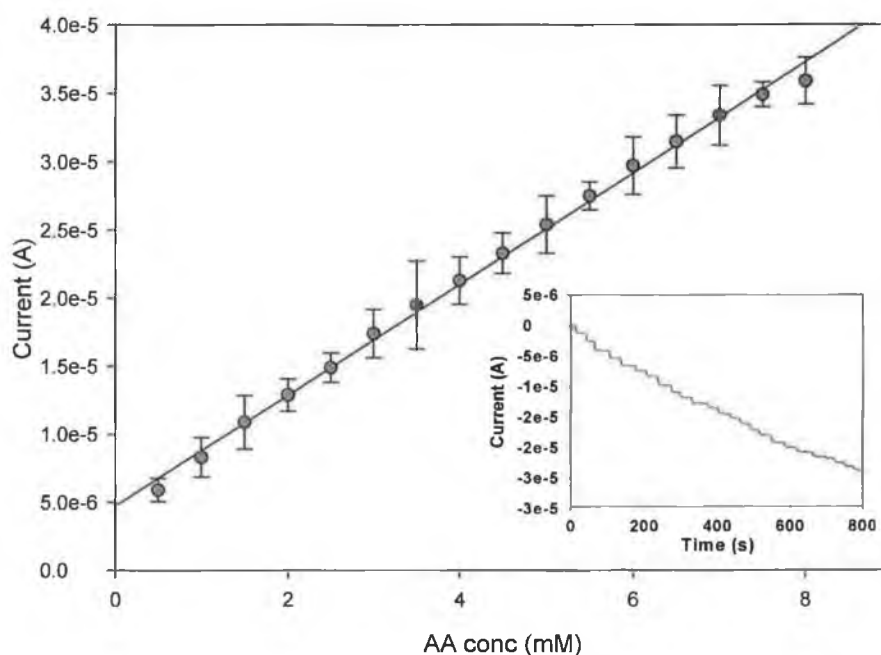


**Figure 2.13.** Calibration curve for the detection of ascorbic acid in batch system at the working potential of 0 V (vs. Ag/AgCl) and using PBS (pH 6.8) as the working buffer. ( $y = 4.07 \times 10^{-6}x + 4.73 \times 10^{-6}$ ,  $r^2 = 0.996$ , electrode surface area:  $0.07 \text{ cm}^2$ ). Inset: step-shaped amperogram generated by the ascorbic acid injections.

Polymer film	Potential applied	pH	LOD	LRR	Ref
PANI on GC electrode	+ 0.1 V vs. Ag/AgCl	6	0.4 $\mu\text{M}$ Batch	0.4 $\mu\text{M}$ –2 mM	21
PANI on GC electrode	+ 0.1 V vs. Ag/AgCl	6	2.45 $\mu\text{M}$ FIA	5 $\mu\text{M}$ –0.1 mM	21
PANI on GC electrode	+ 0.350 V vs. Ag/AgCl	7	1.0 $\mu\text{M}$	1.0 $\mu\text{M}$ –0.7 mM	20
PANI-poly(vinylsulfonic acid) on GC electrode	+ 0.1 V vs. SCE	7	0.06 mM	0.06 $\mu\text{M}$ –30 mM	28
Copolymer of aniline and <i>o</i> - aminobenzoic acid on Au electrode	+ 0.1 V vs. SCE	7	2.0 $\mu\text{M}$	12 $\mu\text{M}$ –2.4 mM	26
Copolymer of aniline and <i>m</i> - aminobenzoic acid on Pt electrode	+ 0.05 V vs. Ag/AgCl	7	20 $\mu\text{M}$	up to 6 mM	27
Copolymer of aniline and 3,4- dihydroxybenzoic acid on Au microdisk	+ 0.2 V vs. SCE	7	50 $\mu\text{M}$	0.1–10 mM	25
Poly(3-methylthiophene) on Au electrode	+ 0.4 V vs. Ag/AgCl	7	0.01 $\mu\text{M}$	10 $\mu\text{M}$ –1 mM	24
PPY doped with hexacyanoferrate on GC electrode	+ 0.24 V vs. SCE	4	0.5 mM	0.5–16 mM	76

**Table 2.1.** Application of electrogenerated polymer coated electrodes for ascorbic acid analysis.

### 2.3.6 Application of nanoPANI-modified electrode for the analysis of hydrogen peroxide

After the investigation on the catalysis of ascorbic acid using a nanoPANI-modified electrode, the electrochemical behaviour of hydrogen peroxide with the same electrode was also investigated. Sensing applications for the detection of hydrogen peroxide generally exploit the catalytic properties of enzymes (peroxidases)<sup>39</sup> as well as metal catalysts<sup>48</sup>. The electrocatalysis of hydrogen peroxide without the use of any catalyst would represent a great advantage for the PANI NPs due to the fact that they can be used for simple fabrication of electrochemical sensing devices. Coupling this nanoparticulate formulation of PANI with inkjet printing deposition technique, sensing devices for the analysis of both ascorbic acid and hydrogen peroxide could be easily fabricated without the addition of enzymes or inorganic catalysts. After the printing process the sensor would be ready to use.

In order to investigate the catalytic properties of PANI NPs towards the reduction of hydrogen peroxide, comparison studies were made between nanoPANI-modified, bulk PANI-modified and unmodified screen-printed electrodes. *Figure 2.14* shows cyclic voltammograms recorded in PBS (pH 6.8) for (a) unmodified and (b) nanoPANI-modified screen-printed electrode in the presence of hydrogen peroxide.

Similarly to the oxidation of ascorbic acid, both voltammograms presented a very similar trend with the reduction peak currents recorded using the nanoPANI-modified SPE being an order of magnitude higher. The nanoPANI film seemed to possess catalytic properties towards the reduction of H<sub>2</sub>O<sub>2</sub>. Another comparison was carried out recording the amperometric signals in a batch system with PBS in the presence of H<sub>2</sub>O<sub>2</sub> at concentrations between 0.5 and 3 mM, at the fixed potential of -0.1 V (vs. Ag/AgCl) (*Figure 2.15*).

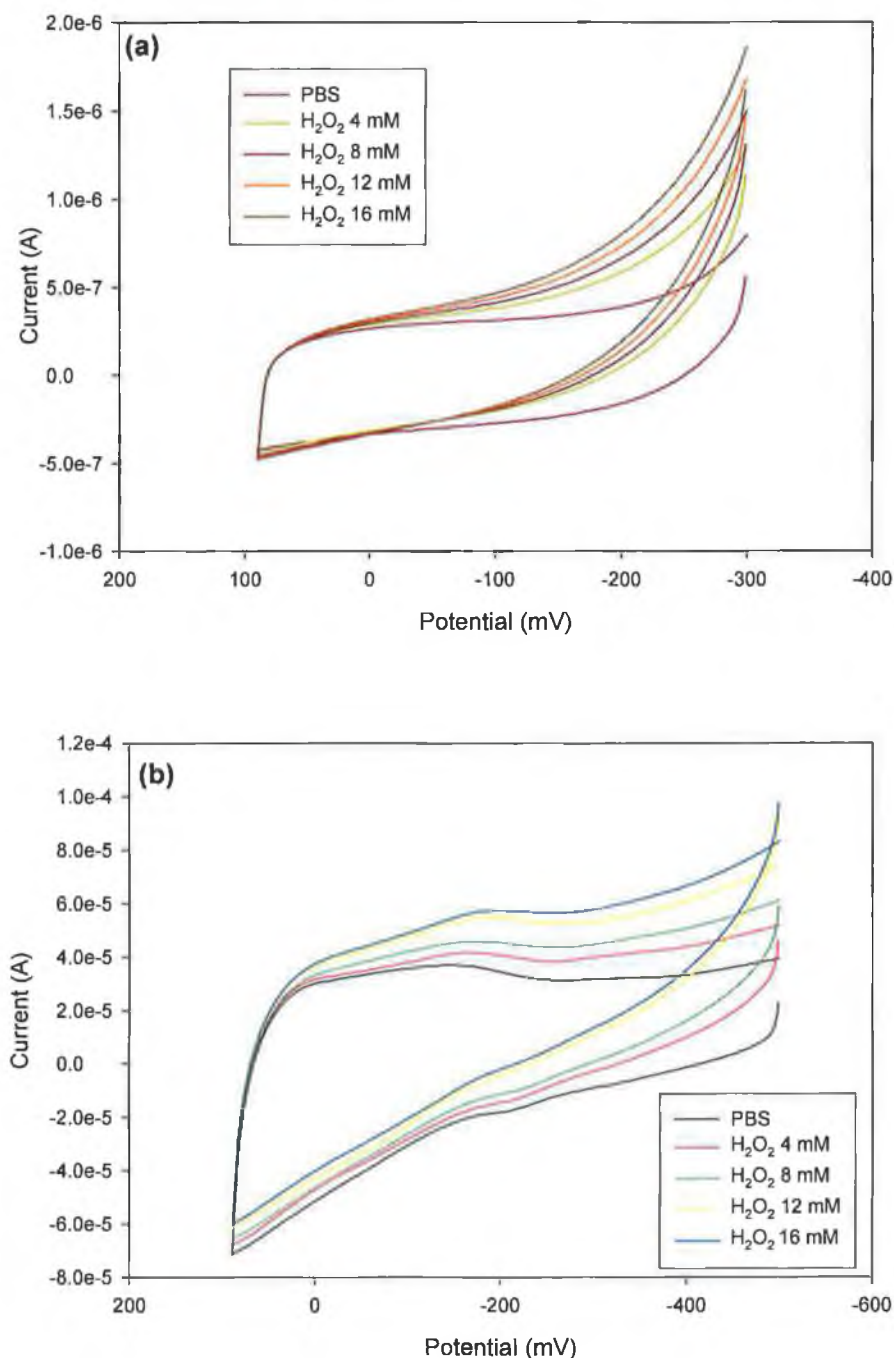


**Figure 2.14.** Cyclic voltammograms for the reduction of hydrogen peroxide at (a) bare SPE and (b) nanoPANI-modified SPE in PBS and containing H<sub>2</sub>O<sub>2</sub> at concentrations 4, 8, 12, 16 mM. (vs. Ag/AgCl). (Electrode surface area: 0.07 cm<sup>2</sup>).

It can be clearly seen from the graph in *Figure 2.15* that the nanoPANI-modified electrode gave a much higher response compared to that of bare SPE and bulk PANI-modified electrode with signals recorded of about two order of magnitude higher. For the catalytic oxidation of ascorbic acid, both the nanoPANI and the bulk PANI/PVS-



modified electrodes showed very similar behaviour. It appeared clear, in this case that the nanoPANI film possesses a new property which cannot be related only to a simple surface effect. Both types of polyaniline films used to modify the electrode contained no catalysts in the structure (as in traditional methods) but only organic dopants: DBSA for the nanoPANI and PVS for the bulk PANI which are not known to possess any catalytic properties. The catalysis exhibited towards the reduction of hydrogen peroxide, therefore, seemed to appear for the nanoPANI specifically because of the nanoparticulate structure of the organic polymer. It represents another example of a nanomaterial which possesses novel properties that are different from those of the bulk material.

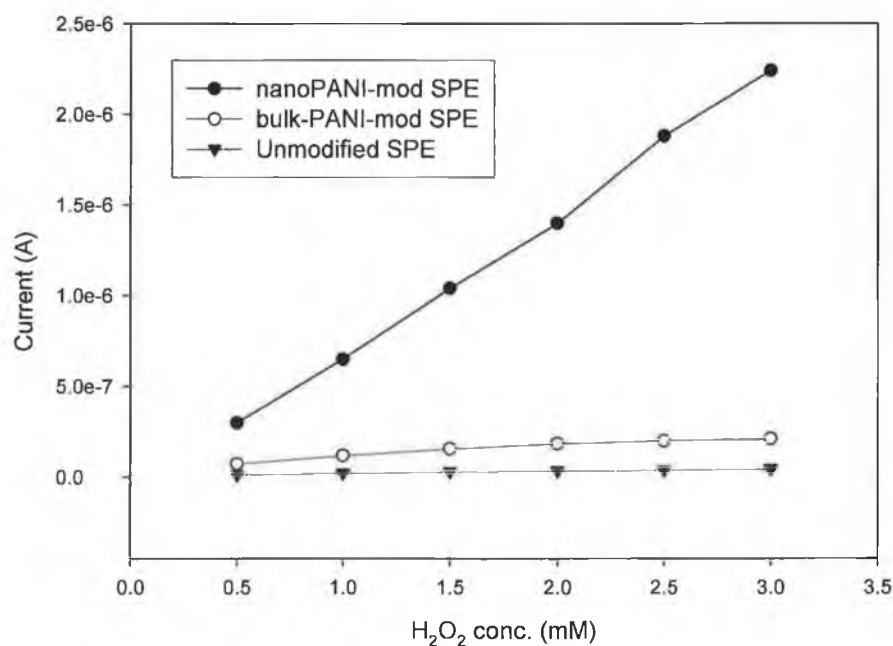


**Figure 2.15.** Signals recorded for the reduction of H<sub>2</sub>O<sub>2</sub> at potential of -0.1 V (vs. Ag/AgCl) for bare SPE, bulk PANI-modified and nanoPANI-modified SPE at concentrations of H<sub>2</sub>O<sub>2</sub> between 0.5 and 3 mM. (Electrode surface area: 0.07 cm<sup>2</sup>).

A scan rate study was also carried out and similarly to the oxidation of ascorbic acid, the reaction of hydrogen peroxide with the nanoPANI film on the electrode surface appeared to be mass transport controlled. Again, it could be supposed that the catalytic reaction occurs at the polymer surface rather than within the film. *Figure 2.16a* shows the cyclic voltammograms recorded in the batch system, in PBS (pH 6.8) containing 16 mM H<sub>2</sub>O<sub>2</sub>. The scan rate was varied from 25 to 100 mV and plotting

the current values taken at the potential of -0.2 V (vs. Ag/AgCl) against the square root of the scan rate, which resulted in a linear trend ( $r^2 = 0.999$ ). (Figure 2.16b).

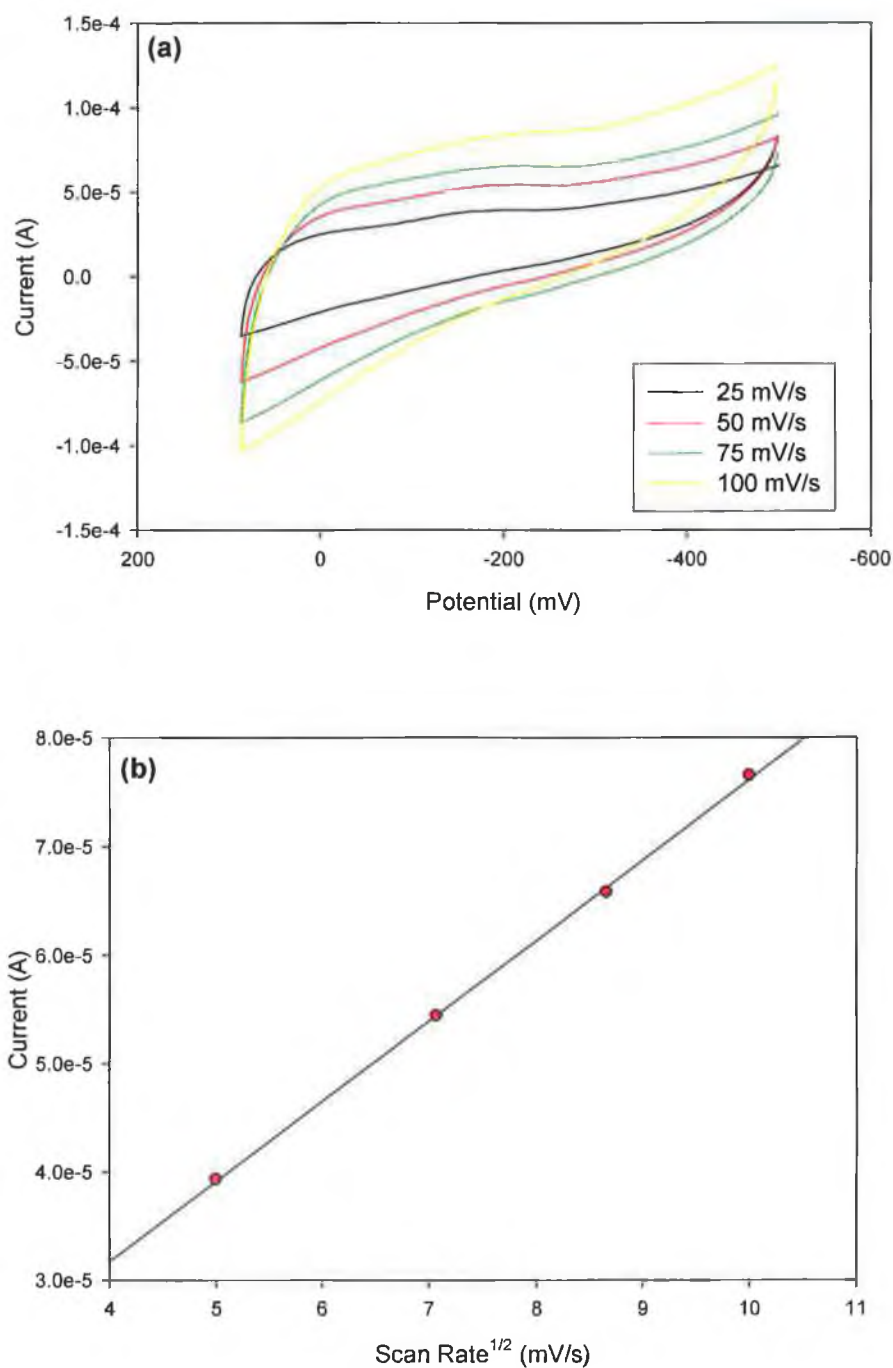


**Figure 2.16.** Scan rate study for the reduction of  $\text{H}_2\text{O}_2$  at nanoPANI-modified SPE. (a) Cyclic voltammograms recorded in the presence of  $\text{H}_2\text{O}_2$  16 mM at scan rates between 25 and 100 mV/s. (b) Plot of the current values as function of the square root of scan rate at potential of -100 mV vs. Ag/AgCl. ( $y = 7.40 \times 10^{-6} + 2.13 \times 10^{-6} x$ ,  $r^2 = 0.999$ , electrode surface area:  $0.07 \text{ cm}^2$ ).

### 2.3.7 Investigation of the working potential for the analysis of hydrogen peroxide

From the cyclic voltammograms there did not appear a clear and precise reduction peak of hydrogen peroxide, probably due to the mediation via the PANI film which generates only a large reduction wave. For this reason, in order to select the optimal potential to be used for the analysis, a potential study was performed similarly as for the ascorbic acid analysis. In batch system, current signals were recorded for the reduction of 8 mM solution of  $\text{H}_2\text{O}_2$  at different potentials applied, in the range  $-350$  to  $+100$  mV. The results are shown in *Figure 2.17*. There is a very small response applying the potential of  $+100$  and  $+50$  mV, which are probably too anodic for the reaction to occur. Then, from 0 to  $-200$  mV there was an increase of the signal response reaching the plateau from  $-200$  to  $-350$  mV. Again, however, the applied potential influenced the background noise, which affected the analysis due to the variation of the signal to noise ratios. In order to evaluate and quantify the effect of the background noise, the limit of detections were calculated at each applied potential. These were correlated to the signal as high as three times the background noise and considering the signal recorded injecting 8 mM solution of  $\text{H}_2\text{O}_2$ . The results are illustrated in the graph at *Figure 2.18*.

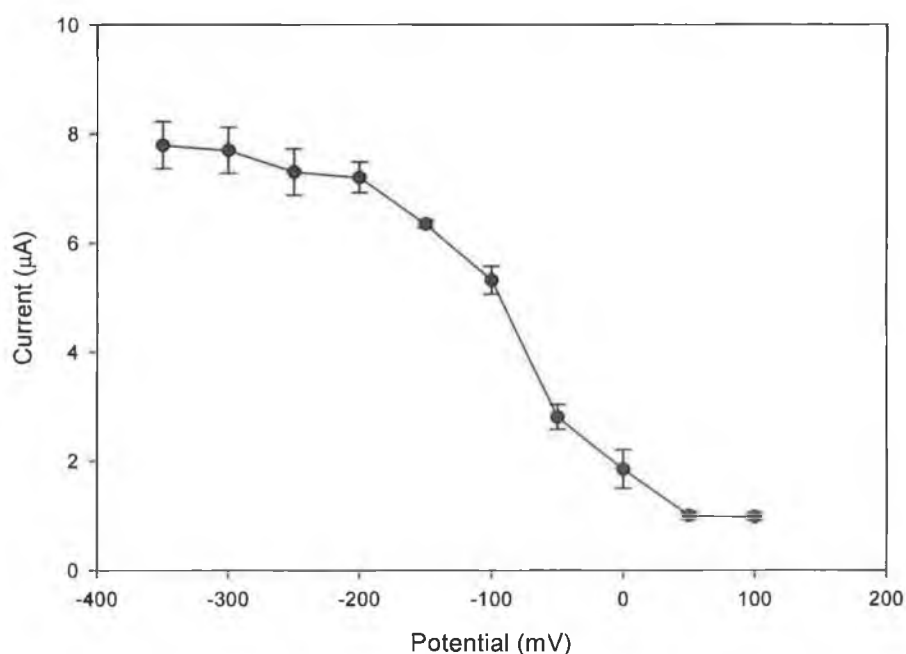


**Figure 2.17. Working potential optimisation. Amperometric signals generated by the reduction of 8 mM solution of  $\text{H}_2\text{O}_2$  in batch system with PBS buffer (pH 6.8) at applied potentials between  $-350$  and  $+100$  mV (vs. Ag/AgCl). (Electrode surface area:  $0.07 \text{ cm}^2$ ).**

The highest signal to noise ratio was found to be at a potential around -100 mV where, therefore, the lowest limit of detection was calculated. Potentials more cathodic than -100 mV generated higher signals but equally balanced by the increase of the background noise resulting, therefore, in a slightly lower signal to noise ratio. The potential of -100 mV was thus chosen as the optimal working potential.

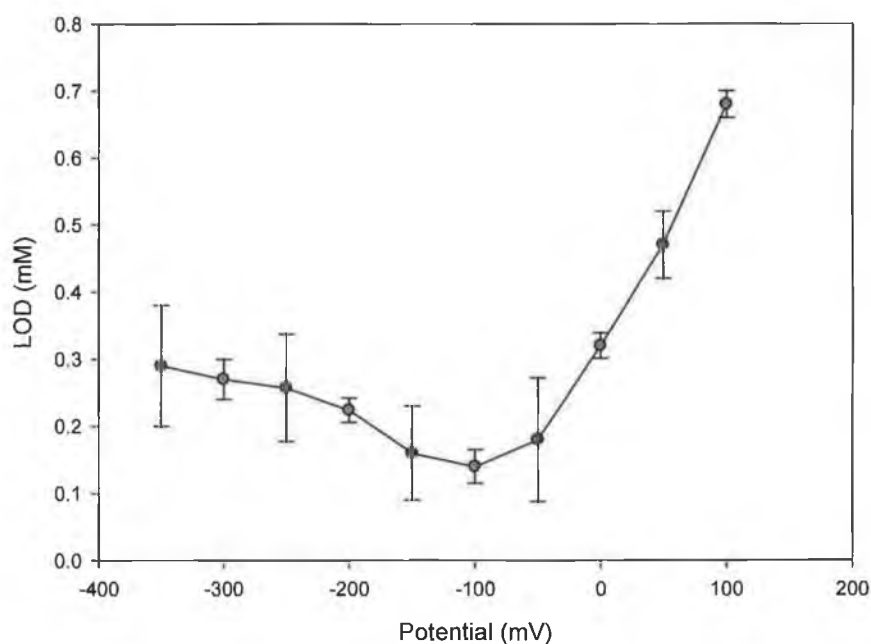


**Figure 2.18.** Investigation of the limit of detection for the analysis of  $\text{H}_2\text{O}_2$  as a function of the potential applied. Experimental set up as in *Figure 2.17*.

### 2.3.8 Optimisation of the working pH and calibration of the nanoPANI based sensor for the analysis of hydrogen peroxide

In order to select the optimal pH, an experiment was carried out in a batch system measuring the signal generated by a solution of 8 mM  $\text{H}_2\text{O}_2$  in buffers at different pH at the applied potential of -0.1 V. Citrate buffer was used to prepare solutions at pH between 4.0 and 5.5 and phosphate buffer for the solutions at pH from 6.0 to 9.0. The results are presented in *Figure 2.19*. It can be seen that the catalytic reduction of hydrogen peroxide at the nanoPANI-modified electrode appeared to be independent of pH. In fact, the amperometric signals which resulted were of the same magnitude across the entire pH range tested. This could be explained by the fact that the reduction process of  $\text{H}_2\text{O}_2$  does not involve protons. It has already been stated that the

presence of DBSA inside the polymer structure guarantees the electroactivity and conductivity of the polymer itself over a wide range of pH and even at alkaline pH, so therefore the intrinsic catalytic property is not affected by the acidity of the solution<sup>28</sup>. At the applied potential of -0.1 V it also appeared that the background noise was of the same amplitude at all the pH tested, so the investigation of the signal to noise ratio was not necessary in this case. Considering the fact that the pH did not influence the performance of the sensor, pH 6.8 was chosen as the working pH for further analysis.

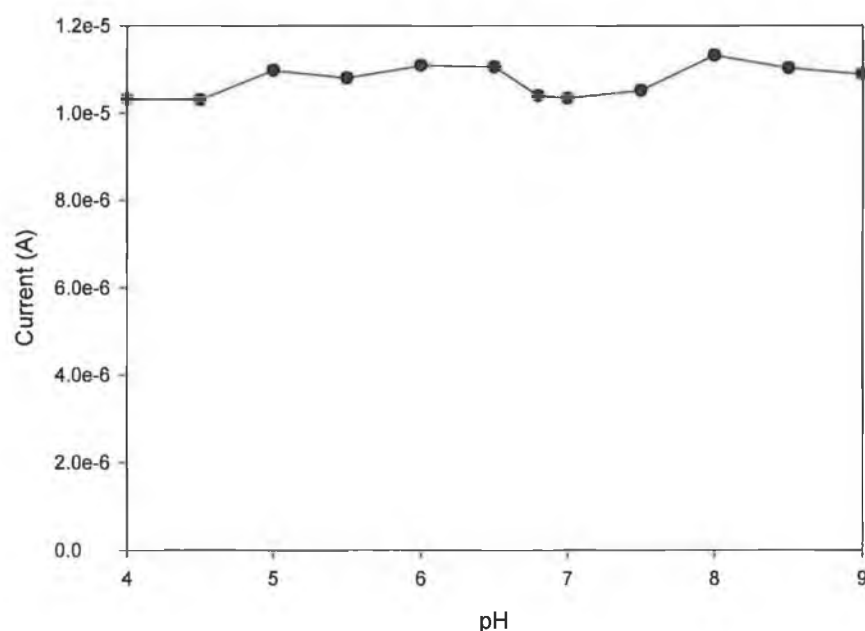


**Figure 2.19.** Working buffer optimisation. Amperometric signals generated by the reduction of 8 mM solution of H<sub>2</sub>O<sub>2</sub> in batch system at potential of -0.1 V (vs. Ag/AgCl) and using different working buffers at pH between 4 and 9. (Electrode surface area: 0.07 cm<sup>2</sup>).

The excellent processability of PANI NPs allows the development of different sensing and biosensing platforms. In the latter case, for example, biomolecules (enzymes) could be added to the nanoPANI suspension for a co-deposition onto electrode surfaces, in order to have a biosensing device specific for the enzyme substrate analyte and exploiting at the same time the catalytic properties of the polymer film itself. An example could be represented by the incorporation of GOX to the nanoPANI film for the development of a glucose sensor, through the detection of hydrogen peroxide by the nanoPANI film-modified electrode. It is important for this biosensing developments that the nanoPANI suspension presents a good

biocompatibility, so that the interaction with biomolecules do not cause functionality alterations.

The natural pH of the nanoPANI suspension after the synthesis is about 4.3 as stated in section 2.2 due to the presence of DBSA. This acidic pH could represent a problem for the processability of this material together with pH-sensitive biomolecules such as enzymes in the fabrication of biosensors. A study was thus performed in order to investigate the effect of the nanoPANI suspension pH on the catalytic properties towards hydrogen peroxide.

Different electrodes were prepared using the nanoPANI suspension at the natural pH 4.3 and then at pH adjusted to the values 5, 5.5, 6, 6.5 and 7. The nanoPANI modified electrodes so prepared were tested in the batch system, in PBS buffer (pH 6.8) recording the signals generated by the reduction of a 8 mM solution of  $H_2O_2$  at the potential of -0.1 V. As it can be seen in the *Figure 2.20* the nanoPANI suspension pH could be varied without altering the catalytic response of the sensor. In fact, the signals recorded in the experiment were much the same amplitude for the entire range of pH tested. A practical consequence of this is the possibility to adjust the suspension pH at optimal values for biomolecules, so that both the PANI NPs and an enzyme, for example, could be processed together in the construction of a biosensor<sup>69</sup>.

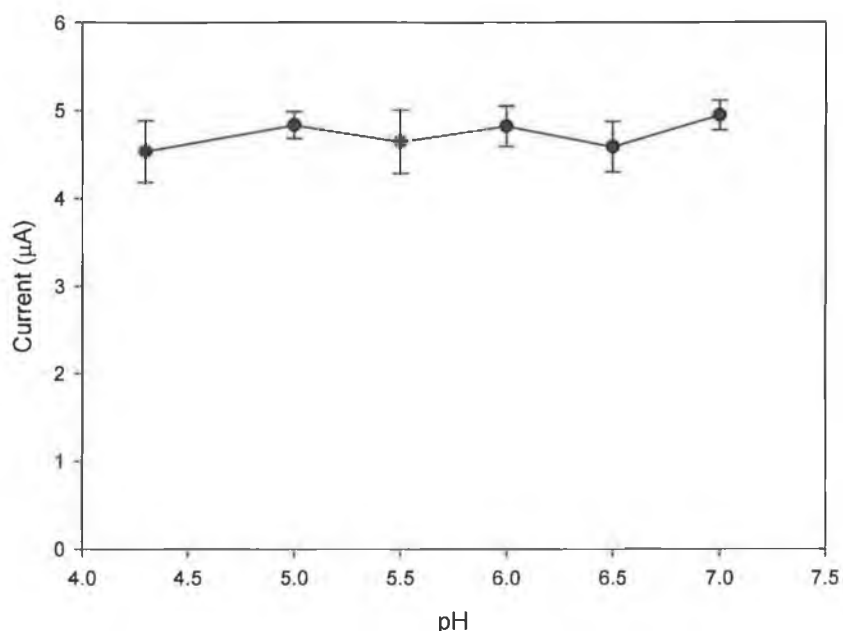


**Figure 2.20.** Effect of the nanoPANI suspension pH on the catalytic reduction of  $H_2O_2$ . NanoPANI modified SPEs were prepared using the nanoPANI suspension at pH adjusted to the values 4.3, 5, 5.5, 6, 6.5 and 7 and tested in batch system at the working potential of -0.1 V (vs. Ag/AgCl), using PBS (pH 6.8) as the working buffer in the presence of  $H_2O_2$  8 mM. (Electrode surface area:  $0.07 \text{ cm}^2$ ).

Using the optimised conditions such as working potential, working buffer, nanoPANI suspension pH, the sensor was calibrated for the analysis of hydrogen peroxide. The calibration curve together with the typical step-shaped amperogram is illustrated in *Figure 2.21*. The sensor showed linearity from 1 mM to 0.1 M with  $r^2 = 0.999$  ( $n = 6$ ). The limit of detection was determined to be 0.14 mM considering the  $S/N=3$ . In terms of reproducibility, it was found that the relative standard deviation (RSD) of the nanoPANI-based sensor was 2.85% for nine successive measurements of 8 mM  $H_2O_2$  (data not shown).

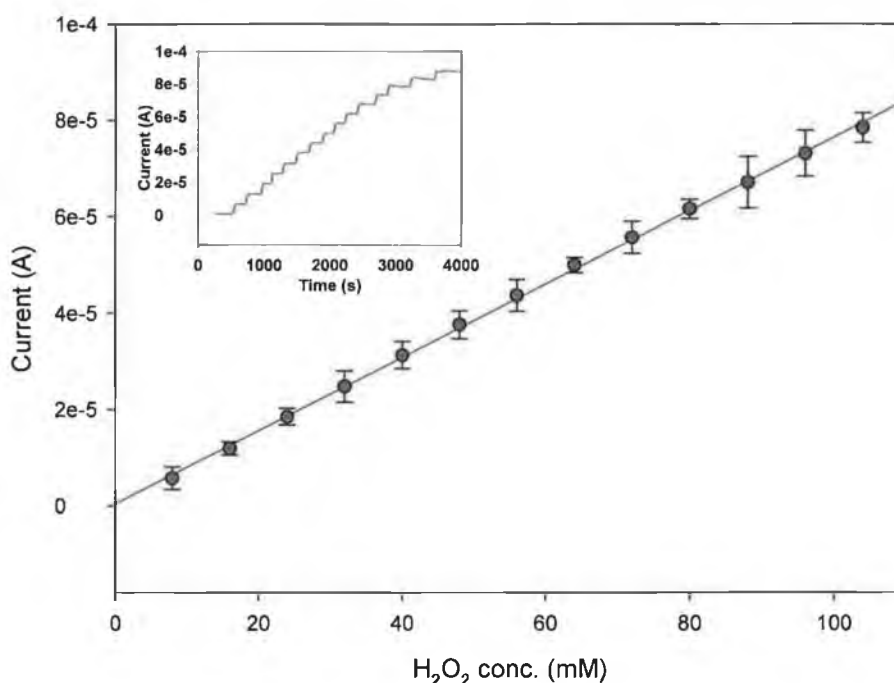


**Figure 2.21.** Calibration curve for the detection of  $H_2O_2$  with nanoPANI modified SPE in batch system at the working potential of  $-0.1$  V (vs. Ag/AgCl) and using PBS (pH 6.8) as the working buffer. ( $y = 7.6 \times 10^{-7}x + 4.6 \times 10^{-7}$ ,  $r^2 = 0.999$ , electrode surface area:  $0.07$  cm<sup>2</sup>). Inset: step-shaped amperogram generated by the hydrogen peroxide injections.

*Table 2.2* summarizes recent biosensing applications based on conducting polymers for the analysis of hydrogen peroxide. It can be seen that the performance of electrochemical sensing devices using enzymes as catalysts are in general better than that of the sensor developed in this work. Enzyme-based catalysis can reach lower limit of detections and higher sensitivities. However, the linearity range is

significantly wide and the sensor reaches the saturation only at very high hydrogen peroxide concentrations (>0.1 M). Further optimisations of the present system may lead to greater improvements in the analytical performance, e.g., smaller nanoparticles etc.

Polymer-based biosensor	pH	Potential applied	LOD	LRR	Ref
Hb/DNA/PPD on Au electrode	5.5	-0.3 V vs. SCE	1.0 $\mu$ M	1.7 $\mu$ M - 3 mM	77
Ordered mesoporous PANI/HRP on GC electrode	7	-0.1 V vs. SCE	0.63 $\mu$ M	1.0 $\mu$ M - 2.0 mM	78
HRP/AuNP/Thi/poly ( <i>p</i> -ABSA) on GC electrode	7	-0.45 vs. SCE	0.64 $\mu$ M	2.6 $\mu$ M - 8.8 mM	79
Silica-PANI/HRP on GC electrode	7	-0.1 V vs. Ag/AgCl	0.18 $\mu$ M	0.3 - 8.8 $\mu$ M	80
CNT/PANI/HRP on GC electrode	7	-0.1 V vs. Ag/AgCl	68 nM	0.2 - 19 $\mu$ M	81
PMAS/PLL/HRP on GC electrode	7	-0.1 V vs. Ag/AgCl	10 $\mu$ M	0.01 - 0.1 mM	82
HRP/PPy on Pt electrode	6	+0.15 V vs. Ag/AgCl	0.1 $\mu$ M	0.5 $\mu$ M - 0.6 mM	40
HRP/PANI on Pt electrode	7	-0.4 V vs. Ag/AgCl	0.25 mM.	0.25 mM - 5 mM	83

**Table 2.2.** Biosensing applications based on conducting polymers for the analysis of hydrogen peroxide.



### 2.3.9 Development of an inkjet printed nanoPANI film electrode for ascorbic acid and hydrogen peroxide detection

In this work various electrodes were prepared using the inkjet printing technology to deposit the PANI nanoparticles onto the screen-printed electrodes. This technique had already been investigated and optimised by Morrin *et al*<sup>71</sup>. Using the procedure discussed in section 2.2.8 a batch of electrodes were prepared by inkjet printing 25 layers of nanoPANI on the active screen-printed electrode surface. From a previous work the sensors prepared with 25 layers were found to be the best in terms of the amperometric response and also presented an electrochemical behaviour similar to the sensors prepared by drop-coating 5  $\mu\text{l}$  of the nanoPANI suspension (data not shown). The electrodes prepared were then tested for the analysis of ascorbic acid and hydrogen peroxide using exactly the same conditions optimised and discussed in sections 2.3.5 and 2.3.8. As can be seen in *Figure 2.22* for both analyses, the electrodes prepared by means of the inkjet printing technique demonstrated very similar performance to those prepared by using the drop-casting method. As a matter of fact, for the analysis of ascorbic acid the sensitivities for the sensors prepared by the drop-coating and the inkjet printing method were found to be 4.07  $\mu\text{A}/\text{mM}$  and 4.59  $\mu\text{A}/\text{mM}$ , respectively. The linear range resulted for both from 0.5 to 8 mM. The limit of detections were found to be 8.3  $\mu\text{M}$  for the drop-coated sensor and 7.4  $\mu\text{M}$  for the inkjet-printed (S/N=3).

With regard to the analysis of hydrogen peroxide the sensitivities were found to be 0.76  $\mu\text{A}/\text{mM}$  for the drop-coated sensor and 0.66  $\mu\text{A}/\text{mM}$  for the inkjet-printed. Again, the linear range was similar and resulted for both from 1 mM to 0.1 M with the limit of detections of 0.14 and 0.21 mM for the drop-coated and the inkjet-printed, respectively (S/N=3).

The significant correspondence in the electrochemical behaviour of the two types of sensors could find two explanations. Firstly, the two sensors presented a very similar nanoPANI film thickness, which guaranteed a similar conductivity and thus the same electrochemical responses towards the analysis of both hydrogen peroxide and ascorbic acid. Secondly, the inkjet printing process, although different from the drop-coating one, did not affect the chemical and physical characteristics of the PANI NPs, which did not alter the catalytic electrode's properties.

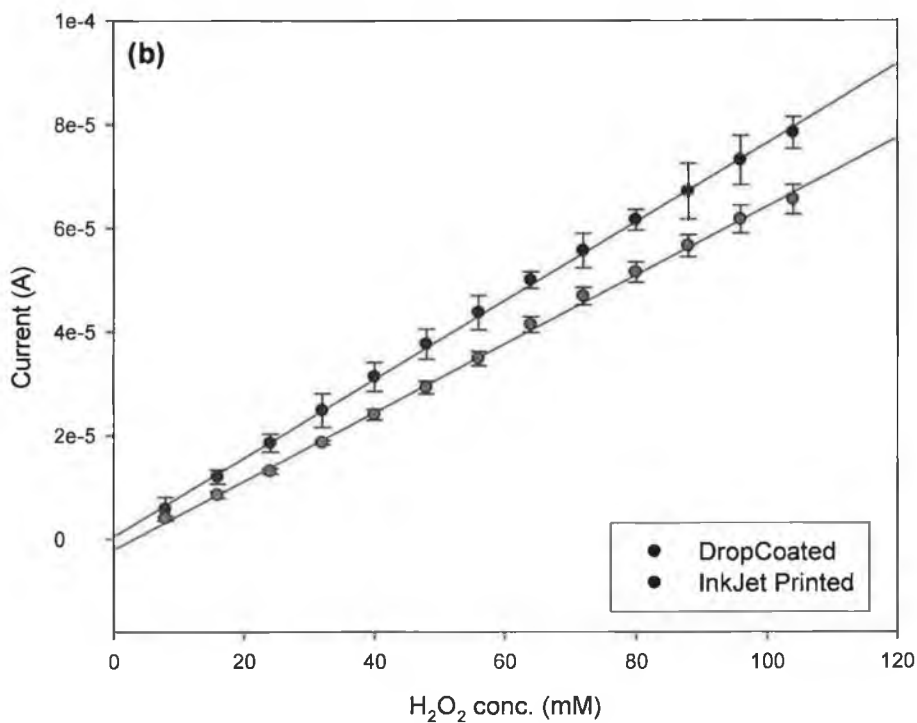
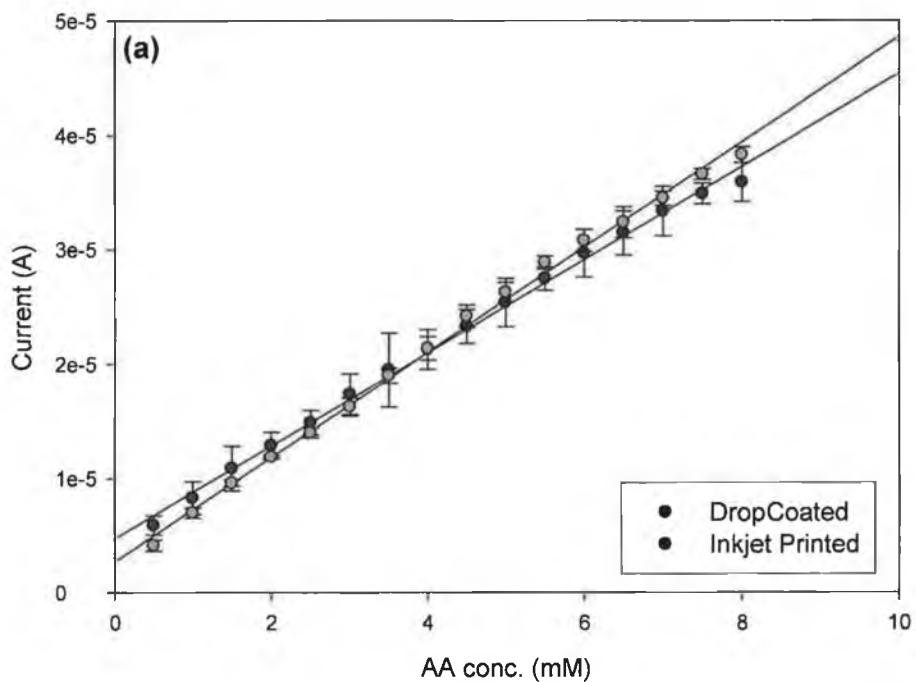


**Figure 2.22.** Calibration curve for the detection of (a) ascorbic acid and (b)  $H_2O_2$  with nanoPANI-modified SPEs prepared using the drop-coating and the inkjet printing techniques. Working potential:  $-0.1$  V (vs. Ag/AgCl) in PBS (pH 6.8) working buffer. (Electrode surface area:  $0.07$  cm<sup>2</sup>).

SEM analysis was also carried out to image the nanoPANI films inkjet printed on screen-printed electrodes. *Figure 2.23a* shows the morphology of a bare carbon paste electrode, where it can be seen to be quite a rough, nodular structure. *Figure 2.23b, c* and *d* show 10, 20 and 30 prints, respectively, of the nanoPANI on carbon paste electrodes. It can be seen that the nodular structure of the carbon paste becomes more concealed as the inkjet printed film builds on the surface, resulting in increasingly smoother, featureless surfaces. Increasing the number of prints to 30 (*Figure 2.23d*) results in a homogeneously smooth film at the length scale of the original nodules. The large ridges that are observed are as a direct result of the cracks in the underlying carbon paste. Even at higher magnifications, the individual nanoPANI particles were not visible, as it would appear that, on this substrate, they coalesce to form a homogeneous film rather than result in a nanostructured interface.

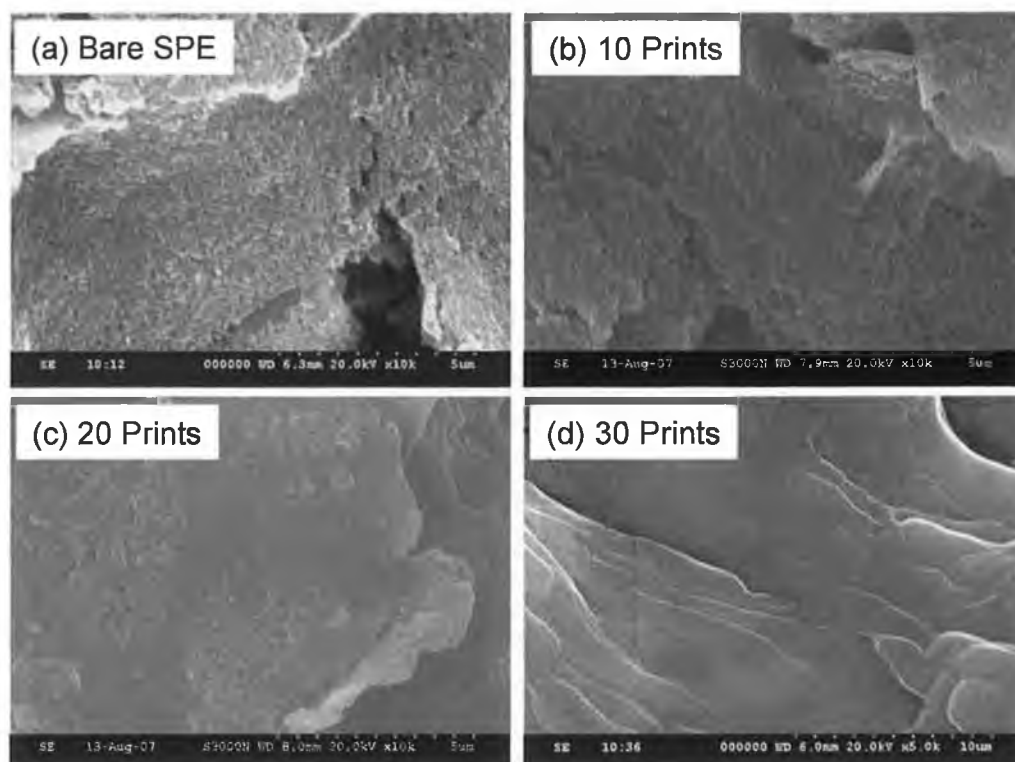


**Figure 2.23.** SEM images of (a) bare carbon paste and (b) 10, (c), 20 and (d) 30 inkjet printed films of nanoPANI on the carbon paste substrate. All samples were gold sputtered before the analysis.

The inkjet printed nanoPANI film morphology observed after 30 prints represent a further proof that the catalytic properties toward ascorbic acid and hydrogen peroxide cannot derive only from a surface area enhancement. In fact, as it can be seen from the image 2.23d, the particles form a continuous film, losing any nanostructural surface morphology, resulting in a surface area probably smaller than that of the porous bulk PANI film.

The mechanism may be linked to the synthetic pathway of the PANI NPs, being formed on a micellar template of DBSA where they polymerize to form morphologically distinct polymer chains. In the traditional electrosynthesized bulk PANI film, there may be a limited number of suitable catalytic sites for the electrocatalysis to proceed efficiently, while through this synthetic procedure, the number of such sites seems to be enhanced substantially, making these nanoparticles efficient nanoorganoelectrocatalysts.

The results presented open novel economical avenues for conducting polymer applications. Coupling the use of conducting polymer nanoparticles as the building material with the inkjet printing deposition technique, enabled a practical and rapid route to the fabrication of sensing devices.

## **2.4 CONCLUSION**

Polyaniline is one of the most widely studied conducting polymers and because it possesses a broad range of tuneable properties derived from its structural flexibility, it has been adopted in numerous applications including chemical and biological sensors. However, it presents several drawbacks in relation to its processability especially for mass production processes. It is insoluble in common solvents, the monomer, aniline, is a carcinogen, it must be distilled prior to use, stored under nitrogen, and also strong acidic conditions are required for the formation of the most highly conductive form of PANI. These drawbacks have been overcome by the possibility of synthesising a nanodispersed polyaniline with enhanced electroactivity and conductivity but also with much greater applicability.

Drop-coating deposition methods were used to modify the surface of screen-printed electrodes with these novel PANI NPs for the preparation of two chemical sensors for the analysis of both ascorbic acid and hydrogen peroxide.

The ability to catalyze the oxidation of ascorbic acid was well known for the bulk polyaniline, but it has been demonstrated here also for this conducting polymer in a nanodimension structure. The sensor was able to detect ascorbic acid at the very low potential of 0 V vs. Ag/AgCl reducing considerably possible interferences. The resulting linear range from 0.5 to 8 mM allows the sensor to be applied for example, to the analysis of ascorbic acid in beverages and pharmaceutical formulations. However, the nanoPANI film did not exhibit any distinct difference in electrocatalytic behaviour than bulk electropolymerized films.

With regard to the second analytical development, the ability to catalyse the reduction of hydrogen peroxide at -0.1 V vs. Ag/AgCl seemed to appear for this material only at nanodimension scale. In fact the bulk PANI was nearly incapable of electroreduction of hydrogen peroxide at the same potential. Initial observations excluded that the catalytic reduction of hydrogen peroxide resulted from a simple nanoparticle surface area enhancement and that the mechanism could possibly be linked to the synthetic pathway of these polymer nanoparticles. However, while the reaction mechanism for the oxidation of ascorbic acid at PANI films has been extensively investigated and published in the past, the mechanism for the reduction of hydrogen peroxide still needs deeper investigation for a complete understanding. The work presented here focused mainly on the optimisation of all the analytical conditions for the best sensing performance. This was found to be not as good as for other sensors exploiting enzymes to catalyse the reaction, but was extremely promising taking into account the simplicity of the sensor fabrication methodology and the opportunities for future refinements.

The high processability of PANI NPs was also demonstrated at the end of the work by preparing various sensors by means of the inkjet printing deposition technique. This method allowed a simple and precise patterning of the nanoparticulate conducting polymer onto screen-printed electrode surfaces. The sensors so prepared were tested for the analysis of both ascorbic acid and hydrogen peroxide using the conditions

optimised previously and resulted in performances very similar to the sensors prepared with the casting method. The inkjet printing deposition technique then, resulted in extremely precise patterning of the PANI NPs onto the electrode surface without affecting their catalytic properties. Coupling, therefore, the use of this novel and highly processable nanoparticulate conducting polymer with the rapid and simple inkjet printing deposition technique, resulted in a promising novel methodology applicable to the mass production of chemical but also biological sensing devices.

## 2.5 REFERENCES

---

- 1 A. Mirmohseni, R. Solhjo. Preparation and characterization of aqueous polyaniline battery using a modified polyaniline electrode. *European Polymer Journal*, **39**, (2003), 219-223.
- 2 M. Kraljić, Z. Mandić, L. Duić. Inhibition of steel corrosion by polyaniline coatings. *Corrosion Science*, **45**, (2003), 181-198.
- 3 M. Malta, E.R. Gonzalez, R.M. Torresi. Electrochemical and chromogenic relaxation processes in polyaniline films. *Polymer*, **43**, (2002), 5895-5901.
- 4 S. Mu, H. Xue. Bioelectrochemical characteristics of glucose oxidase immobilized in a polyaniline film. *Sensors and Actuators, B: Chemical*, **31**, (1996), 155-160.
- 5 A. Morrin, A. Guzman, A.J. Killard, J.M. Pingarron, M.R. Smyth. Characterisation of horseradish peroxidase immobilisation on an electrochemical biosensor by colorimetric and amperometric techniques. *Biosensors and Bioelectronics*, **18**, (2003), 715-720.
- 6 D. Mackey, A.J. Killard, A. Ambrosi, M.R. Smyth. Optimizing the ratio of horseradish peroxidase and glucose oxidase on a bienzyme electrode: Comparison of a theoretical and experimental approach. *Sensors and Actuators B: Chemical*, **122**, (2007), 395-402.

- 
- 7 A. Malinauskas. Electrocatalysis at conducting polymers. *Synthetic Metals*, **107**, (1999), 75-83.
  - 8 R. Mazeikienė, G. Niaura, A. Malinauskas. In situ Raman spectroelectrochemical study of electrocatalytic oxidation of ascorbate at polyaniline-and sulfonated polyaniline-modified electrodes. *Electrochimica Acta*, **51**, (2006), 5761-5766.
  - 9 J. Yano, K. Ogura. The kinetic difference between hydroquinone and Fe<sup>2+</sup> in the electrochemical response of a polyaniline-film-coated electrode. *Synthetic Metals*, **52**, (1992), 21-31.
  - 10 P.N. Bartlett, P.R. Birkin, E.N.K. Wallace. Oxidation of β-nicotinamide adenine dinucleotide (NADH) at poly(aniline)-coated electrodes. *Journal of the Chemical Society - Faraday Transactions*, **93**, (1997), 1951-1960.
  - 11 Z. Mandić, L. Duić. Polyaniline as an electrocatalytic material. *Journal of Electroanalytical Chemistry*, **403**, (1996), 133-141.
  - 12 A. Maines, D. Ashworth, P. Vadgama. Enzyme electrodes for food analysis. *Food technology and biotechnology*, **34**, (1996), 31-37.
  - 13 G.N. Bijur, M.E. Ariza, C.L. Hitchcock, M.V. Williams. Antimutagenic and promutagenic activity of ascorbic acid during oxidative stress. *Environmental and molecular mutagenesis*, **30**, (1997), 339-345.
  - 14 E. Shohami, E. BeitYannai, M. Horowitz, R. Kohen. Oxidative stress in closed-head injury. *Journal of Cerebral Blood Flow and Metabolism*, **17**, (1997), 1007-1012.
  - 15 I. Koshiishi, T. Imanari. Measurement of ascorbate and dehydroascorbate contents in biological fluids. *Analytical Chemistry*, **69**, (1997), 216-220.
  - 16 A. Malinauskas, R. Garjonyte, R. Mazeikiene, I. Jureviciute. Electrochemical response of ascorbic acid at conducting and electrogenerated polymer modified electrodes for electroanalytical applications: a review. *Talanta*, **64**, (2004), 121-129.
  - 17 L. Castelletti, S.A. Piletsky, A.P.F. Turner, P.G. Righetti, A. Bossi. Development of an integrated capillary electrophoresis/sensor for L-ascorbic acid detection. *Electrophoresis*, **23**, (2002), 209-214.
  - 18 A. Bossi, S.A. Piletsky, E.V. Piletska, P.G. Righetti, A.P.F. Turner. An assay for ascorbic acid based on polyaniline-coated microplates. *Analytical Chemistry*, **72**, (2000), 4296-4300.

- 
- 19 G.G. Wallace, G.M. Spinks, L.A.P. Kane-Maguire, P.R. Teasdale. Conductive electroactive polymers: intelligent materials systems, 2nd ed. Boca Raton, FL: CRC Press., 2002.
  - 20 I.G. Casella, M.R. Guascito. Electrocatalysis of ascorbic acid on the glassy carbon electrode chemically modified with polyaniline films. *Electroanalysis*, **9**, (1997), 1381-1386.
  - 21 P.J. O'Connell, C. Gormally, M. Pravda, G.G. Guilbault. Development of an amperometric L-ascorbic acid (Vitamin C) sensor based on electropolymerised aniline for pharmaceutical and food analysis. *Analytica Chimica Acta*, **431**, (2001), 239-247.
  - 22 S.L. Mu, J.Q. Kan. The electrocatalytic oxidation of ascorbic acid on polyaniline film synthesized in the presence of ferrocenesulfonic acid. *Synthetic Metals*, **132**, (2002), 29-33.
  - 23 R.P. Kalakodimi, M. Nookala. Electrooxidation of ascorbic acid on a polyaniline-deposited nickel electrode: surface modification of a non-platinum metal for an electrooxidative analysis. *Analytical Chemistry*, **74**, (2002), 5531-5537.
  - 24 G. Erdogdu, A.E. Karagozler. Investigation and comparison of the electrochemical behavior of some organic and biological molecules at various conducting polymer electrodes. *Talanta*, **44**, (1997), 2011-2018.
  - 25 J.J. Sun, D.M. Zhou, H.Q. Fang, H.Y. Chen. The electrochemical copolymerization of 3,4-dihydroxybenzoic acid and aniline at microdisk gold electrode and its amperometric determination for ascorbic acid. *Talanta*, **45**, (1998), 851-856.
  - 26 J.J. Xu, D.M. Zhou, H.Y. Chen. Amperometric determination of ascorbic acid at a novel 'self-doped' polyaniline modified microelectrode. *Fresenius Journal of Analytical Chemistry*, **362**, (1998), 234-238.
  - 27 D.M. Zhou, J.J. Xu, H.Y. Chen, H.Q. Fang. Ascorbate sensor based on self-doped polyaniline. *Electroanalysis*, **9**, (1997), 1185-1188.
  - 28 P.N. Bartlett, E.N.K. Wallace. The oxidation of ascorbate at poly(aniline)-poly(vinylsulfonate) composite coated electrodes. *Physical Chemistry Chemical Physics*, **3**, (2001), 1491-1496.
  - 29 J. Yáñez Heras, A.F. Forte Giacobone, F. Battaglini. Ascorbate amperometric determination using conducting copolymers from aniline and N-(3-propane sulfonic acid) aniline. *Talanta*, **71**, (2007), 1684-1689.
  - 30 I. Jurevičiūtė, K. Brazdžiuvienė, L. Bernotaitė, B. Šalkus, A. Malinauskas. Polyaniline-modified electrode as an amperometric ascorbate sensor. *Sensors and Actuators B: Chemical*, **107**, (2005), 716-721.



- 
- 31 R. Mažeikienė, G. Niaura, A. Malinauskas. In situ Raman spectroelectrochemical study of electrocatalytic oxidation of ascorbate at polyaniline- and sulfonated polyaniline-modified electrodes. *Electrochimica Acta*, **51**, (2006), 5761-5766.
- 32 E.C. Hurdis, H. Romeyn Jr. Accuracy of determination of hydrogen peroxide by cerate oxidimetry. *Analytical Chemistry*, **26**, (1954), 320-325.
- 33 Z. Genfa, P.K. Dasgupta, W.S. Edgmond, J.N. Marx. Determination of hydrogen peroxide by photoinduced fluorogenic reactions. *Analytica Chimica Acta*, **243**, (1991), 207-216.
- 34 F.R.P. Rocha, E.R. Torralba, B.F. Reis, A.M. Rubio, M. de la Guardia. A portable low cost equipment for flow injection chemiluminescence measurements. *Talanta*, **67**, (2005), 673-677.
- 35 P.A. Tanner, A.Y.S. Wong. Spectrophotometric determination of hydrogen peroxide in rain water. *Analytica Chimica Acta*, **370**, (1998), 279-287.
- 36 K.S. Tseng, L.C. Chen, K.C. Ho. Amperometric detection of hydrogen peroxide at Prussian blue-modified FTO electrode. *Sensors and Actuators B: Chemical*, **108**, (2005), 738-745.
- 37 Y. Lin, X. Cui, L. Li. Low-potential amperometric determination of hydrogen peroxide with a carbon paste electrode modified with nanostructured cryptomelane-type manganese oxides. *Electrochemistry Communications*, **7**, (2005), 166-172.
- 38 G.G. Guilbault, G.J. Lubrano, An enzyme electrode for the amperometric determination of glucose, *Analytica Chimica Acta*, **64**, (1973), 439-455.
- 39 A. Lindgren, T. Ruzgas, L. Gorton, E. Csoregi, G. Bautista Ardila, I.Y. Sakharov, I.G. Gazaryan. Biosensors based on novel peroxidases with improved properties in direct and mediated electron transfer. *Biosensors and Bioelectronics*, **15**, (2000), 491-497.
- 40 S. Razola Serradilla, B. Ruiz Lopez, N. Diez Mora, H.B. Mark, J.M. Kauffmann. Hydrogen peroxide sensitive amperometric biosensor based on horseradish peroxidase entrapped in a polypyrrole electrode. *Biosensors and Bioelectronics*, **17**, (2002), 921-928.
- 41 U. Wollenberger, V. Bogdanovskaya, S. Bobrin, F. Scheller, M. Tarasevich. Enzyme electrodes using bioelectrocatalytic reduction of hydrogen peroxide. *Analytical Letters*, **23**, (1990), 1795-1808.
- 42 T. Ruzgas, L. Gorton, J. Emnéus, G. Marko-Varga. Kinetic models of horseradish peroxidase action on a graphite electrode. *Journal of Electroanalytical Chemistry*, **391**, (1995), 41-49.

- 
- 43 A. Mulchandani, C.L. Wang, H.H. Weetall. Amperometric detection of peroxides with poly(anilinomethylferrocene)-modified enzyme electrodes. *Analytical Chemistry*, **67**, (1995), 94-100.
- 44 T. Tatsuma, K. Ariyama, N. Oyama. Electron transfer from a polythiophene derivative to compounds I and II of peroxidases. *Analytical Chemistry*, **67**, (1995), 283-287.
- 45 F. Ricci, G. Palleschi. Sensor and biosensor preparation, optimization and applications of Prussian blue modified electrodes. *Biosensors and Bioelectronics*, **21**, (2005), 389-407.
- 46 Y. Yang, S. Mu. Bioelectrochemical responses of the polyaniline horseradish peroxidase electrodes. *Journal of Electroanalytical Chemistry*, **432**, (1997), 71-78.
- 47 P. Santhosh, K.M. Manesh, A. Gopalan, K.P. Lee. Fabrication of a new polyaniline grafted multi-wall carbon nanotube modified electrode and its application for electrochemical detection of hydrogen peroxide. *Analytica Chimica Acta*, **575**, (2006), 32-38.
- 48 C. Coutanceau, A. El Hourch, P. Crouigneau, J.M. Leger, C. Lamy. Conducting polymer electrodes modified by metal tetrasulfonated phthalocyanines: Preparation and electrocatalytic behaviour towards dioxygen reduction in acid medium. *Electrochimica Acta*, **40**, (1995), 2739-2748.
- 49 A. Morrin, F. Wilbeer, O. Ngamna, S.E. Moulton, A.J. Killard, G.G. Wallace, M.R. Smyth. Novel biosensor fabrication methodology based on processable conducting polyaniline nanoparticles. *Electrochemistry Communications*, **7**, (2005), 317-322.
- 50 S. Park, M. Cho, H. Choi. Synthesis and electrical characteristics of polyaniline nanoparticles and their polymeric composite. *Current Applied Physics*, **4**, (2004), 581-583.
- 51 P. Somani. Synthesis and characterization of polyaniline dispersions. *Materials Chemistry and Physics*, **77**, (2003), 81-85.
- 52 R. Gangopdhyay, A. De, G. Ghosh. Polyaniline-poly(vinyl alcohol) conducting composite: material with easy processability and novel application potential. *Synthetic Metals*, **123**, (2001), 21-31.
- 53 S. Moulton, P. Innis, L. Kane-Maguire, O. Ngamna, G. Wallace. Polymerisation and characterisation of conducting polyaniline nanoparticle dispersions. *Current Applied Physics*, **4**, (2004), 402-406.
- 54 M. Han, S. Cho, S. Oh, S. Im. Preparation and characterization of polyaniline nanoparticles synthesized from DBSA micellar solution. *Synthetic Metals*, **126**, (2002), 53-60.

- 
- 55 J.X. Huang, R.B. Kaner. Nanofiber Formation in the Chemical Polymerization of Aniline: A Mechanistic Study. *Angewandte Chemie International Edition*, **43**, (2004), 5817-5821.
- 56 O. Ngamna, A. Morrin, A.J. Killard, S.E. Moulton, M.R. Smyth, G.G. Wallace. Inkjet printable polyaniline nanoformulations. *Langmuir*, **23**, (2007), 8569-8574.
- 57 H.S. Xia, Q. Wang. Synthesis and characterization of conductive polyaniline nanoparticles through ultrasonic assisted inverse microemulsion polymerization. *Journal of Nanoparticle Research*, **3**, (2001), 401-411.
- 58 J. Wang, B. Zou, X. Hong, D.M. Collard. Photoinduced vibrational absorptions from poly(3-octylthiophene)/Fe<sub>2</sub>O<sub>3</sub> nanoparticle composite, a time-resolved FTIR study. *Synthetic Metals*, **113**, (2000), 223-226.
- 59 K.Grennan, A.J. Killard, C. Hansen, A. Cafolla, M.R. Smyth. Optimisation and characterisation of biosensors based on polyaniline. *Talanta*, **68**, (2006), 1591-1600.
- 60 A. Fujii, H. Mizukami, Y. Hashimoto, T. Umeda, Y. Nishihara, M. Ozaki, K. Yoshino. Highly efficient photovoltaic cells composed of interpenetrating conducting polymer/C[60] heterojunction. *Synthetic metals*, **152**, (2005), 121-124.
- 61 Y. Zhang, Y. Guan, J. Liu, J. Xu, W. Cao. Fabrication of covalently attached conducting multilayer self-assembly film of polyaniline by in situ coupling reaction. *Synthetic Metals*, **128**, (2002), 305-309.
- 62 G. Li, C. Martinez, S. Semancik. Controlled Electrophoretic Patterning of Polyaniline from a Colloidal Suspension. *Journal of the American Chemical Society*, **127**, (2005), 4903-4909.
- 63 P. Calvert. Inkjet printing for materials and devices. *Chemistry of Materials*, **13**, (2001), 3299-3305.
- 64 B. Chen, T. Cui, Y. Liu, K. Varahramyan. All-polymer RC filter circuits fabricated with inkjet printing technology. *Solid-State Electronics*, **47**, (2003), 841-847.
- 65 K. Paul, W.S. Wong, S. Ready, R. Street. Additive jet printing of polymer thin film resistors. *Applied Physics Letters*, **83**, (2003), 2070-2072.
- 66 H. Sirringhaus, T. Kawase, R.H. Friend, T. Shimoda, M. Inbasekaran, W. Wu, E.P. Woo. High-resolution inkjet printing of all-polymer transistor circuits. *Science*, **290**, (2000), 21232-21236.
- 67 M.F. Mabrook, C. Pearson, M.C. Petty. An inkjet printed chemical fuse. *Applied Physics Letters*, **86**, (2005), 346-351.
- 68 J.P. Ferraris, T.H. Dam, D. Meeker. Method of creating colour-changing displays. (2002). Patent No: US 6,501,587.

- 
- 69 L. Setti, A. Morgera, B. Ballarin, A. Filippini, D. Frascaro, C. Piana. An amperometric glucose biosensor prototype fabricated by thermal inkjet printing. *Biosensors and Bioelectronics*, **20**, (2005), 2019-2026.
- 70 B. Ballarin, A. Fraleoni-Morgera, D. Frascaro, S. Marazzita, C. Piana, L. Setti. Thermal inkjet microdeposition of PEDOT:PSS on ITO-coated glass and characterization of the obtained film. *Synthetic Metals*, **146**, (2004), 201-205.
- 71 A. Morrin, O. Ngamna, A.J. Killard, S.E. Moulton, G.G. Wallace, M.R. Smyth. Inkjet printing: Novel fabrication approach for a catalytic sensor for hydrogen peroxide based on polyaniline nanoparticles. (2007). In Press.
- 72 K. Grennan, A.J. Killard, M.R. Smyth. Physical Characterizations of a Screen-Printed Electrode for Use in an Amperometric Biosensor System. *Electroanalysis*, **13**, (2001), 745-750.
- 73 J. Huang, R.B. Kaner. Nanofiber formation in the chemical polymerization of aniline: A mechanistic study. *Angewandte Chemie International Edition*, **43**, (2004), 5817-5821.
- 74 I.-F. Hu, T. Kuwana. Oxidative mechanism of ascorbic acid at glassy carbon electrodes. *Analytical Chemistry*, **58**, (1986), 3235-3239.
- 75 S.P. Perone, W.J. Kretlow. Application of controlled potential techniques to study of rapid succeeding chemical reaction coupled to electro-oxidation of ascorbic acid. *Analytical Chemistry*, **38**, (1966), 1760-1763.
- 76 M.H. Pournaghi-Azar, R. Ojani. Electrochemistry and electrocatalytic activity of polypyrrole/ferrocyanide films on a glassy carbon electrode. *Journal of Solid State Electrochemistry*, **4**, (2000), 75-79.
- 77 Z. Tong, R. Yuan, Y. Chai, S. Chen, Y. Xie. Amperometric biosensor for hydrogen peroxide based on Hemoglobin/DNA/Poly-2,6-pyridinediamine modified gold electrode. *Thin Solid Films*, **515**, (2007), 8054-8058.
- 78 Q. Xu, J.-J. Zhu, X.-Y. Hu. Ordered mesoporous polyaniline film as a new matrix for enzyme immobilization and biosensor construction. *Analytica Chimica Acta*, **597**, (2007), 151-156.
- 79 F. Gao, R. Yuan, Y. Chai, S. Chen, S. Cao, M. Tang. Amperometric hydrogen peroxide biosensor based on the immobilization of HRP on nano-Au/Thi/poly (*p*-aminobenzene sulfonic acid)-modified glassy carbon electrode. *Journal of Biochemical and Biophysical Methods*, **70**, (2007), 407-413.
- 80 X. Luo, A.J. Killard, A. Morrin, M.R. Smyth. In situ electropolymerised silica-polyaniline core-shell structures: Electrode modification and enzyme biosensor enhancement. *Electrochimica Acta*, **52**, (2007), 1865-1870.

- 
- 81 X. Luo, A.J. Killard, A. Morrin, M.R. Smyth. Enhancement of a conducting polymer-based biosensor using carbon nanotube-doped polyaniline. *Analytica Chimica Acta*, **575**, (2006), 39-44.
- 82 O. Ngamna, A. Morrin, S.E. Moulton, A.J. Killard, M.R. Smyth, G.G. Wallace. An HRP based biosensor using sulphonated polyaniline. *Synthetic Metals*, **153**, (2005), 185-188.
- 83 G. Ntlatseng, R. Mathebe, A. Morrin, E.I. Iwuoha. Electrochemistry and scanning electron microscopy of polyaniline/peroxidase-based biosensor. *Talanta*, **64**, (2004), 115-120.

## **Chapter 3**

**Development of an electrochemical immunosensor  
platform based on enhancement of enzyme-  
channeling using nanoparticles**

### 3.1 INTRODUCTION

Amperometric, enzyme-based biosensors are devices in constant development because of their wide use in fields such as environmental monitoring<sup>1,2,3</sup>, food and beverage quality analysis<sup>4</sup>, process monitoring<sup>5</sup> or biomedicine<sup>6</sup>. They are simple, sensitive, rapid analytical tools constructed by immobilization of enzymes on the electrode's surface. One of the most used strategies to improve analytical performances of enzyme-based biosensors, is represented by the introduction of multiple enzymes schemes. This biosensor configuration is based on the combination of two or more enzymes immobilised on the electrode surface in a way that the reaction product of one enzyme represents the substrate of the other. In *Figure 3.1* a mono-enzyme and a bi-enzyme biosensor configuration are illustrated.

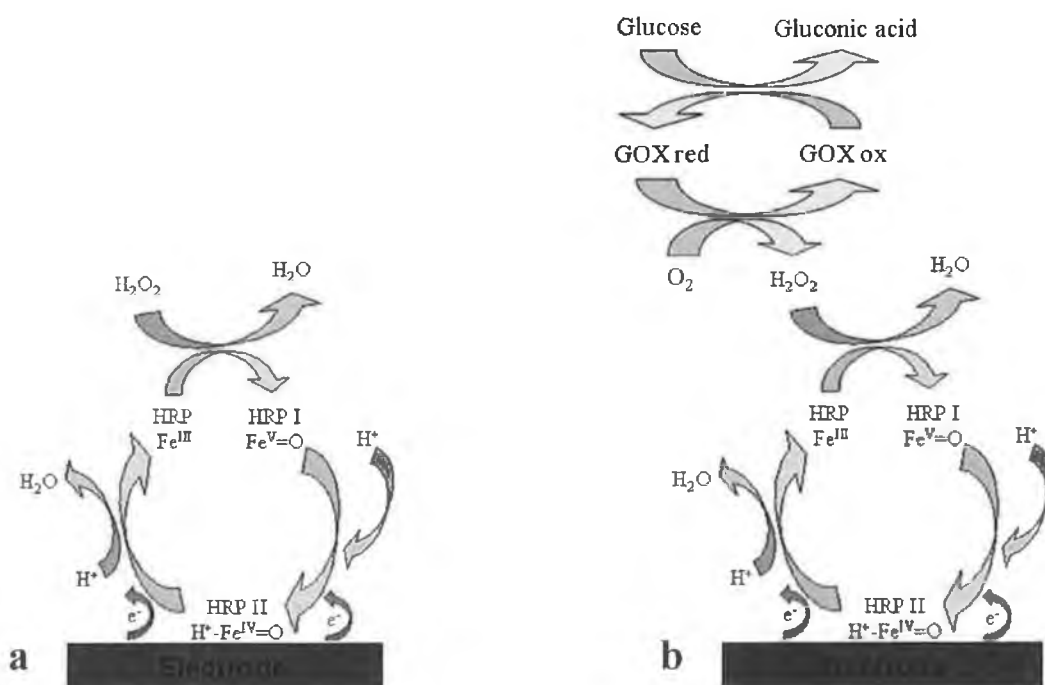


**Figure 3.1.** Different configurations for enzyme-based biosensors. (a) a mono-enzyme system. (b) a bi-enzyme system.

The advantages resulting by the use of multi-enzyme strategies could be summarized as follows:

1. Several enzymes facilitate the biological recognition by sequentially converting the substrates of a series of enzymatic reactions into a final electroactive form; this set-up allows a much wider range of possible analytes detectable<sup>7</sup>;
2. Multiple enzymes, applied in series, may regenerate the first enzyme co-substrate and a real amplification of the biosensor output signal may be achieved by efficient regeneration of another co-substrate of the first enzyme<sup>8</sup>;
3. Multiple enzymes, applied in parallel, may improve the biosensor selectivity by decreasing the local concentration of electrochemical interfering substances: this set-up is an alternative to the use of either a permselective membrane or differential set-up, i.e. subtraction of the output signal generated by the biosensor and by a reference sensor having no biological recognition element<sup>9</sup>.

### 3.1.1 Bienzyme biosensors

The major problem that appears in the use of these enzyme-based devices is the electron transfer between the enzyme's active centre and the electrode. The first-developed, oxidase-based, amperometric biosensors usually involved electrochemical oxidation of  $\text{H}_2\text{O}_2$  resulting from the enzyme's reaction with its natural cofactor,  $\text{O}_2$  or reduction of molecular oxygen. In this type of biosensor, a high operational potential needed to be applied on the interface, which leads to high background currents and to the non-selectivity of the electrodes. Since this drawback became very important in real sample measurements, many solutions to avoid high applied potentials have been developed, leading to the second and third generation of the amperometric enzyme-based biosensors<sup>10</sup>. Addressing the interference elimination problem, Kulys *et al.*, designed the first oxidase/peroxidase bienzyme electrode with a film containing HRP, and GOX that detected glucose by measuring the amount of  $\text{H}_2\text{O}_2$  produced through



the peroxidase. The electron exchange between the peroxidase-active centre and the electrode was carried out by potassium ferrocyanide<sup>11</sup>. Using oxidase/peroxidase bienzyme systems, the detection principle switches from an electrochemical oxidation to a reduction process that is happening at much lower potentials, and therefore, improves considerably the selectivity of the device. Peroxidases are among the very few enzymes able to efficiently transfer electrons from an electrode at relatively low applied potentials<sup>12</sup>. However, in order to improve sensitivity, mediated electron transfer involving a multitude of redox mediators has also been investigated.

Immobilized mediators such as ferrocene derivatives, quinones, quinoid dyes, Ru or Os complexes<sup>13,14</sup> in a polymer matrix have been used to improve electron transfer. However, an alternative and promising approach consists of modifying the electrode surface with conducting polymers such as polyacetylene, polypyrrole (PPy), polyaniline (PANI), and polythiophene<sup>15</sup>. These polymers are attractive materials for application in biosensors due to the considerable flexibility in their chemical structures and their redox characteristics. They have played an important role in the development of novel enzyme-based biosensors, where rapid electron transfer at the electrode surface is required<sup>16</sup>.

Nowadays, the combination of an oxidase and a peroxidase enzyme is widely used to develop biosensors with improved characteristics for the detection of the appropriate substrates (amine oxidase<sup>17</sup>, alcohol oxidase<sup>18</sup>, glucose oxidase<sup>19</sup>, diamine oxidase<sup>20</sup>, choline oxidase<sup>21</sup>, putrescine oxidase<sup>22</sup>, glutamate oxidase<sup>23</sup>, oxalate oxidase<sup>24</sup>, xanthine oxidase<sup>25</sup> and lysine oxidase<sup>26</sup>). Peroxidase from horseradish is usually used in these bienzyme biosensors.

Many different ways exist to immobilize the two enzymes (oxidase and peroxidase) onto an electrode surface. De Benedetto *et al.* in 1995 developed an amperometric bienzyme based biosensor immobilising HRP and GOX on a glassy carbon electrode by an electrosynthesized polypyrrole conducting film. The two enzymes were present in the pyrrole solution so that they could be entrapped in the film during the polymerisation, which was performed at a constant potential of 0.6 V vs Ag/AgCl<sup>27</sup>. Guzman *et al.* proposed a graphite-Teflon<sup>®</sup> composite biosensor where GOX, alcohol oxidase (AOX) and HRP were co-immobilised by simple physical inclusion in the

bulk of the electrode matrix. This trienzyme-based biosensor yielded amperometric responses similar to those obtained with graphite-Teflon<sup>®</sup>-GOX-HRP-ferrocene and graphite-Teflon<sup>®</sup>-AOX-ferrocene electrodes for glucose and ethanol, respectively<sup>28</sup>.

Min-Chol *et al.* designed a heterobilayer biosensor where polypyrrole/GOX and polypyrrole/HRP films were grown potentiostatically at 750 mV vs Ag/AgCl alternately in a solution containing pyrrole and GOX for the first film and pyrrole and HRP for the second<sup>29</sup>. Delvaux *et al.* in 2004 proposed two different geometries to develop a HRP/GOX bienzyme based biosensor. A monolayer enzyme geometry was realised by the covalent immobilisation of both enzymes in the same layer on gold nanotube electrodes using a self-assembled layer of mercaptoethylamine (MPE) and glutaraldehyde as linking agent. The second geometry was composed of a bilayer enzyme electrode where the inner layer (closest to the electrode) was composed of HRP and the outer layer contained GOX<sup>30</sup>. Min *et al.* prepared an enzyme-modified carbon paste (EMCP) electrode containing the two enzymes (GOX and HRP). The solid paste was obtained by adding polyethylenimine and polyester sulfonic acid cation exchanger before drying under reduced pressure. A silver wire inserted into the paste provided the electrical contact<sup>31</sup>. Kobayashi *et al.* prepared enzyme multilayer films on the surface of a glassy carbon electrode by a layer-by-layer deposition of alternate layers of concanavalin A (Con A) with HRP or GOX. The enzyme thin films were formed through biological affinity between Con A and sugar chains intrinsically located on the surface of the enzymes<sup>32</sup>.

### 3.1.2 Bienzyme immunosensors

The use of a bienzyme system has also brought considerable advantages in the development of amperometric immunosensors. They were initially based on the ELISA technique, where the measurements of electrochemically active products were carried out using redox-enzyme labels of either antigen or antibody. Generally, in the case of competitive assay, an analyte and a labelled analyte compete for a limiting number of immobilised antibody binding sites. The amount of bound conjugate is inversely proportional to the amount of analyte in the sample. However, the limiting factor in the development of rapid and separation-free electrochemical

immunosensors is the background noise induced by non-specific reactions. Such noise is most often due to the excess of enzyme-antigen conjugate in solution, which makes it difficult to discriminate between a signal that is obtained from small amounts of immuno-bound enzyme label and high background levels of signal that emanate from the conjugate in the bulk solution. The general approaches to overcome the non-specific signal of the conjugate in solution are to link the enzyme label catalytically to an additional system, such as a substrate cycle, or to other enzymes to form "cascades"<sup>33,34,35</sup>. This has led to the development of the enzyme-channeling immunoassay. A specific antibody (Ab) is co-immobilised with an enzyme onto an electrode surface. The solution contains the antigen and also the antigen conjugate of a second enzyme<sup>36</sup>. The immunological reaction between the immobilised Ab and the antigen, brings the two enzymes into immediate proximity at an electrode surface and the signal is amplified through the enzyme-channeling system.

The two enzymes are chosen so that the final product of the reaction catalysed by the first enzyme, is the substrate for the second enzyme. A typical enzyme couple used is GOX and HRP where the H<sub>2</sub>O<sub>2</sub> produced by GOX is reduced by the HRP at the electrode surface generating an amperometric signal.

Wright *et al.* developed a model "homogeneous" format enzyme-channeling specific binding assay for biotin. Avidin was immobilised onto the surface of printed carbon HRP enzyme electrodes and a competition assay between free biotin and biotinylated GOX was studied. A catalase was added to the bulk solution to scavenge H<sub>2</sub>O<sub>2</sub> generated from the excess of the biotinylated GOX<sup>37</sup>. Keay and McNeil developed a competitive ELISA incorporating disposable screen printed HRP-modified electrodes as the detector element in conjunction with single-use atrazine immuno-membranes. The assay was based on competition for available binding sites between free atrazine and an atrazine-GOX oxidase conjugate. Again, a catalase was used to scavenge H<sub>2</sub>O<sub>2</sub> formed in the bulk solution by unbound atrazine-GOX conjugate<sup>38</sup>. Dzantiev *et al.* in 2004 used a similar platform for the electrochemical determination of the herbicide chlorsulfuron<sup>39</sup>. Zeravik *et al.* developed an integrated flow-through amperometric biosensor for detection of environmental pollutants such as s-triazine herbicides<sup>40</sup>. Darain *et al.* developed a disposable and mediatorless immunosensor based on a conducting polymer (5,2':5'2"-terthiophene-3'-carboxylic acid) coated

screen-printed carbon electrode using a separation-free homogeneous technique for the detection of rabbit IgG as a model analyte<sup>41</sup>.

The enzyme-channeling system has brought several advantages in developing electrochemical immunosensors. The immunological reaction brings the two enzymes in close proximity at an electrode surface and this facilitates the rapid conversion of the initial substrate into the final product. In this scenario the background level of signal due to the unbound conjugate in the bulk solution is minimised and there is no need for washing steps. Cascade schemes, where an enzyme is catalytically linked to another enzyme can produce signal amplification and therefore increase the sensitivity. HRP has been successfully used as label in biosensing due to the extremely high turn over rate and very efficient electron transfer. For bienzyme systems based on HRP coupled with GOX, the substrate used to generate the signal is glucose, which is more stable and biocompatible than H<sub>2</sub>O<sub>2</sub>. However, the lower turn over rate of GOX compared to that of HRP, the increased complexity of the sensing device with an extra protein to be immobilised on the surface and diffusion issues affecting the response, represent the main drawbacks to be considered for bienzyme systems.

The aim of the work in this chapter was to establish an enzyme channeling system using GOX and HRP, to adapt this system to a conducting polymer platform and to investigate its efficiency and applicability to an immunosensor platform as a means of reporting the immunological interaction between avidin and biotin.

Modification of electrodes with PANI can be found in many biosensing applications due to its interesting electrical, electrochemical and optical properties. PANI can act as a non-diffusional mediating specie in enzyme biosensors, coupling electrons directly from the enzyme active site to the electrode. It can also be used as an effective substrate for immobilisation of biomolecules<sup>42</sup>.

Electroactive PANI/PVS has been used as the mediator in a reagentless peroxide biosensor operating at pH 6.8<sup>43</sup>. It has been applied to examine the amperometric behaviour of immobilised HRP<sup>44</sup> and has since been extended to develop rapid, single-step separation-free immunosensors for real-time monitoring<sup>45</sup> and incorporating multi-calibrant measurement<sup>46</sup>.

The first part of the work consisted of the development and optimisation of a bienzyme-based biosensor with HRP and GOX immobilized on PANI/PVS-modified screen-printed electrodes, exploiting the direct electron transfer between the modified electrode and the peroxidase enzyme. This bienzyme configuration was then applied to an immunosystem in which avidin and HRP were immobilised on the electrode surface, and GOX acted as the biotin label. This work was used as a foundation for comparison of this system with one enhanced by the use of AuNPs.

The second part of the work consisted of the production of AuNPs, and their use in forming conjugates with HRP, GOX and finally biotin-GOX to be applied in the immunosystem. Spectrophotometric and amperometric techniques were then proposed to characterise the conjugates, in order to determine the amount of the enzymes bound to the AuNPs, evaluating also the enzymatic activity after the conjugation process. These enzyme-NP conjugates were then applied to the bienzyme-based immunosensing system developed in the first part of the work, in order to see whether signal enhancements and improved sensor performances could be achieved.

## **3.2 MATERIALS AND METHODS**

### **3.2.1 Materials**

Aniline was purchased from Aldrich (13,293-4), vacuum distilled and stored frozen under nitrogen. Avidin, bovine serum albumin (BSA), biotin, *o*-phenylenediamine dihydrochloride (OPD), glucose and polyvinylsulphonate (PVS, 27,842-4) were purchased from Aldrich. HRP (250 U/mg) and GOX (270 U/mg) were purchased from Biozyme Laboratories. Biotin-GOX conjugate was from Rockland Immunochemicals. 30% (v/v) hydrogen peroxide solution and ethanol (99.9% w/v) were purchased from Merck. Trisodium citrate and H<sub>2</sub>AuCl<sub>4</sub> were purchased from Aldrich. Silver/silver chloride (Ag/AgCl) electrodes were purchased from Bioanalytical Systems Ltd. (Cheshire, UK). The platinum mesh (29,809-3) was purchased from Aldrich.

### 3.2.2 Buffers and solutions

Unless otherwise stated, all electrochemical measurements were carried out in phosphate buffered saline (PBS), (0.002 M  $\text{KH}_2\text{PO}_4$ , 0.008 M  $\text{Na}_2\text{HPO}_4$ , 0.137 M  $\text{NaCl}$ , 0.003 M  $\text{KCl}$ , pH 6.8 or 7.4). Unless otherwise stated, all biochemicals were prepared in PBS.

### 3.2.3 Instrumentation

Screen-printed carbon-paste electrodes were produced using an automated DEK 248 machine (Weymouth, UK). Electrode modification and protein immobilisation were performed using a CH1000 electrochemical analyser with CH1000 software, setting either cyclic voltammetry or time- based amperometric modes. An  $\text{Ag}/\text{AgCl}$  pseudo reference electrode and a platinum mesh auxiliary electrode were used for bulk electrochemical experiments. Electrochemical batch and flow cells were used according to Killard *et al.* (1999)<sup>43</sup>. They were composed of polycarbonate, and designed to house the screen-printed electrodes. Both cells incorporated internal  $\text{Ag}/\text{AgCl}$  reference and platinum wire auxiliary electrodes (*Figure 3.2*). Cell volumes of the batch and flow cells were 2 ml and 26  $\mu\text{l}$ , respectively. Peristaltic pump (Gilson Miniplus 3) was used to perform flow-injection analysis at the set flow rate of 400  $\mu\text{l}/\text{min}$ . Ultracentrifuge (Sorvall RC5Bplus) was used during the purification process of the conjugate.

### 3.2.4 Screen printed electrode modification with PANI/PVS

Electrodes were placed in 10 ml of 0.2 M  $\text{H}_2\text{SO}_4$ , prior to the polymerisation of aniline. A platinum mesh auxiliary and a silver/silver chloride reference electrode were used. Electrodes were cleaned and activated using cyclic voltammetry between  $-1200$  and  $+1500$  mV versus  $\text{Ag}/\text{AgCl}$  electrode at scan rate of 100 mV/s, sensitivity of  $1 \times 10^{-3}$  A over one cycle. A mixture of 7.8 ml 1 M  $\text{HCl}$ , 186  $\mu\text{l}$  aniline and 2 ml PVS was degassed under nitrogen for 10 min. Aniline was polymerised on the surface of the working electrode using 10 voltammetric cycles between  $-500$  and  $+1100$  mV versus  $\text{Ag}/\text{AgCl}$  electrode at 100 mV/s.

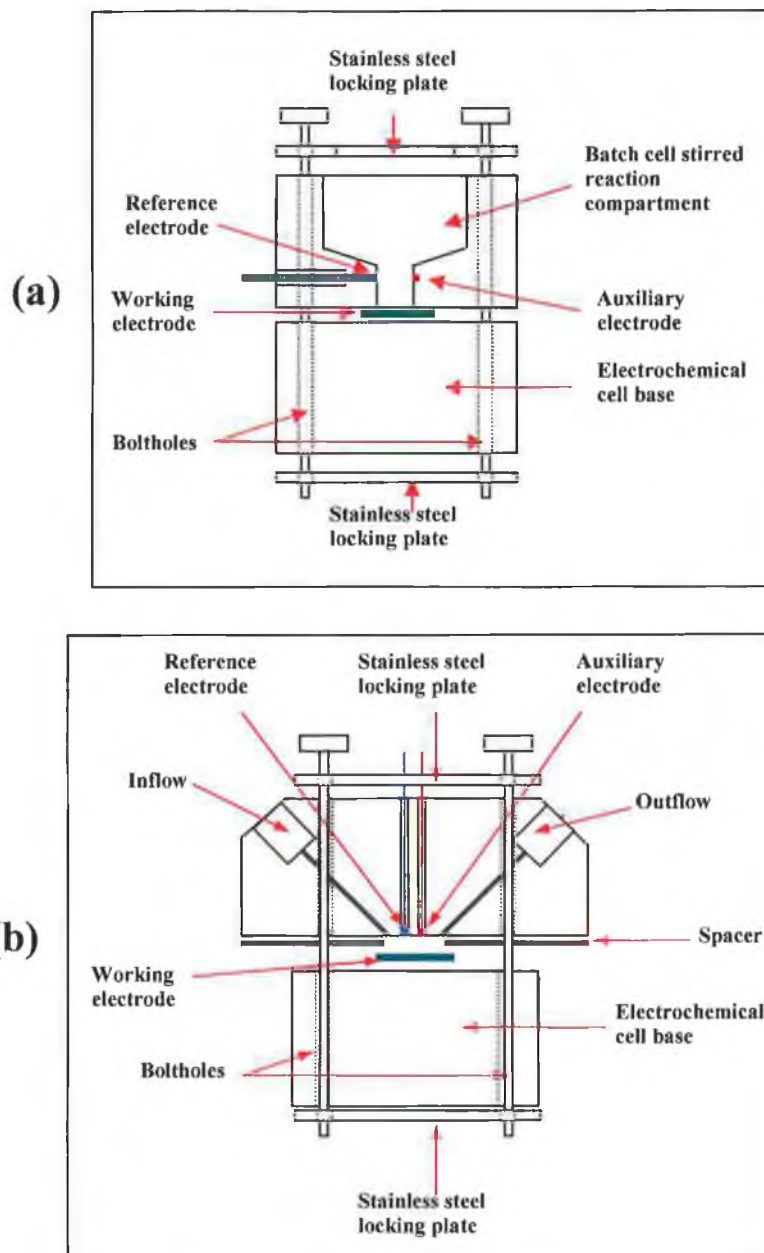


**Figure 3.2.** Batch and flow cell configurations. (a) The polycarbonate batch cell comprised an upper reaction vessel and a lower base, between which was clamped the screen-printed electrode. Platinum wire auxiliary and pseudo silver/silver chloride wire reference electrodes were incorporated into the reaction vessel with external connections as shown. (b) The flow injection cell was composed of polycarbonate into which had been drilled holes for inflow and outflow. Platinum and silver/silver chloride electrodes were placed at the base of the cell to come into close association with the screen-printed working electrode. The flow chamber was formed by the use of a PET spacer (50  $\mu\text{m}$  thickness). The screen-printed electrode was clamped into place between the upper and lower sections as shown. (Adapted from Killard *et al.*<sup>43</sup>).

### 3.2.5 Immobilisation of HRP on PANI/PVS-modified screen printed electrode

Following polymerisation of aniline, the electrode was transferred to a 2 ml batch cell. The isoelectric point of HRP is 7.2, therefore carrying a negative charge could be adsorbed on the oxidized PANI film at  $\text{pH} > 7.2$ . The polymer surface was firstly reduced in 2 ml of PBS (pH 7.4) (degassed for 10 min. under nitrogen or argon) at  $-500$  mV vs. Ag/AgCl, sample interval of 500 ms, over 300 s. HRP was prepared in PBS (pH 7.4) prior to use. After reduction was complete, PBS buffer was removed from the cell and quickly replaced with the enzyme solution, not under stirring or degassing. Oxidation was then performed at  $+700$  mV vs. Ag/AgCl for 300 s. The protein solution was carefully recovered from the cell and re-stored for later use.

### 3.2.6 Flow-injection analysis of $\text{H}_2\text{O}_2$

The HRP/PANI/PVS modified screen-printed electrode prepared according to sections 3.2.4 and 3.2.5 was tested for the analysis of  $\text{H}_2\text{O}_2$  using a flow-injection system illustrated in *Figure 3.3* where a peristaltic pump assures a constant flow ( $400 \mu\text{l}/\text{min}$ ) of the reagents through the flow-cell (*Figure 3.2.b*) and therefore over the sensor surface. The flow-cell is connected with a potentiostat interfaced with a PC to record chronoamperometric measurements at the constant potential of  $-0.1 \text{ V}^{44}$ . A PBS buffer solution (pH 6.8) was initially passed over the sensor surface until the system reached a steady current signal. Then standard samples of  $\text{H}_2\text{O}_2$ , prepared in the same buffer, were passed over the surface and the current signals recorded.

### 3.2.7 Immobilisation of HRP and GOX in a single step

A simple bienzyme-based biosensor was built immobilising HRP and GOX in one single step according to the section 3.2.5. The isoelectric point of GOX is 4.2, so again a solution at  $\text{pH} > 7.2$  was used to electrostatically attach both enzymes carrying a negative charge on the oxidised PANI film. Solutions with different molar ratios of the two enzymes were prepared in PBS (pH 7.4) and used for the preparation of different bienzyme platforms.



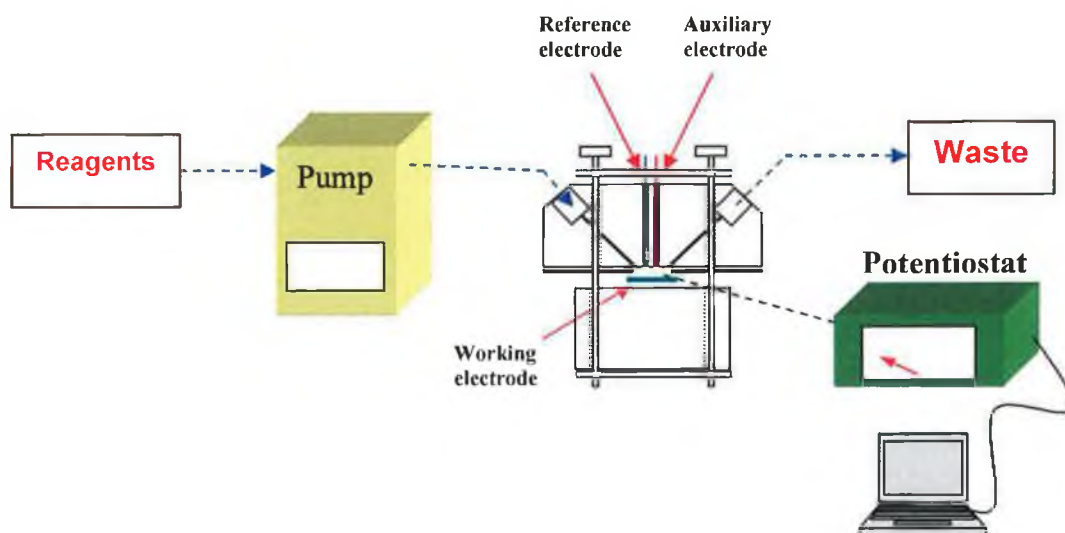


**Figure 3.3.** Experimental set-up for FIA experiments incorporating screen-printed electrode-based biosensors. The buffered reagents are injected in the electrochemical flow cell by means of a peristaltic pump. The auxiliary and reference electrodes present in the cell, and the screen-printed working electrode inserted, are connected to a potentiostat interfaced with a PC which controls the electrochemical settings and records the responses.

### 3.2.8 Investigation of the bienzyme-based biosensor using a mathematical approach

This section was a collaborative work with Dr. Dana Mackey at School of Mathematical Sciences, Dublin Institute of Technology, Dublin 8, Ireland.

In this study the behaviour of the electrochemical bienzyme biosensor based on the enzyme channelling configuration, employing the enzymes GOX and HRP, was investigated with a theoretical analysis based on a mathematical model and numerical simulation. The sensing configuration was modelled by a system of partial differential equations and boundary conditions representing convective and diffusive transport of the substrates glucose and  $H_2O_2$ , as well as reaction kinetics of the bienzyme electrode. The main parameter investigated was the ratio of the two immobilised enzymes, with the aim of maximising the amperometric signal amplitude.

### **3.2.9 Flow-injection analysis of glucose**

The bienzyme-based biosensor prepared immobilising HRP and GOX onto the PANI/PVS modified screen-printed electrode was tested for the analysis of glucose using a flow-injection system according to section 3.2.6. For this experiment, after reaching the steady state, different standard samples of glucose, prepared in PBS buffer (pH 6.8), were passed over the sensor surface and the current signals recorded.

### **3.2.10 Immobilisation of avidin and HRP in a single step**

A platform for the evaluation of biospecific interactions between avidin and biotin was built immobilising avidin and HRP on PANI/PVS modified electrodes in one single step using a slightly different procedure to that illustrated in section 3.2.5. The isoelectric point of avidin is 10.5. In order to immobilize avidin and HRP together, the two proteins were prepared in PBS buffer at pH 6.8 to have them positively charged. In this case the surface of the polymer was firstly oxidised in 2 ml of PBS (pH 6.8) (degassed for 10 min. under nitrogen or argon) at +700 mV vs. Ag/AgCl, sample interval of 500 ms, over 300 s. After oxidation was complete, PBS buffer was removed from the cell and quickly replaced with the solution containing avidin and HRP, not under stirring or degassing. The electrostatic attachment was then performed reducing the PANI film at -500 mV vs. Ag/AgCl for 300 s. Different solutions containing HRP at a concentration 0.4 mg/ml and avidin at concentrations between 0 and 1.1 mg/ml, were prepared and used during the immobilisation process.

### **3.2.11 Assessment of different avidin/HRP platforms on binding GOX or biotin-GOX**

Different avidin/HRP platforms prepared as described in section 3.2.10 were tested to evaluate the specific binding of biotin-GOX and non-specific binding of GOX. The experiment was carried out in two successive steps. In the first part, GOX or biotin-GOX solution was passed over the electrode surface modified with avidin/HRP, using the flow-injection system. Subsequently, a solution of glucose was passed over the same surface. GOX or biotin-GOX catalyses the oxidation reaction of glucose to

gluconic acid with production of  $\text{H}_2\text{O}_2$ , while HRP, adsorbed on the surface, catalyses the reduction of  $\text{H}_2\text{O}_2$  to  $\text{H}_2\text{O}$  at a potential of  $-0.1$  V. The catalytic signal measured while passing the glucose solution was proportional to the amount of GOX or biotin-GOX binding the electrode surface.

### **3.2.12 Calibration curve for GOX and biotin-GOX on avidin/HRP platform**

The specific binding between avidin and biotin was compared to a non-specific binding between GOX and the electrode surface. Using the same avidin/HRP platform, solutions at varying concentrations of GOX or biotin-GOX were passed over the electrode surface. According to section 2.2.9, the signal was recorded after passing across a glucose solution.

### **3.2.13 Competition assay system for real-time biotin determination**

The optimised avidin/HRP platform was tested for a real-time biotin determination using a competition assay system. Solutions with free biotin at different concentrations and biotin-GOX were passed over an avidin/HRP modified electrode surface. The signal was recorded after passing across a glucose solution.

### **3.2.14 Preparation of gold nanoparticle solutions**

AuNPs were prepared by the conventional citrate reduction of  $\text{HAuCl}_4$  in water at boiling point according to the literature<sup>47</sup>. All glassware used in the procedures was cleaned in a bath of freshly prepared  $\text{HNO}_3$ - $\text{HCl}$  (3:1) and rinsed thoroughly in water prior to use. A solution of 1% (w/v) trisodium citrate was added to a boiling solution of 0.01% (w/v)  $\text{HAuCl}_4$ . After the solution turned red, it was left to cool down while stirring. UV-Vis spectrophotometry was used to characterise the AuNPs solution.

### **3.2.15 Formation and characterisation of gold-HRP and gold-GOX conjugates**

The Au colloid solution's pH was adjusted to pH 6.8, adding drop by drop a solution 0.01 M HCl, for the conjugation with HRP enzyme (pI=7.2), and to pH 4 for the conjugation with GOX (pI=4.2)<sup>53</sup>. A preliminary titration, also called Au aggregation test, was carried out to establish the optimal amount of enzyme to be added to the Au solution. The HRP and GOX solutions were then added drop-wise to the Au colloid suspension while stirring rapidly at room temperature. After 10 min the solutions with gold-GOX and gold-HRP conjugates were centrifuged at 15,000g for 1 h, the clear supernatant was removed to eliminate the excess of enzyme and the conjugates were resuspended in PBS and stored at 4°C. Spectrophotometric and amperometric techniques were used to characterise the two conjugates in order to evaluate the enzyme bioactivity after the conjugation process. The colorimetric assay based on the reaction between HRP and OPD substrate, was used to characterise the Au-HRP conjugate. Two novel amperometric methods were also developed and optimised for the analysis of HRP and GOX in a sample.

### **3.2.16 Application of Au-biotin-GOX conjugates to the immunosensing system**

A set of measurements have been carried out with the aim of evaluating the possibility of AuNPs bringing benefits in the performances of the enzyme-channeling-based immunosensing platform developed. The use of biotin-GOX solutions prepared with and without AuNPs has been considered the best way to compare the performances of the two types of conjugates. A flow-injection set-up was used to pass over the electrode surface, solutions at different concentrations of biotin-GOX prepared either in PBS (pH 6.8) or prepared in the Au colloid solution (at pH adjusted to 6.8), in the range 1 – 25 µg/ml. A 20 mM glucose solution was passed after each of the solution described in order to generate the amperometric signal. Before use, the solutions of biotin-GOX prepared in the Au colloid suspension were gently mixed for 10 min. in order to form the Au-biotin-GOX conjugate.

### 3.3 RESULTS AND DISCUSSION

#### 3.3.1 HRP binding capacity of PANI/PVS modified electrode

A series of sensors were prepared by modifying PANI/PVS-coated electrodes with a range of concentrations of HRP in order to evaluate the optimal amount of protein to yield the best coating efficiency on the electrode surface. According to section 3.2.5, HRP was immobilised on the electrode surface for 5 min., using solutions at concentrations between 0.005 mg/ml and 1.0 mg/ml. The HRP-based sensor so prepared, was then tested for the analysis of  $\text{H}_2\text{O}_2$  using a flow-injection system. In *Figure 3.4* the graph represents the response of different electrodes at different concentrations of  $\text{H}_2\text{O}_2$ . It appears clear that the electrodes prepared immobilising the lowest concentrations of enzyme, 0.005 mg/ml and 0.01 mg/ml, showed the lowest signals.

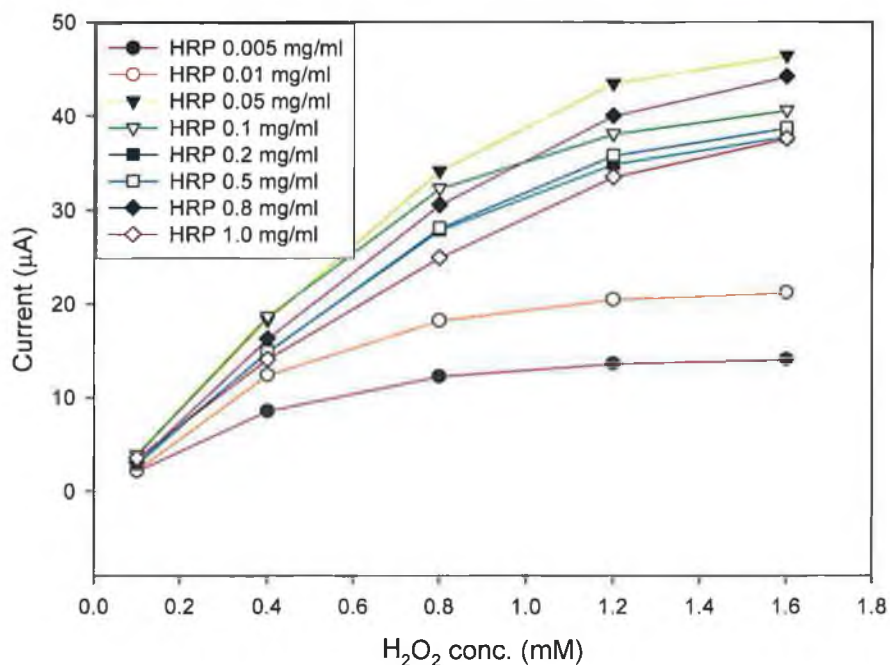


*Figure 3.4.* Amperometric response for the analysis of  $\text{H}_2\text{O}_2$  using flow-injection system and electrodes modified with different concentrations of HRP. The electrode modified using solutions 0.005 mg/ml (●) and 0.01 mg/ml (○) of HRP, showed the lowest signal responses (-0.1 V vs. Ag/AgCl). (Electrode surface area:  $0.07 \text{ cm}^2$ ).

At low concentrations of  $\text{H}_2\text{O}_2$  (between 0.1 and 0.8 mM) the signal responses could be considered linear and the related slopes from each curve represented the sensitivity of the biosensor. The graph in *Figure 3.5* shows the sensitivity of the sensor versus HRP concentrations used during the immobilisation procedure. It suggests that using HRP concentrations between 0.05 mg/ml and 0.8 mg/ml, biosensor platforms with similar performances can be derived. As a matter of fact, the sensitivity of the specific electrodes appears very similar. Concentrations below 0.05 mg/ml of HRP yielded the lowest catalytic signals, due to the very low amount of enzyme attached to the electrode surface, which, might suggest, therefore, that there is still space available for further protein adsorption. The concentration of 1.0 mg/ml of enzyme produced a biosensor with a remarkably lower sensitivity compared to the other values. In this case the reason could be found in the excess of protein attached on the electrode surface in a multiple layer form which may cause a less efficient electron transfer between the enzyme's active centre and the electrode, or block the diffusion of  $\text{H}_2\text{O}_2$  from the bulk to the enzyme/electrode interface.

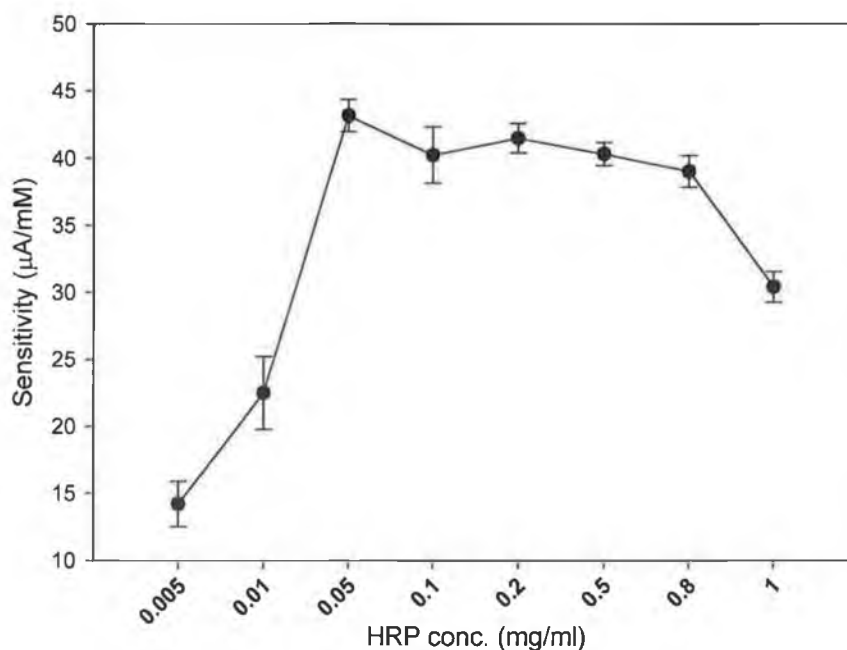


**Figure 3.5.** HRP binding capacity of PANI/PVS modified electrode surface. HRP concentrations in the range 0.005 – 0.8 mg/ml produced the highest catalytic signals. (Electrode surface area: 0.07 cm<sup>2</sup>).

### 3.3.2 Assessment of immobilisation time of HRP

A study to evaluate the efficiency of the electrostatic adsorption of proteins on PANI/PVS modified electrode surface was carried out. As described in section 3.2.5, the electrode was firstly subjected to a potential of  $-0.5$  V for 300 s in PBS buffer (pH 7.4) and then oxidised at potential of  $+700$  mV in the presence of the enzyme solution for incubation times between 1 and 40 min. In this study, a 0.1 mg/ml solution of HRP, which is within the optimal range of concentrations for the best coverage of the electrode surface (section 3.3.1), was used for the immobilisation. *Figure 3.6* shows the signals recorded in a flow-injection analysis of  $H_2O_2$  for the various electrodes. It can be seen how all the electrodes showed a very similar performance and the difference between the electrode prepared immobilising HRP for just 1 min. and the one prepared using an incubation time of 40 min. was very small. This result suggests that the electrostatic attraction taking place at the very beginning of the process between the positively charged polymer and the negatively charged HRP (pI= 7.2, prepared in PBS, pH 7.4), plays the most important role in the overall protein adsorption.

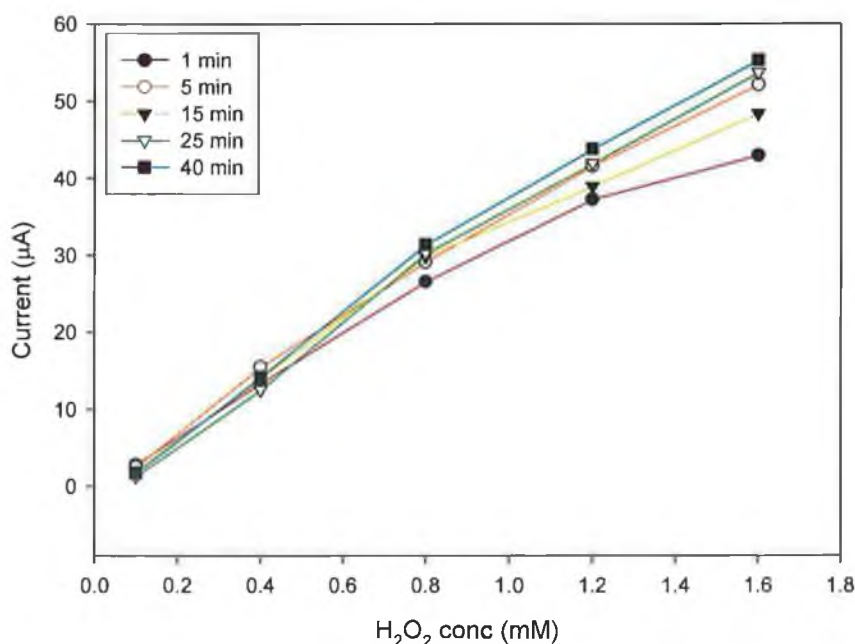


**Figure 3.6.** HRP immobilisation time optimisation. Flow-injection analysis of  $H_2O_2$  using HRP-based electrodes prepared with different immobilisation times of the enzyme ( $-0.1$  V vs. Ag/AgCl). (Electrode surface area:  $0.07$  cm<sup>2</sup>).

### 3.3.3 Assessment of the optimal pH for the immobilisation of HRP

Considering the electrostatic attraction between the enzyme and the polymer as the main phenomenon taking place, it was of interest to carry out a study to evaluate the effect of the pH during the immobilisation process. Enzyme solutions at pH between 6.0 and 8.0 were made up at a concentration of 0.1 mg/ml and were used in the immobilisation procedure at a chosen incubation time of 5 min. The electrodes prepared as described above were then tested in a flow-injection analysis system, passing 1.6 mM H<sub>2</sub>O<sub>2</sub> solutions over the surface at pH 6.8 and recording the catalytic signals.

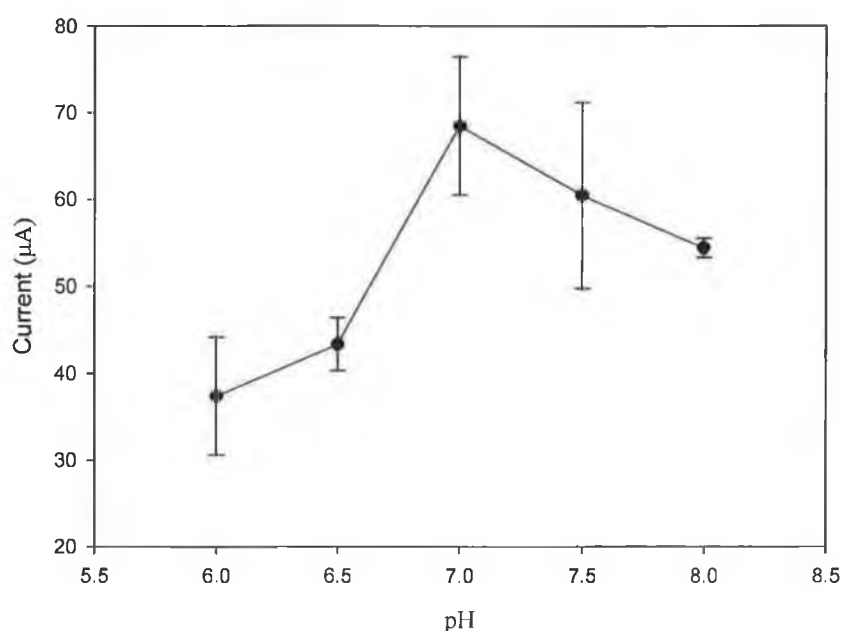


**Figure 3.7.** HRP solutions of 0.1 mg/ml were prepared at different pH in the range 6 – 8 and used for the immobilisation process (5 min). The graph shows the catalytic signals recorded in a flow-injection analysis system passing over the surface H<sub>2</sub>O<sub>2</sub> solution at a concentration of 1.6 mM (n = 3) (-0.1 V vs. Ag/AgCl). (Electrode surface area: 0.07 cm<sup>2</sup>).

As expected, using HRP solutions at pH lower than 7 the amperometric responses were reduced. This may be because at these pH the protein was positively charged and the electrostatic attachment onto the positive charged PANI film was less efficient (Figure 3.7). However, using HRP solutions at pH higher than 7 the response decreased again despite the protein becoming more negatively charged by increasing the pH. This suggests that the electrostatic attraction cannot be considered as the only



phenomenon taking place. The acidity of the solution might modify in some way the structure of the polymer either increasing or decreasing its protein binding ability. It is well known, for example, that at alkaline pH the conductivity of doped PANI film decreases and that might also affect the adsorption of proteins<sup>48</sup>.

### 3.3.4 Calibration of the HRP-based biosensor for H<sub>2</sub>O<sub>2</sub> analysis and stability study

The HRP-based biosensor prepared under optimal conditions was tested for the analysis of H<sub>2</sub>O<sub>2</sub> with a flow-injection system. Linear range, detection limit and stability were evaluated. *Figure 3.8* shows a typical amperogram recorded passing five H<sub>2</sub>O<sub>2</sub> concentrations between 0.05 mM and 2.0 mM over the electrode surface. The current signals generated from the reduction of H<sub>2</sub>O<sub>2</sub> by HRP were clearly proportional to the concentration of H<sub>2</sub>O<sub>2</sub> present in the sample. As can be easily seen, the equilibrium of the reduction reaction was reached in about 100 s when the current reached the maximum at a steady value. For concentrations of H<sub>2</sub>O<sub>2</sub> higher than 1 mM, the HRP-based biosensor under study seemed to lose linearity, and the signal at 2mM of H<sub>2</sub>O<sub>2</sub> was very noisy and not as high as expected for that concentration, possibly due to the saturation of the enzyme with substrate.

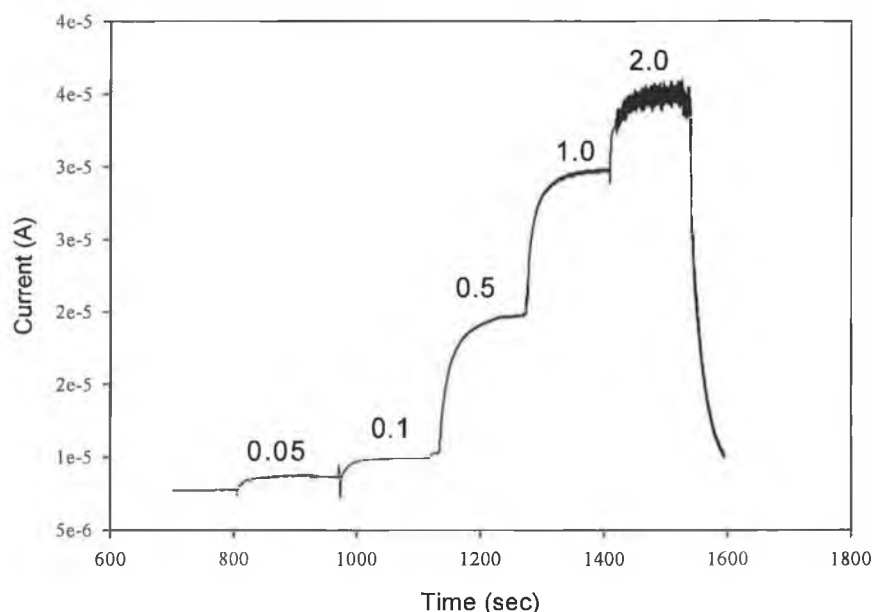


**Figure 3.8.** Amperogram of H<sub>2</sub>O<sub>2</sub> solutions at a range of concentration passed over the HRP/PANI/PVS modified electrode surface at the applied potential of -0.1 V vs. Ag/AgCl. (Electrode surface area: 0.07 cm<sup>2</sup>).

The same electrode was tested for four days and stored at 4°C in a dry atmosphere. As the graph in *Figure 3.9* shows, the electrode yielded a stability at the highest concentration of 2 mM H<sub>2</sub>O<sub>2</sub> only over a 24 h time, with a recorded signal 12% lower. However, after four days, similar responses were recorded only for very low concentrations of H<sub>2</sub>O<sub>2</sub> (0.0025 – 0.5 mM). This could be due to an initial loss of HRP molecules from the electrode surface which made the system unable to fully reduce higher concentrations of H<sub>2</sub>O<sub>2</sub>. The graph in *Figure 3.10* shows the stability over four days of another electrode tested using H<sub>2</sub>O<sub>2</sub> solutions at concentrations between 0.0025 and 0.25 mM. It confirms that for low concentration of H<sub>2</sub>O<sub>2</sub>, despite the possible loss of enzyme molecules, the system was still able to fully reduce the H<sub>2</sub>O<sub>2</sub> present, generating signals proportional to the concentration. Finally, *Figure 3.11* illustrates the calibration curve of the HRP-based biosensor for H<sub>2</sub>O<sub>2</sub> analysis. The linear range achieved was for concentrations of H<sub>2</sub>O<sub>2</sub> between 0.0025 and 2 mM (slope: 424.2 mA/Mcm<sup>2</sup>). The sensitivity of this enzyme-based sensor toward the analysis of H<sub>2</sub>O<sub>2</sub> was much higher than other sensors found in the literature<sup>49</sup>. This enzyme-based sensor resulted also more sensitive than the nanoPANI-based sensor described in chapter 2 (slope: 10.8 mA/M cm<sup>2</sup>) which presented, however, a much wider linearity range (1 mM to 0.1 M).

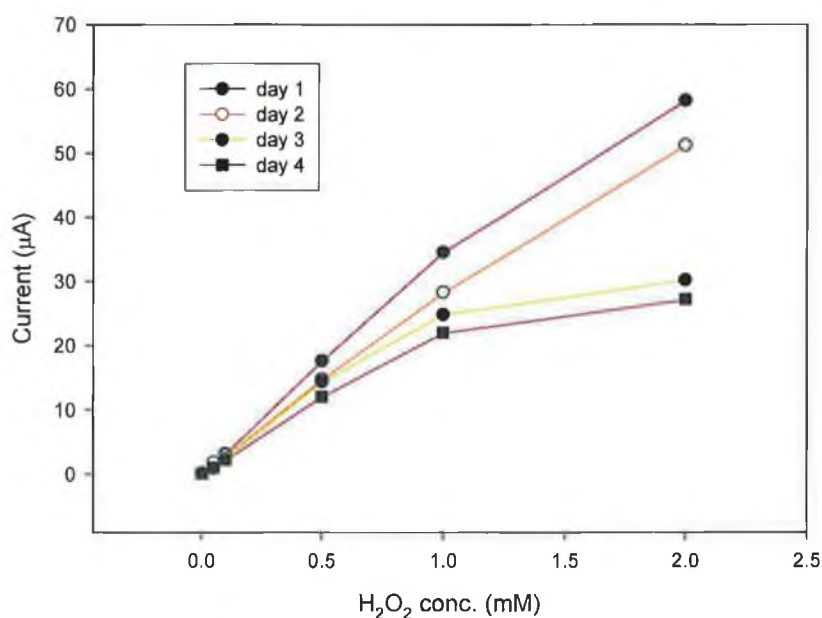


**Figure 3.9.** Stability study of the HRP-based biosensor, using a flow-injection analysis system. The electrode was tested over four days and stored at 4°C in a dry atmosphere. The range of H<sub>2</sub>O<sub>2</sub> concentrations used was between 0.0025 – 2.0 mM (-0.1 V vs. Ag/AgCl). (Electrode surface area: 0.07 cm<sup>2</sup>).

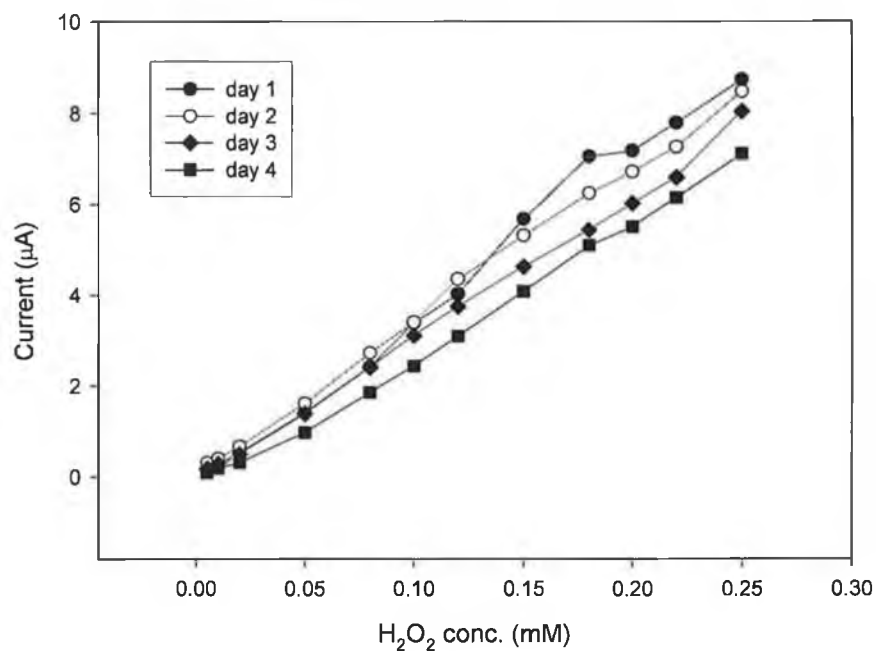


**Figure 3.10.** Stability study for the HRP-based biosensor in a flow-injection analysis using a range of H<sub>2</sub>O<sub>2</sub> concentrations between 0.0025 – 0.25 mM (-0.1 V vs. Ag/AgCl). (Electrode surface area: 0.07 cm<sup>2</sup>).

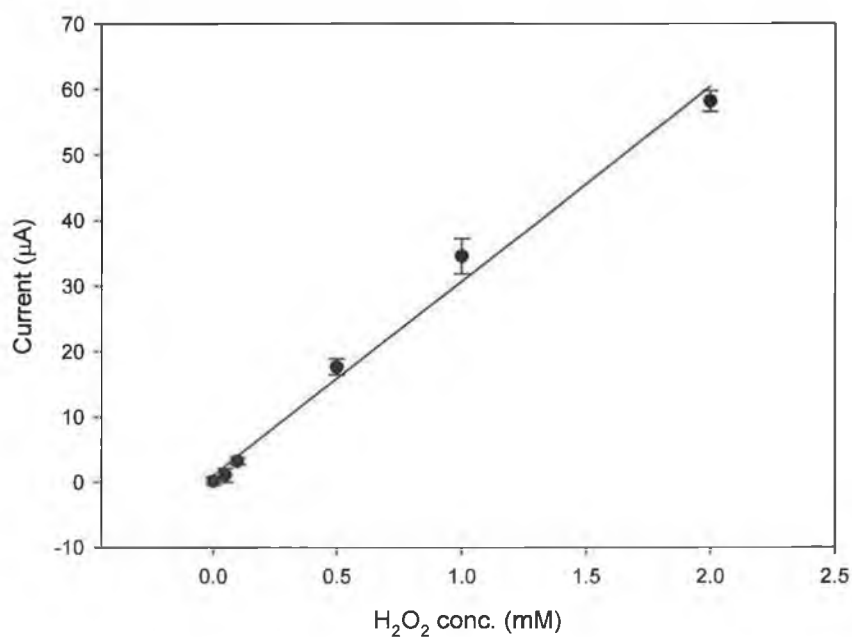


**Figure 3.11.** Calibration curve for H<sub>2</sub>O<sub>2</sub> analysis with an HRP-based biosensor. Linear range (0.0025 – 2.0 mM), intercept = 1.05 µA, slope = 424.2 mA/Mcm<sup>2</sup>, r<sup>2</sup> = 0.990 (-0.1 V vs. Ag/AgCl). (Electrode surface area: 0.07 cm<sup>2</sup>).

### 3.3.5 Optimisation of HRP/GOX ratio for the bienzyme-based biosensor for glucose analysis

Experiments were carried out with the aim of creating a bienzyme-based biosensor for glucose analysis. HRP and GOX were immobilised together in a single step according to section 3.2.7. Solutions of the two enzymes at different ratios were prepared, maintaining a total concentration of 0.8 mg/ml, which was the highest value within the optimal range seen in *Figure 3.5*. GOX (160 kDa) is approximately four times larger than HRP (44 kDa) and because of the difference in size of the two enzymes, 0.8 mg/ml was chosen to ensure a good coverage of the electrode surface. Different solutions containing the two enzymes were made at the mass ratio of HRP/GOX from 1:7 to 7:1 and used to prepare electrodes. The enzyme-immobilisation was performed by immersing the electrode into the enzymes solution and applying a static potential of +0.7 V for 5 min. Due to the ability of polyaniline to bind biomolecules, the two enzymes became electrostatically and hydrophobically adsorbed on the electrode surface and because of the nature of this immobilisation, it was assumed that the distribution of the enzyme molecules over the surface was equal in ratio to that of the solution used, i.e. that there was no difference in binding efficiency. Each electrode was then tested in a flow-injection analysis of glucose using standard solutions at concentrations between 0.5 and 20 mM. *Figure 3.12* shows a typical amperogram recorded at -0.1 V vs. Ag/AgCl. The enzyme-channeling between GOX and HRP generated step-type signals after passing across glucose solutions. Once again, a time of about 100 s seemed necessary to reach the steady state. It can also be seen that even at higher concentrations of glucose, the signals recorded were significantly lower than the signals recorded for the monoenzyme HRP-based biosensor (*Figure 3.8*) for equivalent H<sub>2</sub>O<sub>2</sub> concentrations. This suggests that the bienzyme system has a lower overall efficiency than the HRP system in its ability to couple substrate consumption into electron transfer.

The sensitivities of the electrodes were compared using the slope of the glucose calibration curves. The mass ratios of HRP/GOX in the solutions used for the immobilisation can be more conveniently expressed as molar ratios in order to visualise approximately the relative molecular distribution on the electrode surface of the two enzymes.

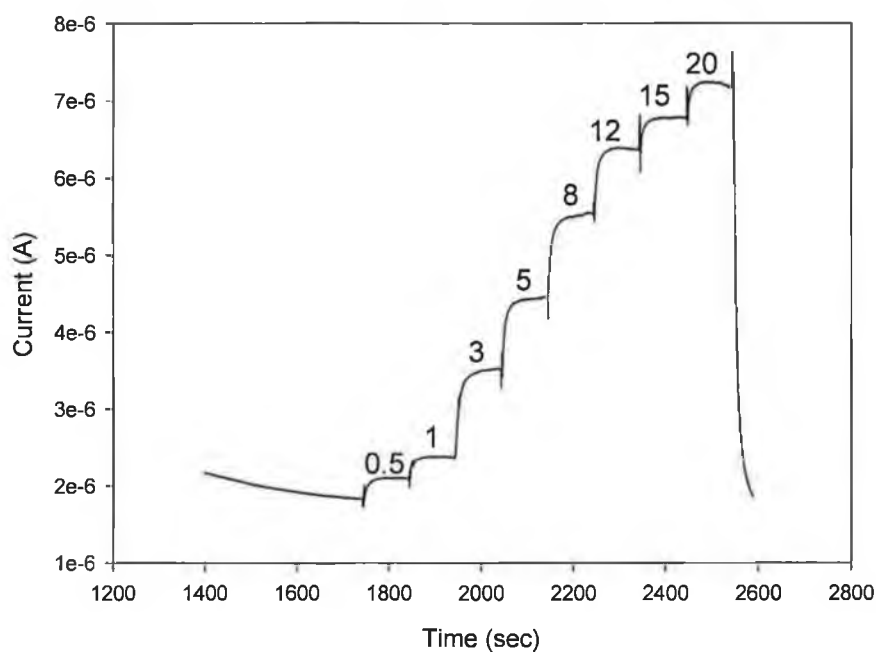


**Figure 3.12.** Amperometric responses of a HRP/GOX (mass ratio 2:6) bienzyme electrode to a range of glucose concentrations between 0.5 – 20 mM at -0.1 V vs. Ag/AgCl. (Electrode surface area: 0.07 cm<sup>2</sup>).

Figure 3.13 shows the calibration curves achieved with the optimal electrode configuration (HRP 0.2, GOX 0.6 mg/ml, which is a molar ratio HRP/GOX of 1:1) and with the worst (HRP 0.7, GOX 0.1 mg/ml, which is a molar ratio HRP/GOX of 26:1). Interestingly, the former calibration lost linearity above 12 mM glucose, where it appears to adopt the same slope as the latter electrode. This could be due to the GOX reaching saturation at this concentration. Figure 3.14 shows a comparison between all the sensitivities of the electrodes with the different molar ratios of HRP/GOX. The electrode prepared with HRP/GOX at a molar ratio of 1:1 yielded the highest sensitivity.

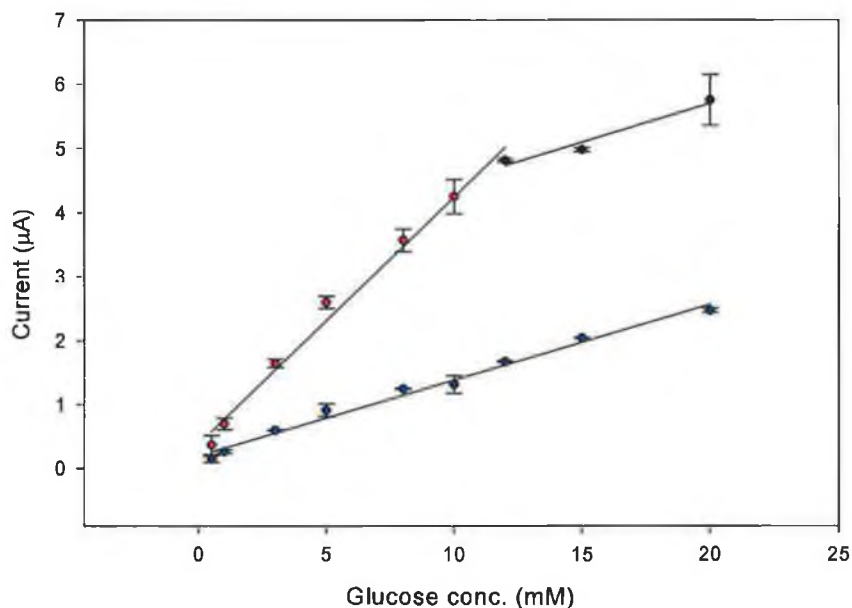


**Figure 3.13.** Glucose calibration curves for the bienzyme electrode yielding the highest and lowest sensitivities. The curve with the highest slope (red) was achieved using the molar ratio HRP/GOX of 1:1 (linearity range = 0.5 – 12 mM, slope = 5.51 mA/Mcm<sup>2</sup>, intercept = 0.38 µA, r<sup>2</sup> = 0.989); and the curve with the lowest slope (blue) was achieved using the molar ratio HRP/GOX of 26:1 (linearity range = 0.5 – 20 mM, slope = 1.7 mA/Mcm<sup>2</sup>, intercept = 0.201 µA, r<sup>2</sup> = 0.987) (-0.1 V vs. Ag/AgCl). (Electrode surface area: 0.07 cm<sup>2</sup>).

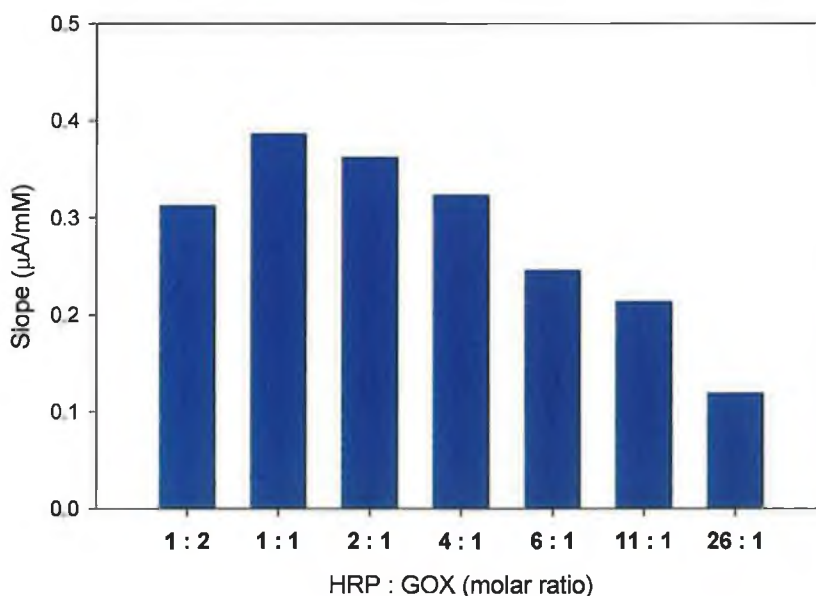


**Figure 3.14.** Comparison of HRP/GOX ratio and sensitivity to glucose. The electrode prepared immobilising HRP and GOX at the molar ratio of 1:1 (HRP 0.2, GOX 0.6 mg/ml) yielded the highest catalytic signals and the highest sensitivity (-0.1 V vs. Ag/AgCl). (Electrode surface area: 0.07 cm<sup>2</sup>).

The GOX adopted in the experiment had an activity of 270 U/mg protein, and HRP 250 U/mg protein. Expressing the two activities in U/mol they are 1.7 for GOX and 5.7 for HRP. Thus, HRP was approximately three times more active than GOX. Considering the difference in activity between the two enzymes, a platform with GOX in excess with respect to HRP was expected to be the most efficient. The fact that the platform with HRP and GOX present at a molar ratio of 1:1 produced the highest signals, suggests that other phenomena occur and contribute to influence the response. Diffusion of the reactants in solution over the electrode surface to reach the enzymes, the relative distance between GOX and HRP molecules and also, the actual activity of HRP after its immobilisation on the electrode surface and its reliance on direct electron transfer, are certainly important factors to be considered. A theoretical homogeneous distribution of an equal number of HRP and GOX molecules on the electrode surface is represented in *Figure 3.15*. This distribution may ensure the shortest distance between the two enzymes and therefore produce the most efficient channeling. A similar average spatial distribution could be suggested for the real bienzyme system under study with HRP and GOX at a molar ratio of 1:1 and with the distance between them minimised.

In this configuration  $H_2O_2$  produced by GOX is more rapidly and efficiently reduced by HRP, so producing the signal. Configurations with a higher molar quantity of GOX resulted in a lower response despite the higher concentration of  $H_2O_2$  which would be produced, probably as a consequence of the increased distance between GOX and HRP molecules, which resulted in a less efficient channelling process, as diffusional losses may have been a significant feature.

Agreement with this explanation has been found by a mathematical approach in which the bienzyme system under investigation was approximated to the model illustrated in *Figure 3.16*. This was based on the existence of a convection layer, where the glucose concentration remained constant, and a diffusion layer. The two enzymes form a monolayer on the electrode so all reactions can be assumed to take place at the lower boundary of the diffusion domain. For computational simplicity, the flow effects were not explicitly modelled and the existence of the convective zone was only reflected in the boundary conditions imposed at the top of the diffusion layer. The equations were therefore one-dimensional, where the spatial variable  $x$  measures the distance from the electrode.

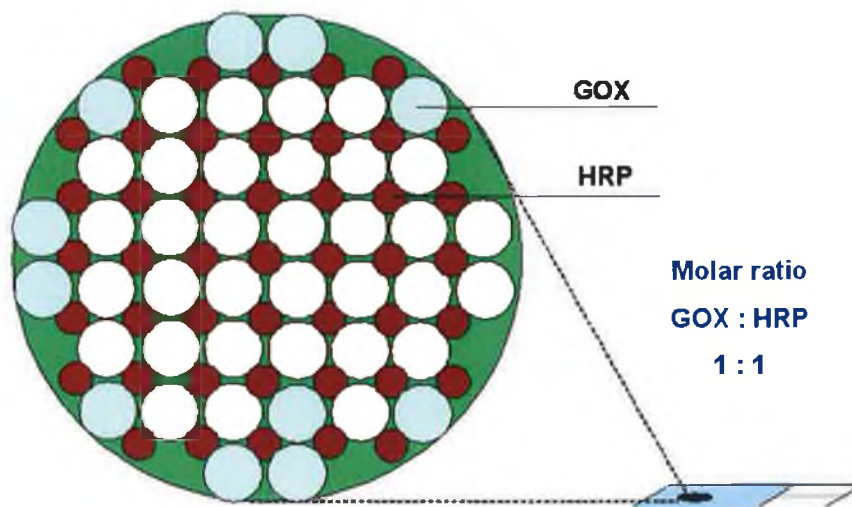


**Figure 3.15.** Molecular distribution of HRP and GOX on the electrode surface at a molar ratio of 1:1. This configuration platform ensuring the shortest distance between the enzymes molecules resulted the most sensitive. (Electrode surface area:  $0.07 \text{ cm}^2$ ).

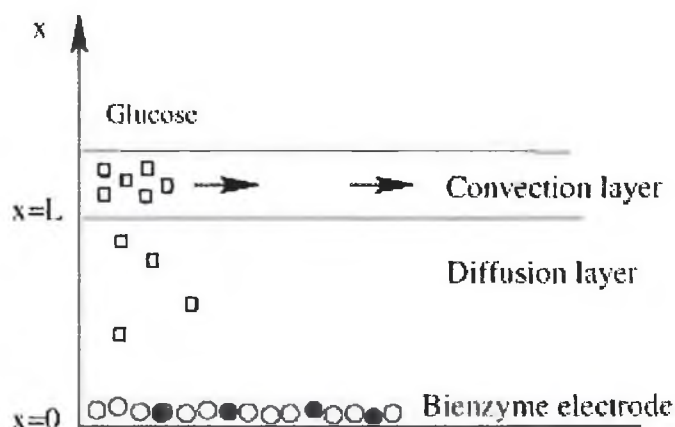
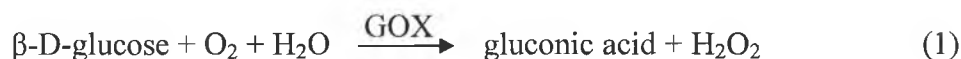


**Figure 3.16.** Mathematical model representing the experimental set-up. Glucose is considered present in two solution layers, a convection layer, where the concentration remains constant, and a diffusion layer. The two enzymes form a monolayer on the electrode. To have one-dimensional equations, only the diffusion layer was taken into account for the calculations, where the spatial variable  $x$  measures the distance from the electrode.



A cascade reaction takes place at the electrode. Glucose oxidase catalyses the oxidation reaction of glucose to gluconic acid, with production of H<sub>2</sub>O<sub>2</sub>. HRP is oxidised by hydrogen peroxide and then subsequently reduced by electrons provided by the electrode, as shown in the following abbreviated reactions.



The two reactions were modelled by standard Michaelis–Menten equations. This simple scheme has been used extensively for modelling glucose–glucose oxidase kinetics<sup>50</sup> and it was also shown to be appropriate for the case of immobilised HRP<sup>44</sup>. For the purpose of this comparative analysis, using similar kinetics for the two consecutive reactions was a necessary simplifying assumption. The kinetic scheme was thus given by the Equations 4 and 5 below:



where  $E_1(t)$  is GOX concentration as function of time,  $E_2(t)$  represents the HRP concentration as function of time,  $S_1(x,t)$  is the first substrate (glucose),  $S_2(x,t)$  is the second substrate (hydrogen peroxide), both as function of time and distance from the electrode,  $C_1(t)$  and  $C_2(t)$  represent the first and the second complex as function of time and  $P(x,t)$  is the final product as function of time and distance from the electrode. The numerical integration of the partial differential equations governing the behaviour of the relevant chemical species in the proposed model, resulted in the final graph illustrated in *Figure 3.17*. It represents the current dependency on the molar ratio of HRP/GOX at different glucose concentrations. It can be seen that at higher glucose concentrations, the optimum response approaches at molar ratio GOX:HRP of 1:1. As the substrate concentration is reduced, this optimum becomes gradually less defined

as the enzyme system is operating well below its optimum capacity. Taking into account the kinetics of the enzymes with the respective  $k_{\text{cat}}$  and  $K_M$  a mathematical study of the signal response varying the kinetic characteristic associated with each step of the two reactions, was also carried out. The graph in *Figure 3.18* shows the current as a function of the molar ratio GOX:HRP, for different values of  $k_4/k_2$  ranging from 0.5 to 8. It is interesting to note that the second curve, which corresponds to  $k_4 = k_2$ , indicates that the highest sensitivity is obtained for a molar ratio GOX:HRP of 1.

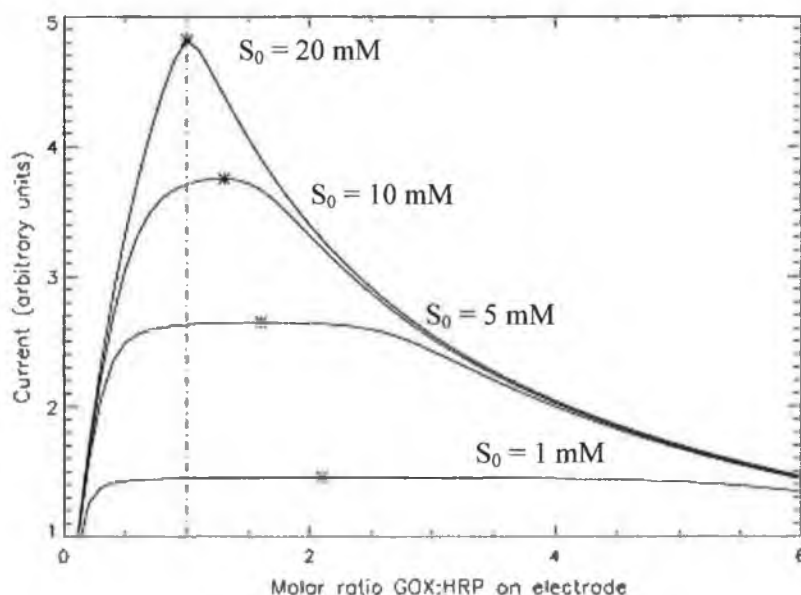


**Figure 3.17.** Dependence of current on the electrode GOX:HRP ratio for different initial glucose concentrations,  $S_0$ . From bottom to top the curves correspond to  $S_0 = 1, 5, 10$  and  $20 \text{ mM}$ . The position of the maximum current value is indicated on each curve.

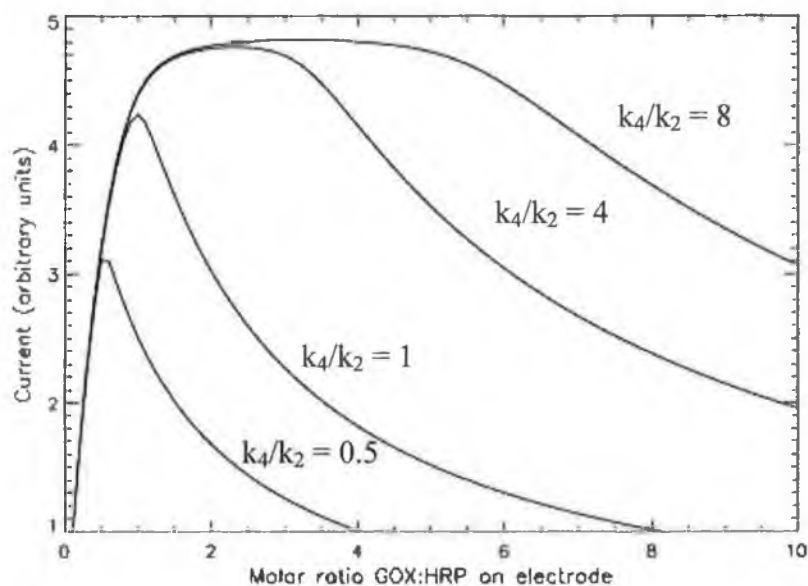


**Figure 3.18.** Dependence of current on the electrode GOX:HRP ratio for different  $k_4/k_2$  values. The lower curve corresponds to  $k_4/k_2 = 0.5$  and the upper curve to  $k_4/k_2 = 8$ .

The numerical simulations presented show that, when the two consecutive reactions are assumed to be equally fast ( $k_4/k_2 = 1$ ), the optimal ratio of immobilised enzymes converges to 1 as the glucose concentration increases. Moreover, the results obtained by fixing the glucose concentration and varying the kinetic rates of the GOX and HRP reactions strongly suggest that an optimal ratio GOX:HRP of 1 is associated with the two consecutive reactions proceeding at the same speed.

Since the mathematical model on which the simulations are based uses kinetic rate constants for the immobilised enzymes, while the specific activities quoted in the experimental work refer to the enzymes in the PBS solution, it is reasonable to conclude that these conditions might be brought about by a reduction in the actual activity of immobilised HRP. This could be due to the efficiency of electron transfer to the enzyme active site from the conducting polymer surface, which is affected by the random orientation of enzyme on the surface, possibly making much of the immobilised material completely inactive.

### 3.3.6 Assessment of different avidin/HRP platforms on binding GOX or biotin-GOX

After investigating the performance of the bienzyme electrode, an enzyme-channeling system based on the same enzyme coupling was developed in order to detect in real-time, the immunological interaction between avidin and biotin. The specific avidin-biotin interaction brings the biotin-GOX conjugate in proximity to HRP on the electrode surface to create a so-called “cascade”. The diagram in *Figure 3.19* shows a schematic of the biosensor platform with avidin and HRP immobilised on the PANI/PVS modified electrode surface. Biotin-GOX conjugate produces  $H_2O_2$  by glucose and HRP attached to the surface to produce a catalytic signal reducing  $H_2O_2$  by direct electron transfer.

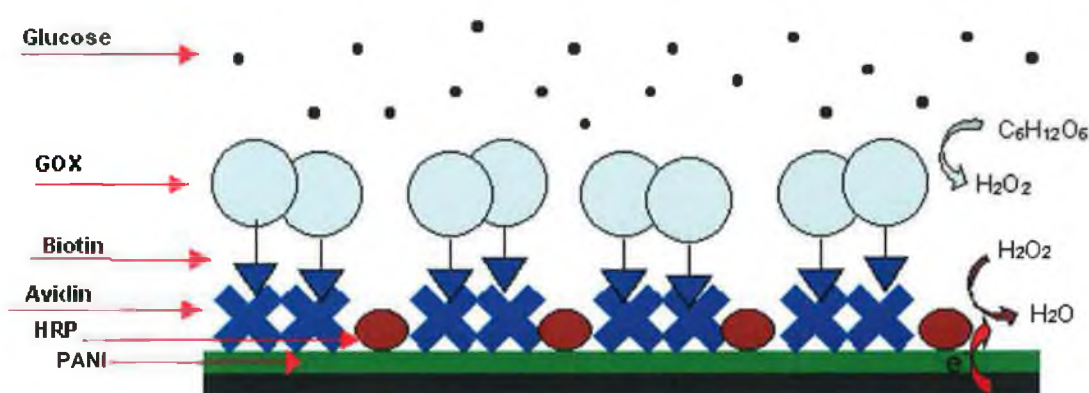


**Figure 3.19.** The enzyme-channeling-based biosensor with avidin and HRP immobilised on PANI/PVS electrode surface and biotin-GOX specifically binding to avidin via a biotin-avidin interaction. The two enzymatic reactions occurring are also shown.

Experiments were carried out to test the ability of the biosensor to specifically bind biotin-GOX conjugate. GOX enzyme without the attached biotin was chosen as a control protein to evaluate the specificity of the protein interactions. An avidin/HRP-based biosensor was prepared according to section 3.2.10, using a solution with HRP 0.4 mg/ml and avidin 0.8 mg/ml (which corresponds to a molar ratio of HRP/Avidin of 1:1) for the immobilisation procedure. A direct evaluation of the biosensor behaviour in relation to biotin-GOX conjugate and in relation to GOX was made, testing the sensor in a flow-injection system. A two-step analysis was carried out

according to the section 3.2.11 where during the first step, the protein solution was injected, and during the second step, the glucose solution was passed over the surface to generate the signal. *Figure 3.20* shows the typical signals recorded after passing the relevant solutions in succession over the electrode surface. After reaching the steady state injecting PBS buffer, solutions of glucose (20 mM), GOX (20  $\mu\text{g/ml}$ ), glucose (20 mM), biotin-GOX (20  $\mu\text{g/ml}$ ), glucose (20 mM) and  $\text{H}_2\text{O}_2$  (1 mM) were passed over the surface in this order. The first glucose solution was used as a control to prove that without GOX no signal is generated; a second glucose solution was passed after a GOX solution and the signal recorded was about 1.5  $\mu\text{A}$ . A third glucose solution was passed over after a biotin-GOX solution, and the signal recorded was about 6.0  $\mu\text{A}$ . The final  $\text{H}_2\text{O}_2$  solution was injected to test the HRP activity on the surface and the signal recorded was about 17  $\mu\text{A}$ .

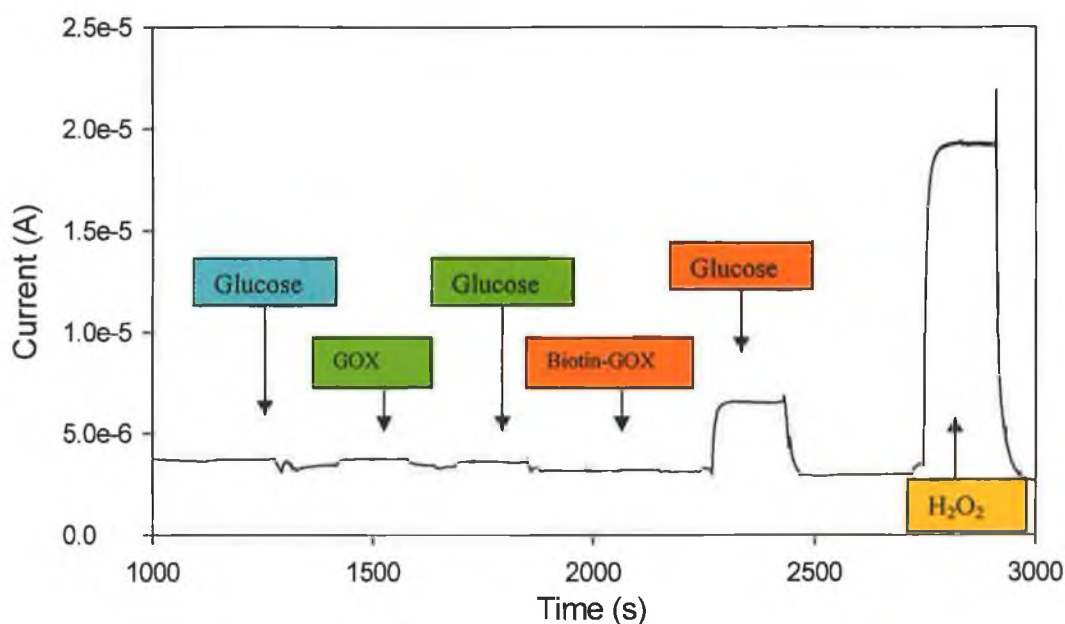


**Figure 3.20.** Amperogram recorded using an avidin/HRP-based biosensor (molar ratio 1:1) in a flow-injection system analysis. The signal generated from biotin-GOX is about four times higher than the signal generated from GOX. The final  $\text{H}_2\text{O}_2$  solution was passed to test the HRP activity (-0.1 V vs. Ag/AgCl). (Electrode surface area: 0.07  $\text{cm}^2$ ).

The Biotin-GOX conjugate generated a higher signal compared to that of GOX. This confirmed the presence of the specific interaction between avidin and biotin that promotes the conjugate attachment. However, the signal generated by GOX without biotin attached was about 22% of the specific signal and this suggested that non-specific binding was taking place. The high signal generated at the end by adding  $H_2O_2$  via HRP suggests that the enzyme-channeling system was highly subject to the diffusion phenomenon of the reactants. The signal generated from the enzyme-channeling system depends on the relative turn over rate of the two enzymes and also from the diffusion of the glucose in the first step and of  $H_2O_2$  from GOX to HRP in the second step. All of these events may have produced a lower local concentration of  $H_2O_2$  in the vicinity of HRP resulting, therefore, in a lower catalytic signal. Experiments were also carried out to optimise the avidin/HRP platform. Different electrodes were formed using solutions with fixed 0.4 mg/ml of HRP and avidin at concentrations between 0 and 1.1 mg/ml, for the immobilisation process. The biosensors were tested in a flow-injection system using biotin-GOX and GOX at concentrations of 20  $\mu$ g/ml and glucose at 20mM as a substrate.

The graphs in *Figure 3.21* show the catalytic signals achieved from the biosensor with different avidin/HRP ratios in the flow-injection set-up. It can be seen in *Figure 3.21(a)* that the activities of the two GOX enzymes (the one free and the other one conjugated to biotin) were different. As a matter of fact, in the absence of avidin on the electrode surface, the signal from the free GOX was higher than from the biotin-GOX. This is very likely due to the fact that the conjugation with biotin caused a loss of activity. However, both GOX and biotin-GOX show the ability to bind non-specifically to the electrode surface. Increasing the amount of avidin on the surface resulted in a reversal of this trend because at a concentration of avidin of 0.2 mg/ml, (which resulted in a molar ratio avidin/HRP of 1:5) the signal achieved from biotin-GOX was higher than from GOX. The non-specific signal reached a minimum value at the avidin concentration of 0.4 mg/ml and remained constant at higher concentrations. This appears to suggest that at that concentration the electrode surface was fully covered by the two proteins. The specific signal, on the other hand, generated from biotin-GOX started to be dependent on the molar ratio of avidin/HRP on the electrode surface. It can be seen, that the maximum response was achieved at the avidin concentration of 0.7 mg/ml which corresponds to a molar ratio avidin/HRP of 1:1. This result agrees very well with that for the bienzyme platform, where the

best performance corresponded to the molar ratio HRP/GOX of 1:1 (section 3.3.5). Once again then, it can be suggested that the spatial molecular disposition on the electrode surface for the two proteins at molar ratio of 1:1 was the one which ensured highest sensor efficiency (see *Figure 3.15*).

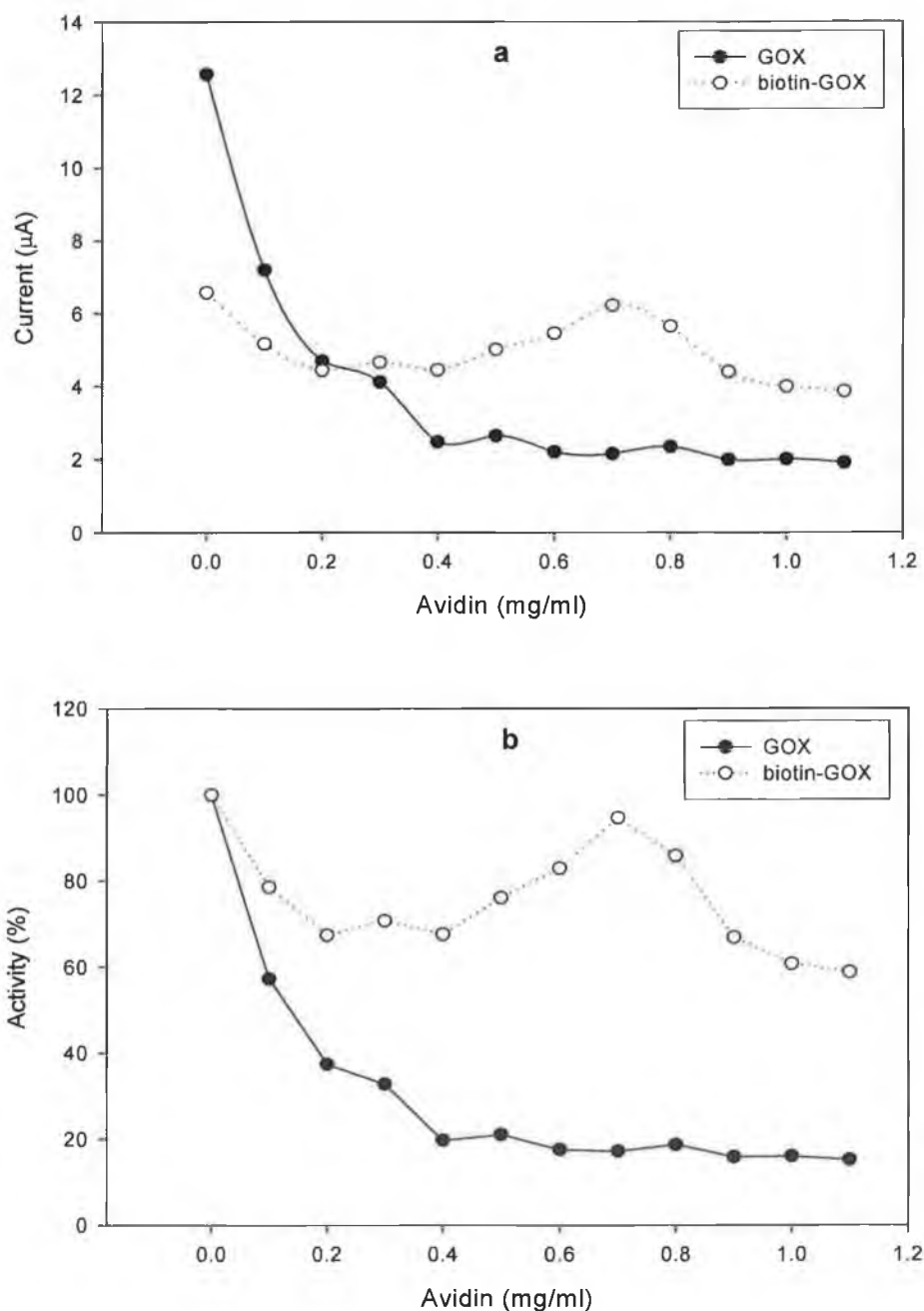


**Figure 3.21.** (a) Flow-injection analysis with sensors prepared using solutions with HRP at concentration 0.4 mg/ml and avidin at concentrations between 0 and 1.1 mg/ml. GOX or biotin-GOX at a concentration of 20 µg/ml were passed over the electrode surface, followed by glucose at 20 mM. Response measured at -0.1 V vs. Ag/AgCl. (b) The responses of the GOX and biotin-GOX assays assuming the same activity for the two GOX enzymes. (Electrode surface area: 0.07 cm<sup>2</sup>).

The difference between the two signals, (specific and non-specific), appears clearer from *Figure 3.21(b)*. In this graph the current values were recalculated to take account of the difference in activity of the two enzymes (free GOX and biotin-GOX conjugate).

### **3.3.7 Calibration curve for GOX and biotin-GOX on avidin/HRP platform**

An avidin/HRP platform was established using an immobilisation solution of 0.7 mg/ml of avidin and 0.4 mg/ml of HRP to ensure the minimum non-specific signal, the total coverage of the surface and the highest current signal. This platform was tested in a flow-injection assay where different concentrations of biotin-GOX or GOX were passed over the electrode surface. *Figure 3.22* shows the signals generated by GOX and biotin-GOX at different concentrations. It can be seen that for lower concentrations of GOX or biotin-GOX, the signal achieved from GOX was similar to the signal generated by biotin-GOX. Above 10  $\mu\text{g/ml}$ , the signal for GOX reached a plateau, while the signals recorded from biotin-GOX increased from 10 to 22  $\mu\text{g/ml}$ . This suggests that for lower concentrations, the higher activity of the free GOX was predominant despite the small amount non-specifically attached. However, at higher concentrations, proportionately more biotin-GOX was specifically attached, resulting in higher specific signals. Above 20  $\mu\text{g/ml}$ , a constant signal ratio of approximately 2:1 was achieved. If we here again take into account the relative activities of the two enzyme materials, this ratio would be approximately 4:1 which still represents an estimably poor ratio of specific-to-non-specific signal.



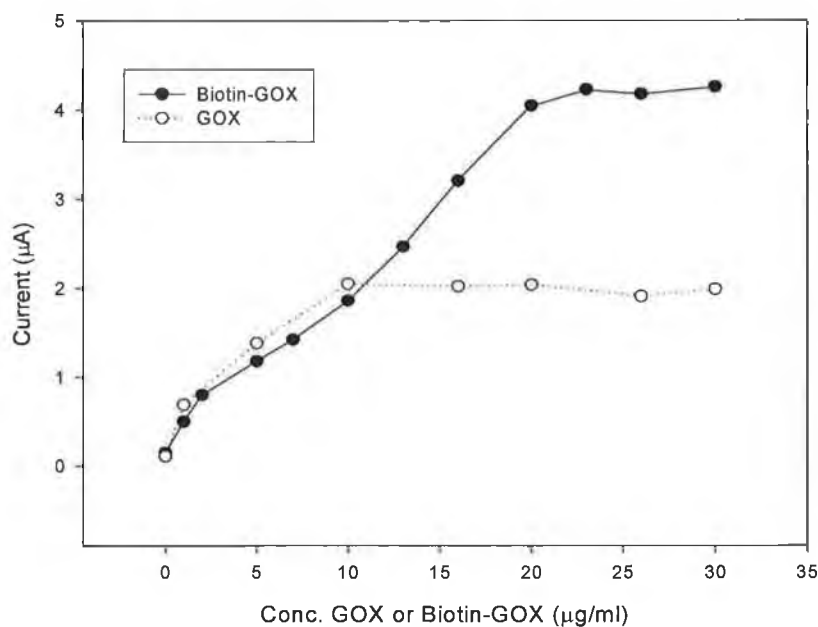


**Figure 3.22.** Flow-injection assay using an avidin/HRP-based biosensor (avidin 0.7 mg/ml and HRP 0.4 mg/ml). Concentrations between 1 and 30  $\mu\text{g/ml}$  of GOX or biotin-GOX were passed over the surface followed by 20 mM glucose solution. Response measured at -0.1 V vs. Ag/AgCl. Above 10  $\mu\text{g/ml}$  the signals generated by biotin-GOX ( $\bullet$ ) were higher than the signals recorded from GOX ( $\circ$ ). (Electrode surface area:  $0.07 \text{ cm}^2$ ).

### 3.3.8 Competition assay system for real-time biotin determination

The avidin/HRP-based biosensor (avidin 0.7 mg/ml, HRP 0.4 mg/ml) was further tested for biotin determinations in a competition assay system. In this assay, free biotin competes with biotin-GOX conjugate to bind specifically to avidin, resulting in lower signals generated by biotin-GOX with increasing free biotin concentration. Using a constant biotin-GOX concentration, but increasing the concentration of free biotin it was possible to calibrate the biosensor to determine biotin in a sample. The amperogram in *Figure 3.23* shows two signals recorded in two different experiments where, in the first one, biotin-GOX at a concentration of 20  $\mu\text{g/ml}$  was passed over the surface (a), and in the second one, biotin-GOX at a concentration of 20  $\mu\text{g/ml}$  and free biotin at a concentration of 50  $\mu\text{g/ml}$  were passed over the surface together (b). It can be seen that the signal decreased when free biotin was present which suggests that a specific, competitive binding was occurring. However, there was no reproducibility in these experiments. The signal generated by biotin-GOX decreased disproportionately to the concentration of free biotin added. This would need to be studied more

carefully as in its current form it could not be used as an assay platform. However, problems with producing functioning competitive assays with these particular biotin/avidin reagents has been found previously<sup>43</sup> and may be due to the immunochemicals used and not the assay itself.

The platform configuration based on avidin and HRP immobilised on the electrode surface resulted in the ability to discriminate between a specific interaction with biotin-GOX labelled and the non-specific interaction with GOX. However, the specific response generated by biotin-GOX was extremely poor and a sensitive evaluation in real-time of the immunological interaction for avidin-biotin was not practical. The preliminary study carried out on the bienzyme-based biosensor helped to better understand the phenomena influencing the efficiency of the enzyme-channeling system. From this study it was established that an equimolar distribution of the two enzymes on the electrode surface produced the highest signals. A similar configuration could be adopted for avidin/HRP-based immunosensor with a maximum difference between specific and non-specific signal achieved with a molar ratio avidin/HRP of 1:1.

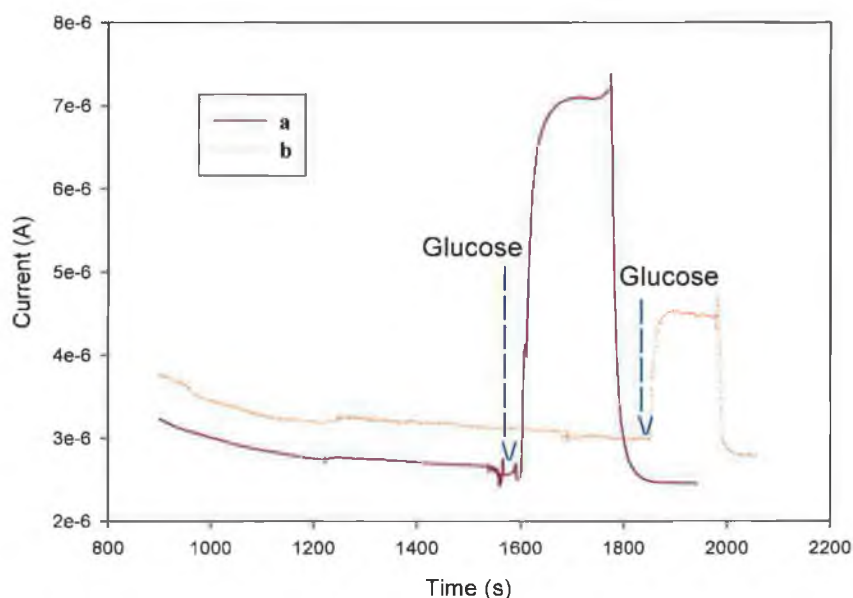


**Figure 3.23.** Flow-injection assay with an avidin/HRP-based biosensor (avidin 0.7 mg/ml, HRP 0.4 mg/ml). Signal recorded passing over the surface biotin-GOX at a concentration of 20  $\mu\text{g/ml}$  followed by glucose at concentration of 20 mM (a) and signal recorded passing over the electrode surface a solution containing biotin-GOX at a concentration of 20  $\mu\text{g/ml}$  and free biotin at a concentration of 50  $\mu\text{g/ml}$  followed by glucose at concentration of 20 mM (b). Responses measured at -0.1 V vs. Ag/AgCl. The competition occurring between biotin and biotin-GOX reduced the signal generated from biotin-GOX alone. (Electrode surface area: 0.07  $\text{cm}^2$ ).

In this situation a possible enhancement of the performance of the biosensor might be obtained by the use of AuNPs. AuNPs have been adopted in many systems exploiting their ability to stably bind a higher number of biomolecules. In the system under study here, these NPs might be used to carry over the electrode surface a higher molar ratio of biotin-GOX molecules than could be achieved by the normal configuration, resulting in possible signal amplification by the large increase in  $H_2O_2$  production (Figure 3.24). That is, by the deposition of biotin-GOX on AuNPs, the number of GOX molecules in close proximity to HRP would be increased.

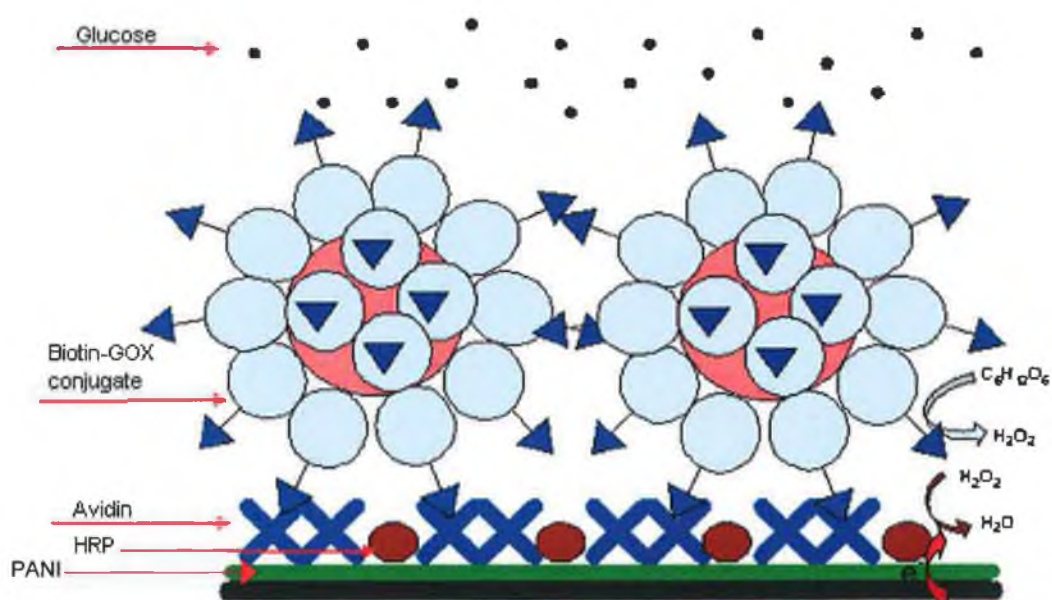


**Figure 3.24.** The enzyme-channeling-based biosensor with avidin and HRP immobilised on PANI/PVS electrode surface and biotin-GOX molecules carried by AuNPs. A higher number of conjugates come into close proximity with the surface via the specific avidin-biotin interaction resulting in a possible signal amplification.

### 3.3.9 Conjugation of AuNPs with GOX and HRP

For conjugation, enzymes were directly adsorbed onto the colloidal gold particle surfaces, mediated mainly by electrostatic forces with, in addition, hydrophobic interaction or possible chemisorption through thiol groups present on the external shell of the protein. AuNPs were negatively charged due to the citrate molecules which surround them, ensuring their stability after the synthesis. Positively charged protein would, therefore, be electrostatically adsorbed to the Au particles. However,

from other studies carried out to evaluate the effect of uncharged compounds on colloidal suspensions, it was found that colloids could behave as hydrophobic sols maintained in suspension by forces of non-electric nature<sup>51</sup>. The interaction of protein-gold colloids, might be, therefore, the result of forces of both electrostatic and hydrophobic nature giving the extraordinary stability to the formed conjugate.

A preliminary titration was performed in order to judge the optimal enzyme concentration to be used for the conjugation. The conjugation was best performed at, or near to the isoelectric point of the protein where the strongest attraction is achieved without loss of activity<sup>52</sup>. The colloidal Au was formed in solution by virtue of a balance between electrostatic repulsion and van der Waals attraction among the particles. However, on addition of ionic substances, the attracting force becomes greater than the repulsion, which leads to an aggregation accompanying a colour change from red ( $\lambda_{\text{max}} \approx 520 \text{ nm}$ ,  $A_{520}$ ) to blue ( $\lambda_{\text{max}}$ ,  $A_{580}$ )<sup>53</sup>. *Figure 3.25* shows the UV-vis spectrum for the Au colloid solution where it can be seen the typical absorption peak at 520 nm. Coating the colloidal surfaces with protein molecules, can prevent this instability.

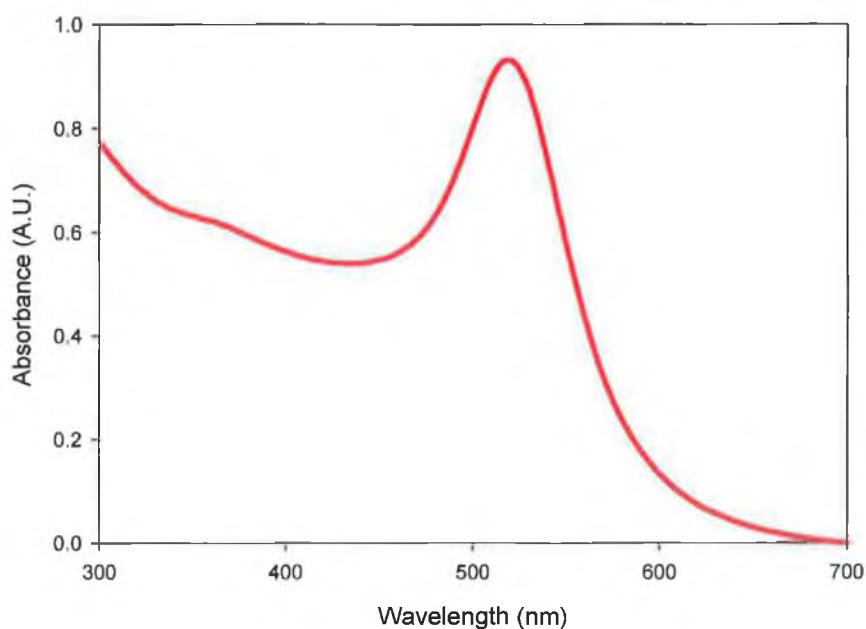


**Figure 3.25.** UV-Vis spectrum of Au colloid solution with the characteristic absorbance band at 520 nm indicating the surface plasmon transition of Au.

Optimal enzyme concentration for the conjugation was determined by the Au aggregation test by comparing the absorption at 520 and 580 nm ( $A_{520}-A_{580}$ ). According to the section 3.2.14 Au colloid suspensions, adjusted to pH 6.8 for the conjugation with HRP and to pH 4 for the conjugation with GOX, were pipetted (300  $\mu$ l) into a series of wells of a test plate (12x8). 30  $\mu$ l of the enzyme solutions (0 – 18  $\mu$ g/ml HRP and 0 – 28  $\mu$ g/ml GOX) were added to each colloidal Au solution. After 5 min., each well received 30  $\mu$ L of 10% (w/v) NaCl to cause the gold aggregation. Absorption from each well at 520 and 580 nm was determined after 5 min. of mixing.

*Figure 3.26* shows the results achieved for the titrations of the two enzymes in the conjugation to AuNPs. It can be seen that the minimal concentration required to stabilize colloidal Au was 6  $\mu$ g/ml for HRP and 11  $\mu$ g/ml for GOX, which corresponded to 0.13  $\mu$ M and 0.07  $\mu$ M, respectively. AuNPs concentration in solution was calculated and found to be about 2 nM.

From all these data it was possible to estimate the number of HRP and GOX molecules attached to each Au particle. It was found that the number of molecules required to stabilize Au particles preventing their aggregation, was 57 for HRP and 28 for GOX. These values were verified geometrically by using the close packed sphere model<sup>54</sup>. GOX and HRP molecules were approximated to spheres with diameter of 4.19 nm and 2.58 nm, respectively. A spherical packing corresponds to the placement of  $n$  spheres around a central unit sphere. By the use of trigonometric calculations with the radius of the central sphere (AuNP, 7.5 nm) and of those surrounding (enzyme molecules), it was possible to approximate the maximum number of spheres touching the central one. It was found that about 50 HRP molecules and about 25 GOX molecules can be arranged around a AuNP central sphere of 7.5 nm radius. A good correspondence between experimental data and geometrical calculations, was thus obtained.

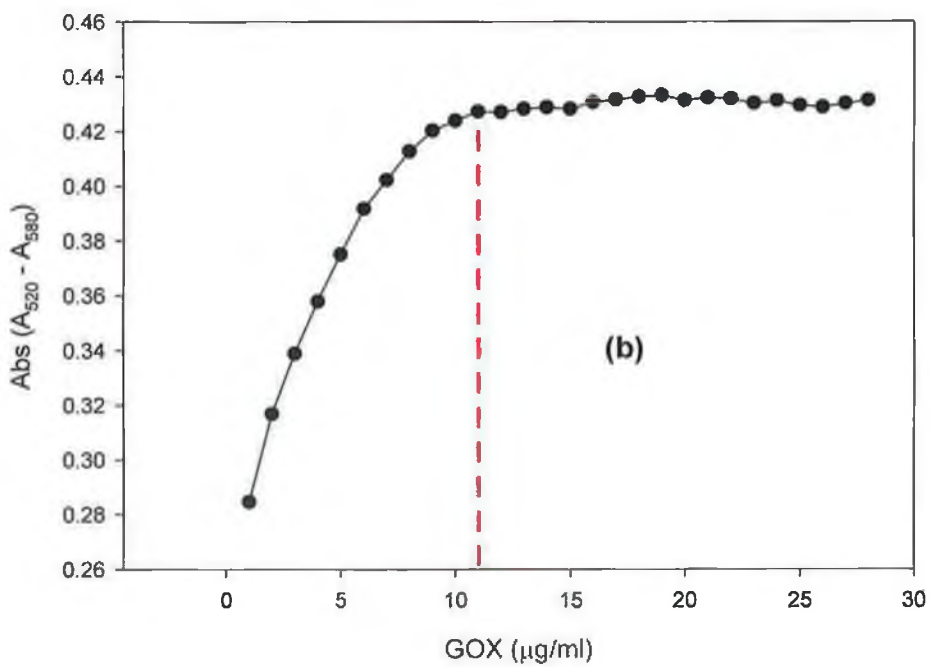
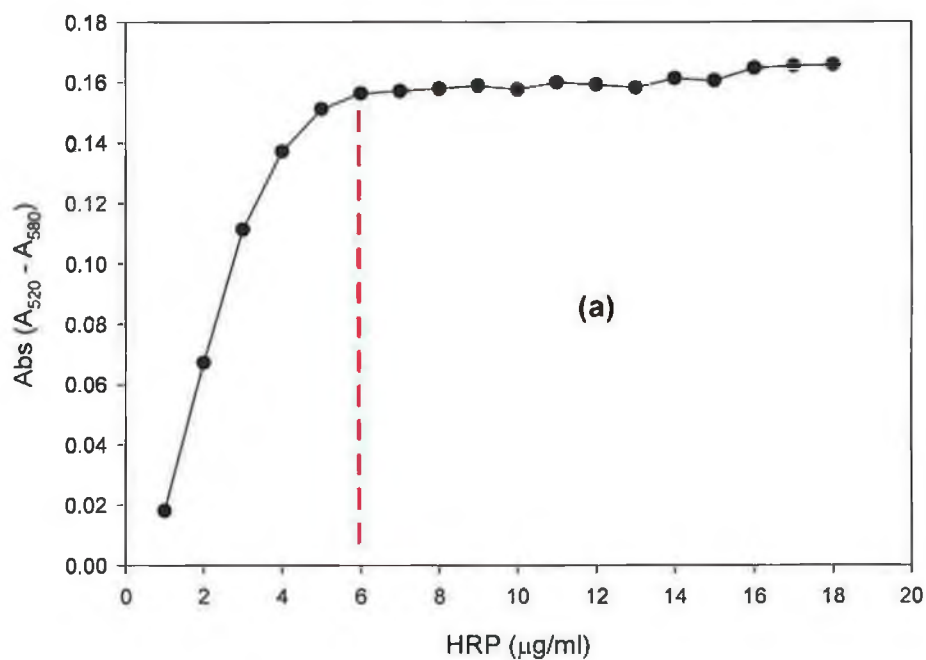


**Figure 3.26. Gold aggregation test for HRP and GOX. (a) The minimal HRP concentration to stabilize gold nanoparticles was found to be 6  $\mu\text{g/mL}$  (0.13  $\mu\text{M}$ ). (b) The minimal GOX concentration was found to be 11  $\mu\text{g/ml}$  (0.07  $\mu\text{M}$ ).**

The two enzyme-Au conjugates were then prepared by mixing 10 ml of Au colloid solution (adjusted at pH 6.8 for HRP and pH 4 for GOX) with the two enzyme solutions at the concentrations determined by the titration plus a 10% and precisely HRP 7  $\mu\text{g/ml}$  and GOX 12  $\mu\text{g/ml}$ . The mixtures were stirred for 10 min. and then to remove the excess of enzyme, were centrifuged at 15,000 g for 1 h at 4°C. The clear supernatants were carefully removed and the precipitated Au-HRP and Au-GOX conjugates were resuspended in 10 ml of PBS buffer (pH 6.8) and stored at 4°C. Spectrophotometric and electrochemical analyses were then carried out to evaluate the enzyme activity after the conjugation process.

### 3.3.10 Spectrophotometric activity study of HRP on gold nanoparticles

Protein adsorption to solid surfaces often induces structural changes that may affect the entire molecule. This is a frequently observed phenomenon, and the resulting changes in structure, and function, can have profound consequences in various fields, such as biology, medicine, biotechnology, and food processing. Therefore, an understanding of the conformational behavior of proteins at solid-solution interfaces is desirable for a variety of reasons. For example, detailed mapping of conformational changes is necessary for understanding the mechanism of protein adsorption and can help to identify optimal conditions to preserve functionality following protein immobilization. A schematic mechanism for protein adsorption to solid surfaces can be illustrated as follows:



where P is the native protein, S is the surface, and DP denotes an ensemble of non-native protein conformations. After the protein has transformed to the DP-S state it usually sticks to the surface, and the reverse reaction, whereby the protein desorbs from the particle (with or without renaturation), rarely occurs unless the chemical

environment changes (with respect, for instance, to pH or ionic strength). The degree of conformational change and the rate at which the protein undergoes this conformational change depend on the protein's specific chemical properties, its stability, and the surface's chemical properties<sup>56</sup>.

In ELISA tests the well known reaction between HRP and OPD-H<sub>2</sub>O<sub>2</sub> substrate is generally used to quantify the enzyme-based label and the related analyte under investigation, exploiting the fact that the reaction product is colored and adsorbs in UV-Vis. The same reaction was also used to quantify the active enzyme attached to each AuNP.

An enzymatic assay was carried out in a 96-well plate utilizing OPD as a colorimetric substrate. In the presence of HRP, the reaction with urea/hydrogen peroxide and OPD generates a soluble yellow-brown product, the intensity of which is proportional to the concentration of HRP. A calibration curve with standard HRP solutions was generated measuring the absorbance after the reaction with the substrate at a wavelength of 450 nm. *Figure 3.27* shows the calibration curve where the linear range was achieved for HRP concentrations between 0.015 µg/ml and 2.0 µg/ml. Comparing the absorbance measured from the Au-HRP conjugate solution with this calibration curve resulted in a concentration of active HRP of 1.67 µg/ml (0.038 µM). This concentration corresponds to 16 active HRP molecules per AuNP. From the previous section, it was established that the number of HRP surrounding the Au particle was as much as 57. The percentage activity retention after conjugation was therefore about 28%. This could be due partially to the detachment of some enzyme molecules during the centrifugation and also to the loss of bioactivity by conformational changes in the protein structure during the conjugation process.



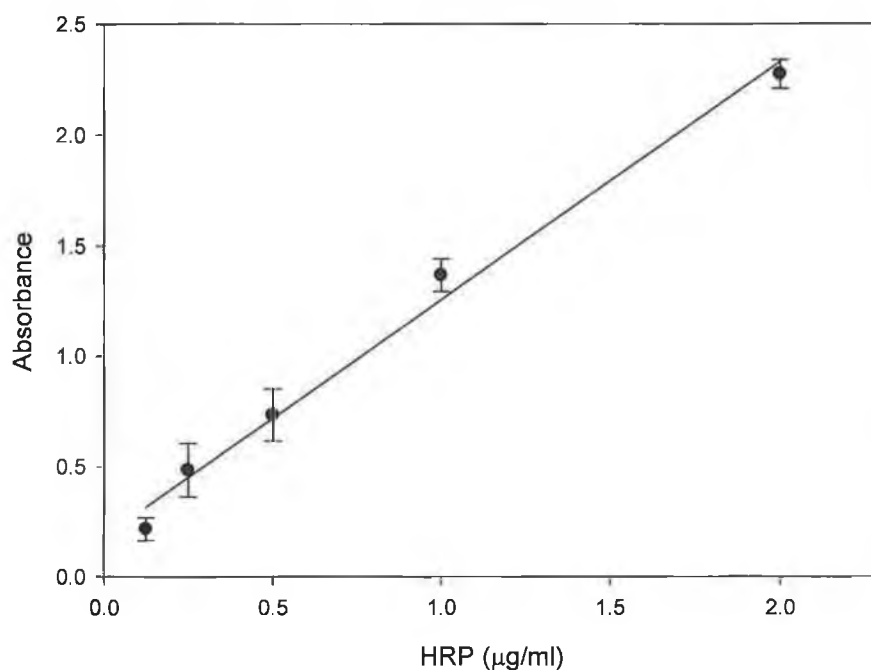


**Figure 3.27. Spectrophotometric analysis of HRP. The reaction between HRP and urea/hydrogen peroxidase/OPD generates a colored product ( $\lambda=450$  nm,  $a=1.276$ ,  $b=0.084$ ,  $r^2=0.9915$ ).**

This result is in agreement with data present in the literature. From studies carried out to evaluate the activity of enzymes after conjugation with NPs, it was found that the particle size had a big effect on the biomolecule conformation and functionality. It seems that the loss of activity for the enzyme increases for larger particle sizes, due to more prominent structural deformation<sup>55</sup>. Smaller particles, with greater surface curvature promote the retention of more native-like protein structure and function when compared to their larger (and hence less curved) particle counterparts. The influence of surface curvature is not entirely unexpected. Nature presents examples of nanoscale surfaces that are highly curved, such as, the molecular components of subcellular organelles and membranes. These curved surfaces may result in the stabilization of proteins, nucleic acids, and other biological macromolecules with significant secondary and tertiary structure<sup>56</sup>. In *Figure 3.28* is shown the curvature radius effect on the protein deformation.

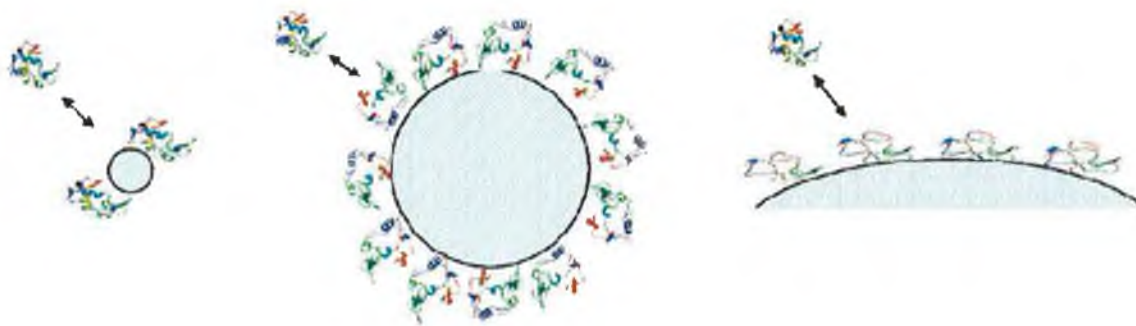


**Figure 3.28. Diagram of enzyme adsorption onto NPs with different sizes. Stronger protein-particle interactions exist in the case of larger nanoparticles, resulting in more protein unfolding and less enzymatic activity<sup>56</sup>.**

The activity studies carried out to evaluate the functionality of the Au-HRP conjugate, revealed a big loss of activity after the conjugation process. Due to the enormous particle size effect on the functionality of the protein, NPs with a smaller diameter (< 15 nm) would be expected to preserve higher percentage native protein functionality after the conjugation and should certainly be the object of future work. Alternatively, specific affinity interactions could be exploited to attach enzymes to AuNPs retaining their biofunctionality. For example, streptavidin-functionalized AuNPs could be used for the affinity binding of biotinylated enzymes<sup>57</sup>.

### **3.3.11 Amperometric activity study of HRP on gold nanoparticles**

A novel analytical amperometric methodology was developed and proposed to determine the concentration of active HRP in a sample as alternative to the spectrophotometric method. As discussed earlier in this chapter, polyaniline conducting polymer adopted for the construction of the bienzyme-based biosensor, showed adequate ability to bind proteins, which has been exploited to immobilise HRP, GOX and avidin. This ability was tested in a flow-injection analysis system. A freshly prepared PANI/PVS modified screen-printed electrode was inserted into the flow-cell and PBS buffer solution (pH 6.8) was passed over the surface until a steady current signal was recorded at a potential of -0.1 V vs. Ag/AgCl. A 3 ml solution containing 10 µg/ml of HRP and H<sub>2</sub>O<sub>2</sub> (1 mM) was then passed over the surface. *Figure 3.29* shows the signal recorded while the enzyme was passing over the

polymer surface and presents a typical curve of saturation where the maximum net current value of  $36 \mu\text{A}$  was reached gradually due to the kinetic of the binding interaction of the enzyme with the polymer. In a further experiment, with a new PANI/PVS modified electrode, after reaching the steady state, instead of injecting a solution with both the enzyme and  $\text{H}_2\text{O}_2$  present, two solutions were added at different times; 1 ml of HRP at  $10 \mu\text{g/ml}$ , followed by 1 ml of  $1 \text{ mM}$   $\text{H}_2\text{O}_2$  solution. In this case, as it can be seen in *Figure 3.30*, the maximum net current signal was reached much more quickly, generating the typical step-shape curve, with, however, the same current value recorded as in the previous experiment ( $\sim 36 \mu\text{A}$ ). These experiments proved that the enzyme was adsorbed onto the conducting polymer during the flow-injection. The two different kind of signals; the kinetic in the first experiment and the direct in the second, are more clearly illustrated in *Figure 3.31*.

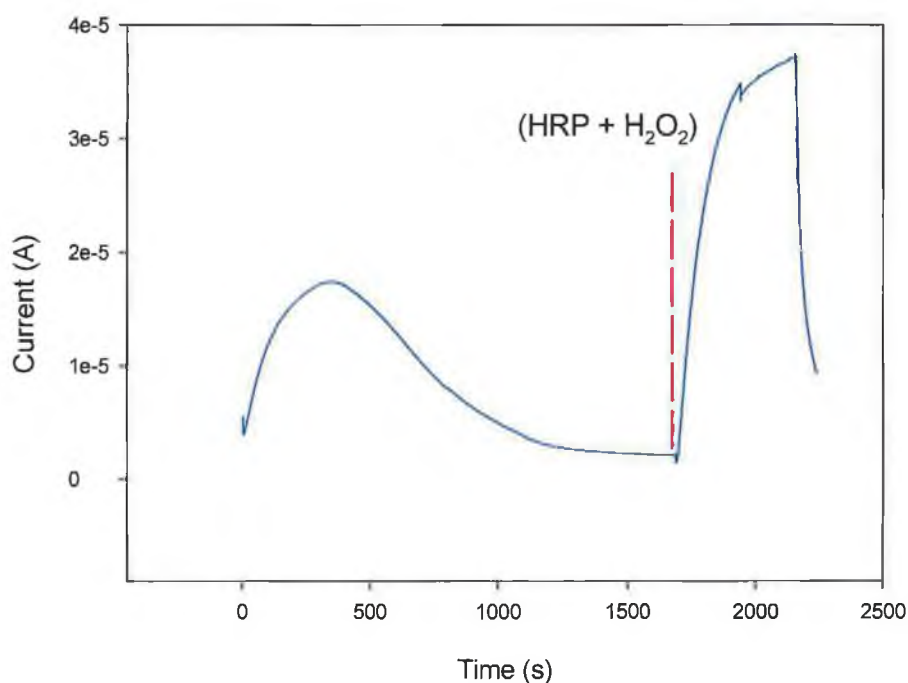


**Figure 3.29.** Amperogram recorded by passing HRP ( $10 \mu\text{g/ml}$ ) and  $\text{H}_2\text{O}_2$  ( $1 \text{ mM}$ ) over a PANI/PVS modified electrode. The maximum current value reached was  $36 \mu\text{A}$  at  $-0.1 \text{ V vs. Ag/AgCl}$ . (Electrode surface area:  $0.07 \text{ cm}^2$ ).

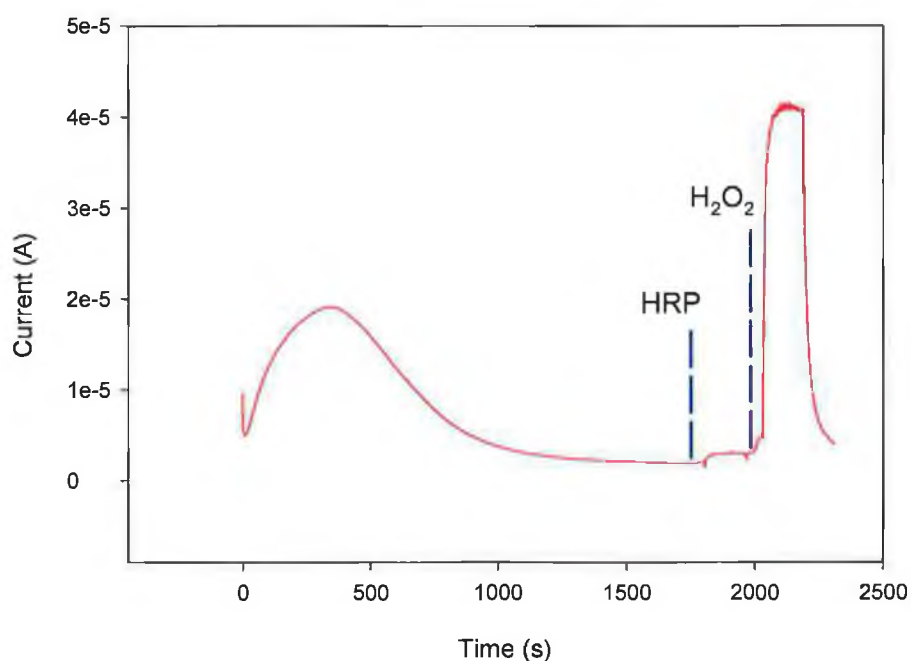


**Figure 3.30.** Amperogram recorded by passing HRP (10  $\mu\text{g/ml}$ ) first, and subsequently  $\text{H}_2\text{O}_2$  (1 mM). The typical step-shape curve recorded after passing  $\text{H}_2\text{O}_2$  shows that the enzyme was adsorbed onto the polymer surface during the previous step (-0.1 V vs. Ag/AgCl). (Electrode surface area:  $0.07 \text{ cm}^2$ ).

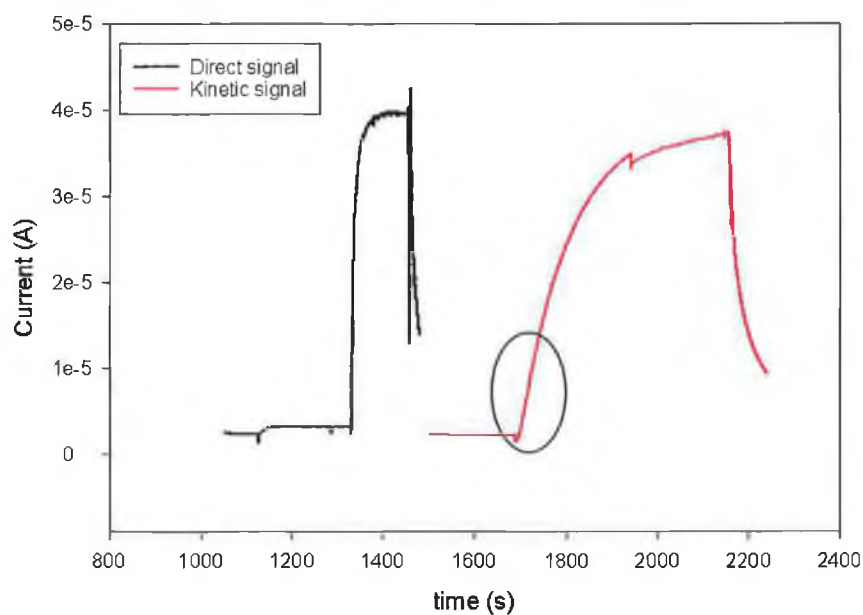


**Figure 3.31.** Comparison between the direct amperometric signal generated passing first HRP and then  $\text{H}_2\text{O}_2$  (black) and the kinetic signal passing HRP and  $\text{H}_2\text{O}_2$  together (red). The early part of this second curve can be considered linear.

The graph shown in *Figure 3.29* represents the saturation curve of the electrode surface with HRP. Considering the early part of the curve, during which, mass transport is not limited by lack of available binding sites, it can be assumed that the curve is linear. The slope of this curve was found to be proportional to the concentration of HRP passing<sup>46</sup>. A very sensitive method was, therefore, optimised for the calibration. Since the analysis of a HRP sample takes only few seconds the surface does not become saturated and a multi-calibration is possible using the same electrode. Various experiments were carried out to optimise the contact time of the enzyme with the surface and the optimum was found to be 30 s. *Figure 3.32* shows the multi-calibration curve recorded by passing five different solutions of HRP at concentrations between 0.1 and 5  $\mu\text{g/ml}$  over the electrode surface for 30 s each. As it can be seen, the kinetic signal generated by the different HRP solutions presents an increased slope for higher concentrations.

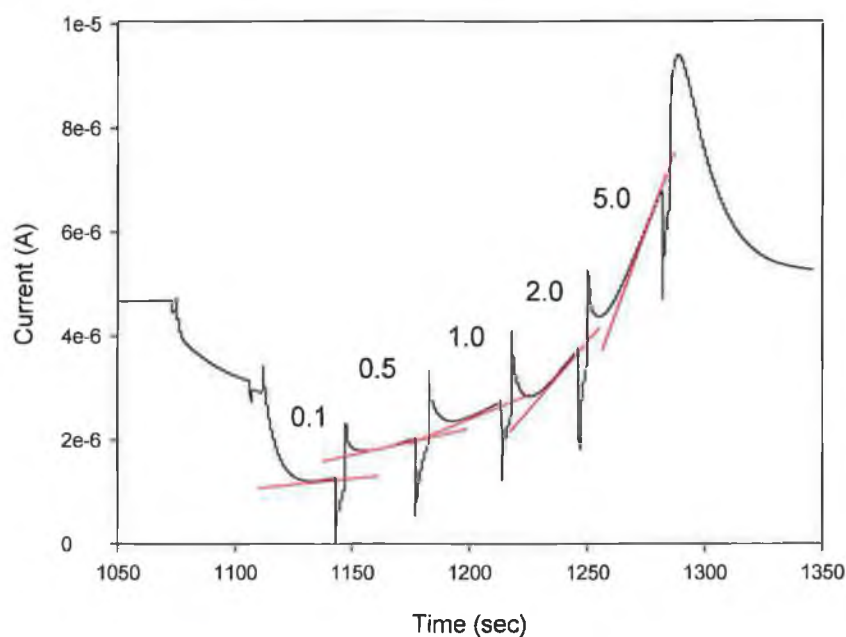


**Figure 3.32.** Multicalibration analysis of HRP. Solutions of 0.1, 0.5, 1.0, 2.0 and 5.0  $\mu\text{g/ml}$  of HRP were passed each over a PANI/PVS modified electrode surface for 30 s (-0.1 V vs. Ag/AgCl). (Electrode surface area: 0.07  $\text{cm}^2$ ).

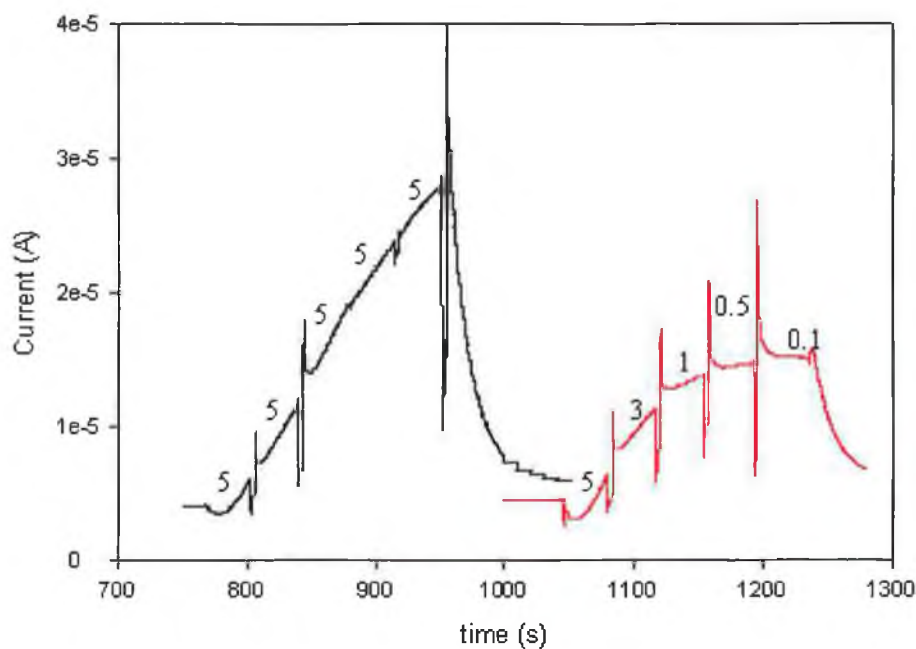


**Figure 3.33.** Control experiments showing the direct proportionality between the HRP concentration injected and the slope of the current signal. The black curve shows five injections of 5.0  $\mu\text{g/ml}$  of HRP. The red curve shows five injections with 5, 3, 1, 0.5 and 0.1  $\mu\text{g/ml}$  of HRP (-0.1 V vs. Ag/AgCl). (Electrode surface area: 0.07  $\text{cm}^2$ ).

Two control experiments were then carried out in order to demonstrate the independence of the signals from each other and the genuine proportionality of the slope with the enzyme concentration. In the first one five HRP solutions at the same concentration (5  $\mu\text{g/ml}$ ) were passed over the surface. In the second one, a “negative” multi-calibration platform was used where the five different solutions were passed in a decreasing order, starting from 5  $\mu\text{g/ml}$  to 0.1  $\mu\text{g/ml}$ .

Figure 3.33 shows the two control experiment amperograms on the same graph. It can be seen that passing five times HRP solutions at the same concentration, the slope of the five kinetic signals were very similar. The last two signal slopes became only slightly reduced probably due to the fact that the electrode surface was reaching the saturation, having used the highest HRP concentration for the test. The second amperogram clearly shows that the signal generated by one solution of HRP is independent from the previous one because a decrease of the slope result from a decrease in the HRP concentration passed. In order to prevent early saturation of the electrode surface, for a more accurate response, the “positive” multi-calibration platform was used to create the calibration curve. The HRP solutions were passed,

starting from the most dilute to the most concentrated. *Figure 3.34* shows the calibration curve for the amperometric, real-time detection of HRP using PANI/PVS modified screen-printed electrode in a flow-injection set-up. The response was linear over the range 0.1 – 5.0  $\mu\text{g/ml}$  of HRP with sensitivity of  $2.3 \times 10^{-8}$  A/ $\mu\text{g/ml/s}$ .

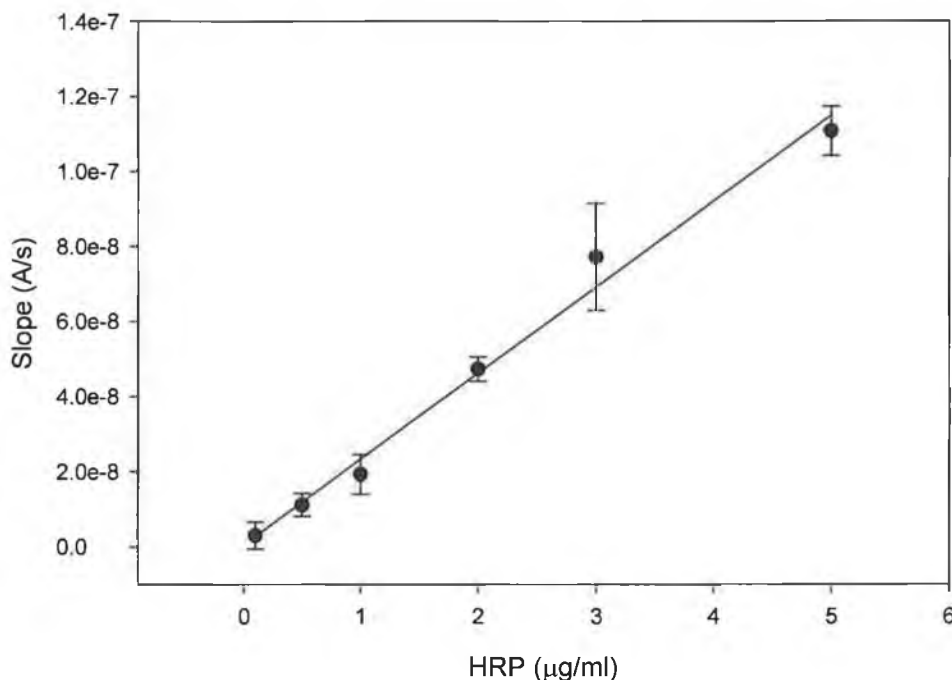


**Figure 3.34.** Calibration curve for amperometric detection of HRP. ( $y = 2.3 \times 10^{-8}x + 4.63 \times 10^{-10}$ ,  $r^2 = 0.988$ ). Working potential: -0.1 V vs. Ag/AgCl, electrode surface area:  $0.07 \text{ cm}^2$ .

Samples containing an unknown concentration of HRP could be analysed using the internal standard method. Precisely, injecting sequentially two standard solutions of HRP and then the unknown sample, a form of two points calibration could be achieved for each analysis, avoiding problems associated with reproducibility between different batches of electrodes. Comparing the three slopes, the one generated by the standard 1, the one generated by the standard 2 and the one generated by the sample, the unknown concentration could be derived.

This method was then applied to determine the amount of active HRP conjugated to AuNPs. Analysing the same Au-HRP suspension characterised previously with the spectrophotometric method (as discussed in section 3.3.10), an average value of  $1.05 \mu\text{g/ml}$  ( $0.023 \mu\text{M}$ ) of HRP resulted from the amperometric method. This HRP

concentration corresponds to 10 active HRP molecules per AuNP, when the value determined by the spectrophotometric method was 16 active HRP molecule per AuNP.

The fact that, from the amperometric analysis, lower values were achieved with respect to the spectrophotometric method, could be explained by an accurate analysis of the phenomena taking part in both methods. The spectrophotometric technique is based on the measurement of a coloured solution, the absorbance of which depends on all the active enzymes present in the entire solution. The amperometric analysis presents a disadvantage with respect to the colorimetric, because the measured signals are generated only by the active enzymes in direct electronic contact with the electrode surface, where the electron transfer takes place. Comparing, therefore, the signal generated by the conjugate with those generated by the two standard HRP-free solutions results in an unavoidable underestimate of the actual value. In conclusion, then, the amperometric analysis underestimated the value because a certain percentage (~ 40 %) of active HRP present on the particles did not participate in generating the signal because they were not in electrical communication with the electrode. Further optimisation could possibly quantify this consistent method error with the aim of adjusting automatically the final result in relation, for example to the particle size. This method, however, was much quicker than the colorimetric one, representing a valid alternative for the quantification of active, immobilised HRP in a sample and could possibly be extended to the analysis of other enzymes with similar characteristics.

### **3.3.12 Amperometric activity study of GOX on gold nanoparticles**

Unlike the analysis of active HRP, a spectrophotometric determination of active GOX conjugated to AuNPs could not be performed due to the lack of a suitable substrate. In enzyme assays involving GOX, generally it has made use of 5-bromo-4-chloro-3-indolyl phosphate/Nitro blue tetrazolium (BCIP/NBT) which is, however, a precipitating substrate and therefore not suitable for colorimetric determinations. A novel amperometric method was then proposed and optimised for the determination of GOX in a sample. GOX produces  $H_2O_2$  by the oxidation of glucose to D-gluconolactone; the concentration of  $H_2O_2$  produced can, therefore, be related to the amount



of enzyme. The simple HRP-based biosensor described in sections 3.3.1-3.3.4 was here adopted for the analysis of the  $\text{H}_2\text{O}_2$  produced by GOX in a flow-injection set-up. Preliminary experiments were then carried out, flowing a sample of GOX together with glucose over an electrode surface modified with HRP and recording the catalytic signal generated by HRP reducing  $\text{H}_2\text{O}_2$  at  $-0.1$  V vs. Ag/AgCl. The first responses showed time-dependent current values which meant that the amount of  $\text{H}_2\text{O}_2$  produced by GOX was dependent on the reaction time with glucose. The analysis could not be accurate if the different samples were prepared at different times. To avoid this problem, a reaction blocker was introduced to be added at the same time for each sample. In detail,  $100 \mu\text{l}$  of glucose ( $1$  M) was added to five solutions ( $200 \mu\text{l}$ ) of GOX at concentrations between  $0.01$  and  $100 \mu\text{g/ml}$ . After  $5$  min. the reaction was blocked adding, to the samples at the same time,  $50 \mu\text{l}$  of HCl ( $3$  M) to denature the enzyme. After mixing for  $1$  min., all the samples were neutralised by adding  $2.65$  ml of PBS ( $\text{pH } 6.8$ ) so that the final volume for all was  $3$  ml. At this point, each sample should contain a different concentration of  $\text{H}_2\text{O}_2$  proportional to the amount of GOX present. *Figure 3.35* shows the signals recorded by passing all the five samples over the HRP-modified electrode surface.

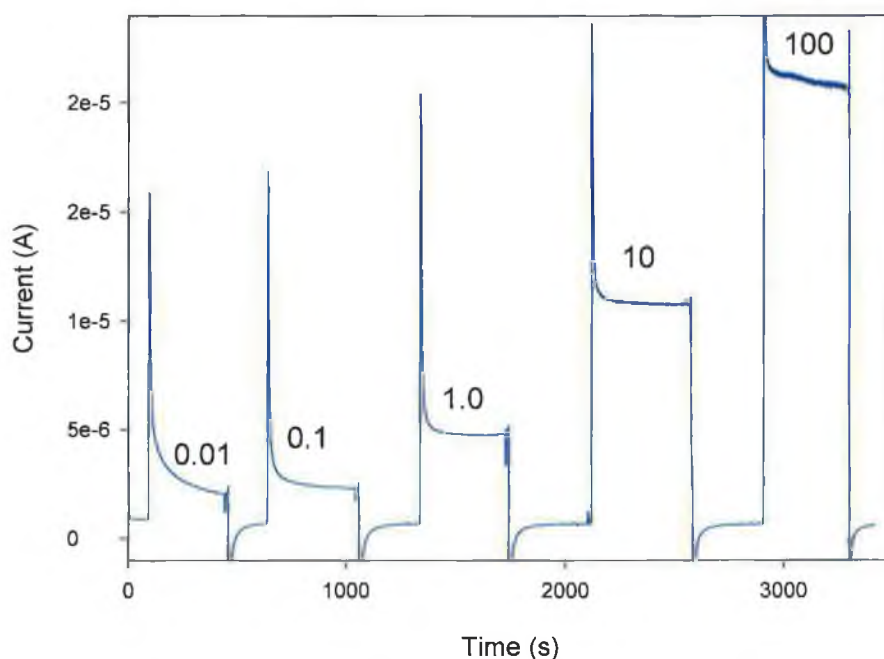


**Figure 3.35.** Amperogram recorded in a flow-injection analysis system, passing over the HRP-modified electrode surface, five different samples of GOX at concentrations of  $0.01$ ,  $0.1$ ,  $1.0$ ,  $10$ ,  $100 \mu\text{g/ml}$  after the reaction with glucose ( $1$  M). The reaction was blocked with HCl ( $3$  M) after  $5$  min. ( $-0.1$  V vs. Ag/AgCl). (Electrode surface area:  $0.07 \text{ cm}^2$ ).

The same procedure was followed for reaction times of 15 and 30 min. All the results are compiled in *Figure 3.36*, which shows that the reaction time clearly influenced the amperometric responses. For longer reaction times the signals recorded were higher.

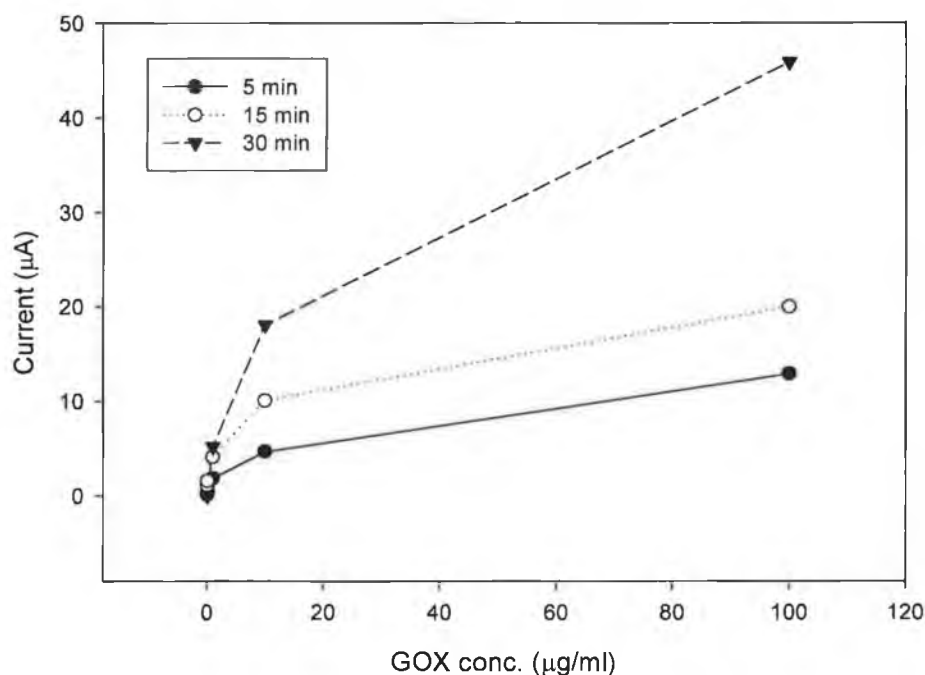


**Figure 3.36.** Peak amperometric responses for the analysis in flow-cell of GOX. The reaction with glucose (1 M) was blocked after 5, 15 and 30 min. with HCl (3 M) before passing the solution over the HRP-modified electrode.

It can be seen also from the graph in *Figure 3.36* that the amperometric response presented a logarithmic trend. A more linear response was found for the reaction times of 5 and 15 min. showing both the current signals and the GOX concentration in a logarithm scale (*Figure 3.37*). 5 min. was chosen as the reaction time for the calibration of the sensor towards the detection of GOX in a sample. Different experiments with the same set-up were carried out and the signal recorded. The resulting calibration curve is represented in *Figure 3.38*. Similarly to the amperometric analysis of HRP the internal standard method was used, passing over the electrode surface two solutions derived from standard concentrations of GOX and one from the unknown conjugate sample and comparing then the three current signals.

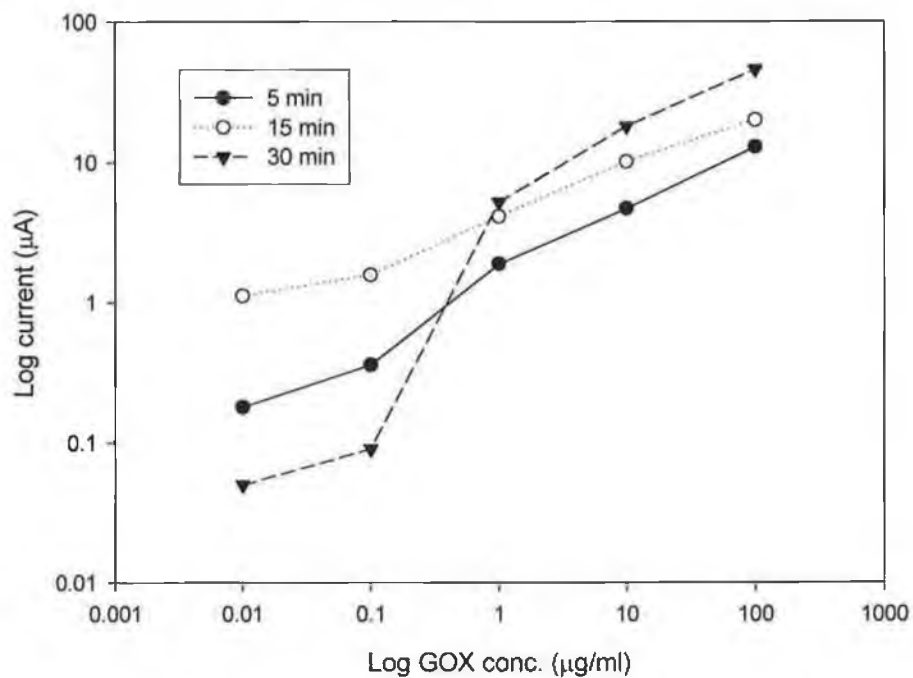


**Figure 3.37.** Log-log plots of the amperometric responses in the analysis of GOX. A linear trend was found for the reaction times of 5 and 15 min.

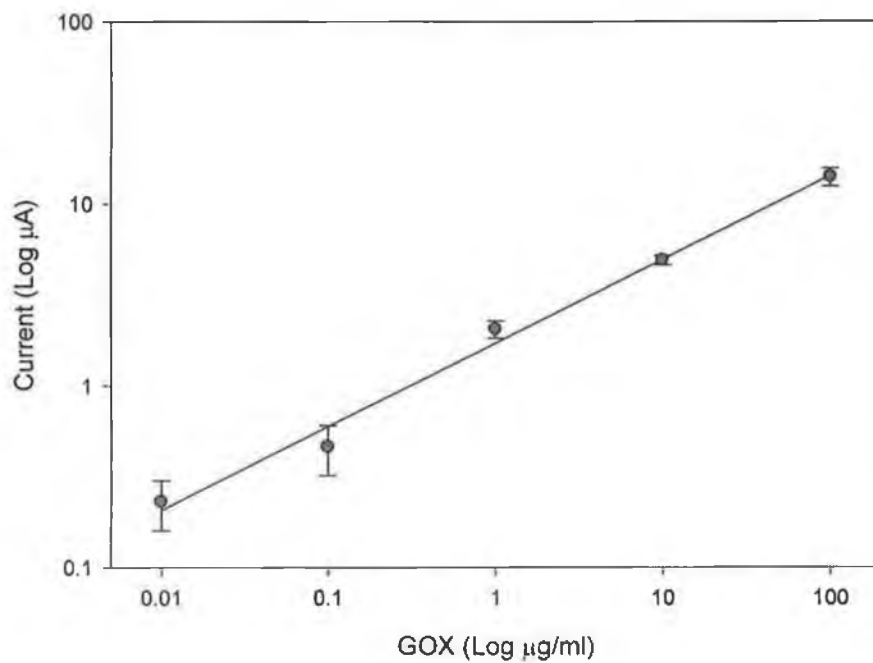


**Figure 3.38.** Log-log calibration curve for the analysis of GOX. A reaction time of 5 min. was used. ( $\text{Log } y = 0.23 \text{ Log } x + 0.459$ ,  $r^2 = 0.990$ ).

Even though this method was not particularly sensitive considering the logarithmic nature of the calibration curve, it was adopted to quantify the enzyme GOX conjugated to AuNP, evaluating also the number of active molecule per NP. The analysis of the Au-GOX suspension previously prepared gave as a result, an average value of 7.3  $\mu\text{g/ml}$  of active GOX which corresponds to 18 molecules per AuNP. Once again, according to this analysis, a big loss of bioactivity resulted from the conjugation process. However, the methodology described was not compared to other techniques, and so therefore, an exact estimation of its accuracy could not be determined.

### **3.3.13 Comparison between free biotin-GOX and Au-biotin-GOX conjugate applied to the immunosystem**

In order to make a valid comparison in performance using biotin-GOX or Au-biotin-GOX conjugate, a set of experiments were carried out as follows: the immunosensor platform was prepared as described in section 3.3.6 immobilising avidin (0.7 mg/ml) and HRP (0.4 mg/ml) onto a PANI/PVS modified screen-printed electrode. A flow-injection set-up was then used to pass over the electrode surface, solutions at different concentrations of biotin-GOX prepared either in PBS, pH 6.8 or prepared in the Au colloid solution at pH 6.8, in the range 1 – 25  $\mu\text{g/ml}$ , followed each time by a solution of 20 mM glucose. The signals generated were recorded for each biotin-GOX concentration used. The intention was therefore to compare two different types of solution, but containing the same amount of enzyme. It was believed that this was a valid way to compare the performances of the sensor using the enzyme free or the enzyme conjugated to AuNPs and to evaluate any possible benefit in using this nanomaterial.

The graph in *Figure 3.39* shows the results recorded for each solution used. It can be clearly seen that the use of AuNPs did not bring any benefit. On the contrary, the signals generated by the free enzyme were, for the entire range, higher than those generated by the Au-enzyme conjugate.

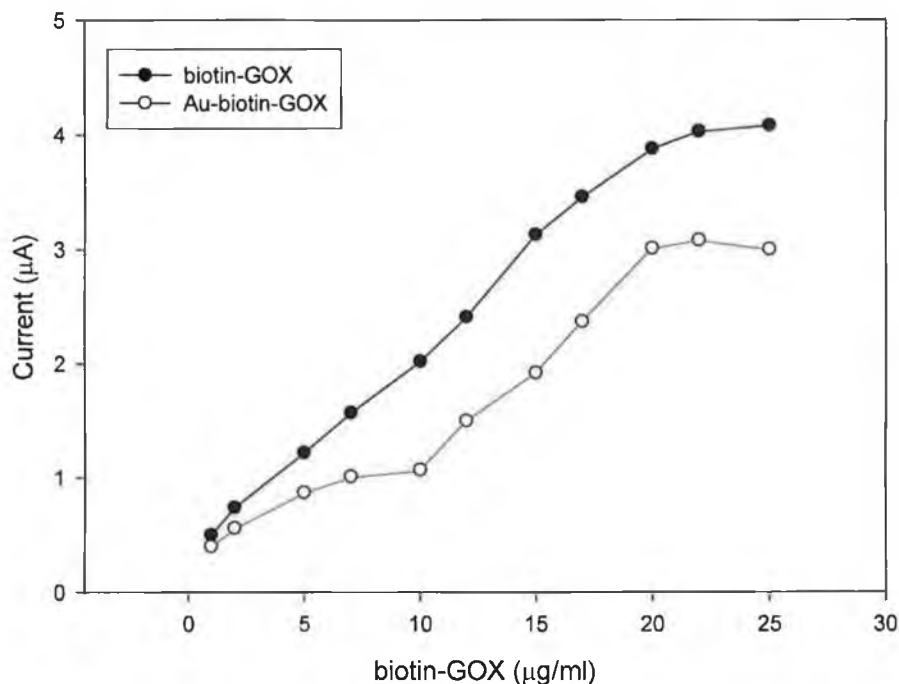


**Figure 3.39.** Response comparison between free biotin-GOX and Au-biotin-GOX conjugates in a flow-injection analysis. After the injection of each solution a 20 mM glucose solution was passed over the electrode to generate the signal at potential -0.1 V vs. Ag/AgCl. (Electrode surface area: 0.07 cm<sup>2</sup>).

Some further information can be extracted from the graph with a more detailed examination. From 1 to 10 µg/ml the signals generated by the Au-biotin-GOX conjugates seemed to reach a little plateau, while after 10 µg/ml the trend seemed to be very similar to that of the free enzyme. In fact, both systems have the same slope which reach a plateau at the same biotin-GOX concentration. This could be explained by the fact that by increasing the concentration of biotin-GOX from 1 to 10 µg/ml a higher number of enzymes resulted attached to the AuNPs, which, however, do not participate in the generation of the signal, probably due to the increased distance from the HRP immobilised on the surface. In other words, only the biotin-GOX molecules directly connected to avidin on the surface were responsible for the generation of the signal because these were sufficiently close to HRP. The other biotin-GOX molecules, present for example on top of the AuNP, may be too far from the surface and the H<sub>2</sub>O<sub>2</sub> produced may be transported away by the flow (see diagram in *Figure 3.24*). After 10 µg/ml the signals have the same trend for both the free biotin-GOX and the Au-biotin-GOX solutions. The gold aggregation test graph in *Figure 3.26* showed that

11  $\mu\text{g/ml}$  of GOX was the minimum concentration to fully cover the AuNPs and corresponded to 28 enzyme molecules. In the present situation, this means that for concentrations higher than 10  $\mu\text{g/ml}$ , free biotin-GOX molecules were present in the Au solution and these interacted with the surface normally. From the experiment carried out it can be concluded once again, that the greatest issue for an efficient enzyme-channeling interaction is represented by the relative distance between the two enzymes. The same conclusion was drawn in the first part of this chapter when the bienzyme platform was under investigation. In a flow-injection set-up like the one here under study, it is even more important considering the fact that the solvent flow renders problematic the formation of a high local concentration of the reactants. Only a few nanometres of distance from the electrode surface caused the loss of the direct enzyme-enzyme connection. Some data from the literature also supports this explanation. A very efficient enzyme-channeling system was obtained recently by Limoges *et al.* by confining the two enzymes within one or within a small number of monolayers. Avoiding transport limitations, the system so constructed allowed high amplification rates with amplified electrochemical responses<sup>58</sup>.

### 3.4 CONCLUSION

A bienzyme-based biosensor using HRP and GOX was developed and optimised with the aim of evaluating the efficiency of the enzyme-channeling system. Polyaniline conducting polymer deposited on the electrode surface was used to immobilise the enzymes and ensure direct electron transfer between HRP and the electrode. Experiments were carried out in order to optimise the conditions for the immobilisation and to evaluate the performance of different configuration platforms. GOX turn over rate is about three times lower than that of HRP, therefore a configuration with more GOX than HRP immobilised on the surface was expected to generate the highest response. Actually, the configuration with the molar ratio GOX/HRP of 1:1 was found to be the most sensitive. This could be explained both by the fact that the relative distance between the enzymes plays an important role, with a homogeneous distribution of the two enzymes at molar ratio of 1:1 ensuring the minimum inter-enzyme distance; and also from a reduced bioactivity of the HRP

enzyme demonstrated by a mathematical modelling approach. This enzyme-channeling system was then applied to an immunosensor platform to report the immunological interaction between biotin and avidin. Avidin and HRP were immobilised on the electrode surface, biotin-GOX conjugate was used as the interacting species and free GOX was used as a control for non-specific interactions. From the experiments it was found that the electrode was able to discriminate between specific and non-specific interactions with, however, the latter generating a remarkably high signal (22% of the specific signal). The enzyme-channeling system applied to this platform was found to be less efficient than the simple bienzyme biosensor investigated in the first part of the chapter, which generated higher responses. This could be due to the fact that the amount of GOX interacting with avidin via biotin was lower with respect to the bienzyme platform and so less  $H_2O_2$  was produced. Signal amplification could possibly be achieved by the use of AuNPs able to carry a higher number of biotin-GOX conjugates over the electrode surface interacting with avidin in order to achieve a massive production of  $H_2O_2$  to react with HRP. Amperometric techniques were developed and proposed at this point as alternatives to the spectrophotometric ones in the determination of HRP and GOX in a sample. These techniques were applied to the characterisation of the two Au-enzyme conjugates in order to quantify the number of active enzyme molecules attached. The results achieved with these techniques revealed a significant loss of enzyme bioactivity after the conjugation process, mostly due to a conformational deformation of the protein attaching the NP, which caused a decrease in functionality.

Au-biotin-GOX conjugates were applied to the avidin-HRP-based immunosystem with the aim of increasing the local concentration of  $H_2O_2$  close to the electrode surface for a signal enhancement. Once again, however, the relative distance between the two enzymes appeared to represent the limiting factor for signal amplification. The introduction of AuNPs as multi-enzyme carriers revealed a negative effect due to the increased distance between the GOX carried and the HRP on the surface. In order to achieve a signal amplification using an enzyme-channeling system a different approach should be considered. A decrease in the distance between the two enzymes represents the main goal, which could be obtained by the use of smaller NPs or with the contribution of different nanomaterials such as carbon nanotubes. This may also reduce the loss of enzyme activity experienced during conjugation process.

### 3.5 REFERENCES

---

- 1 M.P. Marco, D. Barcelo. Fundamentals and applications of biosensors for environmental analysis. *Techniques and Instrumentation in Analytical Chemistry*, **21**, (2000), 1075-1105.
- 2 D.C. Cowell, A.K. Abass, A.A. Dowman, J.P. Hart, R.M. Pemberton, S.J. Young. Screen-printed disposable biosensors for environmental pollution monitoring. *Environmental Science and Pollution Research*, **56**, (2001), 157-174.
- 3 I. Karube, Y. Nomura. Enzyme sensors for environmental analysis. *Journal of Molecular Catalysis B: Enzymatic*, **10**, (2000), 177-181.
- 4 E. Csöregi, L. Gorton, G. Marko-Varga. Carbon fibres as electrode materials for the construction of peroxidase-modified amperometric biosensors. *Analytica Chimica Acta*, **273**, (1993), 59-70.
- 5 S.L. Brooks, I.J. Higgins, J.D. Newman, A.P.F. Turner. Biosensors for process control. *Enzyme and Microbial Technology*, **13**, (1991), 946-955.
- 6 J. Wang. Amperometric biosensors for clinical and therapeutic drug monitoring: a review. *Pharmaceutical and Biomedical Analysis*, **19**, (1999), 47-53.
- 7 U. Wollenberger, F. Schubert, F.W. Scheller. Enhancing biosensor performance using multienzyme systems. *Trends in biotechnology*, **11**, (1993), 255-262.
- 8 S.C. Changa, K. Rawsonb, C.J. McNeil. Disposable tyrosinase-peroxidase bi-enzyme sensor for amperometric detection of phenols. *Biosensors and Bioelectronics*, **17**, (2002), 1015-1023.
- 9 M.C. Shin, H.C. Yoon, H.S. Kim. In situ biochemical reduction of interference in an amperometric biosensor with a novel heterobilayer configuration of polypyrrole/glucose oxidase/horseradish peroxidase. *Analytica Chimica Acta*, **329**, (1996), 223-230.
- 10 A.E.G. Cass. (1990), *Biosensors: A practical Approach*. IRL Press at Oxford University Press, (Oxford).
- 11 J.J. Kulys, M.V. Pesliakiene, A.S. Samalius. The development of bienzyme glucose electrodes. *Bioelectrochemistry and Bioenergetics*, **8**, (1981), 81-88.
- 12 L. Gorton, A. Lindgren, T. Larsson, F. D. Munteanu, T. Ruzgas, I. Gazaryan. Direct electron transfer between heme-containing enzymes and electrodes as basis for third generation biosensors. *Analytica Chimica Acta*, **400**, (1999), 91-108.
- 13 P.N. Bartlett, P. Tebbutt, R.G. Whitaker. Kinetic aspects of the use of modified electrodes and mediators in bioelectrochemistry. *Progress in reaction kinetics*, **16**, (1991), 55-155.



- 
- 14 B.A. Gregg, A. Heller. Cross-linked redox gels containing glucose oxidase for amperometric biosensor applications. *Analytical Chemistry*, **62**, (1990), 258-263.
  - 15 M. Gerard, A. Chaubey, B.D. Malhotra. Application of conducting polymers to biosensors. *Biosensors and Bioelectronics*, **17**, (2002), 345-359.
  - 16 C.G.J. Koopal, M.C. Feiters, R.J.M. Nolte, B. de Ruiters, R.B.M. Schasfoort. Glucose sensor utilizing polypyrrole incorporated in tract-etch membranes as the mediator. *Biosensors and Bioelectronics*, **7**, (1992), 461-471.
  - 17 M. Niculescu, C. Nistor, I. Frébort, P. Peč, B. Mattiasson, E. Csöregi. Redox hydrogel-based amperometric bienzyme electrodes for fish freshness monitoring. *Analytical Chemistry*, **72**, (2000), 1591-1597.
  - 18 L. Boguslavsky, H. Kalash, Z. Xu, D. Beckles, L. Geng, T. Skotheim, V. Laurinavicius, H. S. Lee. Thin film bienzyme amperometric biosensors based on polymeric redox mediators with electrostatic bipolar protecting layer. *Analytica Chimica Acta*, **311**, (1995), 15-21.
  - 19 F. Tian, G. Zhu. Bienzymatic amperometric biosensor for glucose based on polypyrrole/ceramic carbon as electrode material. *Analytica Chimica Acta*, **451**, (2002), 251-258.
  - 20 S. Tombelli, M. Mascini. Electrochemical biosensors for biogenic amines: a comparison between different approaches. *Analytica Chimica Acta*, **358**, (1998), 277-284.
  - 21 L. Boguslavsky, H. Kalash, Z. Xu, D. Beckles, L. Geng, T. Skotheim, V. Laurinavicius, H. S. Lee. Thin film bienzyme amperometric biosensors based on polymeric redox mediators with electrostatic bipolar protecting layer. *Analytica Chimica Acta*, **311**, (1995), 15-21.
  - 22 X. Yang, G. A. Rechnitz. Dual enzyme amperometric biosensor for putrescine with interference suppression. *Electroanalysis*, **7**, (1995), 105-108.
  - 23 A. Collins, E. Mikeladze, M. Bengtsson, M. Kokaia, T. Laurell, E. Csöregi. Interference Elimination in Glutamate Monitoring with Chip Integrated Enzyme Microreactors. *Electroanalysis*, **13**, (2001), 425-431.
  - 24 E.F. Perez, G. de Oliveira Neto, L.T. Kubota. Bi-enzymatic amperometric biosensor for oxalate. *Sensors and Actuators B: Chemical*, **72**, (2001), 80-85.
  - 25 L. Mao, K. Yamamoto. Amperometric on-line sensor for continuous measurement of hypoxanthine based on osmium-polyvinylpyridine gel polymer and xanthine oxidase bienzyme modified glassy carbon electrode. *Analytica Chimica Acta*, **415**, (2000), 143-150.

- 
- 26 J. Saurina, S. Hernández-Cassou, S. Alegret, E. Fàbregas. Amperometric determination of lysine using a lysine oxidase biosensor based on rigid-conducting composites. *Biosensors and Bioelectronics*, **14**, (1999), 211-220.
- 27 G.E. De Benedetto, F. Palmisano, P.G. Zambonin. One-step fabrication of a bienzyme glucose sensor based on glucose oxidase and peroxidase immobilized onto a poly(pyrrole) modified glassy carbon electrode. *Biosensors and Bioelectronics*, **11**, (1996), 1001-1008.
- 28 A. Guzman-Vázquez de Prada, N. Peña, C. Parrado, A.J. Reviejo, J.M. Pingarrón. Amperometric multidetection with composite enzyme electrodes. *Talanta*, **62**, (2004), 896-903.
- 29 S. Min-Chol, Y.C. Hyun, K. Hak-Sung. In situ biochemical reduction of interference in an amperometric biosensor with a novel heterobilayer configuration of polypyrrole/glucose oxidase/horseradish peroxidase. *Analytica Chimica Acta*, **329**, (1996), 223-230.
- 30 M. Delvaux, A. Walcarius, S. Demoustier-Champagne. Bienzyme HRP-GOX-modified gold nanoelectrodes for the sensitive amperometric detection of glucose at low overpotentials. *Biosensors and Bioelectronics*, **20**, (2005), 1587-1594.
- 31 R.W. Min, V. Rajendran, N. Larsson, L. Gorton, J. Planas, B. Hahn-Hägerdal. Simultaneous monitoring of glucose and L-lactic acid during a fermentation process in an aqueous two-phase system by on-line FIA with microdialysis sampling and dual biosensor detection. *Analytica Chimica Acta*, **366**, (1998), 127-135.
- 32 Y. Kobayashi, J. Anzai. Preparation and optimization of bienzyme multilayer films using lectin and glyco-enzymes for biosensor applications. *Journal of Electroanalytical Chemistry*, **507**, (2001), 250-255.
- 33 K. Di Gleria, H.A.O. Hill, J.A. Chambers. Homogeneous amperometric ligand-binding assay amplified by a proteolytic enzyme cascade. *Journal of Electroanalytical Chemistry*, **267**, (1989), 83-91.
- 34 C.C. Harris, (1984). *Cascade amplification enzyme immunoassay*. US Patent, No. 4,463,090.
- 35 D.J. Litman, T.M. Hanlon, E.F. Ulman. Enzyme channelling immunoassay: a new homogeneous enzyme immunoassay technique. *Analytical Biochemistry*, **106**, (1980), 223-229.
- 36 J. Rishpon, D. Ivnitcki. An amperometric enzyme-channeling immunosensor. *Biosensors and Bioelectronics*, **12**, (1997), 195-204.

- 
- 37 J.D. Wright K.M. Rawson, W.O. Ho, D. Athey, C.J. McNeil. Specific binding assay for biotin based on enzyme channelling with direct electron transfer electrochemical detection using horseradish peroxidase. *Biosensors and Bioelectronics*, **10**, (1995), 495-500.
- 38 R.W. Keay, C.J. McNeil. Separation-free electrochemical immunosensor for rapid determination of atrazine. *Biosensors and Bioelectronics*, **13**, (1998), 963-970.
- 39 B.B. Dzantiev, E.V. Yazynina, A.V. Zherdev, Y.V. Plekhanova, A.N. Reshetilov, S.-C. Chang, C.J. McNeil. Determination of the herbicide chlorsulfuron by amperometric sensor based on separation-free bienzyme immunoassay. *Sensors and Actuators B: Chemical*, **98**, (2004), 254-261.
- 40 J. Zeravik, T. Ruzgas, M. Fránek. A highly sensitive flow-through amperometric immunosensor based on the Peroxidase chip and enzyme-channeling principle. *Biosensors and Bioelectronics*, **18**, (2003), 1321-1327.
- 41 F. Darain, S.-U. Park, Y.-B. Shim. Disposable amperometric immunosensor system for rabbit IgG using a conducting polymer modified screen-printed electrode. *Biosensors and Bioelectronics*, **18**, (2003), 773-780.
- 42 Y. Yang, S. Mu. Bioelectrochemical responses of the polyaniline horseradish peroxidase electrodes. *Journal of Electroanalytical Chemistry*, **432**, (1997), 71-78.
- 43 A.J. Killard, S. Zhang, H. Zhao, R. John, E.I. Iwuoha, M.R. Smyth. Development of an electrochemical flow injection immunoassay (FIIA) for the real-time monitoring of biospecific interactions. *Analytica Chimica Acta*, **400**, (1999), 109-119.
- 44 E.I. Iwuoha, I. Leister, E. Miland, M.R. Smyth, C.O. Fágáin, Reactivities of organic phase biosensors. 2. The amperometric behaviour of horseradish peroxidase immobilised on a platinum electrode modified with an electrosynthetic polyaniline film, *Biosensors and Bioelectronics*, **12**, (1997), 749-761.
- 45 A.J. Killard, L. Micheli, K. Grennan, M. Franek, V. Kolar, D. Moscone, I. Palchetti, M.R. Smyth. Amperometric separation-free immunosensor for real-time environmental monitoring. *Analytica Chimica Acta*, **427**, (2001), 173-180.
- 46 K. Grennan, G. Strachan, A.J. Porter, A.J. Killard, M.R. Smyth. Atrazine analysis using an amperometric immunosensor based on single-chain antibody fragments and regeneration-free multi-calibrant measurement. *Analytica Chimica Acta*, **500**, (2003), 287-298.
- 47 G. Frens. Controlled nucleation for the regulation of the particle size in monodisperse gold suspensions. *Natural Physics Science*, **241**, (1973), 20-22.
- 48 G. Wallace, G. Spinks, L. Kane-Maguire. (2003). *Conductive Electroactive Polymers* (2nd. Ed), CRC Press, London.

- 
- 49 C. Camacho, J.C. Matías, D. García, B.K. Simpson, R. Villalonga. Amperometric enzyme biosensor for hydrogen peroxide via Ugi multicomponent reaction. *Electrochemistry Communications*, **9**, (2007), 1655-1660.
- 50 A. Cambiaso, L. Delfino, M. Grattarola, G. Verreschi, D. Ashworth, A. Maines, P. Vadgama, Modelling and simulation of a diffusion limited glucose biosensor, *Sensors and Actuators B: Chemical*, **33**, (1996), 203–207.
- 51 Y.M. Glazman. Effect of surface-active agents on stability of hydrophobic sols. *Faraday Discussions*, **42**, (1966), 255-258.
- 52 J. Beesley Colloidal Gold. A new perspective for cytochemical marking. *Royal Microscopical Society Handbook No 17*. (1989), Oxford University Press.
- 53 G.T. Hermanson, A.K. Mallia, P.K. Smith. (1992), *Immobilized Affinity Ligand Techniques*, Academic Press, (San Diego).
- 54 L. L. Whyte. Unique arrangement of points on a sphere. *American Mathematics Monthly*, **59**, (1952), 606-611.
- 55 M. Lundqvist, I. Sethson, B.-H. Jonsson. Protein adsorption onto silica nanoparticles: conformational changes depend on the particles' curvature and the protein stability. *Langmuir*, **20**, (2004), 10639-10647.
- 56 A.A. Vertegel, R.W. Siegel, J.S. Dordick. Silica nanoparticle size influences the structure and enzymatic activity of adsorbed lysozyme. *Langmuir*, **20**, (2004), 6800-6807.
- 57 F. Lucarelli, G. Marrazza, M. Mascini. Dendritic-like streptavidin/alkaline phosphatase nanoarchitectures for amplified electrochemical sensing of DNA sequences. *Langmuir*, **22**, (2006), 4305-4309.
- 58 B. Limoges, D. Marchal, F. Mavr e, J.M. Sav eant. High amplification rates from the association of two enzymes confined within a nanometric layer immobilised on an electrode: modeling and illustrative example. *Journal of the American Chemical Society*, **128**, (2006), 6014-6015.

# **Chapter 4**

**Enhanced electrochemical immunoassay  
based on paramagnetic platforms and gold  
nanoparticle labels**

## 4.1 INTRODUCTION

Gold nanoparticles (AuNPs) have been used for analytical and biomedical purposes for many years. Rapid and simple chemical synthesis, a narrow size distribution and efficient coating by thiols or other bio-ligands has enabled AuNPs to be used as transducers for several biorecognition applications. Properties such as their electron dense core, highly resonant particle plasmons, direct visualization of single nanoclusters by scattering of light, catalytic size enhancement by silver deposition, and electrochemical characteristics have made them very attractive for several applications in biotechnology.

AuNPs have been used for several purposes. Bio-conjugated AuNPs for recognizing and detecting specific DNA sequences, that functions as both a nano-scaffold and a nano-quencher (efficient energy acceptor) have been reported.<sup>1</sup> AuNPs conjugated to antibodies are widely used in the field of light and electron microscopy, for visualizing proteins in biological samples.<sup>2</sup> The sensitivity of the detection is usually improved by the silver enhancement method. Beside these applications, an increased interest is shown for their use to quench the fluorescence<sup>3</sup>, tune the enzyme specificity<sup>4</sup>, visualize cellular or tissue components by electron microscopy,<sup>5</sup> electrical contacting or “wiring” between electrodes and redox enzymes,<sup>6</sup> tailoring the DNA loading by changing the nanoparticle size<sup>7</sup> and for labeling DNA strands for sensor and analytical applications.

The combination of biomolecules with AuNPs provides interesting tools for several biological components. Oligonucleotide functionalized AuNPs, and also nanoparticle/protein conjugates have become the basis for an increasing number of diagnostic applications that compete with molecular fluorophores in certain settings<sup>8</sup> such as biochemical sensors, enzyme enhancers, nanoscale building blocks and immunohistochemical probes.<sup>9,10</sup>

NPs in general and AuNPs particularly offer attractive properties to act as DNA tags.<sup>11</sup> Their sensitivity, long life-time along with multiplexing capability have led to extensive applications in electrochemical assays in recent years.<sup>12</sup> Most of the reported assays have been based on chemical dissolution of the AuNP tag (in a hydrobromic acid / bromine mixture) followed by accumulation and stripping analysis of the resulting Au<sup>3+</sup> solution. Due to the toxicity of the HBr/Br<sub>2</sub> solution, direct solid-state detection of a silver precipitate on AuNP-DNA conjugates was reported by

Wang *et al.*<sup>13</sup> However, this method was based on direct detection of precipitated silver, not the AuNP tag itself. Direct detection of colloidal AuNPs, but not in connection with the detection of DNA hybridization, has been reported<sup>14-16</sup>. A novel nanoparticle-based detection of DNA hybridization based on magnetically induced direct electrochemical detection of 1.4 nm Au<sub>67</sub> quantum dot tag linked to the target DNA has been reported previously. The Au<sub>67</sub> nanoparticle tag is directly detected after the DNA hybridization event, without the need of acidic (i.e. HBr/Br<sub>2</sub>) dissolution.<sup>17,18</sup>

The combination of optical and electrochemical properties of AuNPs with the catalytic activity of the HRP enzyme is demonstrated here with a new double-label system. This comprises a AuNP modified with a model anti-human IgG peroxidase-conjugated antibody (anti-human-HRP). This doubly-labelled secondary antibody offers several analytical routes for immunodetection. Spectrophotometric analysis based on either AuNPs absorption or HRP enzymatic activity and the electrochemical detection based on AuNPs is presented and compared. Optical sensitivity enhancement attributable to the use of AuNPs as a multi-IgG-HRP carrier which therefore amplify the enzymatic signal, as well as the high sensitivity in the direct electrochemical detection, represent the most important achievements due to the use of this doubly-labelled protein which can potentially be exploited in several other future applications.

## 4.2 MATERIALS AND METHODS

### 4.2.1 Materials

Streptavidin-coated magnetic beads (MB)(M-280) were purchased from Dynal Biotech. Biotin conjugate-goat anti-human IgG (Sigma B1140, developed in goat and  $\gamma$ -chain specific), human IgG from serum, goat IgG from serum, anti-human IgG peroxidase conjugate (Sigma A8667, developed in goat and whole molecule), *o*-phenylenediamine dihydrochloride (OPD), hydrogen tetrachloroaurate (III) trihydrate ( $\text{HAuCl}_4 \cdot 3\text{H}_2\text{O}$ , 99.9%, w/v), trisodium citrate and hydrogen peroxide were purchased from Sigma-Aldrich. All buffer reagents and other inorganic chemicals were supplied by Sigma, Aldrich or Fluka, unless otherwise stated. All chemicals were used as received and all aqueous solutions were prepared in 18 M $\Omega$  water.

### 4.2.2 Buffers and solutions

The phosphate buffered saline solution (PBS) consisted of 0.002 M  $\text{KH}_2\text{PO}_4$ , 0.008 M  $\text{Na}_2\text{HPO}_4$ , 0.137 M NaCl, 0.003 M KCl (pH 7.4). Blocking buffer solution consisted of a PBS solution with added 5% (w/v) bovine serum albumin (pH 7.4). The binding and washing (B&W) buffer consisted of a PBS solution with added 0.05% (v/v) Tween 20 (pH 7.4). The measuring medium for the electrochemical measurements consisted of a 0.1 M HCl solution. OPD- $\text{H}_2\text{O}_2$  solution for spectrophotometric analysis was prepared by dissolving one as acquired from Sigma OPD tablet in 25 ml of phosphate-citrate buffer (pH 5.0) and then immediately before the analysis 10  $\mu\text{l}$  of a 30% (v/v)  $\text{H}_2\text{O}_2$  solution was added.

### 4.2.3 Instrumentation

All voltammetric experiments were performed using an electrochemical analyzer Autolab 20 (Eco-Chemie, The Netherlands) connected to a personal computer. Electrochemical experiments were carried out in a 10 ml voltammetric cell at room



temperature (25°C), using a three electrode configuration. A platinum electrode served as an auxiliary electrode and an Ag/AgCl as reference electrode. Graphite composite working electrodes were prepared as described in section 4.2.8. The binding of streptavidin-coated paramagnetic beads with biotinylated primary antibody and all the following incubations were performed in TS-100 ThermoShaker (Spain). Magnetic separation was carried out with MCB1200 biomagnetic processing platform (Sigris, CA). The spectrophotometric measurements were performed using a Tecan Sunrise Absorbance Microplate Reader. Transmission electron micrographs (TEM) were taken using a JEOL JEM-2011 (Jeol LTD, Tokyo, Japan). Scanning electron microscopy (SEM) characterisations were performed with a JEOL JSM-6300 (Jeol LTD, Tokyo, Japan) linked to an energy dispersive spectrometer (EDX) LINK ISIS-200 (Oxford Instruments, Bucks, England) for the energy dispersive X-Ray analysis.

#### **4.2.4 Synthesis and characterisation of gold nanoparticles**

AuNPs were synthesized by reducing tetrachloroauric acid with trisodium citrate, a method pioneered by Turkevich *et al.*<sup>19</sup> Briefly, 200 ml of 0.01% (w/v) HAuCl<sub>4</sub> solution were boiled with vigorous stirring. 5 ml of a 1% (w/v) trisodium citrate solution were added quickly to the boiling solution. When the solution turned deep red, indicating the formation of AuNPs, the solution was left to stir and cool down. TEMs were recorded in order to measure the size. To verify the Au metallic structure a Fast Fourier Transform (FFT) of crystalline plane distances were measured. A UV-Vis spectrum was recorded to establish the characteristic absorbance peak of gold at 520 nm. Finally, an Energy Dispersive X-Ray (EDX) analysis was also performed.

#### **4.2.5 Preparation of gold nanoparticle-based immuno label**

The gold-labelled anti-human IgG-peroxidase conjugate antibody (Au-anti-human-HRP), was prepared by following published procedures<sup>20</sup>. A schematic of this preparation is also given at *Figure 4.1*. A preliminary titration was carried out in order to verify the optimal pH for the conjugation of anti-human-HRP to AuNPs. The AuNP solution's pH was adjusted with either 0.01 M HCl or 0.01 M NaOH (buffered

saline solutions cannot be used because this causes the aggregation of AuNPs) to the values: 6.5, 7.0, 7.5, 8.0, 8.5, 9.0, 9.5, 10.0. 200  $\mu$ l of each solution were transferred to 8 wells of a 96-well microtitre plate. Then, 30  $\mu$ l of anti-human-HRP at the fixed concentration of 10  $\mu$ g/ml were added to each well. After 5 min., 30  $\mu$ l of 10% (w/v) NaCl solution were added to each well. NaCl causes the aggregation of AuNPs and shifts the maximum absorbance peak from 520 to 580 nm. A spectrophotometric measurement was then carried out recording the absorbance at 520 and 580 nm. The optimal pH at which the antibody more efficiently prevents gold aggregation is given by the highest absorbance difference. Once the pH had been optimised, a gold aggregation test was carried out to judge the minimum antibody concentration to use for conjugation. Precisely, gold colloid (13 nm) solution was adjusted to the optimal conjugation pH; then several solutions of anti-human-HRP at concentrations between 0 and 12  $\mu$ g/ml were prepared in water to a volume of 30  $\mu$ l and added to 200  $\mu$ l of gold solution. After 5 min., 30  $\mu$ l of 10% (w/v) NaCl solution were added to induce aggregation. The minimum antibody concentration able to prevent gold aggregation was determined measuring again the absorbance at 520 and 580 nm. The actual conjugate preparation was then followed by adding the minimum antibody concentration determined by gold aggregation test plus 10% to the appropriate gold solution volume (10 ml) adjusted to the optimal pH. The mixture was stirred for 10 min., and then to remove the excess of antibody it was centrifuged at 15,000 g for 1 h at 4°C. The clear supernatant was carefully removed and the precipitated Au-anti-human-HRP conjugates were resuspended in 10 ml of B&W buffer and stored at 4°C.

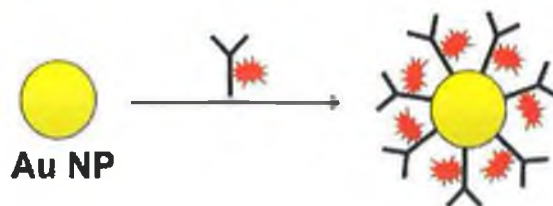


**Figure 4.1.** Schematic of Au-anti-human-HRP conjugate preparation. The anti-human-HRP solution at the concentration determined by gold aggregation test plus 10% was added dropwise to the AuNPs solution (10 ml) adjusted to the optimal pH. The mixture was stirred for 10 min, and then to remove the excess of antibody it was centrifuged at 15,000 g for 1 h at 4°C. The clear supernatant was carefully removed and the precipitated Au-anti-human-HRP conjugates were resuspended in 10 ml of B&W buffer and stored at 4°C.

#### 4.2.6 Preparation of magnetic bead sandwich-type immunocomplexes

The binding of biotinylated anti-human IgG with streptavidin-coated paramagnetic beads was carried out using a slightly modified procedure recommended by Dynal Biotech<sup>21</sup>. *Figure 4.2* is a schematic of all assay steps used in this work. In detail, 150 µg (15 µl from the stock solution) of streptavidin-coated paramagnetic beads (MB) were transferred into 0.5 ml micro test tube (I). The MBs were washed twice with 150 µl of B&W buffer and then resuspended in 108 µl of B&W buffer. 42 µl (from stock solution 0.36 mg/ml) of biotinylated anti-human IgG were added reaching the final concentration of 100 µg/ml. The resulting MB solution with biotinylated anti-human IgG was incubated for 30 min. at 25°C with gentle mixing using a TS-100 ThermoShaker. The formed MB/anti-human IgG complexes (II) were then separated from the incubation solution and washed three times with 150 µl of B&W buffer. The preparation process was followed by the resuspension of MB/anti-human IgG complex in 150 µl of blocking buffer (PBS-BSA 5% (w/v)) to block any remaining active surface of MBs and incubated at 25°C for 20 min. After the washing steps with B&W buffer, the MB/anti-human IgG complexes were incubated at 25°C for 30 min. with 150 µl of human IgG antigen at concentrations ranging between 0.5 ng/ml and 1 µg/ml and forming by this way the immunocomplex MB/anti-human/human IgG (III). Finally, after the washing steps the MB/anti-human/human IgG immunocomplexes were incubated with either the Au-anti-human-HRP conjugate previously prepared or with anti-human-HRP (without Au).

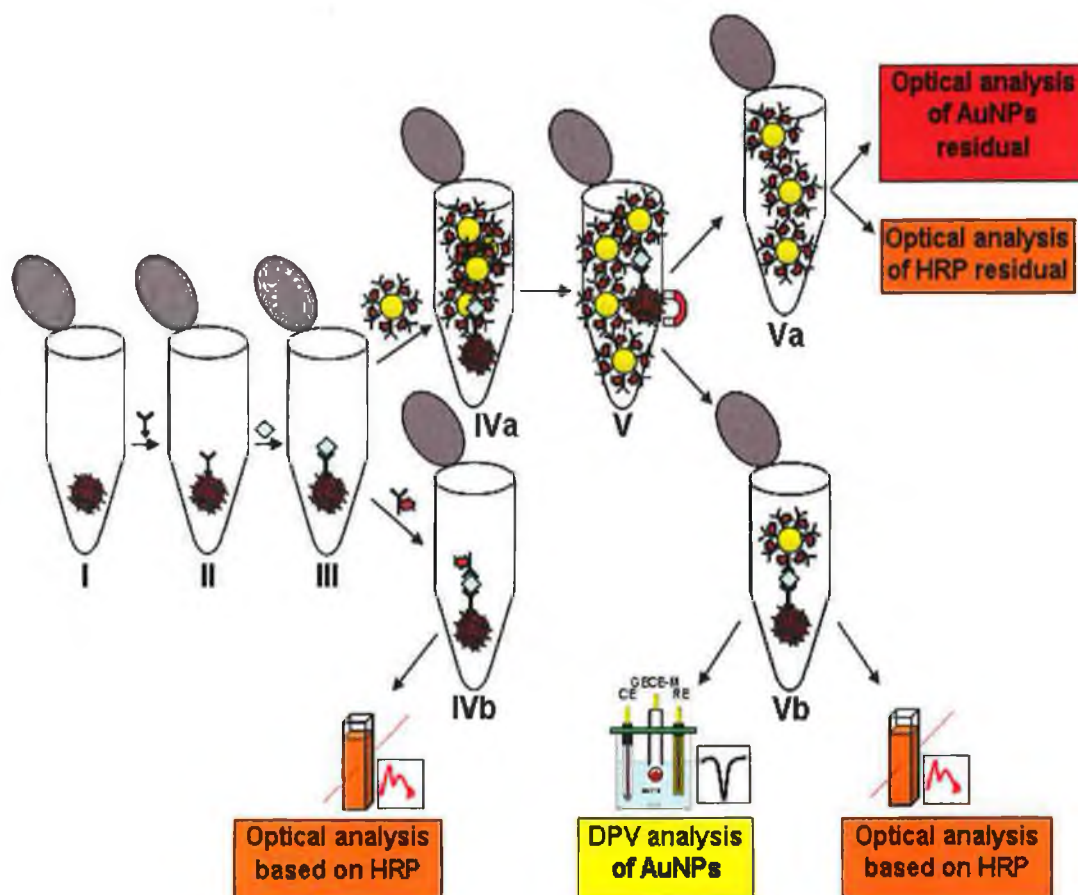


**Figure 4.2.** Schematic of the general assay procedure and characterisations, consisting of the following steps. (I) Introduction of streptavidin-coated paramagnetic beads (MB). (II) Incubation with the primary biotinylated anti-human IgG antibody. (III) Incubation with different concentrations of the antigen human IgG. (IVa) Incubation with Au-anti-human-HRP. (V) Separation of the MB-immunocomplex from the unbound Au-anti-human-HRP. (Va) Au-anti-human-HRP residual for spectrophotometric analysis based on gold and HRP. (IVb) incubation with anti-human-HRP and spectrophotometric analysis based on HRP. (Vb) MB-immunocomplex with Au-anti-human-HRP ready for a double detection: spectrophotometric based on HRP and electrochemical based on direct DPV analysis of AuNPs.

#### *Labelling with Au-anti-human-HRP*

The washed MB/anti-human/human IgG immunocomplex (III) was resuspended and incubated at 25°C for 30 min. with 150 µl of the previously prepared gold-labelled anti-human-HRP conjugate solution (IVa) forming the sandwich-type immunocomplex: MB/anti-human/human IgG/Au-anti-human-HRP. This complex

was then characterized by TEM and also some spectrophotometric analyses were carried out in order to prove the specific interaction between the antigen human IgG and the Au-anti-human-HRP conjugate. Precisely, after the magnetic separation (V), optical measurements were carried out in order to quantify the Au-anti-human-HRP conjugates in excess and not anchored to the MB through the interaction with the antigen human IgG. They were based on either the HRP enzyme (optical analysis based on HRP activity) or the AuNP (optical analysis based on Au absorptivity) both present in the conjugate (Va). In detail, the separated solution of residual Au-anti-human-HRP (Va) was divided into two parts. In Part I, 140  $\mu\text{l}$ , were transferred to a 96-well plate and used directly for the analysis of gold by measuring the absorbance at 520 nm. In Part II, 10  $\mu\text{l}$  were transferred to another plate and used for the reaction between HRP and OPD (150  $\mu\text{l}$ ) which generated a coloured solution. After 2 min. the HRP/OPD reaction was stopped by adding 50  $\mu\text{l}$  of 3 M HCl and the absorbance measurement was carried out at 492 nm. For both experiments, the absorbance measured was directly proportional to the amount of conjugate (Au-anti-human-HRP) present in solution.

#### *Labelling with anti-human-HRP*

The MB/anti-human/human IgG immunocomplex (III) was resuspended and incubated at 25°C for 30 min. with 150  $\mu\text{l}$  of the anti-human-HRP secondary antibody (7  $\mu\text{g/ml}$ ). The resulting MB/anti-human/human IgG/anti-human-HRP immunocomplex was characterised by TEM and used for comparison studies.

#### **4.2.7 Spectrophotometric analysis**

The two MB-immunocomplexes prepared without AuNP (MB/anti-human/human IgG/anti-human-HRP), (IVb) and with AuNP (MB/anti-human IgG/human IgG/Au-anti-human-HRP), (Vb) in the secondary antibody conjugate, were spectrophotometrically analysed exploiting, in both cases, the HRP activity in the label. As the complexes were prepared using different concentrations of the antigen (human IgG), a calibration curve was obtained and a comparison between the two platforms was made in order to evaluate the benefits in using AuNPs. The analysis

procedure is well described in *Figure 4.3*. Each MB-immunocomplex was resuspended in the micro test tube with 150  $\mu$ l of a preliminarily prepared solution of OPD-H<sub>2</sub>O<sub>2</sub> (I). After the optimized time of 2 min., the solution colour changed to yellow-orange in proportion to the concentration of HRP present in the complexes (II) which was also proportional to the concentration of human IgG used during the assay procedure. The reaction was then blocked by adding 50  $\mu$ l of 3 M HCl which denatured the enzyme and ensured the same reaction time in all the tubes. Using an external magnet, the MB-immunocomplexes were then separated from the solution (III) which was subsequently transferred to a 96-well plastic plate. The spectrophotometric analysis (IV) was performed by measuring the absorbance at 492 nm.

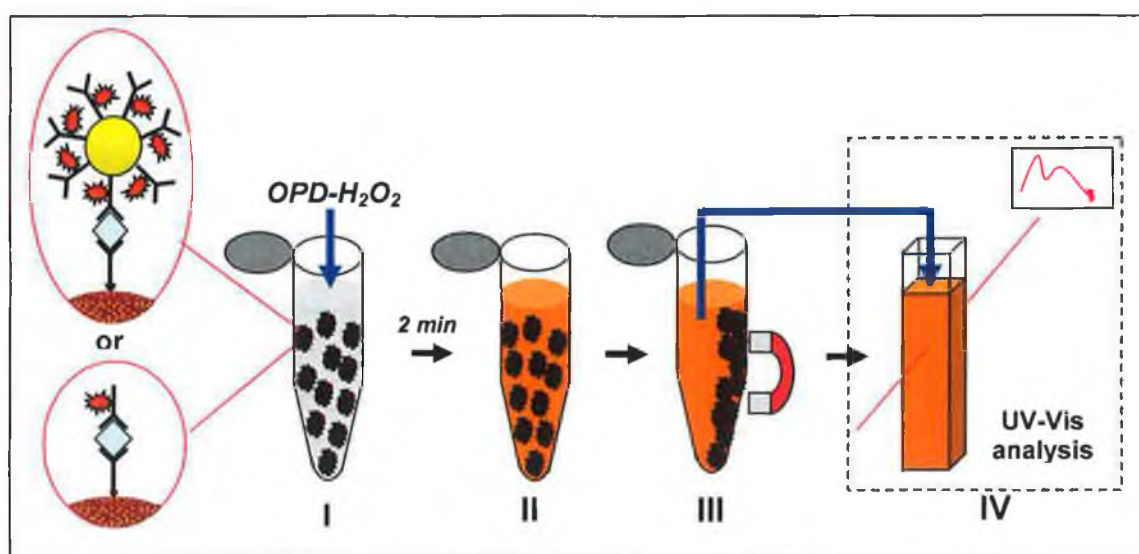


**Figure 4.3.** Spectrophotometric analysis procedure consisting in (I) Resuspension of the MB-immunocomplex (with or without AuNPs) with an OPD-H<sub>2</sub>O<sub>2</sub> solution (OPD ready to use from tablets, H<sub>2</sub>O<sub>2</sub> 0.01% (v/v)) as a specific enzymatic substrate for HRP; (II) After 2 min. the solution turns orange due to the water soluble yellow-orange reaction product of the peroxidase with OPD with maximum absorbance at 492 nm (blocking the reaction with 3M HCl) and intensity proportional to the concentration of the enzyme label; (III) Using a magnet, MB-immunocomplexes are separated from the solution which is then transferred to the measuring cuvette for UV-Vis analysis. (IV) Absorbance measurements are carried out at 492 nm.

#### 4.2.8 Construction of the graphite-epoxy composite-magnet electrodes

Graphite-epoxy composite electrodes without incorporated magnet (GECE) were prepared as described by Cespedes *et al.*<sup>22,23</sup>. Briefly, epoxy resin (Epotek H77A, Epoxy Technology, USA) and hardener (Epotek H77B) were mixed manually in the ratio 20:3 (w/w) using a spatula. When the resin and hardener were well-mixed, the graphite powder (particle size 50  $\mu\text{m}$ , BDH, U.K.) was added in the ratio 1:4 (w/w) and mixed for 30 min. The resulting paste was placed into a cylindrical PVC sleeve (6 mm i.d.). Electrical contact was completed using a copper disk connected to a copper wire. The conducting composite was cured at 40°C for one week. Magnetic graphite-epoxy composite electrodes (GECE-M) were prepared in a similar way by incorporating a neodymium-based magnet ( $\text{Nd}_2\text{Fe}_{14}\text{B}$ , diameter 3 mm, height 1.5 mm, Halde Gac Sdad, Barcelona, Spain, catalog number N35D315) into the body of graphite epoxy composite, 2 mm under the surface of the electrode (*Figure 4.4*). Prior to use, the surface of the electrode was polished with abrasive paper and then with alumina paper (polishing strips 301044-001, Orion, Spain) and rinsed carefully with water.

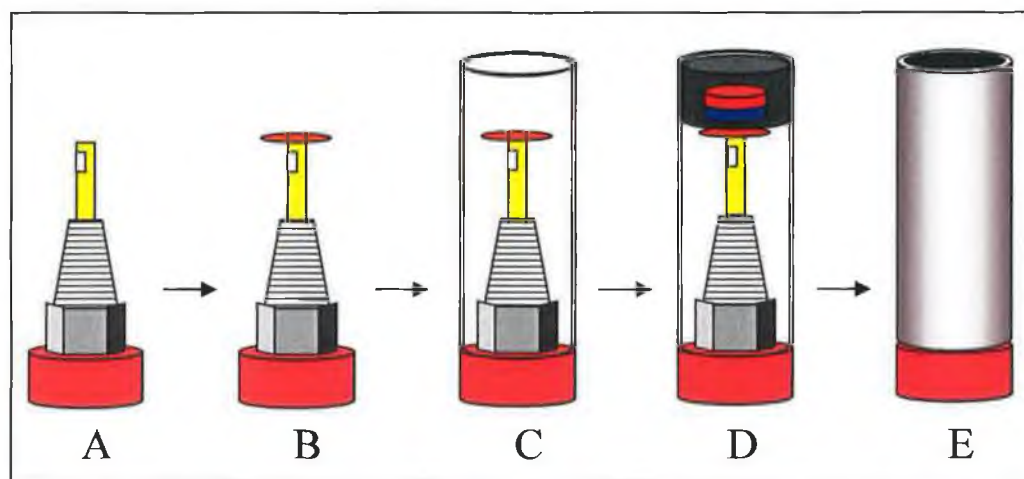


**Figure 4.4.** Schematic of the graphite-epoxy composite-magnet electrode (GECE-M) preparation. A) Electrode connector body. B) copper disk attachment on top of the connector. C) mount of the PVC body. D) introduction of the graphite-epoxy paste including a permanent neodymium magnet on top of the copper disk up to the upper border. E) The ready to use GECE-M assembled after a curing step at 40°C for one week.



#### 4.2.9 Electrochemical analysis

Figure 4.5 is a schematic of the steps followed for the electrochemical analysis. The MB/anti-human/human IgG/Au-anti-human-HRP immunocomplex was resuspended in 150  $\mu\text{l}$  of water. 50  $\mu\text{l}$  of this suspension was brought into contact for 5 min. with the surface of magnetic graphite-epoxy composite electrode in order to allow AuNP to accumulate on it. The inherent magnetic field of the electrode certainly improved the accumulation process keeping the magnetic beads well immobilized. After 5 min. the electrode was transferred without any washing steps to an electrochemical cell containing 0.1 M HCl. A preconcentration process to oxidize AuNPs to  $\text{AuCl}_4^-$  was performed at +1.25 V (vs. Ag/AgCl) for 120 s in a stirred solution. Immediately after the electrochemical oxidation, differential pulse voltammetry (DPV) was performed by scanning from +1.25 V to 0 V (step potential 10 mV, modulation amplitude 50 mV, scan rate 33.5 mV/s, non-stirred solution), resulting in an analytical signal due to the reduction of  $\text{AuCl}_4^-$  at potential +0.45 V<sup>14</sup>.

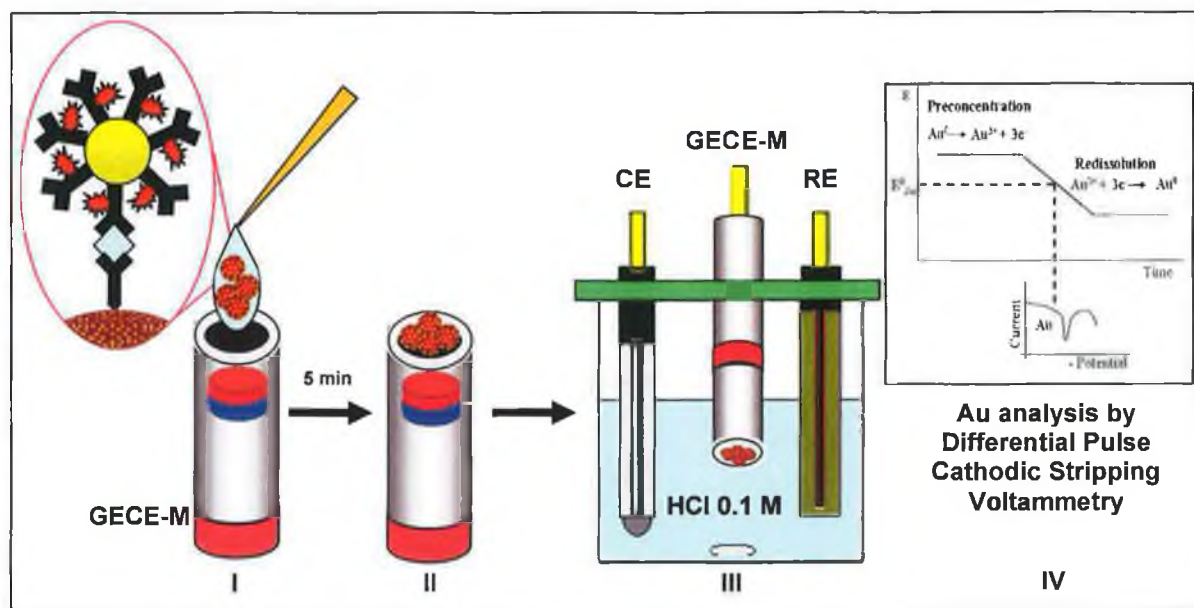


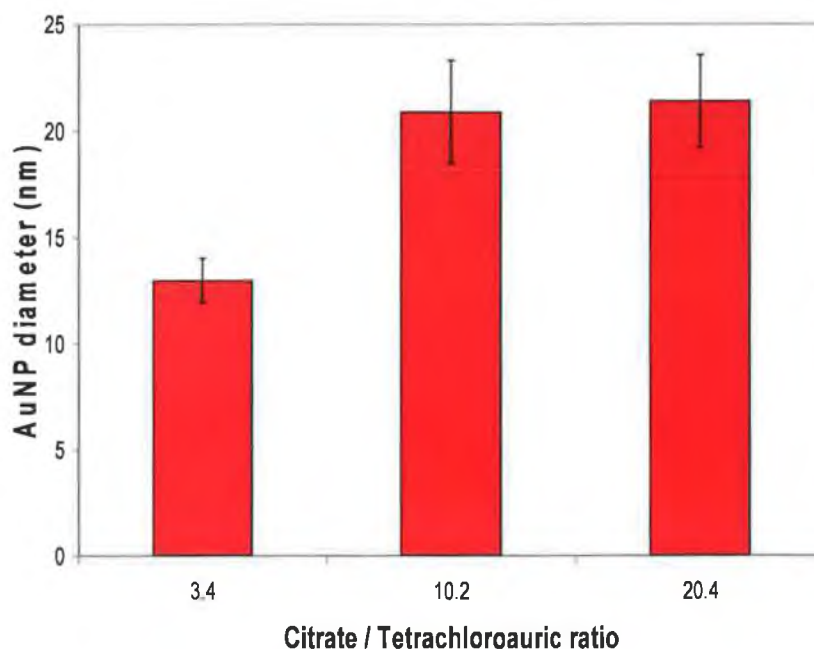
**Figure 4.5.** Electrochemical analysis procedure consisting of: (I) Deposition of 50  $\mu\text{l}$  of the MB-Au-immunocomplex sample onto the electrode surface; (II) Adsorption of the added immunocomplex on the electrode surface for 5 min. at open circuit; (III) Introduction of the electrode without washing step in the measurement cell containing 0.1 M HCl as electrolyte buffer. (IV) Electrochemical analysis consisting of a preconcentration step at 1.25 V for 150 s, followed by a DP cathodic scan from 1.25 to 0 V and measurement of the peak current at 0.45 V. (Step potential 10 mV, amplitude 50 mV, scan rate 33 mV/s (vs. Ag/AgCl)).



## 4.3 RESULTS AND DISCUSSIONS

### 4.3.1 Gold nanoparticles characterisation

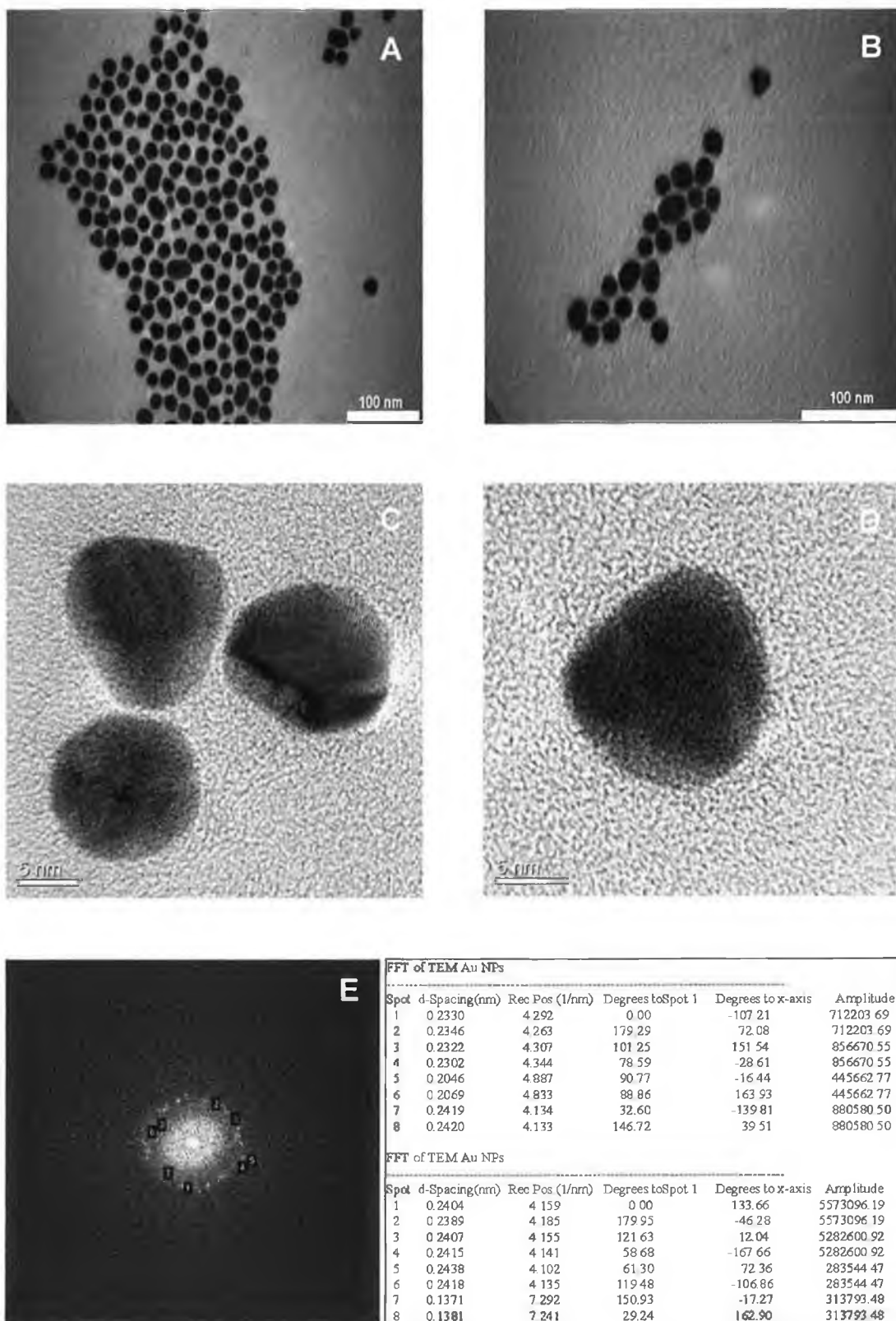
The synthesis of AuNPs was carried out using trisodium citrate as a reducing agent of tetrachloroauric as described in section 4.2.3. A AuNP size study was performed varying the concentration of the citrate during the synthesis and evaluating the effect on the particle size. In detail, 5, 15 and 30 ml of the 1% (w/v) citrate solution were added to the boiling tetrachloroauric solution, resulting in final concentrations of 0.85, 2.55 and 5.10 mM and in ratios citrate/tetrachloroauric of 3.4, 10.2 and 20.4, respectively. The size of the particles was measured using the TEM software, sampling about 30 particles per batch. The graph in *Figure 4.6* shows the results for the size study. It can be seen that surprisingly, for increased concentrations of citrate used for the reduction, a larger particle size resulted, passing from an average size of 13 nm to a size of 22 nm. This result finds correspondence in the literature. Kumar *et al.* (2007) developed a model to predict the gold particle size using the citrate-based reduction method. A mechanism is proposed to explain the dependency of the final particle size from the ratio of citrate/tetrachloroauric used in the synthesis. Their studies suggest that for a ratio of citrate/tetrachloroauric between 0.4 and 2, the particle size decreases by a factor of 7; then the size remains constant for ratios between 2 and 10; ratios greater than 10 cause another increase of the final mean particle size. This is due to a coagulation process taking place only at very high concentrations of citrate where the counterion concentration is high and a double-layer compression phenomenon occurs<sup>24</sup>. In order to guarantee a synthesis of AuNPs with a highly reproducible mean size, the rest of the work was carried out using AuNPs prepared with the lowest concentration of citrate (0.85 mM) being within the range of concentrations of citrate where the particle size remains constant for different ratios of citrate/tetrachloroauric.



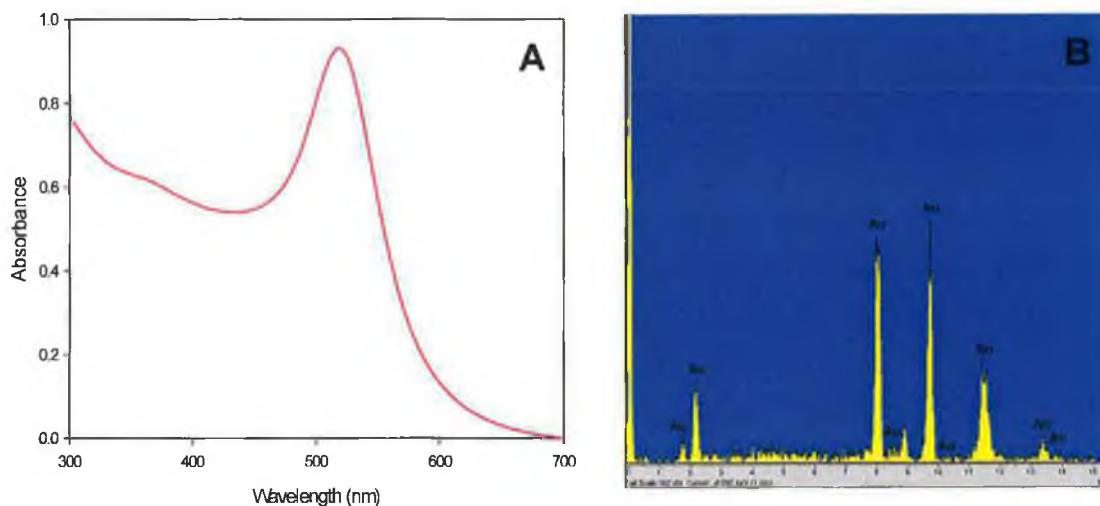
**Figure 4.6.** Mean diameter size for AuNPs synthesized using three different ratios of citrate/tetrachloroauric: 3.4, 10.2 and 20.4. An average diameter of 13 nm, 21 nm and 22 nm was measured, respectively.

Figure 4.7 shows TEM micrographs of AuNPs (13 nm) taken with a low (A and B) and high (C and D) resolution TEM. Using the highest resolution image (Mag. 600k), a FFT of crystalline planes of one AuNP was applied and the measured plane distances corresponded to the cubic system of Au (Figure 4.7 E).

Spectrophotometry, together with EDX analysis were also carried out for further characterisation of the prepared AuNP solutions and the results are shown in Figure 4.8. The UV-Vis analysis resulted in the characteristic absorbance peak at 520 nm for gold colloid solutions (A), while the EDX detection confirmed the presence of metallic gold (B).



**Figure 4.7.** Transmission electron micrographs of AuNPs (13 nm) at A) x 40k, B) x 55k, C) x 500k and D) x 600k magnifications. E) FFT of crystalline planes of one AuNP. Planes distances measured correspond to the cubic system of Au (table). The AuNP sample was diluted in water and ultrasonicated for 20 min. prior the analysis.



**Figure 4.8.** A) UV-Vis spectrum of AuNP solution with the characteristic absorbance peak at 520 nm. B) EDX spectrum of AuNPs confirms the presence of gold.

### 4.3.2 Preparation of gold-labelled anti-human-HRP

In order to form a strong absorption between gold and antibody, preliminary titrations must be performed to determine the optimum conditions for conjugation. First of all it is important to determine the correct pH for the conjugation. This is best performed at, or near to the isoelectric point of the protein<sup>20</sup>. The protein used in this work (anti-human-HRP) represents a double-protein (antibody-enzyme conjugate) and therefore the overall pI cannot be found in the literature. A preliminary titration was then carried out in order to verify the optimal pH for the conjugation of anti-human-HRP to AuNPs. Details of the experiment are given in paragraph 4.2.5. The graph in *Figure 4.9* shows the titration results and it can be seen that a pH around 9.0 resulted in the best for the conjugation in the sense that the protein (anti-human-HRP) more efficiently prevented gold aggregation. However, it can be also seen that at other pH values the conjugation was still quite efficient, and this was probably due to the nature of the conjugated protein. The attachment of AuNPs to different portions of the

protein at different pH may occur, for example, to the enzyme-side at one pH and to the antibody-side at another pH. After the optimisation of the pH, a gold aggregation test was performed to detect salt-induced colloidal gold aggregation and find, in this way, the antibody concentration to be used for conjugation with AuNPs. The antibody concentration that prevented gold aggregation was determined by measuring the difference between the absorbance at 520 and at 580 nm and plotting it against the concentration used (*Figure 4.10*). *Figure 4.11* also shows the spectrum of AuNPs and how this changes with the addition of increasing concentrations of the protein before the addition of NaCl. The minimum antibody concentration giving the highest absorbance difference was found to be 7  $\mu\text{g}$  for 1 ml of AuNPs and that corresponded to a number of protein molecules of 10 for each AuNP. This result was verified by theoretical calculations by using a close packed sphere model<sup>25</sup>. A spherical packing corresponds to the placement of  $n$  spheres around a central unit sphere such that they maximize the minimum distance between them. Using simple trigonometric calculations with the radius of the central sphere (AuNP) and of those surrounding (molecules), it is possible to approximate the maximum number of spheres touching the central one. Anti-human-HRP was approximated to a sphere of a radius of 5.6 nm<sup>26</sup>, hence resulted that 13 molecules can be arranged around a central sphere of radius 6.5 nm (AuNP). The good agreement between theoretical and experimental results supports the belief that the gold aggregation test is a simple but valid method to control protein conjugation to gold nanoparticles (*Figure 4.12*). TEMs in *Figure 4.13* show AuNPs surrounded by anti-human-HRP antibodies. The multiple small dots present inside the biological mass could be attributed to Fe atoms of the prosthetic heme group of HRP enzymes which improve the protein visualization.

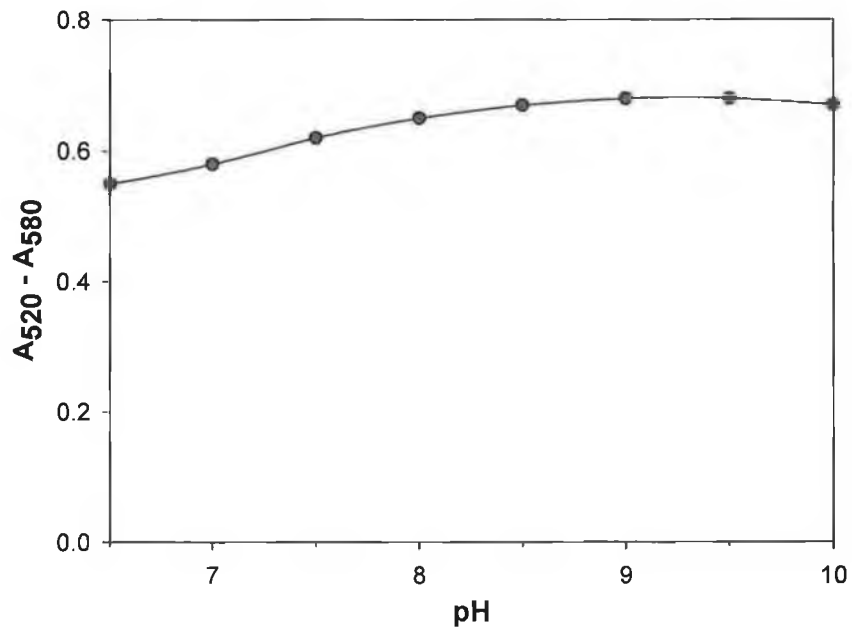


**Figure 4.9.** pH optimisation for the conjugation of anti-human IgG-HRP to AuNPs. The optimal pH at which the antibody most efficiently prevented gold aggregation was found to be around 9, giving the highest absorbance difference.

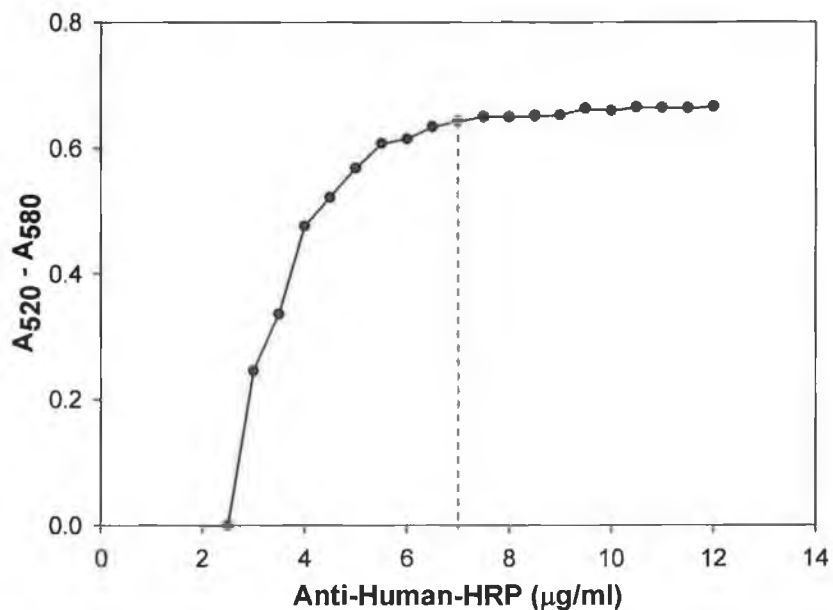


**Figure 4.10.** Gold aggregation test with anti-human-HRP. 7 µg for 1 ml of AuNPs resulted in the minimum protein concentration giving the highest absorbance difference (A520-A580) and resulting therefore the minimum protein concentration able to stabilize the AuNPs.

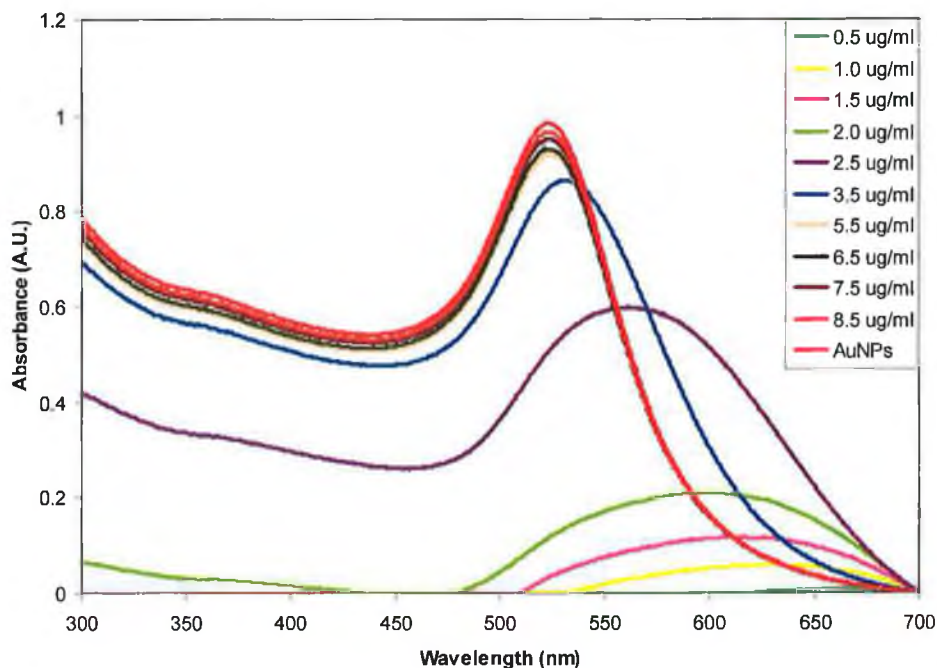


**Figure 4.11.** AuNP spectra recorded after the addition of increasing concentrations of anti-human-HRP antibody and NaCl (10% w/v). The increase of anti-human-HRP stabilized the AuNPs preventing their aggregation which was visible from the shift of the maximum absorbance peak from 520 to 580 nm. It can be seen that the spectra of AuNP-anti-human-HRP conjugate solutions became increasingly similar to that of pure AuNPs (upper line).

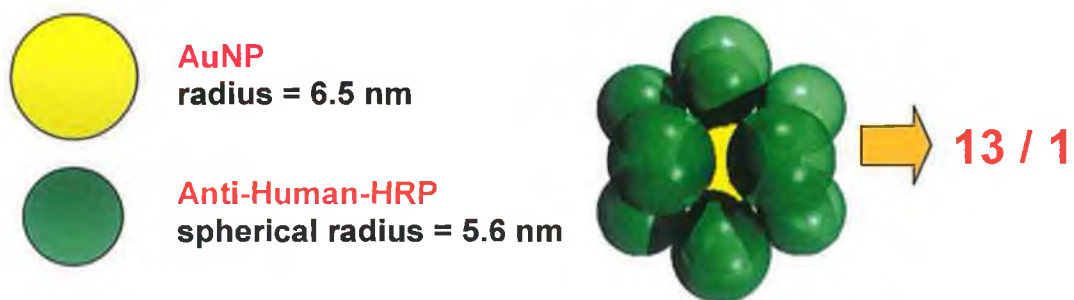


**Figure 4.12.** Theoretical calculation using the geometrical model of sphere packing around a single central sphere. 13 spheres of radius 5.6 nm can be arranged around a central sphere of radius 6.5 nm.

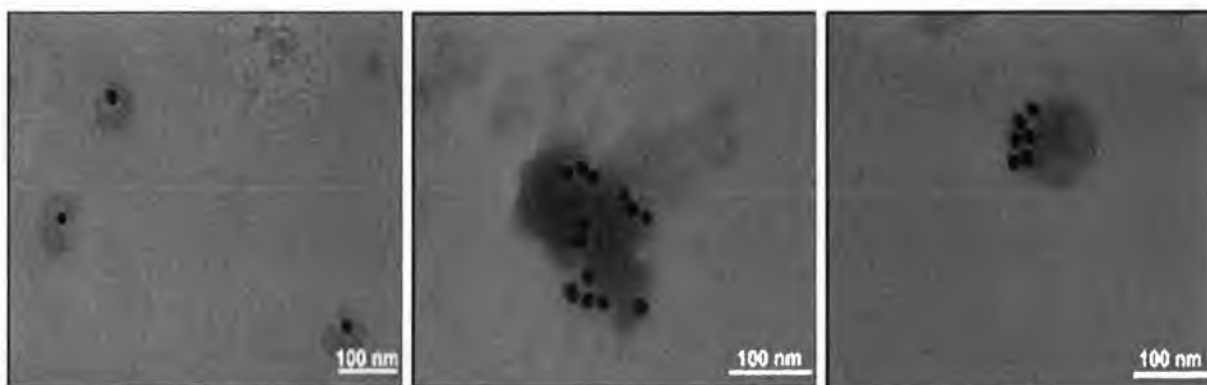


**Figure 4.13.** Transmission electron micrographs (x 40k and x 50k magnification) showing anti-human-HRP antibodies conjugated to AuNPs. The small spots around the black AuNPs can be attributed to iron metals present in the heme group of HRP.

Using the optimised conditions, five batches of Au-anti-human-HRP were prepared as described in the section 4.2.5. The method reproducibility was evaluated spectrophotometrically by measuring the absorbance at 492 nm after the reaction between HRP on AuNPs and OPD chromogen. 5  $\mu$ l of the Au-anti-human-HRP solution (diluted 1:2) from each batch were transferred to a 96-well plate; then 160  $\mu$ l of OPD solution was added. The reaction between HRP and OPD, generating a coloured solution, was stopped after 2 min. by adding 50  $\mu$ L of 3M HCl. The absorbance at 492 nm was then measured for each batch with a Microplate Reader. The absorbance was proportional to the amount of HRP attached to AuNPs. This is not an absolute quantification of HRP carried by each AuNP, but only a relative comparison between the five batches. The five batches yielded an average absorbance of 1.306 with an RSD of 7.8 %. This value represents a good reproducibility in the sense that using the same conditions in the synthesis, the final conjugate results in a consistent and reproducible number of anti-human-HRP per AuNP.



### 4.3.3 Characterisation of magnetic bead-immunocomplexes by TEM and SEM

Classical spectrophotometric immunoassays are usually performed using PVC or polycarbonate-based 96-well plates as supporting material to immobilize either antibodies or antigens. In this work, streptavidin-coated magnetic beads were used to prepare the sandwich-type immunocomplexes. Suspending these magnetic beads in the incubation solutions can shorten the incubation time itself (as confirmed in section 4.3.5) and the possibility of using an external magnet to separate the MB-complexes from the excess/unbound material can also simplify the washing procedures. The preparation of the immunocomplex is well described in section 4.2.6. In *Figure 4.14* SEMs at different magnifications of streptavidin-coated magnetic beads are shown. They are commercially available at different diameters. However, in this work the 2.8  $\mu\text{m}$  size beads were used. It can be seen from the pictures how the beads appeared to be very reproducible with a very narrow size-dispersion and this feature is important with regard to the reproducibility of the assays using these beads.



**Figure 4.14.** Scanning electron micrographs of streptavidin-coated magnetic beads (2,8  $\mu\text{m}$ ) at (A) x 1k, (B) x 5k and (C) x 20k magnification. The MB sample was diluted with water and ultrasonicated for 20 min. prior the analysis. The size-dispersion is very narrow and that ensures a good quality of the assay results.

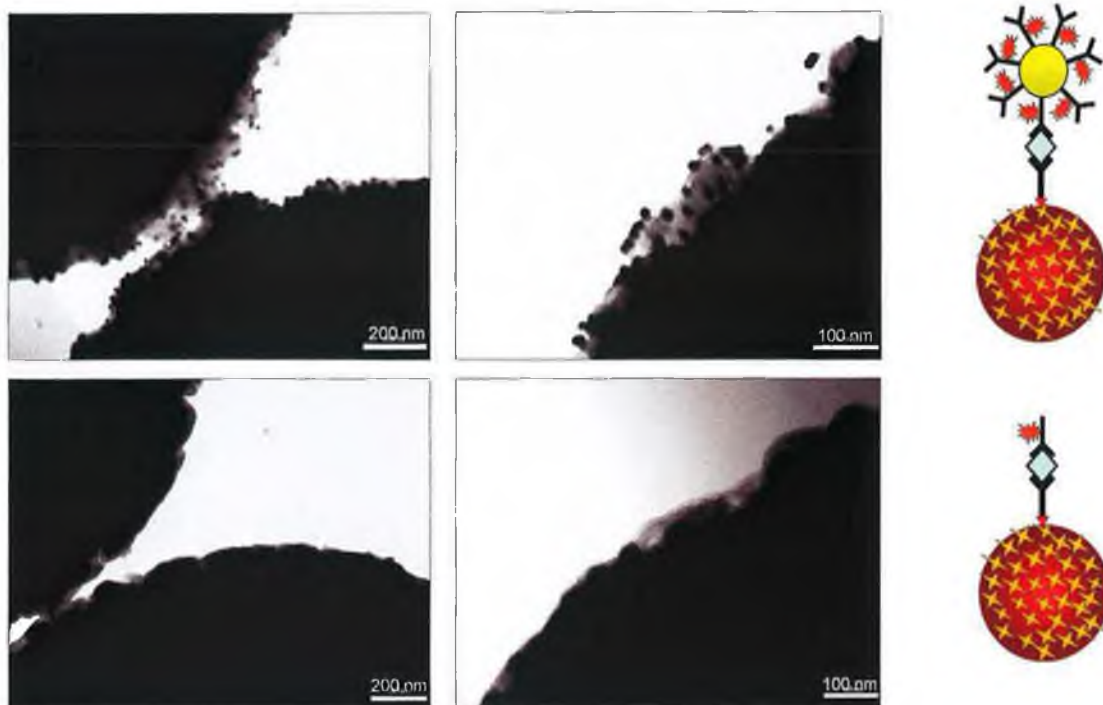


**Figure 4.15.** Transmission electron micrographs (at x 20k (left) and x 40k (right) magnifications) of sandwich-type immunocomplex MB/anti-human/human IgG/Au-anti-human-HRP (Upper part images) and MB/anti-human/human IgG/anti-human-HRP (Lower part images) obtained after the magnetic separation from the unbound Au-anti-human-HRP and anti-human-HRP respectively. The AuNPs are clearly visible on the MB surface when Au-anti-human-HRP was used to prepare the immunocomplex.

TEMs were recorded for the two MB-immunocomplexes prepared as described in section 4.2.6 using either Au-anti-human-HRP (Vb in *Figure 4.2*) or anti-human-HRP (IVb in *Figure 4.2*) as a secondary labelled antibody, respectively (*Figure 4.15*). It can be clearly seen that AuNPs are present on the magnetic bead surface when the Au-anti-human-HRP was used as a secondary antibody. No AuNP is visible on the surface when anti-human-HRP was used.

#### 4.3.4 Spectrophotometric analysis

An ultrasensitive and simple method for detecting and quantifying biomarkers is essential for early diagnosis of diseases. AuNPs are a very good candidate due to their extremely high extinction coefficients at 520 nm. Moreover, different agglomeration states of AuNPs can result in distinctive colour changes. These extraordinary optical

features make AuNPs an ideal colour reporting group for signaling molecular recognition events and render the nanomolar concentration detection possible.<sup>27</sup> In addition to AuNP optical properties the Au-anti-human-HRP secondary antibody, carrying HRP enzyme is sensitive to OPD chromogen showing by this way an alternative optical detection. Taking into account these two properties, two optical detection procedures were developed and optimized for the analyte quantification: (I) indirect analysis of Au-anti-human-HRP conjugates remaining in solution after the final incubation with the immunocomplex (Va in *Figure 4.2*) and based on both the AuNPs absorptivity and the HRP activity; (II) direct analysis of Au-anti-human-HRP conjugates specifically attached to the MB-immunocomplexes (Vb in *Figure 4.2*) and based only on the HRP activity. This direct optical detection based on the gold-conjugate was performed in parallel with the direct analysis based on the anti-human-HRP secondary antibody (IVb in *Figure 4.2*) in order to evaluate the benefits of using AuNPs.

#### *Indirect spectrophotometric determination of human IgG*

*Figure 4.16A & B* show the signals recorded for the analysis based on AuNPs (at 520 nm) (A) and based on HRP (at 492 nm after reaction with OPD) (B) for all the human IgG antigen concentrations used during the preparation of the MB/anti-human/human IgG/Au-anti-human-HRP complexes. The solutions used for the analysis correspond to the excess (residual) of Au-anti-human-HRP conjugate (Va in *Figure 4.2*) non-connected/remained in solution after the magnetic separation of the MB-immunocomplex: MB/anti-human/human IgG/Au-anti-human-HRP. An increased signal (absorbance at 520 nm for AuNP (*Figure 4.16A*) and at 492 nm for HRP/OPD reaction (*Figure 4.16B*) due to a higher concentration of Au-anti-human-HRP conjugate residual is related to the decrease of the bound human IgG antigen. Two negative controls (red bars) are also included in the graphs and correspond to the sample where a non-specific antigen (goat IgG 1  $\mu\text{g/ml}$ ) or no antigen (without human IgG added) was used in the assay, respectively. It can be clearly seen that for increasing concentrations of the human IgG antigen, the concentration of AuNP and HRP present in the residual separated Au-anti-human-HRP conjugate solution decreases, proving that a specific interaction was effectively occurring. These two

indirect spectrophotometric analyses allowed the quantification of human IgG as low as 16 ng/ml and 36 ng/ml by using AuNP and HRP related signals, respectively.

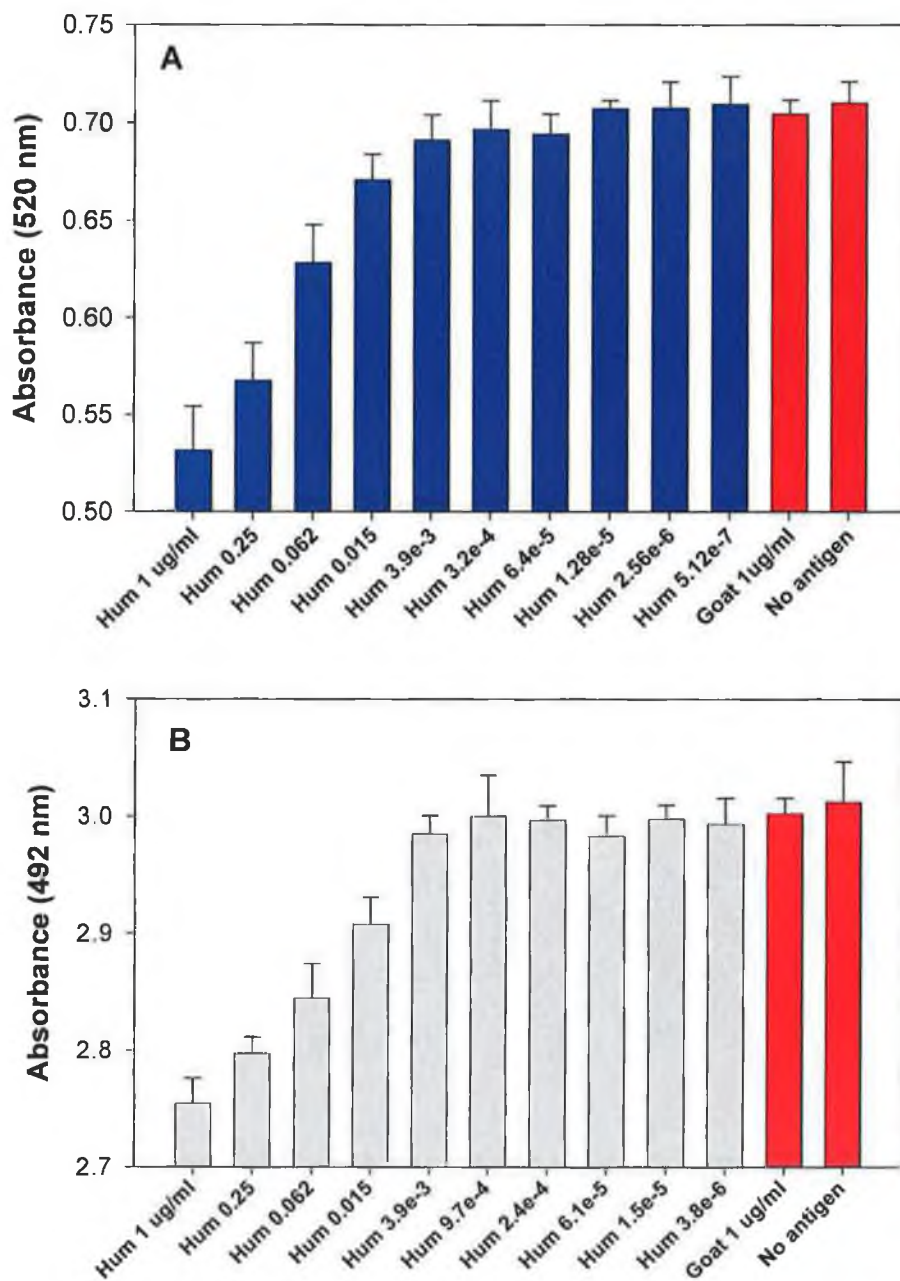


**Figure 4.16.** Spectrophotometric analyses of magnetically separated Au-anti-human-HRP conjugates remaining in solution as excess after the incubation with MB/anti-human/human IgG complexes. The graph (A) shows the absorbance at 520 nm related to the amount of AuNPs and the graph (B) shows the absorbance at 492 nm related to the amount of anti-human-HRP after the reaction with OPD. In both cases it can be seen that for an increased concentrations of the antigen (human IgG), the amount of the gold-conjugate remaining in solution decreased as a proof of the specific interaction with the antigen. The red bars (at both A & B) represent the signals recorded when a non-specific antigen was used (Goat IgG – first red bar) or the antigen was missing (second red bar) in the immunoassay.

### *Direct spectrophotometric determination of human IgG*

A direct spectrophotometric analysis based on the reaction between HRP and OPD was carried out for the sandwich-type immunocomplex MB/anti-human/human IgG/Au-anti-human-HRP (Vb in *Figure 4.2*) and the results were compared with the analysis of the MB/anti-human/human IgG/anti-human-HRP immunocomplex (IVb in *Figure 4.2*).

*Figure 4.17* shows the two calibration curves of human IgG for both immunocomplexes. It can be seen that using the gold-labelled anti-human-HRP as a secondary antibody, an optical signal enhancement occurred, due to the higher number of anti-human-HRP carried on the AuNPs (around 10 HRP for each AuNP). Although the sensitivity of the assay was almost the same ( $0.36 \text{ Abs/ln } \mu\text{g/ml}$ ) for both spectrophotometric detections, the limit of detection using the gold-labelled anti-human-HRP conjugate was about 50 times lower than that obtained using anti-human-HRP without gold reaching the value of  $52 \text{ pg human IgG/ml}$  (which corresponds to  $0.33 \text{ pM}$ ). The increased absorbance achieved using AuNPs was most likely due to a higher number of HRP. However, the resulting LOD decreased because of a lower non-specific signal. It can be seen in *Figure 4.17* that using AuNPs there was a signal enhancement of about 2 units (at the concentration of  $1 \mu\text{g/ml}$  the absorbance increases from 2 to 4 and the same for the rest of the points except for the baseline, which increased only by 0.23 units from 0.12 to 0.35). This could be explained only by the fact that during the washing steps, the non-specific interactions could be eliminated more easily when the antibody was attached to gold than when it was alone. This keeps the baseline at a value lower than that at which it should be, considering the signal enhancement.

In a situation where there are the same non-specific interactions, the signal enhancement would not lower the LOD because all the values for all the concentrations would be increased by the same factor and the final LOD would remain the same. The detection limit obtained using Au-anti-human-HRP was much lower than that normally reached by ELISA. It was lower than reported work in which the electrochemical oxidation of enzyme-generated hydroquinone was measured<sup>28</sup> and it was comparable to the limit of detection ( $190 \text{ fM}$ ) of three protein cancer markers reported by Mirkin's group<sup>10</sup>, utilizing a new multiplexed version of the biobarcode amplification method.

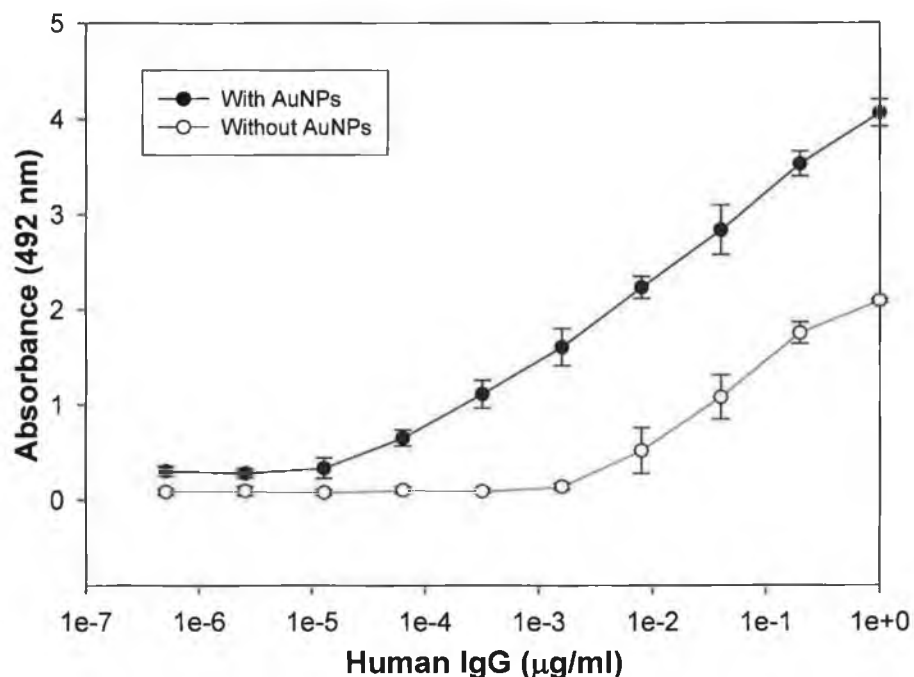


**Figure 4.17.** Calibration curves for the direct spectrophotometric detection of human IgG recorded using anti-human-HRP (red) and Au-anti-human-HRP (black) as a secondary antibody. The two curves present the same slope (0.36 Abs/ln  $\mu\text{g/ml}$ ) but using the gold-labelled anti-human-HRP a 50-fold lower limit of detection was achieved (52 pg human IgG/ml which corresponds to 0.33 pM).

#### 4.3.5 Electrochemical measurements

The use of enzymes as labels in immunosensing systems in general and particularly those based on electrochemical methods is one of the most important strategies reported so far. Various kinds of enzymes such as urease<sup>29</sup>, alkaline phosphatase<sup>30</sup> or HRP<sup>31</sup> have been used as labels for immunosensors based on electrochemical detection. While elegant biosensing designs utilizing optical properties of AuNP have been demonstrated, it is desirable to expand these rather facile/sensitive detection methodologies to new and more versatile applications with special interest to the development of novel biosensor devices: integrated and small, low cost and easy to use. The methods based on electrochemical detection are offering unique opportunities for such applications. Direct differential pulse voltammetric (DPV) detection of AuNPs is of particular interest. This useful detection possibility has been

already exploited for DNA sensing<sup>17</sup>. The proof of concept of a magnetically triggered direct electrochemical detection for monitoring DNA hybridization shows several advantages. The developed method couples a high sensitivity and a good reproducibility with an effective genomagnetic discrimination against non-complementary DNA. The elimination of the need for acid dissolution greatly simplifies particle-based electrical bioassays and obviates the use of toxic HBr/Br<sub>2</sub> solutions. The same detection principle is now applied to the gold-labelled anti-human-HRP in this work. The sandwich-type immunocomplex MB/anti-human/human IgG/Au-anti-human-HRP (Vb in *Figure 4.2*) obtained after the magnetic separation from the unbound Au-anti-human-HRP was directly detected using the differential pulse cathodic scan. The magnet inside the electrode greatly facilitated the adsorption of AuNPs present in the MB-immunocomplexes onto the surface during both the adsorption time and the preconcentration time at 1.25 V in the cell. After the DPV scan from 1.25 V to 0 V, the Au reduction peak at +0.45 V of great amplitude resulted if compared to the gold colloid detection methods performed without the use of a magnet<sup>16</sup>. This reduction peak at +0.45 V was chosen and used as the analytical signal in all of the measurements. *Figure 4.18A* shows typical DPV gold reduction curves corresponding to Au-anti-human-HRP connected to the immunocomplex for human IgG concentrations ranging from  $2.5 \cdot 10^{-6}$  to 1  $\mu\text{g/ml}$ . In contrast, no electrochemical response was observed for the same immunocomplex at the same electrode but without the built-in magnet as would be expected from the absence of magnetic or adsorptive accumulation of the paramagnetic beads. Quantitative results are presented in *Figure 4.18B*, which shows the analytical performance of the magnetically-triggered electrochemical detection of the immunoreaction based on gold-labelled anti-human-HRP secondary antibody. The calibration curve for the DPV analysis of the MB-immunocomplex presented a sensitivity of  $0.5066 \mu\text{A}/\ln \mu\text{g}\cdot\text{ml}^{-1}$  IgG, which was higher than the spectrophotometric detection with a slightly higher detection limit of 0.26 ng human IgG for ml sample (which corresponds to 1.7 pM), as compared to 52 pg/ml or 0.33 pM. The method showed a very good precision ( $\sim 3\%$ ) which represents an attractive and important feature for novel electrochemical immunoassays, compared to ELISA tests for human IgG analysis which present a coefficient of variation in the range 5-10%. It is believed that this is related to the well defined and highly reproducible magnetic collection of the MB/anti-human/human IgG/Au-anti-human-

HRP immunocomplexes on the electrode surface and overall to the direct detection of AuNPs without the need for any preliminary dissolution step that might affect the sensitivity as well as the reproducibility of the method (a series of three replicate immunoreactions with 1  $\mu\text{g}/\text{ml}$  human IgG showed a RSD of around 3%).

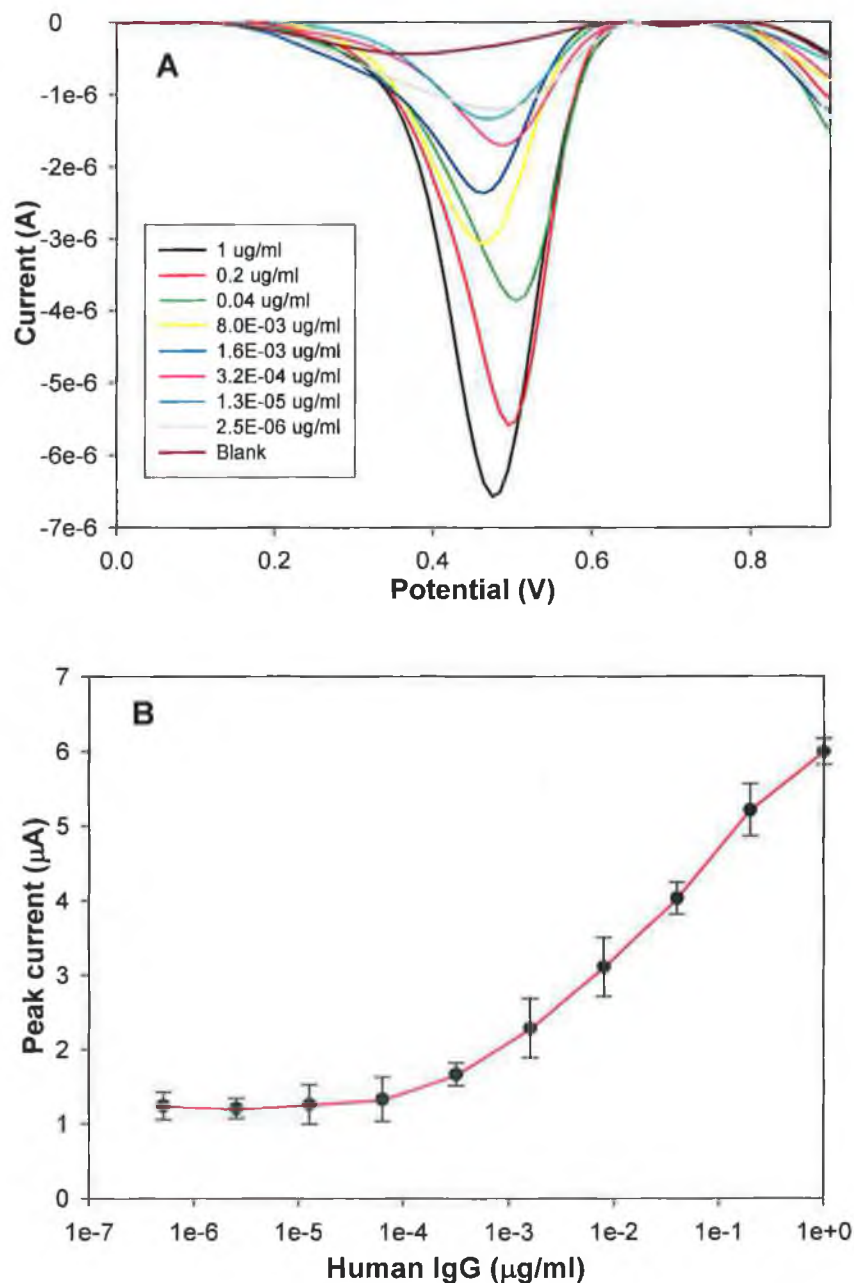


**Figure 4.18.** A) Typical DPV curves corresponding to AuNP analysis for human IgG concentrations of 2.5E-06, 1.3E-05, 3.2E-04, 1.6E-03, 0.008, 0.04, 0.2 and 1  $\mu\text{g}/\text{ml}$ . It also shows the response for 0.1M HCl only as blank solution (vs. Ag/AgCl). B) Calibration curve obtained with the electrochemical detection of gold nanoparticles present in the MB-immunocomplexes, sensitivity 0.506  $\mu\text{A}/\ln \mu\text{g}/\text{ml}$ , detection limit of 0.26 ng human IgG/ml.



Optimization of the entire procedure was carried out using the described electrochemical conditions at the fixed concentration of the antigen human IgG of 1  $\mu\text{g/ml}$ . Various parameters involved in the preparation of the MB-immunocomplexes as well as in the electrochemical detection were examined and optimized. The graph in *Figure 4.19A* represents the optimization of the deposition time of MB-immunocomplexes on the electrode surface, before the electrochemical measurement. After the final wash to eliminate the excess of Au-anti-human-HRP, the MB-immunocomplexes were resuspended in water and then 50  $\mu\text{l}$  from the suspension were dropped onto the electrode surface and left for different time periods to be adsorbed. An increase in the voltammetric peak related to AuNPs for increasing adsorption times on the electrode surface was observed up to 5 minutes. This increase was correlated to a higher number of AuNPs coming through the MB-immunocomplexes and attracted onto the electrode surface by the magnet underneath. Adsorption times longer than 5 minutes caused a signal decrease and this was probably due to a blocking effect taking place on the surface and caused by the thicker layer of magnetic beads as more and more were attracted to the electrode surface. A direct consequence of this seems to be the reduced number of AuNPs that could actually 'be seen' (touching the surface) by the electrode. The signal should indeed have reached a plateau corresponding to the maximum interaction between the electrode and the AuNPs on the magnetic beads, but actually it decreased. The adsorption time of 5 minutes was then chosen for further characterisation as the best in terms of DPV sensitivity. *Figure 4.19B* represents the incubation time optimization of the biological elements at 25°C. It can be seen that using the magnetic beads as a supporting material, the biological interactions could be completed in 20 min., which was much shorter than typical incubation times used in ELISA procedures<sup>32</sup>. Longer incubation time did not improve the signal. *Figure 4.19C* shows the optimization of the magnetic bead concentration. The response increased linearly up to 1 mg magnetic beads/ml and remained almost constant thereafter. The magnetic bead stock solution (10 mg/ml) was therefore diluted 1:10 with PBS buffer before starting the assay procedure.

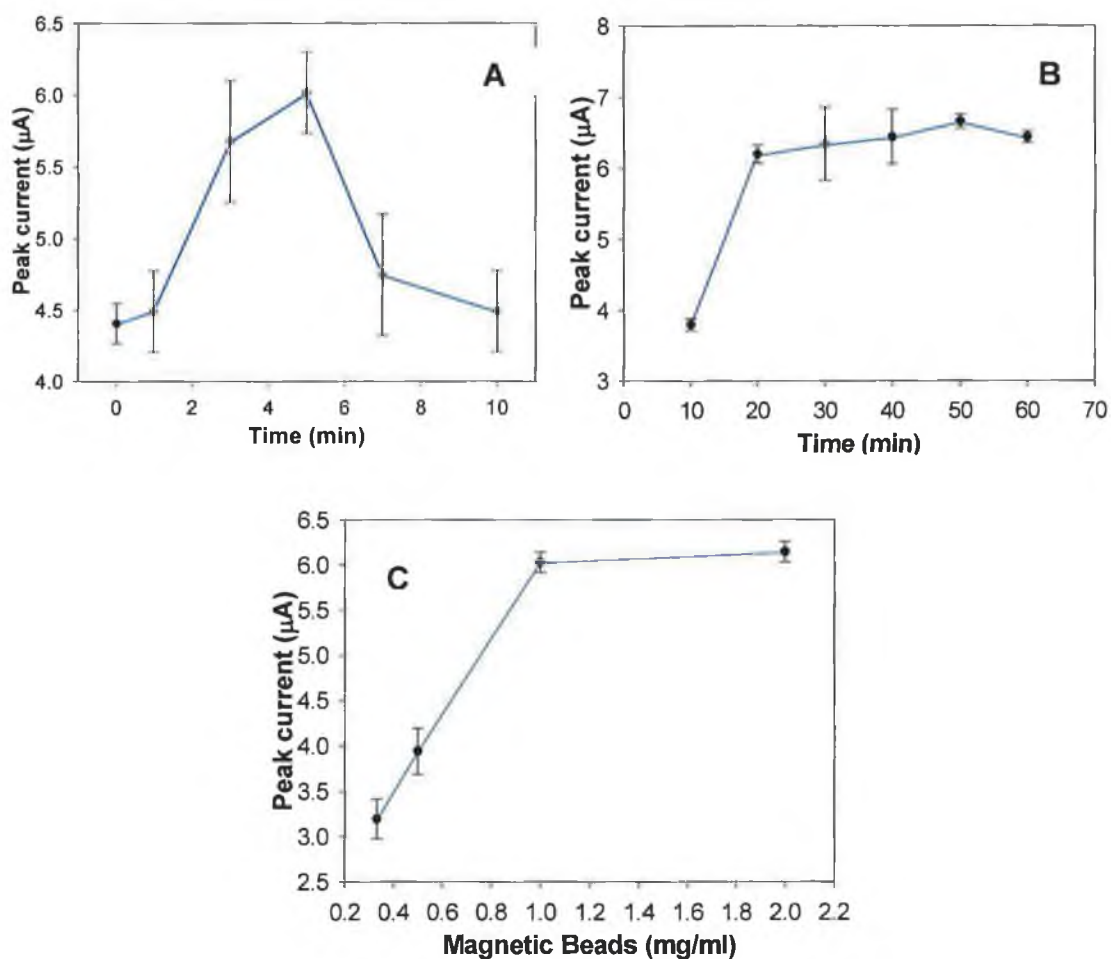


**Figure 4.19.** A) Optimisation graph for the adsorption time of MB-immunocomplexes on the electrode surface. The highest signal was recorded depositing the MB-immunocomplexes on the electrode surface for 5 min. B) Graph of the optimization of the incubation time. Using MB as supporting material the biological interactions between all the immunoreactants could be completed in 20 min. C) Magnetic beads concentration optimisation graph. 1 mg/ml MB solution was found to be the optimal to be used for the best signal response.

The use of Au-anti-human-HRP as a secondary antibody resulted in a significantly improved response for both the electrochemical and the spectrophotometric detection techniques, compared to the classical immunoassays exploiting HRP or other enzymes as labels. The lowest detection limit was obtained using the spectrophotometric detection (52 pg/ml or 0.33 pM). However, the sensitivity of the electrochemical detection resulted slightly higher than that of the spectrophotometric one and with a

limit of detection (260 pg/ml or 1.69 pM), still much lower or comparable with those reported by other authors based on either electrochemical or optical detection<sup>33</sup>, or using chromatographic techniques<sup>34</sup>.

#### 4.4 CONCLUSION

A versatile gold-labelled detection system based on both a spectrophotometric and an electrochemical method was developed. In this work, a doubly-labelled secondary antibody consisting of AuNPs conjugated to an HRP-labelled anti-human IgG antibody, was used to detect human IgG as a model protein. Streptavidin-modified paramagnetic beads were used as supporting material for the preparation of the sandwich-type immunocomplexes. A magnetic separation was then used to isolate the complexes from the unbound components, reducing considerably incubation and washing times. A permanent magnet inserted inside a graphite-epoxy-composite electrode allowed an efficient and very reproducible collection of the MB-immunocomplexes on the electrode surface for an enhanced adsorption and direct electrochemical determination of AuNPs. The use of the doubly-labelled antibody allowed immunoassays using both the electrochemical and the spectrophotometric technique to be performed obtaining for both detection methods better results in terms of detection limits (0.33 pM and 1.69 pM for the antigen by the optical – HRP-based and the electrochemical – AuNP-based analysis, respectively) and in terms of method sensitivity if compared to the classical ELISA. This proof-of-concept of a double immunodetection method showed very good performance, was rapid, straightforward, and inexpensive (no special equipment was required). In addition, this system established a general detection methodology that could be applied to a variety of immuno and DNA detection systems including lab-on-a-chip technology.

## 4.5 REFERENCES

---

- 1 D.J. Maxwell, J.R. Taylor, S. Nie. Self-assembled nanoparticle probes for recognition and detection of biomolecules. *Journal of the American Chemical Society*, **124**, (2002), 9606-9612.
- 2 M. Horisberger. Colloidal gold: a cytochemical marker for light and fluorescent microscopy and for transmission and scanning light microscopy. *Scanning Electron Microscopy*, **11**, (1981), 9-31.
- 3 T. Huang, R.W. Murray. Quenching of  $[\text{Ru}(\text{bpy})_3]^{2+}$  fluorescence by binding to Au nanoparticles. *Langmuir*, **18**, (2002), 7077-7081.
- 4 C.C. You, S.S. Agasti, M. De, M.J. Knapp, V.M. Rotello. Modulation of the catalytic behavior of  $\alpha$ -Chymotrypsin at monolayer-protected nanoparticle surfaces. *Journal of the American Chemical Society*, **128**, (2006), 14612-14618.
- 5 J.M. De la Fuente, C.C. Berry, M.O. Riehle, A.S.G. Curtis. Nanoparticle targeting at cells. *Langmuir*, **22**, (2006), 3286-3293.
- 6 M. Zayats, E. Katz, R. Baron, I. Willner. Reconstitution of Apo-glucose dehydrogenase on pyrroloquinoline quinone-functionalized Au nanoparticles yields an electrically contacted biocatalyst. *Journal of the American Chemical Society*, **127**, (2005), 12400-12406.
- 7 S.J. Hurst, A.K.R Lytton-Jean, C.A. Mirkin. Maximizing DNA loading on a range of gold nanoparticle sizes. *Analytical Chemistry*, **78**, (2006), 8313-8318.
- 8 A.K.R. Lytton-Jean, C.A. Mirkin. A thermodynamic investigation into the binding properties of DNA functionalized gold nanoparticle probes and molecular fluorophore probes. *Journal of the American Chemical Society*, **127**, (2005), 12754-12755.
- 9 C.J. Ackerson, P.D. Jadzinsky, G.J. Jensen, R.D. Kornberg. Rigid, specific, and discrete gold nanoparticle/antibody conjugates. *Journal of the American Chemical Society*, **128**, (2006), 2635-2640.
- 10 S.I. Stoeva, J.-S. Lee, J.E. Smith, S.T. Rosen, C.A. Mirkin. Multiplexed detection of protein cancer markers with biobarcode nanoparticle probes. *Journal of the American Chemical Society*, **128**, (2006), 8378-8379.
- 11 A. Merkoçi, M. Aldavert, S. Marin, S. Alegret. New materials for electrochemical sensing V. Nanoparticles for DNA labeling. *Trends in Analytical Chemistry*, **24**, (2005), 341-349.

- 
- 12 E. Katz, I. Willner, J. Wang. Electroanalytical and bioelectroanalytical systems based on metal and semiconductor nanoparticles. *Electroanalysis*, **16**, (2004), 19-44.
  - 13 J. Wang, D. Xu, R. Polsky. Magnetically-induced solid-state electrochemical detection of DNA hybridization. *Journal of the American Chemical Society*, **124**, (2002), 4208-4209.
  - 14 D. Hernandez-Santos, M.B. Gonzales-Garcia, A.C. Costa-Garcia. Metal nanoparticles based electroanalysis. *Electroanalysis*, **14**, (2002), 1225-1235.
  - 15 M. Pumera, M. Aldavert, C. Mills, A. Merkoçi, S. Alegret. Direct voltammetric determination of gold nanoparticles using graphite-epoxy composite electrode. *Electrochimica Acta*, **50**, (2005), 3702-3707.
  - 16 M.B. González-García, A. Costa-García. Adsorptive stripping voltammetric behaviour of colloidal gold and immunogold on carbon paste electrode. *Bioelectrochemistry and Bioenergetics*, **38**, (1995), 389-395.
  - 17 M. Pumera, M.T. Castañeda, M.I. Pividori, R. Eritja, A. Merkoçi, S. Alegret. Magnetically triggered direct electrochemical detection of DNA hybridization based Au67 Quantum Dot – DNA – paramagnetic bead conjugate. *Langmuir*, **21**, (2005), 9625-9629.
  - 18 M.T. Castañeda, A. Merkoçi, M. Pumera, S. Alegret. Electrochemical genosensors for biomedical applications based on gold nanoparticles. *Biosensors and Bioelectronics*, **22**, (2007), 1961-1967.
  - 19 J. Turkevich, P. Stevenson, J. Hillier. A study of the nucleation and growth processes in the synthesis of colloidal gold. *Discussions of the Faraday Society*, **11**, (1951), 55-59.
  - 20 J. Beesley Colloidal Gold. A new perspective for cytochemical marking. *Royal Microscopical Society Handbook No 17*. (1989), Oxford University Press.
  - 21 Dynal Biotech, Technote 010 for product 112.05.
  - 22 F. Cespedes, E. Martinez-Fabregas, J. Bartroli, S. Alegret. Amperometric enzymatic glucose electrode based on an epoxy-graphite composite. *Analytica Chimica Acta*, **273**, (1993), 409-417.

- 
- 23 M. Santandreu, F. Cespedes, S. Alegret, E. Martinez-Fabregas. Amperometric immunosensors based on rigid conducting immunocomposites. *Analytical Chemistry*, **69**, (1997), 2080-2085.
- 24 S. Kumar, K.S. Gandhi, R. Kumar. Modeling of formation of gold nanoparticles by citrate method. *Industrial & Engineering Chemistry Research*, **46**, (2007), 3128-136.
- 25 J.H. Conway, N.J.A. Sloane. Sphere packings, lattices and groups. (Third Edition), Springer-Verlag, NY, 1998.
- 26 A.J. Green, C.J. Johnson, K.L. Adamson, R.H.J. Begent. Mathematical model of antibody targeting: important parameters defined using clinical data. *Physics in Medicine and Biology*, **46**, (2001), 1679-1693.
- 27 R. Jin, G. Wu, Z. Li, C.A. Mirkin, G.C. Schatz. What controls the melting properties of DNA-linked gold nanoparticle assemblies?. *Journal of the American Chemical Society*, **125**, (2003), 1643-1654.
- 28 M.S. Wilson, W. Nie. Electrochemical multianalyte immunoassays using an array-based sensor. *Analytical Chemistry*, **78**, (2006), 2507-2513.
- 29 S. Solé, S. Alegret, F. Céspedes, E. Fàbregas, T.D. Caballero. Flow injection immunoanalysis based on a magnetoimmunosensor system. *Analytical Chemistry*, **70**, (1998), 1462-1467.
- 30 M. Santandreu, F. Céspedes, S. Alegret, E. Fàbregas. Amperometric immunosensors based on rigid conducting immunocomposites. *Analytical Chemistry*, **69**, (1997), 2080-2085.
- 31 E. Zacco, M.I. Pividori, S. Alegret, R. Galve, M.P. Marco. Electrochemical magnetoimmunosensing strategy for the detection of pesticides residues. *Analytical Chemistry*, **78**, (2006), 1780-1784.
- 32 <http://www.chemicon.com/resource/ANT101/a2C.asp>
- 33 M. Wang, L. Wang, H. Yuan, X. Ji, C. Sun, L. Ma, Y. Bai, T. Li, J. Li. Immunosensors based on layer-by-layer self-assembled Au colloidal electrode for the electrochemical detection of antigen. *Electroanalysis*, **16**, (2004), 757-764.
- 34 D.H. Perlman, H. Huang, C. Daully, C.E. Costello, M.E. McComb. Coupling of protein HPLC to MALDI-TOF MS using an on-target device for fraction collection, concentration, digestion, desalting and matrix/analyte cocrystallization. *Analytical Chemistry*, **79**, (2007), 2058-2066.

## **Chapter 5**

**The use of nanoparticle enhancement to characterise immunological interactions at a modified electrode by Scanning Electron Microscopy**

## 5.1 INTRODUCTION

Biosensor behaviour is strongly influenced by the surface geometry and morphology of the immobilised biolayer. In this type of analytical system, the detection limits are primarily determined by the number of active biomolecules immobilised on the transducer<sup>1</sup>. It is critical to be able to measure this number in a reliable and reproducible manner for sensor characterisation. Without this information, sensor-to-sensor calibration cannot be performed and the system detection limits are not known. Immunological interactions between antibodies and antigens on immunosensors are routinely tested using enzyme-linked immunosorbent assays (ELISA), where spectrophotometric measurements are carried out following a reaction with a substrate to generate a coloured product. This type of technique is useful, both for characterizing the properties of the immunoassay (optimizing immobilization conditions, assessing equilibrium affinity constants, etc), as well as a means of analyte quantification. However, such techniques give little information about the spatial distribution of the immobilized biomolecules.

Surface microscopy techniques have become important complementary tools for biosensor characterisation, being capable of providing information about the superficial distribution of the biological element and also to directly evaluate specific interactions between the elements involved in the system. Both light microscopies and scanning probe microscopies have been employed in this regard, including fluorescence microscopy, scanning electron microscopy (SEM), atomic force microscopy (AFM) and scanning electrochemical microscopy (SECM).

Sophisticated fluorescence-based techniques have been developed to characterise bio-specific interactions occurring at a given interface. One of the most sensitive instruments, the Zaptoreader (Duvencek *et al.*, 1997), makes use of the evanescent field generated by light travelling in a waveguide, to excite and detect fluorescence in the near-interface region of a microarray chip<sup>2</sup>. A new sensing platform by Grandin *et al.* was based on fluorescence excitation by an evanescent field that is compatible with an inverted microscope. This microscope can provide images with high spatial resolution combined with the dynamic sensing of biomolecular interactions<sup>3</sup>. Grogan *et al.*, (2002) used fluorescence microscopy to characterise a cantilever-based immunosensor surface. As an example, anti-myoglobin antibody was immobilised



onto a gold-coated microcantilever and the specific reaction with myoglobin antigen was tested<sup>4</sup>.

Atomic Force Microscopy (AFM) which provides images at a molecular resolution, has the ability to measure intermolecular forces between various ligand and receptor pairs and has proven to be a very popular technique for biosensor characterization. Kienberger *et al.* (2005) investigated the molecular recognition of an antibody for an antigen using AFM. In their work, the antibody molecule was immobilized on an AFM tip which was then manoeuvred towards the membrane-bound antigen to promote antibody-antigen association. Then, a steadily increasing force was applied to the specific bond by continuously pulling on the complex until dissociation occurred. In this way, both associative and dissociative forces could be determined for the interaction<sup>5</sup>. Ouerghi *et al.* (2002) were able to visualise immune-complexes of anti-rabbit IgG or anti-rabbit IgG moieties adsorbed on a mica surface, with specific rabbit IgG antigen. They also proposed a method for interpreting these analyses which enabled the discrimination between specific and non-specific interactions<sup>6</sup>. Perrin *et al.* (1998) used AFM to detect the immunological reaction between mouse monoclonal anti-ferritin IgG adsorbed onto silane-modified silicon wafers with either gold-labelled polyclonal anti-mouse, or with the specific ferritin antigen. To control the biospecific activity of the immobilised antibody layer, they used two methods: 1) AFM analysis after reaction with an anti-mouse antibody conjugated to a 40 nm colloidal gold particle with the aim of confirming the anti-ferritin antibodies were physically adsorbed onto the silica surface; and 2) AFM analysis after a direct reaction with the specific ferritin antigen, in order to prove the anti-ferritin antibody's recognition activity to its specific target<sup>7</sup>. Kaur *et al.* (2004) characterised an immunosensor surface using AFM, evaluating specific interactions between two herbicide molecules 2,4-dichlorophenoxyacetic acid and atrazine, with the specific antibodies immobilised on gold<sup>8</sup>.

SECM can yield information about the spatial distribution of electrochemically active species at a conducting interface and is particularly useful for the characterization of proteins with electrochemical properties such as enzymes and was first used by Heineman's group to characterize the immobilization of antibodies using an alkaline-phosphatase-labelled secondary antibody<sup>9</sup>. The technique has since been used to perform immunoassays<sup>10</sup>.

SEM does not have the resolving power of some other techniques and is typically incapable of reaching the molecular level for the direct visualization of proteins. However, it is a widely available instrument and has been used quite extensively as a means of indirectly characterizing the presence of a biological component on a transducer surface. This is typically achieved by the visualization of a carrier component such as nanoparticles<sup>11,12</sup>, the direct visualization of a bound macroscopic component such as a bacterial cell<sup>13,14</sup>, or the observation of gross morphological changes in the surface's appearance<sup>15</sup>. Au-labelled antibodies have been applied in immunosensing to enhance immobilization procedures and also as a tracer for optical and electrochemical detection<sup>16</sup>.

The scanning electron microscope (SEM) is a type of electron microscope capable of producing high-resolution images of a sample surface. Due to the manner in which the image is created, SEM images have a characteristic three-dimensional appearance and are useful for judging the surface structure of the sample. Grennan *et al.* proposed the use of a Au-labelled antibody coupled with the SEM technique to gain information concerning the distribution of protein on a conducting polymer-modified electrode surface following its immobilization. This technique assisted in optimizing the immobilization and assessing the quality of immobilization with regards to total mass loading, uniformity and dispersity<sup>17</sup>.

### 5.1.1 Scanning electron microscopy

In a typical SEM, electrons are thermionically emitted from a tungsten or lanthanum hexaboride (LaB<sub>6</sub>) cathode and travel towards an anode. Alternatively, electrons can be emitted via field emission (FE). Tungsten is used because it has the highest melting point and lowest vapour pressure of all metals, thereby allowing it to be heated for electron emission. The electron beam, which typically has an energy ranging from a few hundred eV to 50 keV, is focused by one or two condenser lenses into a beam with a very fine focal spot sized 1 nm to 5 nm. The beam passes through pairs of scanning coils in the objective lens, which deflect the beam in a raster fashion over a rectangular area of the sample surface. As the primary electrons strike the surface they are inelastically scattered by atoms in the sample. Through these scattering events, the primary electron beam effectively spreads and fills a teardrop-shaped volume, known

as the interaction volume, extending about less than 100 nm to 5  $\mu\text{m}$  deep into the surface. Interactions in this region lead to the subsequent emission of electrons, which are then detected to produce an image. X-rays, which are also produced by the interaction of electrons with the sample, may also be detected in an SEM equipped with Energy dispersive X-ray spectroscopy (EDX) or Wavelength dispersive X-ray spectroscopy (WDX).

The most common imaging mode monitors low energy ( $<50\text{ eV}$ ) secondary electrons (SE). Due to their low energy, these electrons originate within a few nanometers from the surface. The electrons are detected by a scintillator-photomultiplier device and the resulting signal is rendered into a two-dimensional intensity distribution that can be viewed and saved as a digital image. This process relies on a raster-scanned primary beam. As the secondary electrons come from the near surface region, the brightness of the signal depends on the surface area that is exposed to the primary beam. This surface area is relatively small for a flat surface, but increases for steep surfaces. Thus, steep surfaces and edges tend to be brighter than flat surfaces resulting in images with good three-dimensional appearance (*Figure 5.1*). Using this technique, resolutions less than 1 nm are possible.

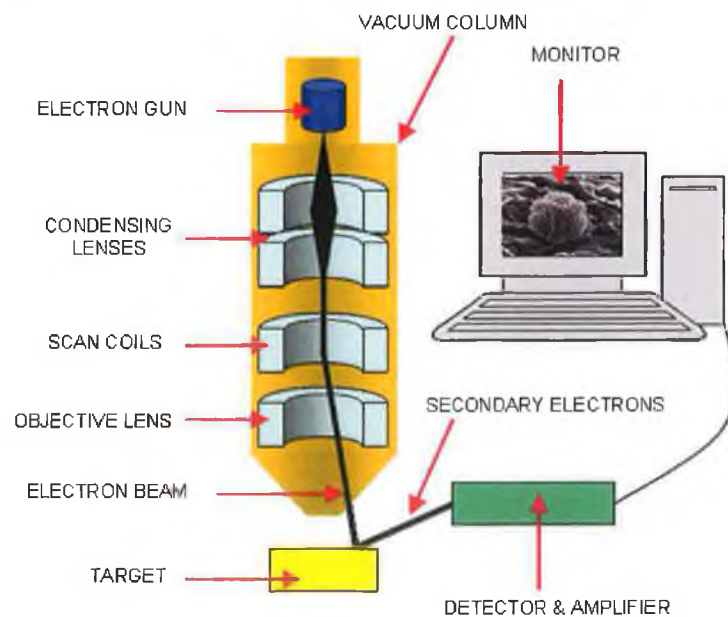


**Figure 5.1.** Schematic representation of the SEM technique. The electron beam emitted from a tungsten or lanthanum hexaboride ( $\text{LaB}_6$ ) cathode is focused by one or two condenser lenses into a beam with a very fine focal spot sized 1 nm to 5 nm. The beam passes through pairs of scanning coils in the objective lens, which deflects the beam in a raster fashion over a rectangular area of the sample surface. The subsequent emission of electrons is detected to produce an image.

In addition to the secondary electrons, or backscattered electrons (BSE) can also be detected. Backscattered electrons may be used to detect contrast between areas with different chemical compositions, especially when the average atomic number of the various regions is different. There are fewer backscattered electrons emitted from a sample than secondary electrons. The number of backscattered electrons leaving the sample surface upward might be significantly larger than those that follow trajectories toward the sides. Additionally, in contrast with the case with secondary electrons, the collection efficiency of backscattered electrons cannot be significantly improved by a positive bias common on Everhart-Thornley detectors. This detector positioned on one side of the sample has low collection efficiency for backscattered electrons due to small acceptance angles. The use of a dedicated backscattered electron detector above the sample in a "doughnut" type arrangement, with the electron beam passing through the hole of the doughnut, greatly increases the solid angle of collection and allows for the detection of more backscattered electrons.

The spatial resolution of the SEM depends on the size of the electron spot, which in turn depends on the magnetic electron-optical system, which produces the scanning beam. The resolution is also limited by the size of the interaction volume, or the extent of material which interacts with the electron beam. The spot size and the interaction volume are both very large compared to the distances between atoms, so the resolution of the SEM is not high enough to image down to the atomic scale, as is possible in the transmission electron microscope (TEM). The SEM has compensating advantages, though, including the ability to image a comparatively large area of the specimen; the ability to image bulk materials (not just thin films or foils); and the variety of analytical modes available for measuring the composition and nature of the specimen. Depending on the instrument, the resolution can fall somewhere between less than 1 nm and 20 nm. In general, SEM images are much easier to interpret than TEM images.

### 5.1.2 Energy dispersive X-ray spectroscopy

Energy dispersive X-ray spectroscopy (EDX or EDS) is a method used to determine the energy spectrum of X-ray radiation. It is mainly used in chemical analysis, in an X-ray fluorescence spectrometer (especially portable devices), or in an electron microprobe (e.g. inside a scanning electron microscope). The detector is a semiconductor, usually silicon-doped with lithium (Si(Li) detector). The semiconductor is polarised with a high voltage. When an X-ray photon hits the detector, it creates electron-hole pairs that drift due to the high voltage. The electric charge is collected, and the increment of voltage of the capacitor is proportional to the energy of the photon. It is thus possible to determine the energy spectrum. The capacitor voltage is reset regularly to avoid saturation. To reduce the electronic noise, the detector is cooled by liquid nitrogen.

In this chapter a further development to the method proposed by Grennan *et al.* is presented. Again, PANI/PVS modified screen-printed carbon electrodes were adopted to immobilise antibodies using the technique optimised and described in chapter three. A colloidal gold-labelled anti-goat antibody was used for the visualisation of two immunosensor platforms where both anti-atrazine single chain antibody and anti-biotin were immobilised on the polymer surface. Firstly, a silver enhancement treatment was optimised in order to improve the visualisation of the gold label. The silver enhancement caused the reduction of silver ions, resulting in the precipitation of metallic silver around the gold colloids, so as to enlarge the gold particles for enhanced visualisation. Subsequently, protein distribution on the surface was evaluated in relation to the immobilisation time and, then, to optimise the process itself. Finally, this method was adopted to evaluate specific immunological interactions. Various incubation and washing steps were carried out to allow specific interactions between the immobilised antibody and anti-goat-gold antibody to occur. Comparing, then, the images of the immunosensor surfaces with those of different control surfaces, it was possible to establish that the immunological interactions were effectively occurring. Energy Dispersive X-ray (EDX) analysis was also performed to quantify the surface coverage.

## 5.2 MATERIALS AND METHODS

### 5.2.1 Materials

Aniline was purchased from Aldrich (13,293-4), vacuum distilled and stored frozen under nitrogen. Polyvinylsulphonate (PVS) was purchased from Aldrich. Anti-atrazine single chain was donated from Haptogen Ltd., Aberdeen, Scotland. Anti-biotin (B-3640), anti-Human Cκ (k-3502) and anti-goat-gold (G-5402) were purchased from Sigma. Tween 20 (P-7949) and bovine serum albumin (BSA) (A-7906) were purchased from Sigma. A silver enhancement kit (SE-1EO) was purchased from Sigma. Silver/silver chloride (Ag/AgCl) electrode was purchased from Bioanalytical Systems Ltd. (Cheshire, UK). The platinum mesh (29,809-3) was purchased from Aldrich.

### 5.2.2 Buffers and solutions

Unless otherwise stated, all electrochemical measurements were carried out in phosphate buffered saline (PBS), (0.002 M  $\text{KH}_2\text{PO}_4$ , 0.008 M  $\text{Na}_2\text{HPO}_4$ , 0.137 M NaCl, 0.003 M KCl, pH 6.8). Unless otherwise stated, all biochemicals were prepared in PBS.

### 5.2.3 Instrumentation

Screen-printed carbon-paste electrodes were produced using a DEK 248 machine (DEK, Poole, Dorset, UK). Electrode modification and protein immobilisation were performed on a CH1000 electrochemical analyser with CH1000 software, using either cyclic voltammetry or time- based amperometric modes. Scanning Electron Microscopy (SEM) using Secondary Electron (SE) detection and Back-Scattered Electron (BSE) detection were carried out with a Hitachi S 3000N. An acceleration voltage of 20 kV was employed.

#### 5.2.4 Electrode preparation

Electrodes were placed in 10 ml of 0.2 M H<sub>2</sub>SO<sub>4</sub>, prior to the polymerisation of aniline. A platinum mesh auxiliary and a Ag/AgCl chloride reference electrode were used. Electrodes were cleaned and activated using cyclic voltammetry between -1200 and 1500 mV versus Ag/AgCl electrode at scan rate of 100 mV/s, sensitivity of  $1 \times 10^{-3}$  A over one cycle.

A conducting polymer film was deposited potentiodynamically. A mixture of 7.8 ml 1 M HCl, 186  $\mu$ l aniline and 2 ml PVS was degassed under nitrogen for 10 min. Aniline was polymerised on the surface of the working electrode using 20 voltammetric cycles between -500 and 1100 mV versus Ag/AgCl electrode at 100 mV/s, and sensitivity of  $1 \times 10^{-4}$  A.

Antibodies were then immobilised onto the electrodes. After modification of the electrode surface with PANI/PVS, the electrode was transferred to a 2 ml batch cell. The polymer surface was reduced in 2 ml of PBS at -0.5 V versus Ag/AgCl, sample interval of 500 ms, over 300 s at sensitivity of  $1 \times 10^{-4}$  A.

Very quickly after reduction was complete, PBS buffer was removed from the cell and replaced with the antibody solution at a concentration of 0.7 mg/ml, not under stirring or degassing. Oxidation was then performed immediately at +0.7 V versus Ag/AgCl. Antibody immobilisation was performed for the necessary time. The protein solution was then recovered from the cell and re-stored for later use.

#### 5.2.5 SEM /EDX Analysis

##### 5.2.5.1. *Optimisation of assay conditions*

After modification of the electrode with PANI/PVS and electrostatic adsorption of the Au-labelled anti-goat antibody, the surface was then treated with silver enhancement solution for 1, 3, 7, 10 and 15 min., before stopping the reaction with a 2.5% (w/v) sodium thiosulphate solution and washing with distilled water. SEM images were

taken and EDX analysis was carried out for comparison of all the different surfaces in order to evaluate the optimal treatment time.

In addition, an immobilisation time optimisation was performed. Again, Au-labelled anti-goat antibody was used at concentration of 0.7 mg/ml to be immobilised on PANI/PVS modified electrode. The electrode was transferred to a batch-cell and after the reduction in PBS at -0.5 V vs Ag/AgCl for 5 min., the antibody solution was added, replacing the buffer, and left on the electrode surface for 1, 5, 15, 25 and 40 min., while a potential of + 0.7 V was applied. After silver enhancement treatment, all electrodes were analysed by SEM and EDX.

#### ***5.2.5.2. Preparation of anti-atrazine immunosensor***

This procedure involved the use of an immunoassay with three components: anti-atrazine scFv antibody on the surface (which possess a human C $\kappa$  domain), goat anti-human C $\kappa$  which interacts and binds specifically with it, and gold labelled anti-goat which interacts and binds specifically with anti-human C $\kappa$ , the gold label of which is possible to visualise with SEM.

After immobilization of anti-atrazine, the electrode was washed with a 0.05% (w/v) Tween 20 solution and incubated with a 20 % (w/v) BSA solution at 37°C for 1 h to block the remaining surface. Then, the electrode was washed again and incubated with anti-human C $\kappa$  antibody at 37°C for 1 h. Finally, after washing, the electrode was incubated with anti-goat-gold at 37°C for 1h. Additional electrodes were prepared as controls for the anti-atrazine immunosensor surface:

1. Anti-Human C $\kappa$  antibody was immobilised on the electrode surface. The remaining surface was blocked with BSA by incubation. Finally, the electrode was incubated with anti-goat-gold antibody at 37°C for 1 h.
2. The electrode was incubated with BSA, and then, after washing, it was incubated with anti-goat-gold antibody at 37°C for 1 h.
3. Anti-goat gold antibody was directly immobilised on the electrode surface.
4. PANI/PVS electrode surface with no protein.

All these electrodes were treated with the silver enhancement solution before being analysed by SEM in BSE and SE mode.



### **5.2.5.3. Preparation of anti-biotin immunosensor**

As anti-biotin was developed in goat, it was possible to use anti-goat-gold directly, which interacts specifically with it. After immobilization of anti-biotin antibody, the electrode was washed with a 0.05 % (w/v) Tween 20 solution and incubated with a 20 % (w/v) BSA solution at 37°C for 1h to block the remaining surface. The electrode was then washed again and incubated with anti-goat-gold at 37°C for 1h.

Additional electrodes were prepared as a control for the anti-biotin immunosensor surface:

1. The electrode was incubated with BSA, and then, after washing, it was incubated with anti-goat-gold antibody at 37°C for 1 h.
2. Anti-goat gold antibody was immobilised on the electrode surface.
3. PANI/PVS electrode surface with no antibody.

All the electrodes were treated with the silver enhancement solution before being analysed by SEM in BSE and SE mode and also by EDX.

## **5.3 RESULTS AND DISCUSSION**

### **5.3.1 Silver enhancement optimisation**

This procedure is based on the reduction of silver ions and the deposition of silver on the surface of a heavy metal such as colloidal gold. Gold catalyses the reduction of silver ions to metallic silver in the presence of a reducing substance. During this physical development, gold particles are encapsulated in growing shells of metallic silver, which become detectable by SEM. Different treatment times were used in order to optimise the visualisation of the gold-labelled protein immobilised onto the electrode surface. In particular, after the immobilisation of gold-labelled anti-goat antibody, 20 µl of the silver enhancement solution (freshly prepared) was deposited on the electrode surface. The silver deposition reaction was stopped after 1, 3, 7, 10 and 15 min. with sodium thiosulphate solution (2.5 %, w/v). One electrode was analysed without silver enhancement treatment for a comparison.

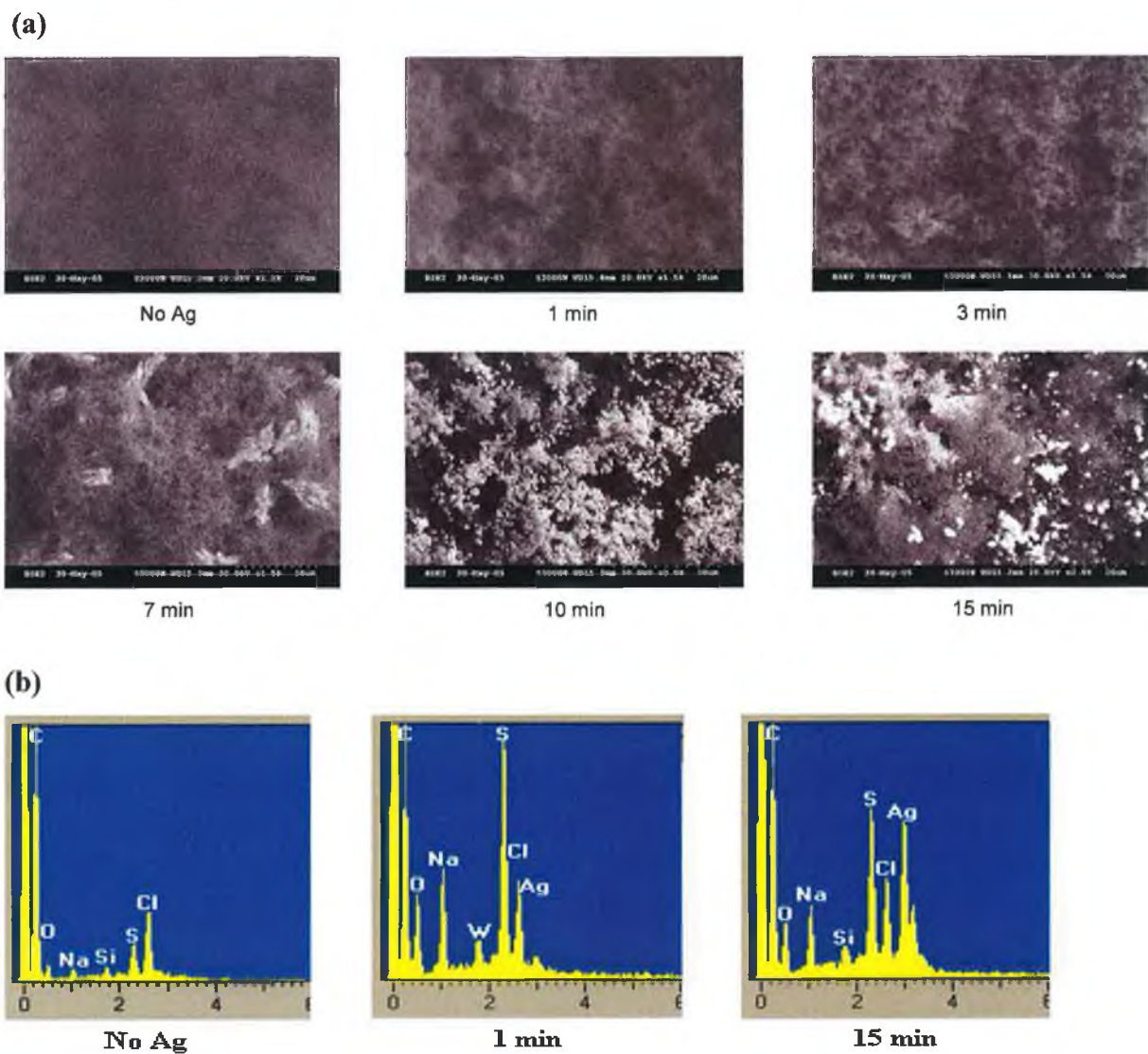


**Figure 5.2.** (a) SEM images in BSE mode showing gold-labelled anti-goat antibody immobilised on the electrode surface with no silver enhancement treatment and treated with silver enhancement solution for 1, 3, 7, 10, 15 min. (1.0k x magnification). (b) EDX spectra for electrode surfaces with no treatment and treated with silver enhancement solution for 1 and 15 min. Silver quantity on the surface clearly increases with longer treatment time.

In *Figure 5.2a*, SEM images (BSE mode) show different intensities of the silver signal, with intensity increasing with silver enhancement treatment time. It can clearly be seen that without silver enhancement, the gold-labelled protein distribution cannot be visualised. A time of 10 min. resulted in the optimal treatment time, considering that, at this time, protein distribution had the best resolution. A treatment time longer than 10 min. produced large silver aggregations which resulted in coverage of the entire surface. *Figure 5.2b* shows the EDX spectra for the electrode with no silver treatment, 1 min. treatment, and 15 min. treatment. These spectra confirm the presence of silver on the electrode surface treated with silver enhancement solution and also show semi-quantitatively how the amount of silver was higher at longer treatment times.

### **5.3.2 Protein immobilisation time optimisation**

To optimize the time necessary for protein immobilization, gold-labelled anti-goat antibody was immobilised on a PANI/PVS modified screen-printed electrode. A potential of -0.5 V was applied for 5 min. to the modified electrode in a batch cell system containing PBS buffer. A solution containing 0.8 mg/ml of the antibody was then added after removing the buffer solution. The immobilisation was performed for different times: 1, 5, 15, 25 and 40 min. One modified electrode was not used for the immobilisation. All the electrodes were then treated with the silver enhancement solution for the optimised time of 10 min. *Figure 5.3* shows SEM images of all the electrode surfaces prepared. The electrode surface with no protein immobilised appears dark with no silver signal. The presence of silver on the surfaces of the electrodes used for the immobilisation confirms that the antibody was immobilised. The silver density all over the surface was higher for the surfaces where the immobilisation time was longer, suggesting an increasing amount of protein for longer incubation times. The protein distribution appears homogeneous with no preferred aggregation points, especially with respect to the images of the surfaces with 5 and 15 min. of immobilisation time. This suggests that the conducting polymer covers the electrode surface with excellent uniformity. However, from these images, no information can be derived with regard to the thickness or the number of protein layers.

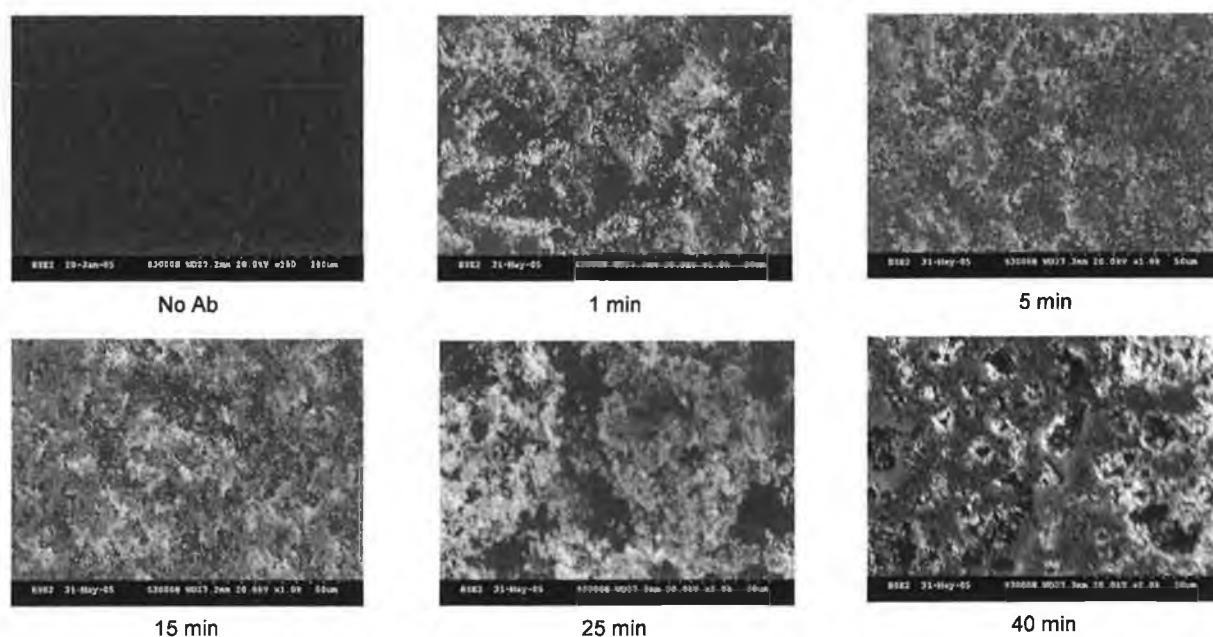


**Figure 5.3.** SEM images of gold-labelled anti-goat antibody adsorbed on the electrode surface using a potential of  $-0.5\text{ V vs Ag/AgCl}$  for 1, 5, 15, 25, 40 min. One image shows the PANI/PVS modified electrode surface with no antibody immobilised (1.0k x magnification).

### 5.3.3 Anti-atrazine immunosensor surface

An attempt at visualizing an immunological interaction was made using SEM. As it has been described in *section 5.2.5.2*, procedures generally adopted in immunoassays (ELISA) were adapted to this system. Anti-atrazine scFv antibody was firstly immobilised on a PANI/PVS modified screen-printed electrode, then after blocking the remaining surface with BSA, two incubations were performed: the first one with anti-human C $\kappa$  which interacts specifically with anti-atrazine, and the second one with gold labelled anti-goat antibody which interacts with anti-human C $\kappa$  (developed in goat). Washing steps were performed to eliminate species non-specifically bound. Additional electrode platforms were prepared as a control (see *section 5.2.5.2*). All the electrodes were analysed in SE or BSE mode by SEM after silver enhancement treatment.

*Figure 5.4* shows all the images recorded in SE detection mode for the immunosensor platform under examination and for all the additional platforms. The small diagram under each picture describes the type of surface analysed. *Figure 5.4(a)* shows the immunosensor surface where anti-atrazine was adsorbed on PANI/PVS modified electrode and the remaining surface blocked with BSA. Anti-human C $\kappa$  Ab and anti-goat-gold were then deposited. *Figure 5.4(b)* shows the surface where anti-human C $\kappa$  was immobilised onto PANI/PVS and the remaining surface blocked with BSA. Anti-goat-gold was then deposited. *Figure 5.4(c)* shows the electrode where the entire surface was blocked with BSA before depositing anti-goat-gold. *Figure 5.4(d)* shows the surface with directly-immobilised gold-labelled anti-goat antibody and finally *Figure 5.4(e)* shows a PANI/PVS modified electrode surface with no protein.

A specific immunological interaction between anti-atrazine, anti-human C $\kappa$  and gold-labelled anti-goat can be proved by comparing all the images. High electron density due to silver-enhanced gold, and therefore due to the gold-labelled anti-goat antibody, resulted for the surface with directly immobilised anti-goat-gold (d) and with similar intensity for the surfaces with immobilised anti-atrazine (a) or anti-human C $\kappa$  (b) in the first layer. The interaction between these antibodies can only be specific because as the image (c) proves, blocking the surface with BSA could prevent any non-specific interaction with the electrode surface. As a matter of fact, this resulted in a surface similar to the surface with no antibody immobilised (e). BSE detection mode was sensitive to the detection of high molecular weight particles such as gold and silver and could be used to reveal the presence of silver on the electrodes examined. *Figure 5.5* shows the images recorded with BSE detection mode and confirms the results achieved in SE mode seen in *Figure 5.4*. Electrode surfaces (a), (b) and (d) revealed the presence of silver, whereas the surface blocked with BSA (c) resulted in a surface similar to that with no protein immobilised (e).



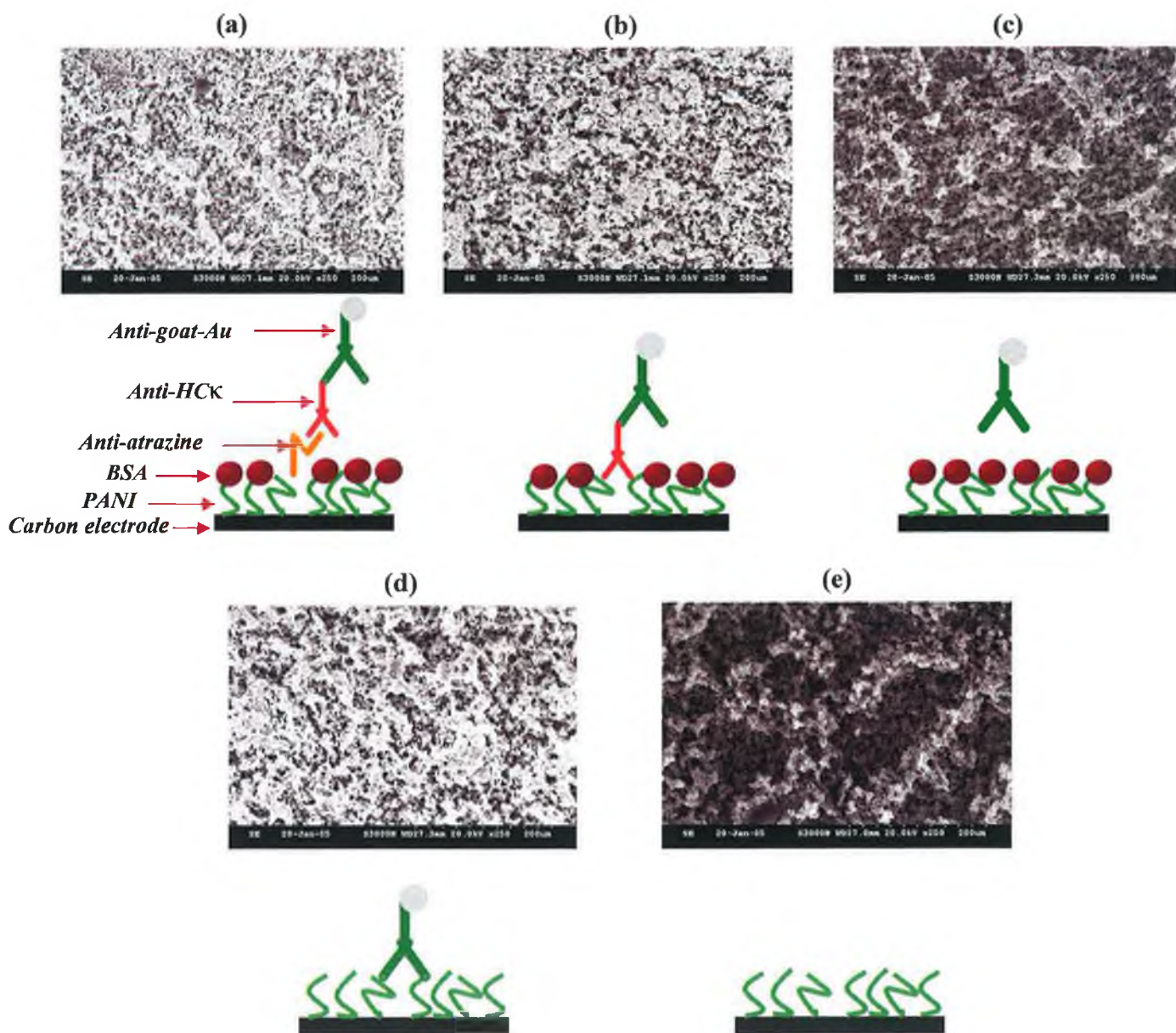


**Figure 5.4.** SEM images of the anti-atrazine immunosensor surface and associated controls (250 x magnification, SE detection mode). (a) Anti-atrazine was adsorbed on PANI/PVS modified electrode and the remaining surface blocked with BSA. Anti-human C $\kappa$  and anti-goat-gold were then deposited. (b) Anti-human C $\kappa$  immobilised onto PANI/PVS and the remaining surface blocked with BSA. Anti-goat-gold was then deposited. (c) BSA was immobilised to block the entire surface and then anti-goat-gold was added. (d) Gold-labelled anti-goat antibody immobilised directly on the surface. (e) PANI/PVS modified electrode surface with no protein.

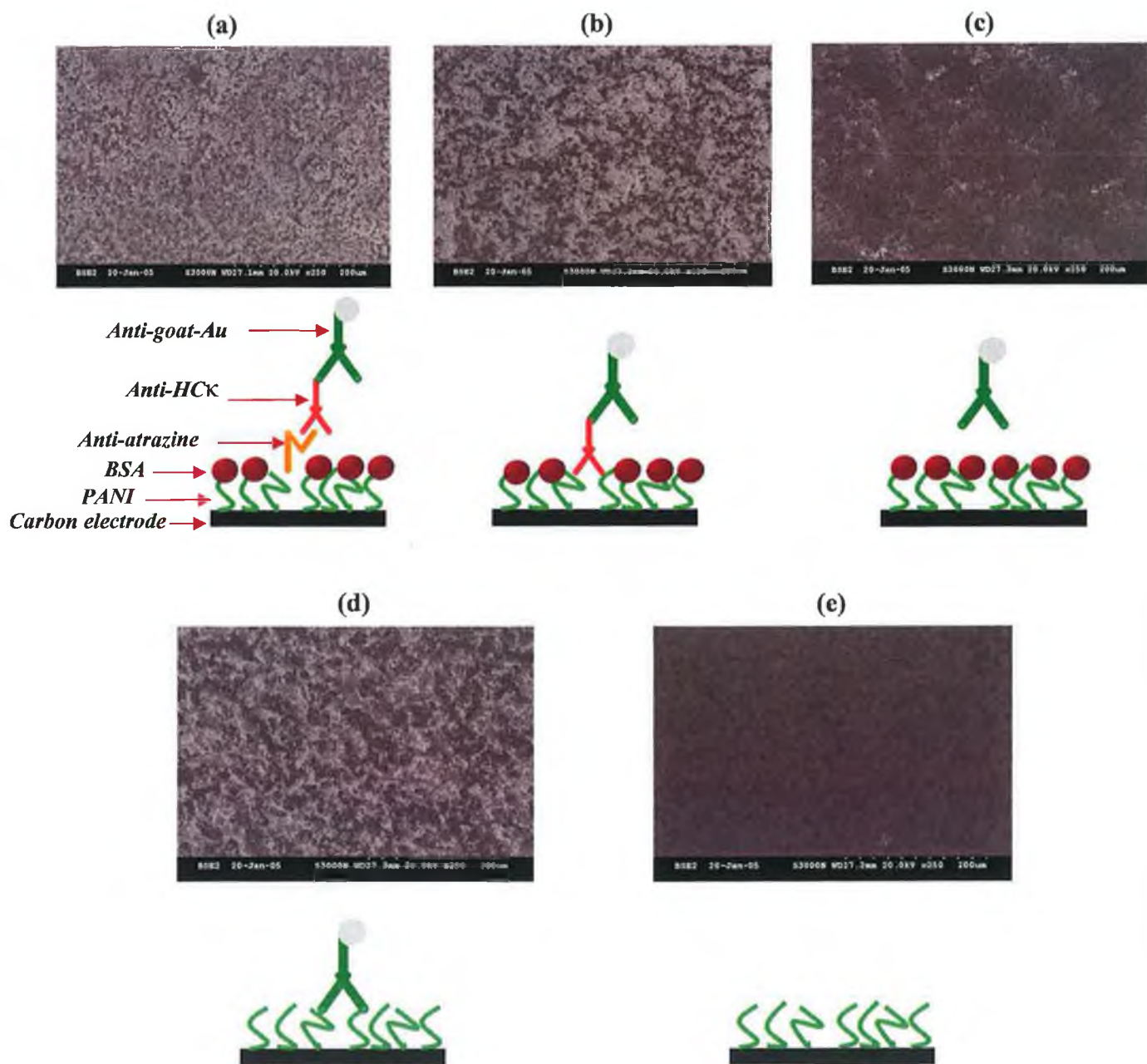


**Figure 5.5.** SEM images of the anti-atrazine immunosensor surface and associated controls (250 x magnification, BSE detection mode). (a) Anti-atrazine was adsorbed on PANI/PVS modified electrode and the remaining surface blocked with BSA. Anti-human C $\kappa$  and anti-goat-gold were then deposited. (b) Anti-human C $\kappa$  immobilised onto PANI/PVS and the remaining surface blocked with BSA. Anti-goat-gold was then deposited. (c) BSA was immobilised to block the entire surface and then anti-goat-gold was added (d) Gold-labelled anti-goat antibody immobilised directly on the surface. (e) PANI/PVS modified electrode surface with no protein.

### 5.3.4 Anti-biotin immunosensor surface

Another immunosensor surface was prepared and analysed using anti-biotin antibody. This antibody was developed in goat so it was possible to reveal its presence on the electrode surface modified again with PANI/PVS, using gold-labelled anti-goat antibody. A procedure similar to that adopted for the characterisation of the anti-atrazine immunosensor, seen in *section 5.3.3*, was followed to prepare the immunosensor with anti-biotin and the associated controls. To visualise the electrode surfaces, silver enhancement treatment was carried out and SEM images were recorded using SE detection mode and to reveal the atomic surface composition, EDX analysis was also performed. *Figure 5.6* shows SEM images of the immunosensor surface and the associated controls with small illustrative diagrams. *Figure 5.6(a)* shows the immunosensor surface with anti-biotin immobilised in the first step. Incubation with BSA was then performed to block the remaining surface and finally anti-goat-gold was added to interact specifically with anti-biotin. *Figure 5.6(b)* shows the electrode where the entire surface was blocked with BSA before depositing anti-goat-gold. *Figure 5.6(c)* shows the surface with directly-immobilised gold-labelled anti-goat antibody and *Figure 5.6(e)* shows a PANI/PVS modified electrode surface with no protein.

It can be seen from *Figure 5.6* that the surface with anti-biotin immobilised (a) presented a brightness similar to the surface with immobilised anti-goat-gold directly (c), confirming the presence of anti-goat-gold interacting with anti-biotin. Blocking the surface with BSA can prevent non-specific interactions, although the resulting surface in this case (b) was slightly brighter than the surface with no protein (d). EDX analysis was carried out to detect the atomic composition of the anti-biotin immunosensor surface, of the surface with BSA immobilised, and of the PANI/PVS surface with no protein immobilised. *Figure 5.7* shows the EDX spectra of the various control and test surfaces. It can be seen that silver was present only for the immunosensor with anti-biotin immobilised on the surface and interacting specifically with anti-goat-gold antibody (silver enhanced).



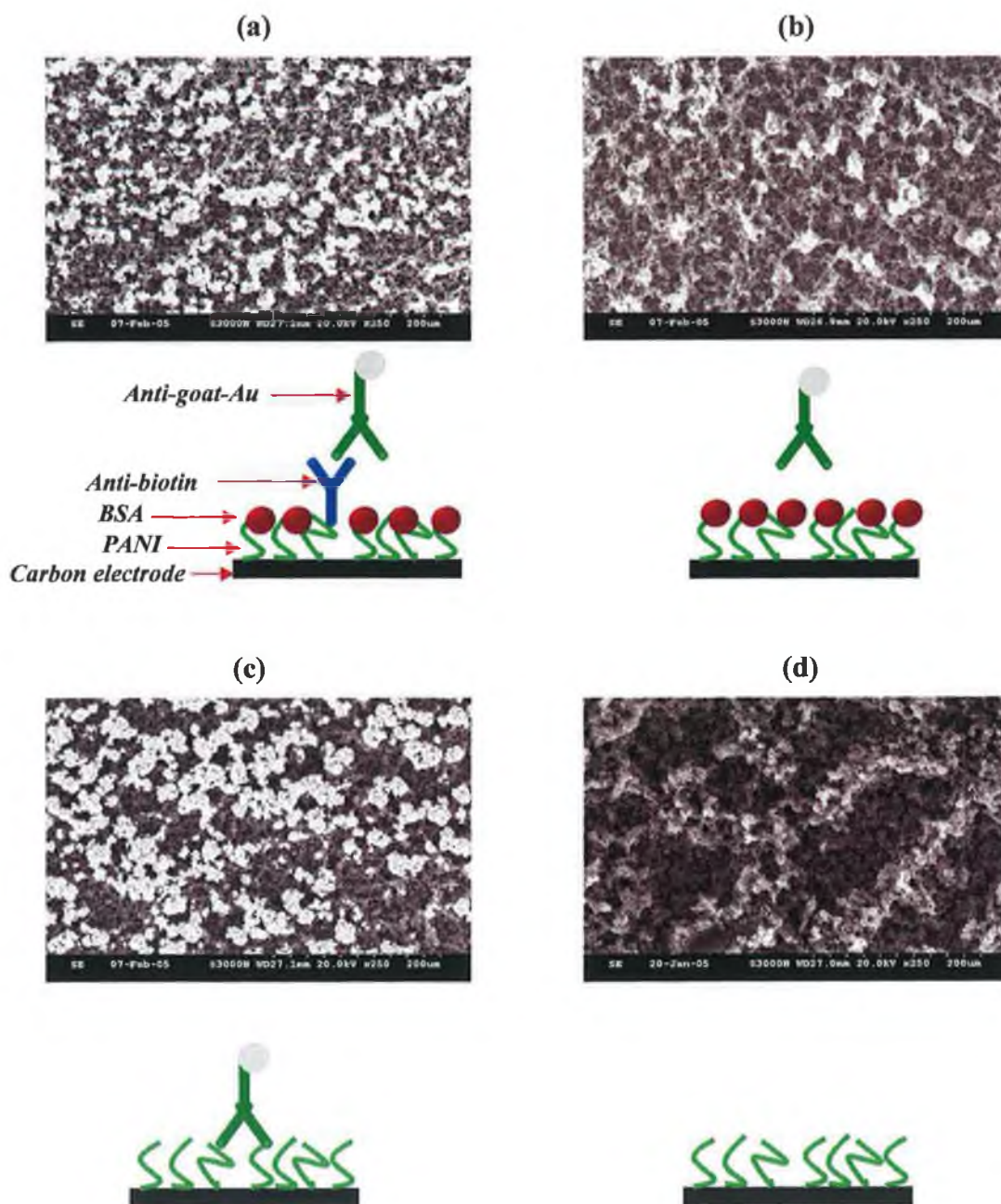


**Figure 5.6.** SEM images of the anti-biotin immunosensor surface and associated controls (250 x magnification, SE detection mode). (a) Anti-biotin was immobilised onto PANI/PVS and the remaining surface blocked with BSA. Anti-goat-gold was then deposited. (b) BSA was immobilised to block the entire surface and then anti-goat-gold was added (c) Gold-labelled anti-goat antibody immobilised directly on the surface. (d) PANI/PVS modified electrode surface with no protein.

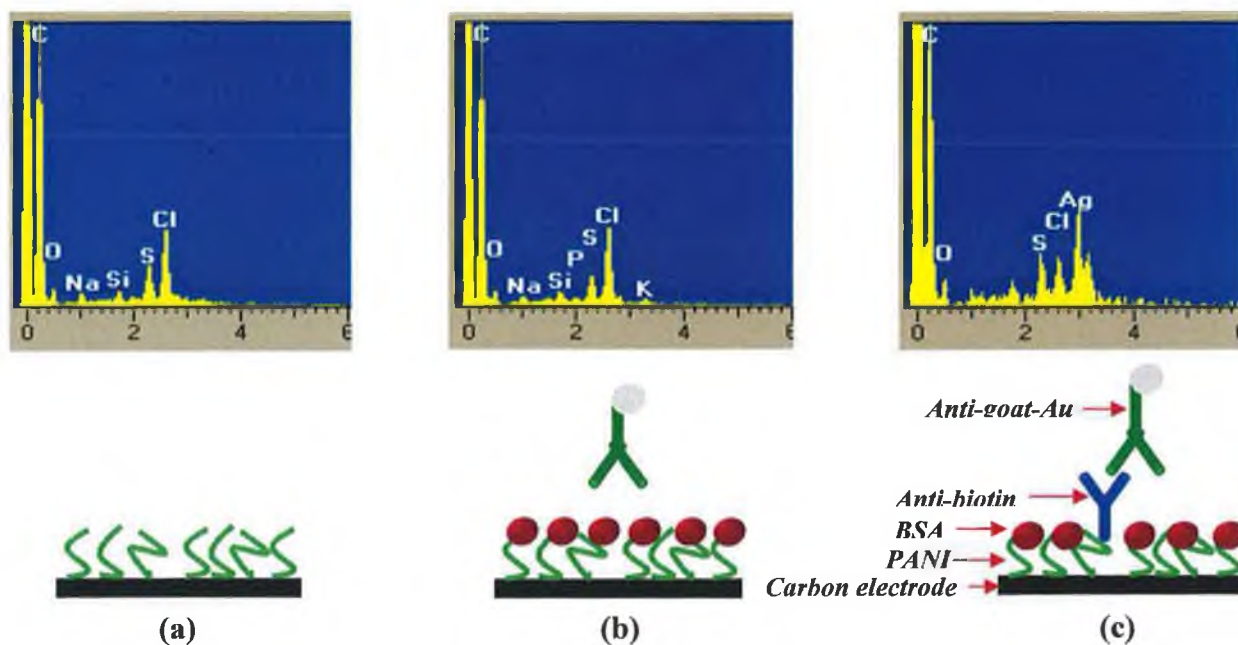


**Figure 5.7.** EDX spectra showing atomic compositions for (a) PANI/PVS electrode surface, (b) PANI/PVS electrode surface blocked with BSA, and (c) anti-biotin immunosensor surface interacting with anti-goat-gold antibody.

#### 5.4 CONCLUSION

AuNP-labelled antibodies have been applied in immunosensing to enhance immobilisation procedures and also as a tracer for electrochemical detections. Grennan *et al.*, proposed the use of this type of label coupled with the SEM technique, to directly gain information concerning the protein distribution on the electrode surface after the immobilisation. In the present work, AuNP-labelled antibody was exploited to visualise the protein distribution on the electrode surface for different immobilisation times and therefore to test the efficiency of the procedure adopted to bind proteins. Moreover, it was possible to use this technique to directly visualise specific immunological interactions occurring at an electrode surface. The comparison between the image of the immunosensor platform and the images of different controls clearly proved that the immunointeraction was occurring. This method was optimised for anti-biotin antibody, anti-human C $\kappa$  antibody and anti-atrazine scFv antibody, using gold labelled anti-goat antibody as a target, but using different gold-labelled

antibodies could certainly be applied to visualise other antibody-antibody or antigen-antibody interactions. Electrochemical techniques have, to date, been the main tool used to characterise immunosensor platforms. However, this research shows that SEM/EDX analysis can provide topological imagery that complements electrochemical data.

## 5.5 REFERENCES

- 1 H. Berney, P. Roseingrave, J. Alderman, W. Lane, J.K. Collins. Biosensor surface characterisation: confirming multilayer immobilisation, determining coverage of the biospecies and establishing detection limits. *Sensors and Actuators B: Chemical*, **44**, (1997), 341-349.
- 2 G.L. Duveneck, M. Pawlak, D. Neuschaefer, E. Baer, W. Budach, U. Pielek, M. Ehrat. Novel bioaffinity sensors for trace analysis based on luminescence excitation by planar waveguides. *Sensors and Actuators B: Chemical*, **38-39**, (1997), 88-95.
- 3 H.M. Grandin, B. Städler, M. Textor, J. Vörös. Waveguide excitation fluorescence microscopy: A new tool for sensing and imaging the biointerface. *Biosensors and Bioelectronics*, **21**, (2006), 1476-1482.
- 4 C. Grogan, R. Raiteri, G. M. O'Connor, T.J. Glynn, V. Cunningham, M. Kane, M. Charlton, D. Leech. Characterisation of an antibody coated microcantilever as a potential immuno-based biosensor. *Biosensors and Bioelectronics*, **17**, (2002), 201-207.
- 5 F. Kienberger, G. Kada, H. Mueller, P. Hinterdorfer. Single molecule studies of antibody-antigen interaction strength *versus* intra-molecular antigen stability. *Journal of Molecular Biology*, **347**, (2005), 597-606.
- 6 O. Ouerghi, A. Touhami, A. Othmane, H. Ben Ouada, C. Martelet, C. Fretigny, N. Jaffrezic-Renault. Investigating specific antigen/antibody binding with the atomic force microscope. *Biomolecular Engineering*, **19**, (2002), 183-188.
- 7 A. Perrin, A. Elaïssari, A. Theretz, A. Chapot. Atomic force microscopy as a quantitative technique: correlation between network model approach and experimental study. *Colloids and Surfaces B: Biointerfaces*, **11**, (1998), 103-112.

- 
- 8 J. Kaur, K.V. Singh, A.H. Schmid, G.C. Varshney, C.R. Suri, M. Raje. Atomic force spectroscopy-based study of antibody pesticide interactions for characterization of immunosensor surface. *Biosensors and Bioelectronics*, **20**, (2004), 284-293.
  - 9 G. Wittstock, K.J. Yu, H.B. Halsall, T.H. Ridgway, W.R. Heineman. Imaging of immobilized antibody layers with scanning electrochemical microscopy. *Analytical Chemistry*, **67**, (1995), 3578-3582.
  - 10 X.L. Zhang, X.W. Peng, W.R. Jin. Scanning electrochemical microscopy with enzyme immunoassay of the cancer-related antigen CA15-3. *Analytica Chimica Acta*, **558**, (2006), 110-114.
  - 11 J.W. Park, S. Kurosawa, H. Aizawa, Y. Goda, M. Takai, K. Ishihara. Piezoelectric immunosensor for bisphenol A based on signal enhancing step with 2-methacryloyloxyethyl phosphorylcholine polymeric nanoparticle. *Analyst*, **131**, (2006), 155-162.
  - 12 L. Yang, W.Z. Wei, X.H. Gao, J.J. Xia, H. Tao. A new antibody immobilization strategy based on electrodeposition of nanometer-sized hydroxyapatite for label-free capacitive immunosensor. *Talanta*, **68**, (2005), 40-46.
  - 13 K.Y. Gfeller, N. Nagaeva, M. Hegner. Micromechanical oscillators as rapid biosensor for the detection of active growth of *Escherichia coli*. *Biosensors and Bioelectronics*, **21**, (2005), 528-533.
  - 14 T. Geng, M.T. Morgan, A.K. Bhunia. Detection of low levels of *Listeria monocytogenes* cells by using a fiber-optic immunosensor. *Applied and Environmental Microbiology*, **70**, (2004), 6138-6146.
  - 15 N.G.R. Mathebe, A. Morrin, E.I. Iwuoha. Electrochemistry and scanning electron microscopy of polyaniline/peroxidase-based biosensor. *Talanta*, **64**, (2004), 115-120.
  - 16 C. Fernandez-Sanchez, C.J. McNeill, K. Rawson, O. Nilsson, H.Y. Leung, V. Gnanapragasam. One-step immunostrip test for the simultaneous detection of free and total prostate specific antigen in serum. *Journal of Immunological Methods*, **307**, (2005), 1-12.
  - 17 K. Grennan, A.J. Killard, C.J. Hanson, A.A. Cafolla, M.R. Smyth. Optimisation and characterisation of biosensors based on polyaniline. *Talanta*, **68**, (2006), 1591-1600.

# **Chapter 6**

## **Future developments**

## 6.1. NOVEL DEVELOPMENTS FOR ELECTROCATALYSIS OF HYDROGEN PEROXIDE (CHAPTER 2)

Chemical sensors are powerful devices for detecting important substances, such as hydrogen peroxide, which is an enzymatic intermediate substance of many enzyme-substrate reactions<sup>1</sup>. Hydrogen peroxide has wide applications in industrial processes as a universal chemical, and it is also a very important intermediate in environmental, biological, and medicinal reactions. It has been reported that the detection of hydrogen peroxide is of interest to many fields, such as food and food additives, medicine, environmental analyses, biosensors<sup>2,3</sup>, etc.

The application of a novel nanoparticulate formulation of polyaniline conducting polymer to the development of a chemical sensor device has been demonstrated in chapter two. The catalytic properties of the resulting nanoPANI film modified electrodes were exploited for the analysis of ascorbic acid and hydrogen peroxide. Additional investigations are required to fully characterise and understand the mechanism involved in the catalytic process, focusing particularly on the catalytic reduction of hydrogen peroxide at low potentials. This significant feature of the nanoPANI film was demonstrated experimentally in this chapter, but further characterisations adopting other analytical techniques would furnish precious information on the chemical and physical characteristic of the nanomaterial under study. In fact, reviewing the physical differences between the PANI NPs and the other forms of PANI could explain why the electrocatalytic reduction of hydrogen peroxide resulted only for this conducting polymer at nanoparticulate form. Resonant Raman spectroelectrochemical (RRS) analysis have been already carried out for in situ studies of electrocatalytic reactions at conducting polymer modified electrode by Malinauskas *et al.* resulting in extremely useful information to elucidate the mechanism of the catalytic oxidation of hydroquinone and ascorbic acid<sup>4,5</sup>. The application of this powerful technique could be useful to study the impact of the nanoparticle size on the observed catalytic phenomenon with particular look at the molecular interaction of hydrogen peroxide with the conducting polymer interface. Another technique useful to gain structural information is the NMR spectroscopy which was already exploited to investigate conducting polymers and metal catalysts<sup>6</sup>.

Next to the full characterisation of the nanomaterial illustrated in the chapter two, further developments could concern the investigation of catalytic properties towards other analytically important species. For example, electrochemical sensing devices could be fabricated for the analysis of nitrite, ammonia, methanol, dopamine etc. as these have been found to be good analytes to be detected with PANI.

A combination of the PANI NPs with enzymes could also open up the possibility of developing biosensing devices for a wider range of analytical applications. The introduction of enzymes producing hydrogen peroxide during their enzymatic reactions can result in a sensor able to specifically detect the enzyme substrate analyte. For example, the immobilisation a GOX enzyme on a nanoPANI modified electrode surface could be used to fabricate a glucose biosensor. Due to the biocompatibility of the nanoPANI dispersion, solutions containing the PANI NPs and the enzymes could be prepared and adopted also for the inkjet printing deposition technique, which was illustrated at the end of chapter two. The simplicity and the efficiency of the inkjet printing technique in combination with the extremely high processability of the PANI NPs, in fabricating disposable sensing devices has already been demonstrated. The possibility of introducing enzymes in combination with the nanoparticulate conducting polymer in the inkjet printing process, with the retention of the enzyme biofunctionality and ensuring the sensor stability, would represent a powerful fabrication methodology for many different sensing and biosensing electrochemical devices.

A different application exploiting the catalytic reduction of hydrogen peroxide is represented by the energy conversion devices, such as fuel and biofuel cells. Hydrogen peroxide has been widely used as an oxidant in biofuel cells<sup>7</sup>. The reduction and the oxidation of hydrogen peroxide is an unfavourable process at a range of electrode interfaces, it requires the application of large overpotentials and the use of catalysts to occur efficiently. To date, the focus has been on the application of transition metals such as platinum, iron and others as catalysts for this purpose. Organic materials are, however, attracting increasing interest as alternatives to traditional metal catalysts due to a number of advantages that organic materials have over the metals such as the efficiency and selectivity of the reactions, cost, availability and ease of use<sup>8</sup>. The PANI NPs investigated in chapter two with their catalytic

features represent a promising building materials also in the development of energy conversion devices based on catalysts.

PANI NPs could be used as either a cathodic or anodic electrode modification to drive oxidation or reduction in a galvanic cell system. Alternately, it could be employed to enhance the performance of a biofuel cell where the enzyme HRP could be removed from the cathode with direct reduction at the nanoparticle surface<sup>9</sup>.

## **6.2. ALTERNATIVE IMMOBILISATION STRATEGIES IN DEVELOPING ELECTROCHEMICAL ENZYME-BASED IMMUNOSENSORS (CHAPTER 3)**

The enzyme-channeling system investigated in chapter three resulted in the ability to furnish a specific response when biotin-GOX conjugate was added to the sensor platform which constituted avidin and HRP immobilised to a PANI/PVS modified electrode surface. However, non-specific responses were recorded by passing free GOX. This was probably due to incomplete coverage of the electrode surface resulting in portions of the conducting polymer being available for non-specific interactions. The sensor performance could, therefore, be enhanced by using additional materials (e.g. BSA, casein, PEG), to block the electrode surface more efficiently and reduce non-specific responses.

As already introduced in the same chapter, the suggestion was made that signal amplification might be achieved by the use of nanoparticles. However, one of the issues reducing the quality and efficiency of the nanoparticle approach was represented by the loss of the enzyme biofunctionality after the conjugation to AuNPs due to large size of the particles used, which caused a partial protein structural denaturation. Further investigations, then, could be focused on the adoption of smaller nanoparticles (< 15 nm) with the aim of retaining higher native protein activity when attached to the particle but also to reduce the relative distance between the enzyme carried and the enzyme immobilised on the electrode surface. Activity improvements



of the enzyme conjugates could be investigated prior to their application in the bienzyme-based platform for possible improvements in signal performance.

Alternative immobilisation strategies could also be taken into consideration as well as the adoption of different nanoparticulate materials. For example the immobilisation of enzymes to AuNPs could be achieved more efficiently exploiting the affinity binding approach. A biotinylated enzyme can be more specifically attached to streptavidin-coated AuNPs without loss of activity<sup>10</sup>.

A further strategy to enhance the performance of this sensor could be the use of nanoparticles with the ability to stably bind biomolecules such as enzymes, while at the same time ensuring direct electron transfer between the electrode and the biomolecule. PANI nanoparticles are novel nanomaterials, which possess both these characteristics and therefore, could be the object of future investigations<sup>11</sup>. Two possible approaches could be taken using PANI nanoparticles: 1) preliminary conjugation with enzymes and subsequent immobilisation of the formed conjugates to a PANI/PVS modified electrode surface; 2) direct attachment of the PANI nanoparticles to the electrode surface with subsequent immobilisation of the enzymes. Methodologies investigated in the formation of enzyme-conjugates and their application to bienzyme-based biosensors, will be transferred to the immunosensor platform based on avidin-biotin interaction. Possible improvements to the enzyme-channeling system based on HRP and GOX could be derived from an increased number of biotin-GOX conjugates in proximity to the electrode surface. After the interaction with biotin, signal amplification could be achieved by the large increases in H<sub>2</sub>O<sub>2</sub> production.

It has been illustrated in the second part of chapter three that a mathematical approach to investigate the enzyme behaviour on the electrode surface represents a promising tool to better optimize biosensing devices. The same approach could be taken also for more complex systems such as immunosensors. Bienzyme immunosensing systems, exploiting the enzyme channelling phenomenon, could be simplified to mathematical models taking into consideration not only the enzyme's kinetic constants, but also the affinity between antigen and antibodies.

### **6.3. TOWARDS MINIATURISATION OF ELECTROCHEMICAL IMMUNOASSAYS (CHAPTER 4)**

Identification and quantification of proteins is becoming more and more important in many fields such as clinical diagnosis, the food industry and environmental monitoring. Immunoassays are nowadays widely used as rapid and efficient tools for screening analysis because they require minimal sample manipulations, small amounts of target analytes and also they are compatible with multiwell or microchip formats.

The electrochemical immunoassay system developed and illustrated in chapter four, made the use of AuNPs as electrochemical tracer for batch mode analysis. A further development could be constituted by the introduction and application of semiconductor nanocrystals (quantum dots)<sup>12</sup> as labels. Different types of nanocrystals, e.g. CdS, PbS, ZnS etc. could be used simultaneously for multi-target assays<sup>13</sup>. However these immunoassays, performed in batch mode, involve a significant number of steps, increasing the possibility of human error, the assay complexity and the assay time. "Lab-on-a-chip" technology offers tremendous potential for obtaining desired analytical information in a simpler, faster and cheaper way compared to traditional batch/laboratory-based technology.

Particularly attractive for multiple biospecific recognition applications is the high-throughput, automation, versatility, portability, reagent/sample economy and high-performance of such micromachined devices<sup>14</sup>. A portable microanalyzer, based on a novel advanced "Lab-on-a-Chip" technology consisting of a magnetic separation and an end-column quantum dot tracers voltammetric detection, would represent an attractive device for automated, fast, sensitive and simultaneous assays. To successfully complete such advanced analytical system, several fundamental and practical issues must be addressed.

Fast mixing of reagents is one of the issues that present a major challenge to the operation of microfluidic devices<sup>15</sup>. Due to their size, microfluidic devices operate in a regime where small Reynold's numbers govern the delivery of fluid samples. Functionalized beads placed in the microchannel can overcome this limitation due to a large surface area for the display of antibody probes. Rapid mixing in microchannels

can be achieved because the distance which must be covered by diffusion is limited to the small interstitial space between the closely packed beads. Analytes will be captured by antibody-covered beads in a flow-through format. The use of paramagnetic beads would not require frits and would provide an automatable approach by using an electroosmotic flow and a magnetic field. Paramagnetic bead-based analysis will be highly selective since only the specific antigen would be entrapped while other materials would be washed out of the microfluidic channel.

There is also urgent need for developing a wide selection of quantum dot tracers, which would create a pool of electrical tags with non-overlapping voltammetric properties. The potential window over which heavy metals (principal constituents of quantum dots) are stripped is of about 1.2 V, therefore, five metals can be measured simultaneously with minimal peak overlap (theoretical peak widths of  $75.5/n$  (mV); where  $n$  is number electrons transferred). Particularly attractive (in addition to CdS, ZnS and PbS) would be the adoption of InAs and GaAs quantum dots.

#### **6.4. CHARACTERISATION OF IMMUNOSENSING SURFACES BY SEM (CHAPTER 5)**

AuNP-labelled antibodies have been applied in immunosensing to enhance immobilisation procedures and also as a tracer for electrochemical detections. In the present work, AuNP-labelled antibody was exploited to visualise the protein distribution on the electrode surface and therefore to test the efficiency of the immobilisation procedure adopted. Moreover, it was possible to use this technique to directly visualise specific immunological interactions occurring at an electrode surface. This method was optimised in chapter five for anti-biotin antibody, anti-human Ck antibody and anti-atrazine scFv antibody, using gold labelled anti-goat antibody as a target. It could be used also, to investigate the interaction occurring between avidin immobilised to the electrode and a biotinylated enzyme, like the system seen in chapter 3. This could be achieved by using a gold-labelled biotinylated

protein, which interacts specifically with avidin and allows its SEM visualisation by the Au particle.

This system could be used to characterise the efficiency of antibody immobilisation and antibody-antigen interaction at nanostructured electrode surfaces designed to bring about an enhancement in the efficiency of immunological interaction at the electrode surface. Such materials are nanoporous conducting polymer films<sup>16</sup>

Using different gold-labelled antibodies the technique developed in chapter five could certainly be applied to visualise other antibody-antibody or antigen-antibody interactions with the aim to provide topological imagery of immunosensing surfaces that complements electrochemical data.

## 6.5. REFERENCES

- 
- 1 Q. Wang, G. Lu, B. Yang. Hydrogen peroxide biosensor based on direct electrochemistry of hemoglobin immobilized on carbon paste electrode by a silica sol-gel film. *Sensors and Actuators B: Chemical*, **99**, (2004), 50-57.
  - 2 J. Wang, M. Musameh, Y. Lin. Solubilization of carbon nanotubes by nafion toward the preparation of amperometric biosensors. *Journal of the American Chemical Society*, **125**, (2003), 2408 -2409.
  - 3 Y. Lin, X. Cui, L. Li. Low-potential amperometric determination of hydrogen peroxide with a carbon paste electrode modified with nanostructured cryptomelane-type manganese oxides. *Electrochemistry Communications*, **7**, (2005), 166-172.
  - 4 R. Mažeikienė, G. Niaura, A. Malinauskas. In situ Raman spectroelectrochemical study of electrocatalytic oxidation of ascorbate at polyaniline-and sulfonated polyaniline-modified electrodes. *Electrochimica Acta*, **51**, (2006), 5761-5766.
  - 5 R. Mažeikienė, G. Niaura, A. Malinauskas. In situ Raman spectroelectrochemical study of electrocatalytic processes at polyaniline modified electrodes: Redox vs. metal-like catalysis. *Electrochemistry Communications*, **7**, (2005), 1021-1026.

- 
- 6 Y.Y. Tong, J.J. Van der Klink. NMR investigations of heterogeneous and electrochemical catalysts. Catalysis and Electrocatalysis at nanoparticle surfaces. CRC Press, (2003), 455-499.
  - 7 A. Ramanavicius, A. Kausaite, A. Ramanaviciene. Biofuel cell based on direct bioelectrocatalysis. *Biosensors and Bioelectronics*, **20**, (2005), 1962-1967.
  - 8 P.I. Dalko, L. Moisan. In the golden age of organocatalysis. *Angewandte Chemie International Edition*, **43**, (2004), 5138-5175.
  - 9 F. Barriere, P. Kavanagh, D. Leech. A laccase-glucose oxidase biofuel cell prototype operating in a physiological buffer. *Electrochimica Acta*, **51**, (2006), 5187-5192.
  - 10 F. Lucarelli, G. Marrazza, M. Mascini. Dendritic-like streptavidin/alkaline phosphatase nanoarchitectures for amplified electrochemical sensing of DNA sequences. *Langmuir*, **22**, (2006), 4305-4309.
  - 11 A. Morrin, F. Wilbeer, O. Ngamna, S.E. Moulton, A.J. Killard, G.G. Wallace and M.R. Smyth. Novel biosensor fabrication methodology based on processable conducting polyaniline nanoparticles. *Electrochemistry Communications*, **7**, (2005), 317-322.
  - 12 J. Wang, G. Liu, R. Polsky, A. Merkoci. Electrochemical stripping detection of DNA hybridization based on cadmium sulphide nanoparticle tags. *Electrochemistry Communications*, **4**, (2002), 722-726.
  - 13 J. Wang, G. Liu, A. Merkoçi. Electrochemical coding technology for simultaneous detection of multiple DNA targets. *Journal of the American Chemical Society*, **125**, (2003), 3214-3215.
  - 14 P.-A. Auroux, D. Iossifidis, D. Reyes, A. Manz. Micro total analysis systems. 2. Analytical standard operations and applications. *Analytical Chemistry*, **74**, (2002), 2637-2652.
  - 15 M.A. Hayes, N.A. Polson, A.N. Phayre, A.A. Garcia. Flow-based micro-immunoassay. *Analytical Chemistry*, **73**, (2001), 5896-5902.
  - 16 X.L. Luo, A.J. Killard, M.R. Smyth. Nanocomposite and nanoporous polyaniline conducting polymers exhibit enhanced catalysis of nitrite reduction. *Chemistry- A European Journal*, **13**, (2007), 2138-2143.

# LIST OF PUBLICATIONS AND PRESENTATIONS

## Scientific Publications

- **Adriano Ambrosi**, Maria Teresa Castañeda, Anthony J. Killard, Malcolm R. Smyth, Salvador Alegret and Arben Merkoçi.  
*Double-codified gold nanolabels for enhanced immunoanalysis. Analytical Chemistry*, 79, **2007**, 5232-5240.
- **Adriano Ambrosi**, Aoife Morrin, Anthony J. Killard, Malcolm R. Smyth.  
*Characterisation of immunological interactions at an immunoelectrode by Scanning Electron Microscopy. Electroanalysis*, 19, **2007**, 244-252.
- Dana Mackey, Anthony J. Killard, **Adriano Ambrosi**, Malcolm R. Smyth.  
*Optimizing the ratio of horseradish peroxidase and glucose oxidase on a bienzyme electrode: Comparison of a theoretical and experimental approach. Sensors and Actuators B: Chemical*, 122, **2007**, 395-402.
- Luigi Campanella, **Adriano Ambrosi**, Francesco Bellanti and Mauro Tomassetti.  
*Comparison between voltammetric and spectrophotometric methods for drug analysis. Current Analytical Chemistry*, 2, **2006**, 229-241.
- **Adriano Ambrosi**, Riccarda Antiochia, Luigi Campanella, Roberto Dragone, Irma Lavagnini.  
*Electrochemical determination of pharmaceuticals in spiked water samples. Journal of Hazardous Materials*, 122, **2005**, 219-225.

## Conference Participations

- **57th Irish Universities Chemistry Colloquium**

National University of Ireland, Maynooth, Ireland, 22-24th June 2005

*Characterisation of an Amperometric Immunosensor Surface by Scanning Electron Microscopy.*

Adriano Ambrosi, Aoife Morrin, Anthony J. Killard, Malcolm R. Smyth.

- **4th Spring Meeting of the International Society of Electrochemistry 2006**

National University of Singapore, Singapore, 17-20th April 2006

*Performance Enhancement of Electrochemical Biosensors by Exploitation of Nanoparticles*

Adriano Ambrosi, Xiliang Luo, Aoife Morrin, Anthony J. Killard and Malcolm R. Smyth.

- **11th International Conference on Electroanalysis ESEAC 2006**

National School of Chemistry and Physics of Bordeaux (ENSCP), France, 11-15th June 2006

*Development of a Novel Electrochemical Immunosensor platform based on enhancement of enzyme channeling using nanoparticles*

Adriano Ambrosi, Anthony J. Killard and Malcolm R. Smyth.

- **XI Trobada Transfronterera sobre Sensors i Biosensors 2006**

Escola Politècnica Superior, University of Girona, Catalonia, Spain, 14-15th September 2006

*Electrochemical Detection Of Antibody-Antigen Interaction Using Nanoparticles*

Adriano Ambrosi, Arben Merkoçi, Malcolm R. Smyth and Salvador Alegret.

- **4th Nanospain Workshop 2007**

Hotel Tryp Macarena, Seville, Spain, 12-15th March 2007

*Enhanced Electrochemical Immunoassay Based on Paramagnetic Platforms and Gold Nanoparticle Labels*

Adriano Ambrosi, Anthony J. Killard, Malcolm R. Smyth, Salvador Alegret and Arben Merkoçi.

- **4th Nanospain Workshop 2007**

Hotel Tryp Macarena, Seville, Spain, 12-15th March 2007

*Electrocatalytical Immunosensing Methods Based on Gold Nanoparticle*

Alfredo de la Escosura Muñiz, Adriano Ambrosi, Marisa Maria Viana Maltez da Costa, Maria Teresa Seabra dos Reis Gomes, Salvador Alegret and Arben Merkoçi.

- **5th Spring Meeting of the International Society of Electrochemistry 2007**

Dublin City University, Dublin, Ireland, 1-4th May 2007

*Direct Electrochemical Detection of Gold Nanoparticle labels for Enhanced Immunoassay*

Adriano Ambrosi, Arben Merkoçi, Anthony J. Killard, Salvador Alegret and Malcolm R. Smyth.

- **RSC Analytical Research Forum 2007**

University of Strathclyde, Glasgow, United Kingdom, 16-18 July 2007

*Enhanced immunoanalysis based on gold nanoparticle labels (Oral Presentation)*

Adriano Ambrosi, Arben Merkoçi, Anthony J. Killard, Salvador Alegret and Malcolm R. Smyth.